YGS Open File 2019-1

Geology of the eastern Lake Laberge area (105E), south-central Yukon

E. Bordet — Yukon Geological Survey
J.L. Crowley — Boise State University
S.J. Piercey — Memorial University of Newfoundland

with contributions from M.L. Golding, R.B. Blodgett and P.J. Sack

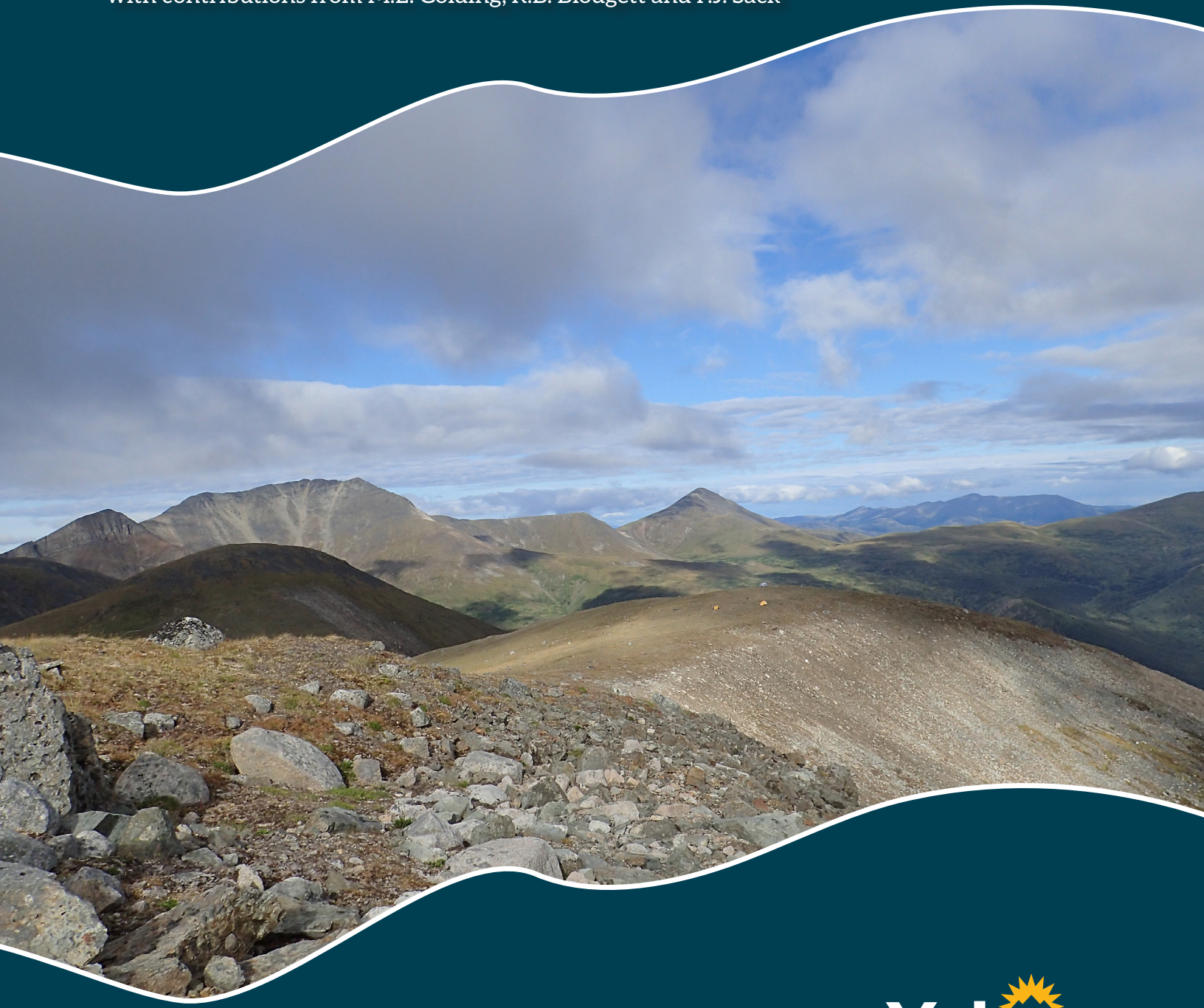

Yukon

Published under the authority of the Department of Energy, Mines and Resources, Government of Yukon http://www.emr.gov.yk.ca.

Printed in Whitehorse, Yukon, 2019.

Publié avec l'autorisation du Ministères de l'Énergie, des Mines et des Ressources du gouvernement du Yukon, http://www.emr.gov.yk.ca.

Imprimé à Whitehorse (Yukon) en 2019.

This, and other Yukon Geological Survey publications, may be obtained from:
Yukon Geological Survey
102-300 Main Street
Box 2703 (K-102)
Whitehorse, Yukon, Canada Y1A 2C6
email geology@gov.yk.ca

Visit the Yukon Geological Survey website at www.geology.gov.yk.ca.

In referring to this publication, please use the following citation:

Bordet, E., Crowley, J.L. and Piercey, S.J., 2019. Geology of the eastern Lake Laberge area (105E), south-central Yukon. Yukon Geological Survey, Open File 2019-1, 120 p.

Cover photo: View of Mount Byng area camp; looking west towards Mount Byng.

Abstract

Results and interpretations from 1:50 000 scale geological mapping of the eastern Lake Laberge area, northeast of Whitehorse, Yukon, are presented. The region is underlain by two Intermontane terranes of the Canadian Cordillera: Stikinia and Cache Creek. Exposed bedrock comprises Middle Triassic to Middle Jurassic volcanic and sedimentary strata, and Late Jurassic to Cretaceous overlap intrusive suites and one volcanic complex.

The Middle Triassic Joe Mountain Formation is characterized by juvenile, tholeiitic basalt flows, gabbroic intrusions, primary volcaniclastic deposits, and minor clastic and carbonate strata. The Upper Triassic Lewes River Group comprises a basal mafic volcanic sequence, the Povoas formation, and a younger, dominantly Norian carbonate to clastic sequence, referred to as the Aksala formation. Lithogeochemistry and Nd-Hf isotope analyses suggest that the Joe Mountain and Povoas formations were formed in primitive intra-oceanic arcs, back-arc basins or mid-oceanic ridge environments. The contact between the Middle and Upper Triassic strata is defined in part by the regional, north-trending, dextral strike-slip Laurier Creek fault. Locally, Joe Mountain Formation mafic volcanic rocks are unconformably overlain by Norian limestone of the Aksala formation. The Joe Mountain arc is interpreted as part of a large Middle Triassic primitive arc subterrane that was situated outboard of Stikinia and Quesnellia. This primitive arc was likely adjacent to the Lewes River arc at least by Late Triassic, and Joe Mountain volcanic rocks were incorporated into a Cache Creek composite terrane during Cordilleran amalgamation in Middle–Late Jurassic.

Triassic strata are unconformably overlain by mudstone, sandstone and conglomerate successions of the Early–Middle Jurassic Laberge Group. The Laberge Group is dominated by cobble to boulder conglomerate in the central part of the map area, and by thin-bedded mudstone–sandstone successions along the east shore of Lake Laberge. Mapping identified an angular unconformity at the base of the Laberge Group, suggesting that a Late Triassic deformation event took place prior to deposition of the Laberge Group strata. The deposition of Laberge Group sediments in the Early Jurassic and their subsequent erosion was likely controlled by pre-existing Triassic topography defined by limestone ridges that acted as buttresses. This pattern was further emphasized by later deformation that thrusted sheets of Triassic rocks over younger Jurassic strata.

Several post-accretion, Jurassic to Cretaceous dikes and plutons and one Late Cretaceous volcanic complex intersect or overlie Triassic to Jurassic stratigraphy. The Early Cretaceous Goddard suite is defined by quartz-phyric rhyolite and rhyodacite dikes dated between 138 and 136 Ma. The Early Cretaceous Teslin and Whitehorse suites are represented by several large plutons and dikes having ages from 116 to 106 Ma. The Late Cretaceous Rancheria suite is expressed by granodioritic and dioritic intrusions at Teslin Mountain (*ca.* 78 Ma) and by the nearby Open Creek volcanic complex, characterized by felsic pyroclastic rocks and dacitic lavas, and similar ages at *ca.* 79 Ma.

At least two deformation events are identified in the eastern Lake Laberge area: one in the latest Triassic, immediately prior to deposition of the Laberge Group basal strata; and the other from the Middle Jurassic through Cretaceous, as part of a Yukon-wide transpressional deformation. These deformation events are expressed by regional faults such as the Laurier Creek and Goddard strike-slip faults, pervasive folding in Triassic and Jurassic strata, unconformable stratigraphic relationships, and hundreds of dikes characterizing local extension synchronous with Cretaceous magmatism.

Several styles of mineral occurrences are either spatially associated with Cretaceous plutons, or result from hydrothermal alteration of the Triassic volcanic rocks. Hematite-rich iron formations are hosted in subaqueous pillowed basalt of the Joe Mountain Formation, and indicate potential for VMS mineralization. Porphyry-style mineralization is reported in the Jurassic Teslin Crossing pluton, or in the mid-Cretaceous Laurier Creek pluton. At the Hartless Joe property, epithermal Au and base metals mineralization is spatially associated with quartz-phyric felsic dikes. Preliminary analytical results indicate that these dikes may belong to the Early Cretaceous Goddard suite.

List of Abbreviations

a.m.u.	atomic mass unit
BABB	Back-arc basin basalt
BC	British Columbia
CAB	Calc-alkaline basalt
CA-TIMS	Chemical Abrasion Thermal Ionization Mass Spectrometry
Cps/pg	centipoise/picogram
HFSE	High field strength elements
HREE	Heavy Rare Earth Elements
IAT	Island arc tholeiite
km	kilometre
m	metre
Ma	Million years
masl	metres above sea level
MC-ICPMS	Multicollector Inductively Coupled Plasma Mass Spectrometry
MORB	Mid-ocean ridge basalt
mV/ng	millivolt/nanogram
m.y.	Million years
LA-ICPMS	Laser Ablation Inductively Coupled Plasma Mass Spectrometry
LFSE	Low field strength elements
LILE	large-ion lithophile element
LREE	Light Rare Earth Elements
REE	Rare Earth Elements
S.I. units	International System of Units
VMS	Volcanogenic Massive Sulphide

Chemical elements

Au	Gold	Ni	Nickel
Cu	Copper	Pb	Lead
Cr	Chromium	Sc	Scandium
Eu	Europium	Ta	Tantalum
Hf	Hafnium	Th	Thorium
La	Lanthanum	Ti	Titanium
Lu	Lutetium	U	Uranium
Mo	Molybdenum	V	Vanadium
Nb	Niobium	Zr	Zirconium

Table of Contents

List of Figures

List of Tables

Appendices

Appendices are provided as digital files only.

Appendix A - Biostratigraphy

A1- Macrofossil report

A2- Conodont report

A3- Compilation table of all fossil collections (this and previous studies) in the eastern Lake Laberge area

Appendix B - Geochronology

B1_Table of LA-ICPMS U/Pb results

B2_Table of CA-TIMS U/Pb results

B3 - Cathodoluminescence imaging for 2015, 2016 and 2017 zircon samples

B4 - Geochronology results from previous studies in the eastern Lake Laberge area

Appendix C - Geochemistry

C1_ Whole rock lithogeochemistry for Triassic volcanic rocks of the Joe Mountain and Povoas fm

C2_Nd-Hf-Isotopes for selected samples of the Joe Mountain and Povoas fm

C3_ Whole rock lithogeochemistry for selected Cretaceous plutons and dikes

C4_QA/QC results and graphs for whole rock lithogeochemistry analyses

Appendix D - Dikes

D1_Database of all dikes mapped in the eastern Lake Laberge area

Appendix E – Assays certificates

WHI17000888_2016

WHI16000320_2016

WH18274924_2018

Chapter 1 - Introduction

The region east of Lake Laberge in south-central Yukon was mapped from 2015–2018 as part of a 1:50 000 scale bedrock mapping program conducted by the Yukon Geological Survey (Fig. 1, red outline). The area encompasses the map sheets of Teslin Mountain (NTS 105E/2), and parts of Lake Laberge (105E/3) and Lower Laberge (105E/6). Parts of Joe Mountain (105D/15) and Mount M'Clintock (105D/16) mapped by Hart and Hunt (1997a,b, 2003a,b) are compiled to provide a comprehensive geological understanding of the area. A 1:50 000 scale bedrock geology map complements this report (Geoscience Map 2019-1; Bordet, 2019).

The area is underlain by Stikinia and Cache Creek, two Intermontane terranes in the Canadian Cordillera (Fig. 1). Bedrock geology is defined by the Middle Triassic Joe Mountain Formation (Hart, 1997a) and Upper Triassic Lewes River Group (Bostock and Lees, 1938; Lees, 1934; Tozer, 1958; Wheeler, 1961; Tempelman-Kluit, 1984, 2009). They are unconformably overlain by the Early–Middle Jurassic Laberge Group, which defines the Whitehorse trough (Fig. 1; Wheeler, 1961; White *et al.*, 2012). Several post-accretion, Early to Late Cretaceous dikes and plutons intrude the Triassic to Jurassic stratigraphy, and are locally associated with mineral occurrences.

Report content and organization

This report includes the most recent field observations of geological units in the Teslin Mountain and Lake Laberge areas, along with results from geochemical and geochronological analyses and a new structural framework. Four geochronology samples from the Triassic volcanic and volcaniclastic sequence were analyzed, as well as 5 detrital zircon samples from the Laberge Group, and 10 igneous samples of various Cretaceous magmatic rocks. Precise U/Pb dates contributed to refining the chronology of basin sedimentation and arc magmatism in south-central Yukon from the Triassic to Cretaceous. The report is organized into seven chapters. Analytical results for geochronology, biostratigraphy and geochemistry are presented in Appendices A to E. All fossil and geochronology sample locations are illustrated on Geoscience Map 2019-1 (Bordet, 2019).

Chapter 1 describes the physiography and access to the region east of Lake Laberge. A combination of geological factors (multiple rock types, deformation), as well as the recent glaciation history shaped the physiography of the area. The tectonic setting and regional geology of the region are introduced, and the terminology of the stratified units is presented. In addition, the main stages of glaciation and resulting post-glacial deposits are briefly described.

Chapter 2 includes unit descriptions from Triassic volcanic rocks, supported by analytical results including petrography, geochemistry and geochronology. New units are defined for the Joe Mountain Formation; they expand the original definition provided by Hart (1997a,b) and redefine the relationship of these rocks within the Intermontane terranes. A new stratigraphic framework is proposed for the Lewes River Group based on the identification of key stratigraphic relationships and lateral facies variations within the dominantly Norian carbonate sequence. Lithogeochemistry and Nd-Hf isotopic analyses of Triassic volcanic rocks outline the tectonic environment in which these rocks were formed.

Chapter 3 includes unit descriptions for the Laberge Group, and how they fit within the broader depositional framework of the Whitehorse trough. In particular, the contact between the Lewes River Group and the overlying Laberge Group is better characterized and is supported by new detrital zircon geochronological data from basal strata of the Laberge Group.

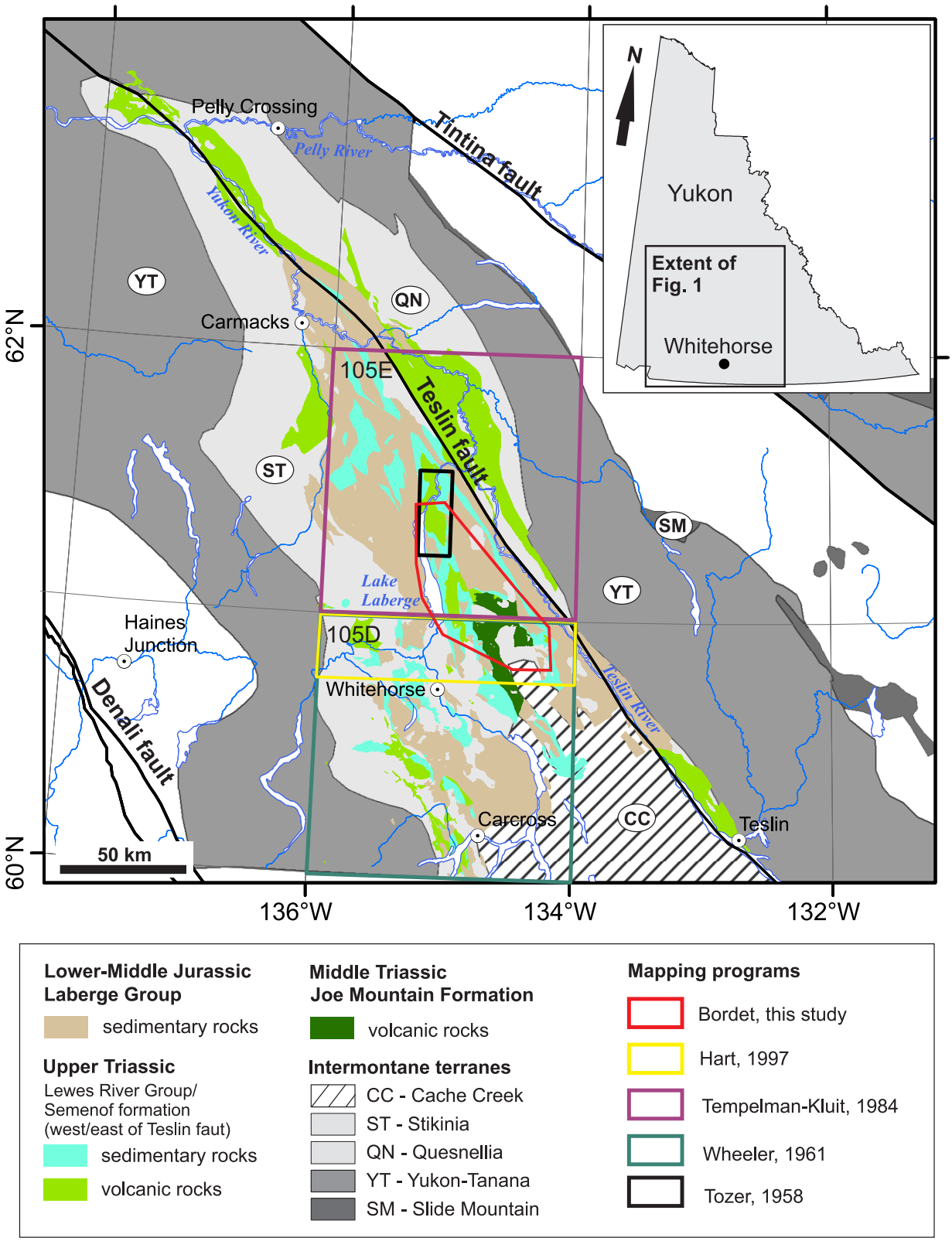

Figure 1. *Terrane map of south-central Yukon illustrating the distribution of the Intermontane terranes and Triassic to Middle Jurassic volcanic and sedimentary units. Red polygon delineates the mapped area and the extent of figures 2, 4, 6. Terrane boundaries after Colpron and Nelson (2011). Geology polygons from Colpron et al. (2016b). Laberge Group corresponds to the extent of the Whitehorse trough (after Hutchison, pers. comm., 2015).*

In **Chapter 4,** the plutons and dikes that intrude Triassic through Jurassic stratigraphy are described, and new U/Pb zircon dates and lithogeochemical data are presented. Combined REE signatures and precise U/Pb dates define a unique profile for each of the different Cretaceous intrusive suites.

Structures are described in **Chapter 5,** supporting interpretations of the deformation history of the area. A recent regional aeromagnetic survey improves the sparse structural information collected in the field. Regional faults, such as the Laurier Creek and Goddard faults, constrain the distribution of Triassic volcanic rocks and Jurassic and younger overlap assemblages, increasing complexity to pre-existing lateral facies transitions in the stratigraphic sequence. A north to northwest-trending fold and thrust belt was identified along the eastern shore of Lake Laberge, characterized by tight east-verging folds ramping up west-dipping thrusts. Dikes are further analyzed with respect to the structural evolution of the area.

Chapter 6 reviews the different styles of mineralization in the map area, including Cu or Mo porphyry, quartz vein related gold and polymetallic veins, and Cu or Mo skarn. Observations and analytical results from the Hartless Joe property suggest possible vectors for mineral exploration in this region.

Chapter 7 is a synthesis and discussion covering two main themes:

1. The evolution of Triassic volcanism and terrane affiliation of volcanic arcs: the Joe Mountain Formation is correlated with other Middle Triassic primitive tholeiitic arc sequences on the basis of similar lithology, geochemistry and geochronology. Data from the literature, compiled with observations in the Lake Laberge area, suggest that these primitive arc sequences may be affiliated with part of the Cache Creek terrane. In contrast, the Lewes River Group and equivalent Upper Triassic volcano-sedimentary sequences in the Canadian Cordillera are affiliated with Stikinia. The Middle and Upper Triassic sequences were likely adjacent by the latest Triassic, as suggested by detrital zircon signatures and stratigraphic relationships.
2. Late Triassic to Cretaceous evolution: field observations of the contact between the Lewes River and Laberge groups in the map area highlight the evolution from carbonate sedimentation on the margin of the Lewes River arc, followed by clastic deposition in the Whitehorse trough. Mapped structures and unconformities support at least two deformation events taking place between the latest Triassic and Cretaceous. Finally, the age and compositional diversity of magmatic rocks indicate a sustained magmatic activity throughout the Cretaceous. The geochemical signature of intrusions records orogen-scale tectonic changes. Intrusions are also linked to several known mineral prospects, suggesting that more mineral potential exists.

Location, physiography & access

The map area is located 40–70 km northeast of Whitehorse, in south-central Yukon (Fig. 1). It displays a diverse and contrasting topography and physiography (Figs. 2 and 3) inherited from a complex geological evolution, and later shaped by several glaciations (Fig. 4).

About 30 km north of Whitehorse, the Yukon River valley widens and opens up to Lake Laberge, a 50 km-long lake formed during the last glacial retreat (Figs. 1 and 2). The map area is located along the eastern shore of Lake Laberge, and is part of the Yukon Plateau physiographic region. The northern half of the map area is delineated by north-northwest trending limestone ridges and rolling hills (Fig. 3a,b) underlain by volcanic rocks. Elevations range from 600 masl on the lake shore, to approximately 1900 masl at Teslin Mountain and Joe Mountain (Fig. 2). Mount Byng is the tallest peak in the area with an elevation of 2089 m (Fig. 2). Rock is exposed along most ridges (Fig. 3c–e), while lowlands are covered with vegetation and blanketed by till deposits (Fig. 3b).

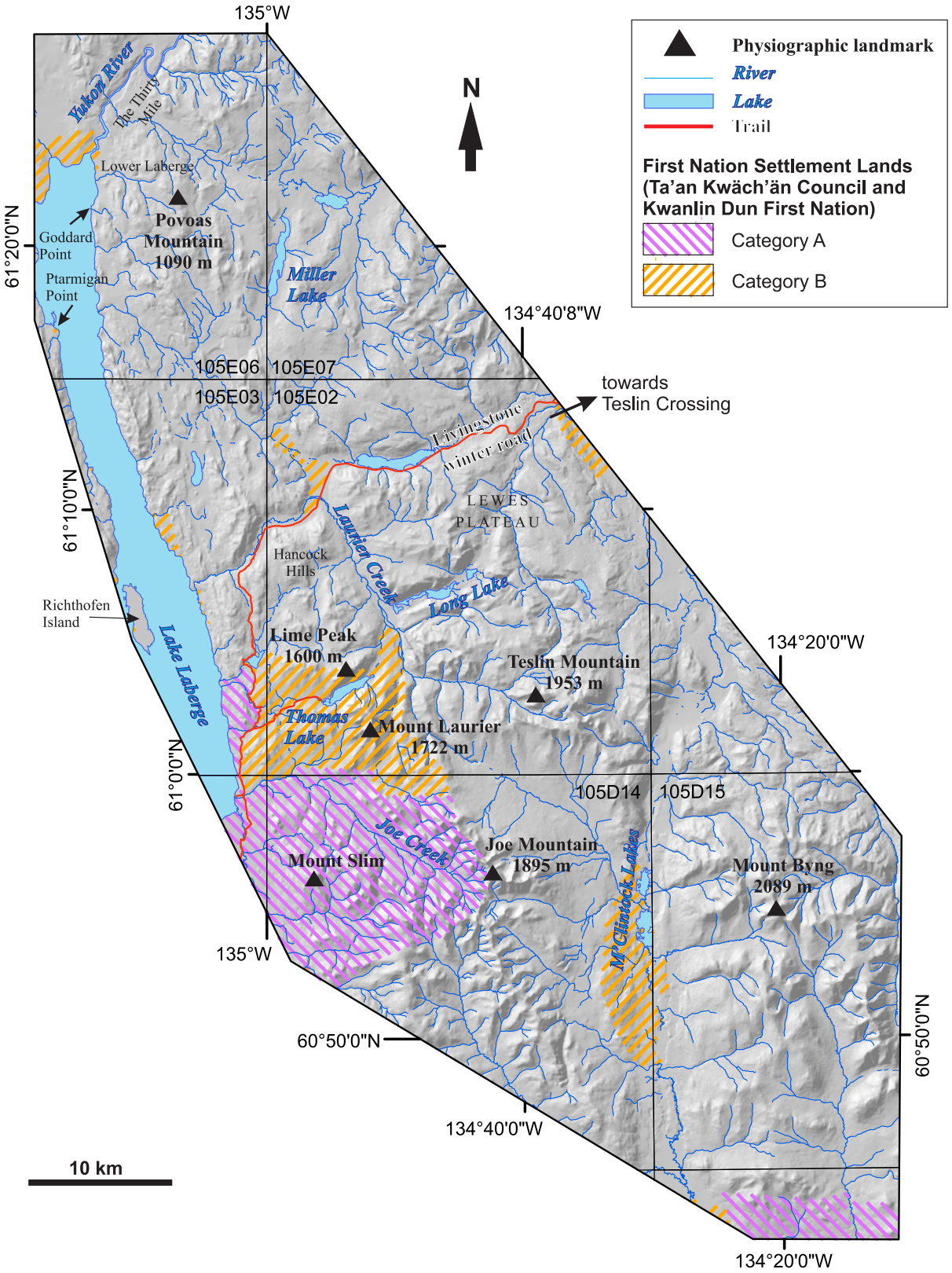

Figure 2. *Physiography of the map area. Main landmarks referred to in text are indicated, including peaks, rivers and lakes. The map area encompasses parts of six different NTS map sheets. First nation settlement lands categories A and B are indicated for reference.*

The southeastern part of the Teslin Mountain map area (105E/02) and northern part of Joe Mountain map area (105D/15) are shaped by four prominent topographic highs displaying rocky ridges and alpine slopes covered by tundra. Joe Mountain and Mount Byng (Fig. 2) feature rugged ridges and peaks with exposed bedrock (Fig. 3c,d), and valley bottom covered in low bushes and tundra. Teslin Mountain (Fig. 2) forms a network of east-trending ridges expanding to a high alpine plateau towards the west and northwest (Fig. 3e). Mount Laurier (Figs. 2 and 3f) is a north–south oriented ridge, with a steep rocky east slope, and a gentler west slope. It is faced by Lime Peak to the north (Figs. 2 and 3f), which is characterized by an ~500 m tall, steep limestone cliff to the south and a smoother northern facing slope. These peaks are separated by deep incised valleys (Laurier Creek valley, between Mount Laurier and Teslin plateau; Fig. 2), or wide glacial valleys (between Joe Mountain and Teslin Mountain; Fig. 2).

Access to the area is primarily by helicopter. The high open ridges and plateau in the southeastern part of the map area offer safe landing zones (Fig. 3e,f). Towards the north, helicopter access is challenging due to the almost continuous tree cover, and only few small open areas bounded by near-vertical cliffs (Fig. 3b). The Livingstone winter road (Fig. 2) connects the southern end of Lake Laberge and Whitehorse to Teslin Crossing, and parts of the trail along the east shore of Lake Laberge are in good condition throughout the year. However the area at the southern tip of Lake Laberge is extremely swampy, and is not accessible by road in the summer time. Access by motorized boat from the west shore of Lake Laberge is possible throughout the summer months. Strong southern winds tend to generate large, uneven and choppy waves and can be a concern while sailing on the lake. It is best to wait for quiet days for navigating, and it is recommended to sail along the east shore of the lake at all times (Fig. 3a).

Glaciation history & post-glacial deposits

The glaciation and deglaciation history of the map area is characterized by ice accumulations during the late Wisconsinan (late Pleistocene), an event referred to as the McConnell glaciation (29.6 to 10.7 ka BP; Bond, 2004). Glacial deposits related to this event became exposed following the retreat of the Cassiar glacial lobe of the Cordilleran Ice Sheet (Fig. 4).

Lake Laberge is a major feature illustrating the deglaciation history of this area. During the second stage of deglaciation, recession of the Cassiar glacial lobe was momentarily paused, leading to the development of a large recessional moraine complex at the north end of Lake Laberge (Fig. 4; Bond, 2004). As the ice receded from this moraine, glacial Lake Laberge developed behind the moraine of stagnating ice and sediment. The lake continued to expand as the Cassiar lobe continued its retreat southward.

Today, the area east of Lake Laberge is dominated by McConnell (late Wisconsinan) glacial deposits, including morainal till deposits, glaciofluvial and glacial lacustrine sediments (Fig. 4). Moraine deposits occupy wide valley bottoms throughout the map area. Towards the northern end of Lake Laberge, the relative proportion of glaciofluvial sediments increases, in association with minor glacial lacustrine sediments in the northern part of the map area at the northern tip of Lake Laberge, south of Miller Lake. Exposed bedrock encompasses about 20% of the area (Fig. 4), including the alpine ridges of Mount Byng, Joe Mountain and Teslin Mountain to the south, and limestone ridges of the Lewes River Group towards the north. Colluvium is found in these areas where the terrain is the most rugged, such as surrounding Mount Laurier, north of Teslin Mountain, and in a series of alpine valleys south of Joe Mountain.

Figure 3. *Field photographs illustrating the physiography of the map area; Q = quaternary deposits.* ***(a)*** *limestone cliffs of the Aksala formation along the eastern shore of Lake Laberge;* ***(b)*** *glacial till form flat-lying terrace deposits in the valley, and east-dipping Triassic strata of the Lewes River Group are exposed in the background;* ***(c)*** *jagged rocky ridge of the main peak at Joe Mountain is underlain by basalt and gabbro;* ***(d)*** *rocky, bare ridge of Mount Byng is underlain by microcrystalline basalt of the Joe Mountain Formation;* ***(e)*** *smooth, tundra-covered alpine ridges of Teslin Mountain are underlain by microcrystalline basalt of the Joe Mountain Formation, and surrounded by wide, U-shaped glacial valleys; and* ***(f)*** *jagged, rocky peaks of Mount Laurier and Lime Peak are surrounded by forested lowlands underlain by glacial deposits.*

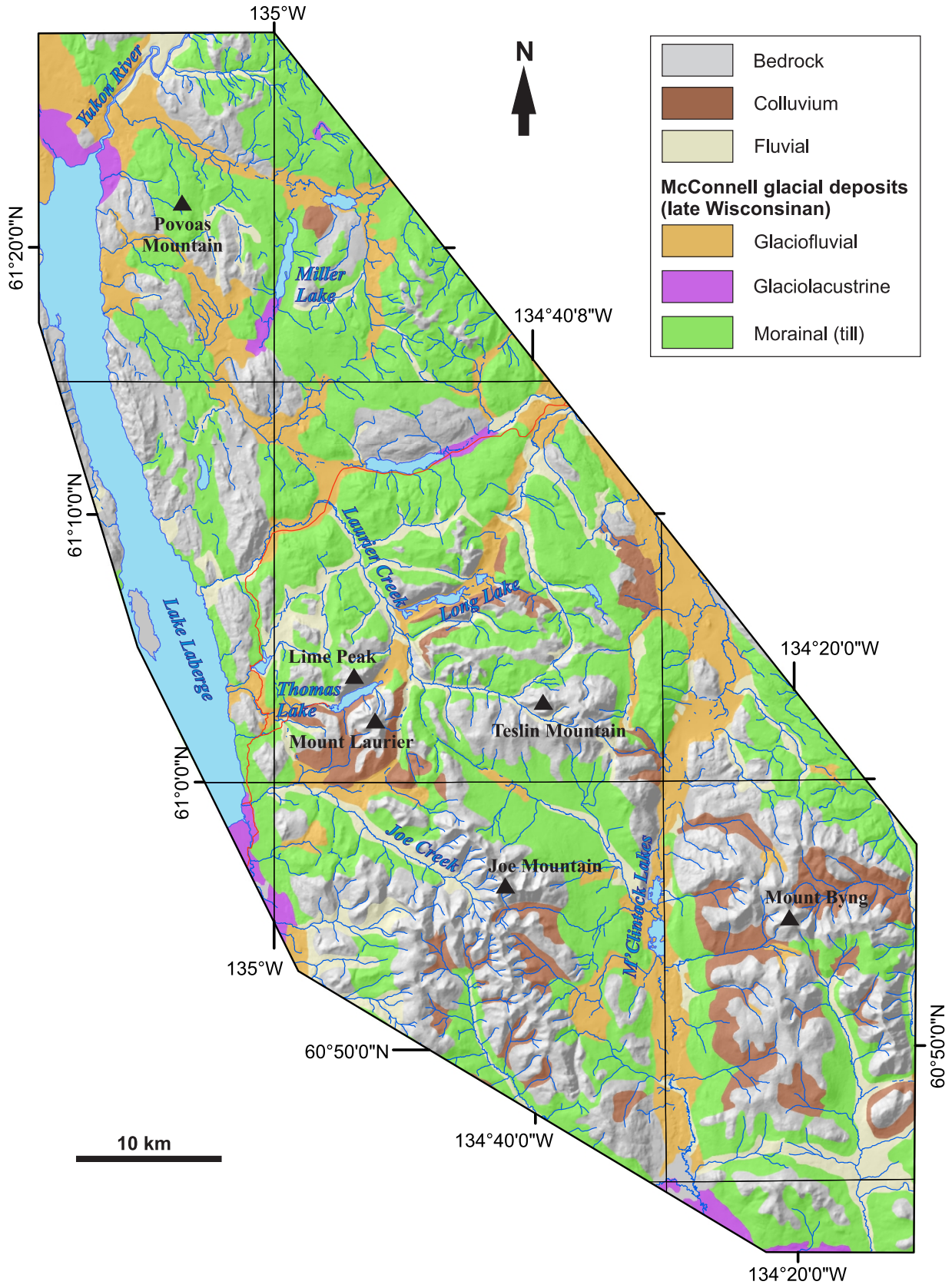

Figure 4. *Surficial geology map of the region east of Lake Laberge after Klassen and Morison (1987).*

Tectonic setting

The Intermontane terranes underlie most of south-central Yukon and British Columbia (BC) southwest of the Tintina fault (Fig. 1). They represent the largest amalgamation of crustal fragments that accreted to the North American margin during the Mesozoic (Coney *et al.*, 1980; Colpron *et al.*, 2007b). In Yukon, the outer margin of the Intermontane terranes is defined by middle Paleozoic (and older) metasedimentary and metavolcanic rocks of the Yukon-Tanana terrane (Fig. 1; Mortensen and Jilson, 1985; Mortensen, 1992). The core and bulk of the Intermontane terranes comprise Mesozoic volcanic arc rocks of Stikinia and Quesnellia (Fig. 1; Colpron and Nelson, 2011; Wheeler *et al.*, 1991), which are juxtaposed along the Teslin fault north of Whitehorse (Fig. 1). Upper Paleozoic to lower Mesozoic accretionary complex rocks of the Cache Creek terrane (*e.g.*, Monger *et al.*, 1991; Struik *et al.*, 2001) are surrounded by Stikinia and Quesnellia (Fig. 1) and extend south of Whitehorse to northern British Columbia. To date, Cache Creek rocks have not been identified north of Whitehorse (Bickerton *et al.*, 2013; Bickerton, 2014).

Subduction of the Panthalassa Ocean along the North American margin during the Mesozoic produced volcanic arcs of Stikinia and Quesnellia (Mihalynuk *et al.*, 1994). In south-central Yukon, arc volcanism and arc-related basinal sedimentation are recorded by Middle and Upper Triassic volcanic and sedimentary rocks of Stikinia, namely the Joe Mountain Formation and Lewes River Group (Wheeler, 1961; Hart, 1997a).

Erosion of the Stikinia and Quesnellia arcs and their plutonic roots from the Early to Middle Jurassic resulted in the deposition of up to 3000 m of sedimentary rocks of the Lower to Middle Jurassic Laberge Group in the Whitehorse trough (*e.g.*, Wheeler, 1961; White *et al.*, 2012). The Whitehorse trough extends approximately 650 km, from Dease Lake, BC to north of Carmacks in central Yukon (Fig. 1). The Whitehorse trough originally developed as a forearc basin and evolved into a northwest-trending, synorogenic, intermontane piggy-back transpressional basin in the Early Jurassic (Colpron *et al.*, 2015; White *et al.*, 2012).

Ongoing eastward subduction of Pacific plates beneath North America during the Cretaceous led to progressive thickening and shortening of the crust, associated with orogen-parallel dextral displacements (Nelson *et al.*, 2013). In this dominantly transpressional and transtensional orogen, corridors of deformation provided pathways for post-accretionary arc activity and the formation of a number of mineral occurrences (Nelson *et al.*, 2013).

Regional geology and terminology

The Teslin Mountain and Lake Laberge areas are underlain by three major layered rock assemblages: the Middle Triassic Joe Mountain Formation and Upper Triassic Lewes River Group are inferred to be part of Stikinia or Cache Creek (Hart, 1997a), and are overlain by the Lower to Middle Jurassic Laberge Group which defines the Whitehorse trough (White *et al.*, 2012; Fig. 5a). Other overlap assemblages include the Upper Cretaceous Open Creek volcanic complex (Tempelman-Kluit, 1984, 2009), and intrusive bodies related to various Cretaceous plutonic suites (Fig. 5b). Paleozoic arc assemblages of Stikinia are not exposed within the map area.

Early reconnaissance geological mapping (1:250 000 scale) was conducted by the Geological Survey of Canada around Whitehorse (NTS 105D, Fig. 1; *e.g.*, Wheeler, 1961), and east of Lake Laberge (NTS 105E, Fig. 1; Bostock and Lees, 1938; Lees, 1934; Tempelman-Kluit, 1984, 2009; Tozer, 1958). The stratigraphic framework and nomenclature most widely used today in this

region is based on the regional mapping by Tempelman-Kluit (1984), and later improved by several 1:50 000 scale maps, and by isotopic and biostratigraphic dates (Hart, 1997a; 105D/2, 3, 6, 11: Hart and Radloff, 1990; 105D/13-16: Hart and Hunt, 1997a,b). This original framework is illustrated on Figure 5a and reviewed below. Bedrock mapping conducted east of Lake Laberge, combined with new high-quality geochemical and geochronological data (see Chapters 2 and 3), suggest that revisions to the stratigraphic framework, and modifications of the existing nomenclature are necessary (Fig. 5b).

The stratigraphic timescale used as a reference in this report is from Cohen *et al.* (2013). Absolute ages of Triassic stages are as followed:

- **Lower Triassic**: 251.902 ± 0.024 to 247.2 Ma
- **Middle Triassic:** Anisian 247.2 to *ca.* 242 Ma; Ladinian *ca.* 242 to *ca.* 237 Ma
- **Upper Triassic:** Carnian *ca.* 237 to *ca.* 227 Ma; Norian *ca.* 227 to *ca.* 208.5 Ma; Rhaetian *ca.* 208.5 to 201.3 ± 0.2 Ma

Joe Mountain Formation

The Joe Mountain Formation was originally defined by Hart (1997a) at Joe Mountain (type-section) and Mount Byng (NTS 105D/15, 16; Fig. 2). It includes a sequence of Middle Triassic (Ladinian) pillow basalt, clastic and calcareous sedimentary rocks, microdiorite, diabase and gabbro. Hart (1997a) suggested that the Joe Mountain Formation may unconformably overlie the upper Paleozoic Takhini assemblage, a package of deformed and metamorphosed mafic volcanic rocks that constitute the oldest unit in Stikinia in southern Yukon (Fig. 5a). The terrane affiliation of the Joe Mountain Formation is further discussed in Chapter 6. In this report, the Joe Mountain Formation refers to Middle Triassic volcanic, volcaniclastic and sedimentary units that underlie the type locality at Joe Mountain (105D/15), Mount Byng (105D/16) and Teslin Mountain (105E/02). Joe Mountain Formation rocks do not extend past the Laurier Creek fault to the west, and are not exposed north of Teslin Mountain, past the basal contact of Laberge Group (Fig. 6; Bordet, 2019).

Lewes River Group

The Lewes River Group comprises Upper Triassic volcanic, clastic and carbonate rocks. The relationship with the underlying Joe Mountain Formation is uncertain (Hart, 1997a; Bordet 2016, 2017, 2018; Fig. 5).

The first stratigraphic framework for the Lewes River Group was established by Lees (1934) and Bostock and Lees (1938). Tozer (1958) conducted mapping and measured several sections northeast of Lake Laberge (Thirty Mile area, Fig. 2), and introduced seven formations (A to G) including four distinct massive or bedded limestone units, interbedded with volcaniclastic and mixed volcano-sedimentary units. Each formation is characterized by unique lithological and textural features, which represent, chronostratigraphic intervals.

Wheeler (1961) mapped the Whitehorse area (Fig. 1), south of Lake Laberge, and divided the Lewes River Group into three belts to reflect lateral changes in lithology from west to east: at the base of the sequence to the west, a coarse-grained, mixed sedimentary and volcaniclastic unit occurs, and finer, more clastic units are mapped to the east; the highest stratigraphic level is dominated by limestone across the three belts. Wheeler (1961) emphasized the complex stratigraphy of the Lewes River Group, by noticing important lateral facies changes across southern Yukon.

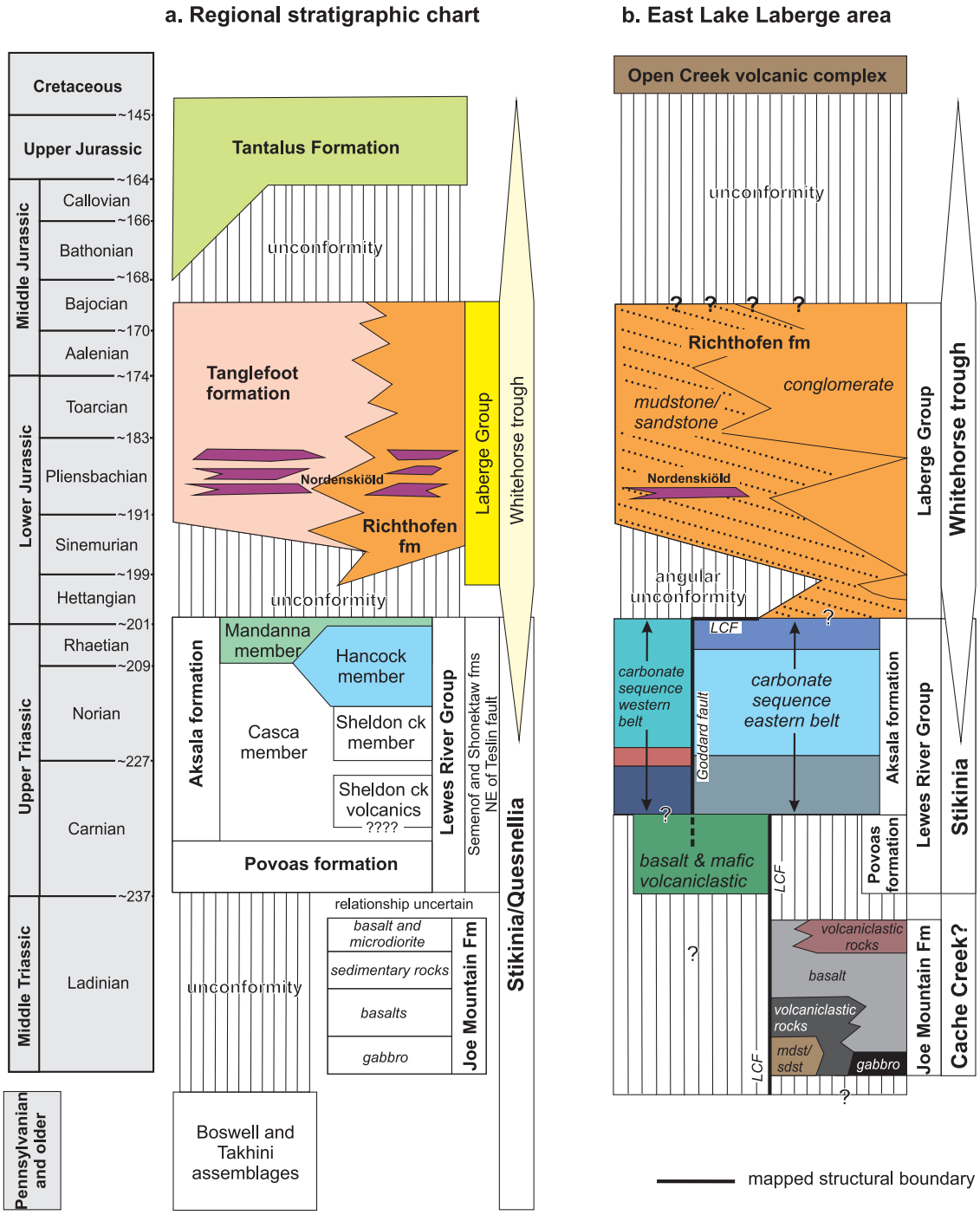

Figure 5. *Stratigraphic relationships between Triassic, Jurassic and younger layered units. Intrusions are not included. Numerical ages for Triassic and Jurassic stage boundaries are from Cohen et al. (2013).* ***(a)*** *Regional composite stratigraphic chart for Stikinia, Quesnellia, and the Whitehorse trough in Yukon (from Colpron et al., 2015; modified from Hart, 1997; Lowey, 2004, 2008). Many of the stratigraphic units in use for Stikinia and the trough are informal (Tempelman-Kluit, 1984, 2009); Upper Triassic strata of the Semenof and Shonektaw formations of Quesnellia, exposed northeast of Teslin fault, are lithologically and age-equivalent to the Lewes River Group; and* ***(b)*** *Local composite stratigraphic chart for the region east of Lake Laberge in south-central Yukon, including the Teslin Mountain, Joe Mountain and Mount Byng areas to the south, and Thirtymile section of the Yukon River to the north. The chart illustrates simplified east-west lateral lithological variations across the region, as well as mapped structural boundaries (LCF = Laurier Creek Fault).*

The current stratigraphic framework for the Lewes River Group comprises four lithological units grouped in two informal formations (Tempelman-Kluit, 1984, 2009; Hart, 1997a).

- The Povoas formation (Fig. 5a,b), comprises aphyric to pyroxene-phyric basalt and volcanic breccia, geochemically distinguished from the underlying Joe Mountain Formation by island arc calc-alkaline geochemical characteristics (Hart, 1997a).
- The Aksala formation (Fig. 5a,b), comprises greywacke-shale with thick limestone lenses, and is divided into four members that variably overlie the Povoas formation: the Casca, Hancock, Mandanna (Tempelman-Kluit, 1984) and Sheldon members (Hart, 1997a). The Casca member is lithologically heterogeneous and includes a variety of calcareous siltstone, argillite, sandstone and conglomerate. The Sheldon member comprises conglomerate, and minor sandstone and limy siltstone, and is only reported at one locality near Mount Byng (Fig. 2; Hart, 1997a; Hart and Hunt, 1997b, 2003b). The Hancock member comprises thick beds of massive to bedded limestone that form a northwest-trending belt east of Lake Laberge (Fig. 3a). The limestone is dominantly Norian and locally Rhaetian (Hoover, 1991; Senowbari-Daryan, 1990; Orchard, 1995). The Mandanna member comprises well-bedded or massive, red and green weathering greywacke and volcanic sandstone, and is mainly observed west and north of Lake Laberge (Colpron *et al.*, 2016b).

A new stratigraphic framework for the Lewes River Group (Fig. 5b) is proposed based on the further characterization of previously defined units, the definition of new map units, and observations supporting the spatial and temporal distribution and relationships between units. This new framework is further detailed in Chapter 2. The stratigraphic subdivision of the Aksala formation into members defined by Tempelman-Kluit (1984, 2009) is not retained here because it significantly lacks at addressing complex vertical and lateral stratigraphic variations. For instance, the Hancock member (Fig. 5a) includes all limestone units regardless of their potentially distinct stratigraphic level, age, and environment of deposition. As for the Casca member (Fig. 5a), it combines any kind of volcaniclastic units mapped throughout the area, with little consideration for their relationship with adjacent volcanic or carbonate rocks. Based on observations made outside of the map area, the Mandanna member may be the only one deserving the status of member (Hart, 1997a; Colpron *et al.*, 2007a).

Laberge Group

The Lewes River Group is overlain by the Lower to Middle Jurassic Laberge Group, but the nature of the contact is uncertain (unconformable contact: Cairnes, 1910; Lowey, 2004, 2005, 2008; Lowey *et al.*, 2009; conformable contact: Bostock and Lees, 1938; Hart, 1997a; Tempelman-Kluit, 1984). The Laberge Group corresponds to deltaic and deep marine sedimentation in the Whitehorse trough from the Early to Middle Jurassic, following shallow-water, arc-related deposition of the Upper Triassic Lewes River Group strata (Colpron *et al.*, 2015; White *et al.*, 2012).

Stratigraphy of the Laberge Group includes shallow marine to fluvial and coal-bearing sandstone, conglomerate and shale deposits of the Tanglefoot formation exposed in the northern part of the trough (Fig. 5a; Hart, 1997a; Lowey, 2004, 2008; Tempelman-Kluit, 1984, 2009), and laterally partially equivalent to deep marine turbidite and mass-flow conglomerate successions of the Richthofen formation mapped in the southern part of the trough (Fig. 5a; e.g., Lowey, 2005; Tempelman-Kluit, 1984, 2009). In northern BC, the western facies of the Laberge Group (Takwahoni formation) may be equivalent to the Tanglefoot formation (Mihalynuk *et al.*, 1999)

and the main facies is equivalent to the Richthofen formation. The Nordenskiöld dacite, a distinct crystal-lithic tuff (Tempelman-Kluit, 1984, 2009), occurs at multiple stratigraphic levels in both the Richthofen and Tanglefoot formations (Fig. 5a,b), and records at least three distinct eruptive events between 188 and 186 Ma (Colpron and Friedman, 2008). The Middle Jurassic to Lower Cretaceous Tantalus Formation disconformably overlies the Laberge Group (Fig. 5a; e.g. Tempelman-Kluit, 1984, 2009). This coal-bearing sequence of fluvial chert-pebble conglomerate and sandstone marks the end of deposition in the Whitehorse trough (White *et al.*, 2012; Long, 2015).

Cretaceous magmatic suites

Several of the Yukon magmatic suites (Colpron *et al.*, 2016a) are represented in the eastern Lake Laberge area and briefly described below.

The Bryde plutonic suite (*ca.* 172-168 Ma; Colpron *et al.*, 2016a) is represented by the Mount Bryde pluton and Fourth of July batholith in southern Yukon (Aitken, 1959), by the Teslin Crossing pluton east of Lake Laberge, and by a distinct phase of the McGregor pluton north of Carmacks. The plutonic rocks are characterized by monzonite, granite, monzodiorite, quartz monzodiorite, hornblende diorite and granodiorite, and rare syenite (Aitken, 1959; Colpron *et al.*, 2016a).

The Teslin plutonic suite (123 to 115 Ma; Colpron *et al.*, 2016a) is defined by a set of plutons located on either side of the Teslin fault between the Teslin Mountain area and the Yukon–BC border. From north to south, it includes the Laurier Creek pluton, the M'Clintock Lakes pluton, the Streak Mountain pluton, the Hayes Peak pluton, the Deadman Creek batholith and the Strawberry Creek pluton (Colpron *et al.*, 2016a). Plutonic rocks of the Teslin suite comprise coarse-grained, biotite-hornblende granodiorite to quartz monzonite (Hart, 1997a).

The Whitehorse plutonic suite (112-98 Ma; Colpron *et al.*, 2016a) is represented by several batholith size plutons west and northwest of Carmacks (*e.g.*, Dawson Range batholith, Coffee Creek pluton, Mount Nansen pluton, Mahoney batholith) and east, west and south of Whitehorse (*e.g.*, Whitehorse pluton, Cap Mountain pluton, Byng Creek pluton, Mount M'Clintock pluton). Plutonic rocks are characterized by several phases dominated by dark-weathering, medium to coarse-grained, biotite-hornblende granodiorite and quartz-diorite, and includes locally mafic compositions (Hart, 1997a; Colpron *et al.*, 2016a). It is associated with several Cu ± Au, Ag, Mo porphyry skarn mineralized occurrences (*e.g.*, Whitehorse Copper belt; Rasmussen, 2013).

The Rancheria plutonic suite (82–77 Ma; Colpron *et al.*, 2016a) comprises a few plutons dominantly located east of the Teslin fault in southern Yukon, such as the Cabin Creek stock, and a phase of the Deadman Creek batholith. Plutonic rocks include biotite-muscovite leucogranite to monzogranite, biotite granodiorite, tonalite, and biotite monzogranite (Colpron *et al.*, 2016a). The Red Mountain Cu-Mo-Au deposit (Turner and Sabag, 1995; Yukon MINFILE 105C 009) is hosted within porphyritic quartz monzonite dated at 81.2 ± 0.9 Ma (Ar/Ar, biotite), 78.7 ± 0.9 Ma (Ar/Ar, whole rock), and 74.4 ± 0.8 Ma (Ar/Ar, whole rock; Brown and Kahlert, 1986; Joyce *et al.*, 2015) and therefore associated with the Rancheria suite. The only known occurrence of this suite west of the Teslin fault is the Teslin Mountain pluton that underlies Teslin Mountain in the eastern Lake Laberge area.

Chapter 2 – Triassic Rocks

This chapter provides new observations and interpretations of the internal stratigraphy and relationships between the Triassic Joe Mountain Formation and the Lewes River Group in the eastern Lake Laberge area. Ages of the different units are constrained when possible by U/Pb geochronology and biostratigraphy. Lithogeochemistry and Nd-Hf isotopic analyses characterize juvenile arc volcanism that led to the formation of the Joe Mountain and Povoas formations. All references to geographic locations (e.g., Joe Mountain, Teslin Mountain, Mount Byng, etc.) are indicated on Figure 2. Detailed bedrock geology and cross sections are available in Geoscience Map 2019-1 (Bordet, 2019).

Lithology and stratigraphy

Joe Mountain Formation (Middle Triassic)

The southeastern part of the map area, east of the Laurier Creek fault, is dominated by coherent pillowed basalt of the Joe Mountain Formation (mTJMb) centred on Joe Mountain, Teslin Mountain and Mount Byng. The unit is overlain by mafic volcaniclastic deposits (mTJMvc) west of Teslin Mountain (Fig. 6). North of Teslin Mountain and at Joe Mountain, basalt and fragmental rocks are underlain or interbedded with clastic, locally thin-bedded and laminated strata, as well as minor calcareous conglomerate and mudstone (mTJMms). To the north, this clastic sequence is also underlying, or locally thrust over a volcanic and volcaniclastic assemblage (mTJMbx). In addition, dark, massive, coarse-grained and locally pegmatitic, pyroxene gabbro and diorite (mTJMg) are reported at Joe Mountain (105D/14; Hart, 1997a; Hart and Hunt, 1997a, 2003a; Fig. 6) and Mount Byng (105D/14; Hart, 1997a; Hart and Hunt, 1997a, 2003a; Fig. 6).

The thickness of the Joe Mountain Formation is estimated at ~3500 m from map relationships, including an ~1000 m-thick basal sedimentary sequence north of Teslin Mountain, a cumulative thickness of 2000-2300 m for the basalt and volcaniclastic sequence, and a thickness of at least 500 m for the younger volcaniclastic sequence. Previous thickness estimates indicate at least 3200 m for the Joe Mountain Formation type-section at Joe Mountain (Hart, 1997a).

The Joe Mountain Formation is folded along a consistent east-west structural trend (Fig. 6). It is locally intruded by Early and Late Cretaceous plutons.

*Clastic sedimentary sequence (*mTJMms*)*

A newly defined, dominantly clastic sedimentary sequence underlies mafic and volcaniclastic strata of the Joe Mountain Formation north of Teslin Mountain (Figs. 6). North of Teslin Mountain, the clastic sedimentary strata display a consistent southern dip. Contact with mafic volcaniclastic rocks (mTJMvc) to the south is interpreted as conformable, whereas the contact to the north with volcanic conglomerate and breccia (mTJMbx) is interpreted as a thrust fault. The sequence is continuously exposed along the northern flank of Teslin Mountain's westernmost ridge, and presumably underlies an east-trending valley covered by vegetation and thick glacial fluvial terraces. The sequence outcrops again south of Long Lake (Fig. 6). The Laurier Creek fault marks the westernmost boundary of this sequence, and it is not exposed north of Long Lake.

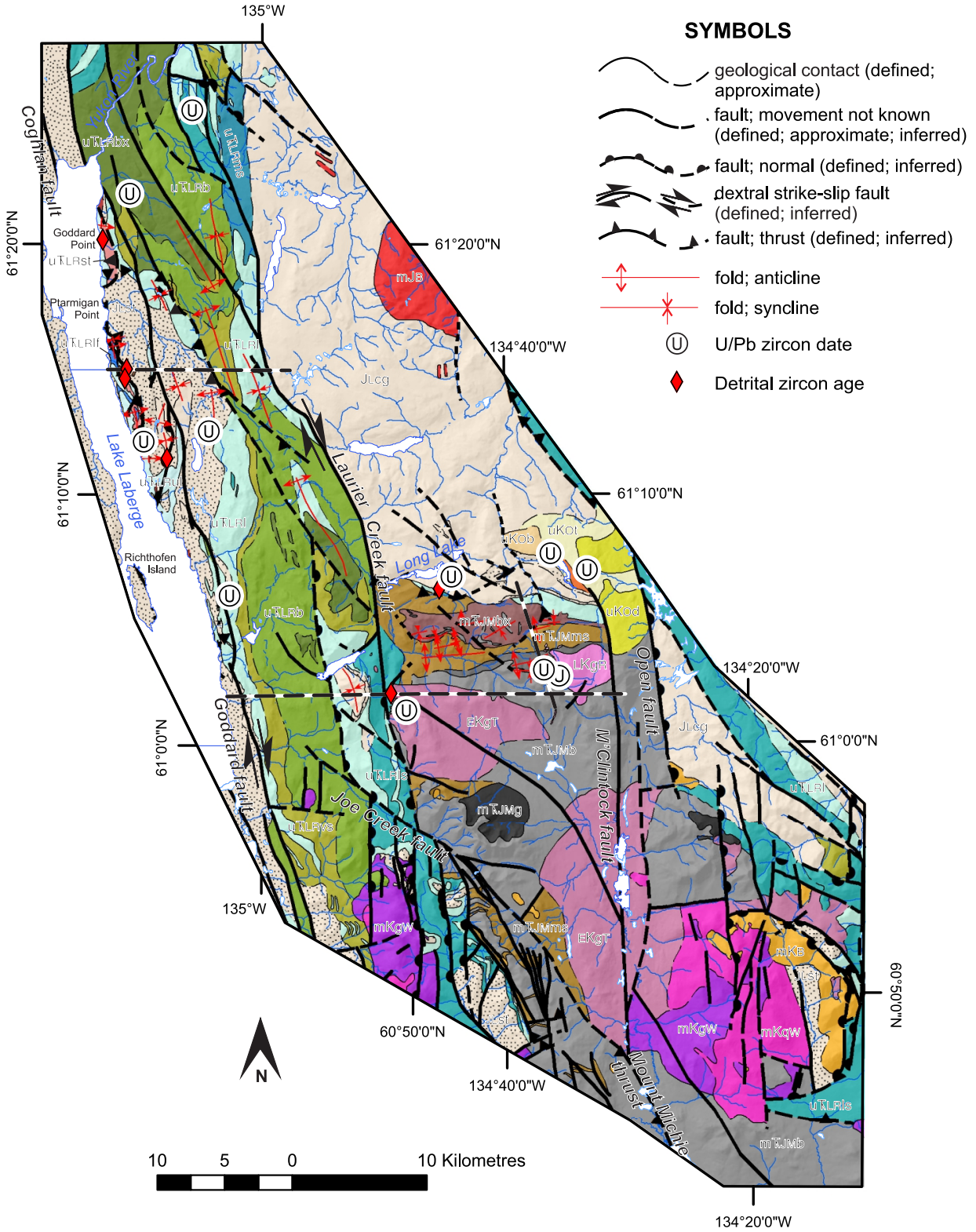

Figure 6. *Simplified geology of parts of the Teslin Mountain, Lake Laberge and Lower Laberge (105E/2, 3, 6) areas based on 1:50 000-scale mapping. Detailed geology and cross sections available in Bordet (2019). Grid in UTM zone 8, NAD 83. Legend on next page.*

UPPER CRETACEOUS

OPEN CREEK VOLCANIC ROCKS

uKOb — Pyroxene-plagioclase porphyritic vesicular to amygdaloidal basalt and gabbro dikes

uKOd — Massive to columnar jointed or flow-banded indurated dacite and scoriaceous dacitic breccia

uKOt — Crystal-rich lapilli tuff and block-and-ash flow forming a ≥400 m thick ignimbrite sequence

uKO — Coarsely plagioclase, biotite, hornblende porphyritic diorite

LATE CRETACEOUS

RANCHERIA SUITE - Teslin Mountain pluton

LKgR — Granodiorite, diorite and quartz diorite

BYNG SUITE

mKB — Quartz-eye rhyolite and dacite flows, tuff, fragmental volcanic rocks

WHITEHORSE SUITE - Cap Creek pluton, M'Clintock plutons

mKgW — Biotite hornblende granodiorite

mKqW — Quartz monzonite

EARLY CRETACEOUS

TESLIN SUITE - Laurier Creek pluton

EKgT — Granodiorite and quartz diorite, monzonite, monzodiorite

GODDARD SUITE

EKqG — Quartz-phyric rhyolite and rhyodacite dikes

MIDDLE JURASSIC

BRYDE SUITE - Teslin Crossing pluton

mJB — Medium to fine-grained, equigranular, leucocratic monzonite, syenite and granite and related dikes

LOWER AND MIDDLE JURASSIC

WHITEHORSE TROUGH, LABERGE GROUP

lJN — Beige-tan weathering, medium grained crystal tuff (Nordenskiöld dacite)

JLcg — Polymictic pebble to boulder conglomerate

JLst — Turbiditic mudstone, siltstone, sandstone; minor granule to pebble conglomerate

JLcbx — Dark grey-green matrix-supported, immature polymictic, chaotic cobble to boulder conglomerate; bright green, volcanic quartz-rich sandstone matrix

UPPER TRIASSIC

LEWES RIVER GROUP - AKSALA FORMATION

uTLRul — Thick-bedded limestone; wackestone; calcareous sandstone and conglomerate

uTLRst — Non-calcareous, polymictic medium to coarse-grained sandstone and matrix supported granule conglomerate

uTLRlf — Thick to medium-bedded lime mudstone; argillaceous, fossiliferous limestone wackestone; thin-bedded calcareous sandstone and mudstone

uTLRms — Argillaceous laminated mudstone with lenses (10 cm thick) of pale grey lime mudstone; non-calcareous fine-grained sandstone

uTLRl — Thick-bedded limestone; wackestone

uTLRls — Fine-grained calcareous and non-calcareous laminated sandstone/mudstone; chaotic limestone conglomerate

WESTERN BELT ↑ ↓ EASTERN BELT

LEWES RIVER GROUP - POVOAS FORMATION

uTLRvs — Volcaniclastic sandstone; pyroxene-phyric lithic mafic sandstone; polymictic cobble conglomerate

uTLRbx — Mafic volcanic conglomerate, angular volcanic breccia and lapilli tuff

uTLRb — Flow-banded to pillowed aphyric to pyroxene-phyric basalt and plagioclase-phyric basalt or andesite

MIDDLE TRIASSIC

JOE MOUNTAIN FORMATION

mTJMbx — Polymictic volcanic breccia, locally interbedded with coherent pillowed to flow-banded basalt and mafic volcanic sandstone and mudstone

mTJMvc — Thick-bedded, polymictic, chaotic volcaniclastic boulder conglomerate; angular lapilli tuff with up to 3 % quartz eyes; silicified laminated mafic ash tuff and minor limestone

mTJMg — Dark-weathering, massive, variably textured, coarse-grained and locally pegmatitic, pyroxene gabbro and diorite (Hart and Hunt, 2003)

mTJMb — Aphyric basalt and basaltic andesite forming blocky, massive to pillowed lava flows; volcanic breccia and volcaniclastic sandstone

mTJMms — Slightly calcareous laminated mudstone; mafic volcanic sandstone, conglomerate and breccia

This unit comprises slightly calcareous, laminated mudstone/sandstone, mafic volcanic sandstone, conglomerate and breccia. A south-dipping sequence of rusty-brown weathering, dark grey to pale grey-green, thin to medium-bedded, fine-grained, slightly calcareous laminated mudstone/sandstone is exposed north of Teslin Mountain and is up to 100 m thick. The same thin-bedded, laminated mudstone lithology is exposed along steeply dipping beds south of Long Lake (Fig. 7a,b). This lithology contains less than 1% disseminated pyrite. Coarse, matrix-supported, angular volcanic conglomerate consisting of volcanic clasts and dark brown, very fine mudstone clasts in a sandstone-rich matrix, contains thick interbeds of laminated sandstone. Brown-grey weathering, calcareous sandstone to pebble conglomerate are found immediately north of the contact with Joe Mountain Formation basalt at Teslin Mountain, and contains rounded to subangular clasts of limestone, shell fragments, and fine-grained, dark grey, aphyric or plagioclase-phyric volcanic rock. North of Teslin Mountain, this sequence is deformed, as indicated by frequent changes of strike and dip, interpreted as successive, parallel east-trending folds (Figs. 6).

A similar unit is also described south of Joe Mountain, as a "chaotic assemblage of recessive-weathering, volcanogenic sandstone-siltstone, shale and gritty sandstone, [which] includes limestone or limy beds, and resistant, dark-weathering, chaotic and massive to poorly bedded, heterolithic, diamictite, conglomerate and fragmental or gritty sedimentary rocks" (Hart and Hunt, 2003a). At Joe Mountain, this unit is interbedded between two distinct units of pillowed basalt (Hart, 1997a), so there is an older episode of mafic volcanism that either did not extend as far as Teslin Mountain, or is not exposed there.

Gabbro and diorite (mTJMg***)***

Dark-weathering, massive, variably textured, coarse-grained and locally pegmatitic, pyroxene gabbro and diorite (Fig. 7c) underlies the highest peaks of Joe Mountain and Mount Byng, where the Joe Mountain Formation was originally defined (Hart, 1997a). This unit underlies and intrudes microdiorite and basalt flows that form the bulk of the formation (Hart, 1997a). It represents subvolcanic intrusions exposed by erosion, and likely corresponds to the remnant of former volcanic centres.

Coherent basalt (mTJMb***)***

The dominant lithology of the Joe Mountain Formation comprises dark grey, grey-green aphyric to microcrystalline coherent basalt and basaltic andesite exposed throughout the area between Joe Mountain, Mount Byng and Teslin Mountain (Fig. 6). Coherent mafic rocks overlie thin-bedded clastic strata exposed north of Teslin Mountain, and are overlain by volcaniclastic strata along the western ridge of Teslin Mountain. The Laurier Creek fault marks the western boundary of the Joe Mountain Formation basalt (Fig. 6). East of this boundary, the contact between Joe Mountain Formation basalt and the overlying Lewes River Group carbonate sequence is folded (see Chapter 5), and is likely a stratigraphic disconformity. Joe Mountain Formation basalt is intruded by several plutons, including monzonite and monzodiorite of the mid-Cretaceous Laurier Creek pluton (EKgT) and granodiorite of the Late Cretaceous Teslin Mountain pluton (LKgR; Fig. 6).

Coherent mafic strata of the Joe Mountain Formation include grey to rusty-brown weathering, dark grey-green, fine to medium-crystalline, locally finely amygdaloidal or vesicular aphyric basalt and basaltic andesite forming thick-bedded (up to 2 m), blocky, massive (Fig. 7d) to pillowed flows (Fig. 7e). The basalt is locally plagioclase-phyric (up to 5%), or displays minor pyroxene cumulates. Locally, layers of volcanic breccia and volcaniclastic sandstone are found interbedded with the basalt. Petrographic observations show that microcrystalline basalt with a groundmass

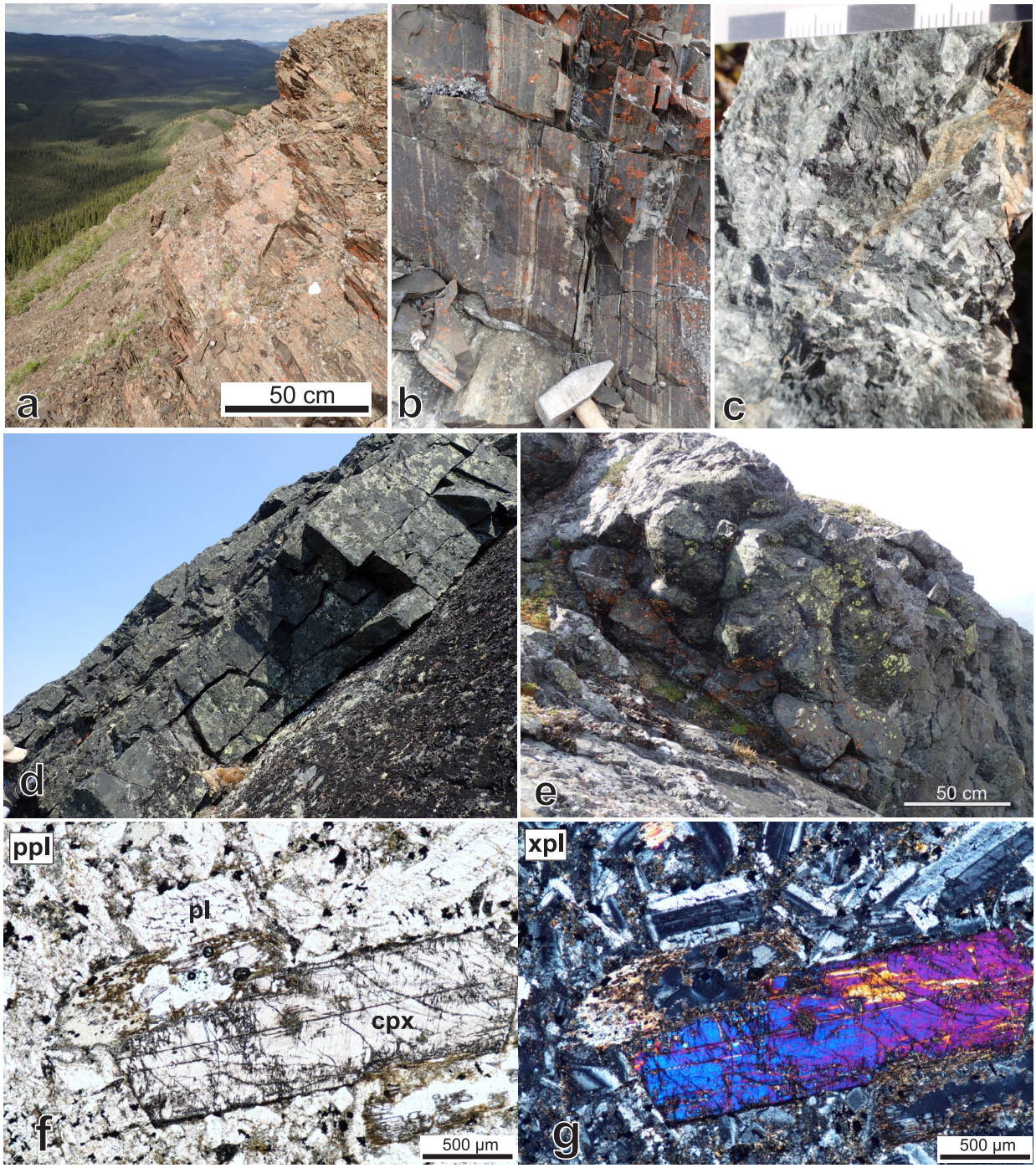

Figure 7. *Coherent units of the Joe Mountain Formation.* ***(a)*** *northeast-dipping, finely laminated mudstone and sandstone;* ***(b)*** *steeply-dipping mudstone-sandstone sequence;* ***(c)*** *grey weathering, dark green coarse-grained pyroxene gabbro forming the intrusive core of Joe Mountain;* ***(d)*** *flow-banded basalt;* ***(e)*** *pillowed aphyric basalt; and* ***(f,g)*** *photomicrographs illustrating the texture and mineralogy of the coherent basalt: clinopyroxene (cpx) phenocryst in an equigranular plagioclase-rich (pl) groundmass (ppl = plain polarized light; xpl = cross-polarized light).*

composed of interlocked equigranular plagioclase crystals dominate around Joe Mountain. At Teslin Mountain, augite phenocrysts or agglomerates are found within an equigranular groundmass of interlocked, fine to medium-grained plagioclase crystals (Fig. 7 f,g). Locally altered crystals of orthopyroxene and clinopyroxene were identified, as well as minor olivine. Chlorite is the main alteration phase (up to 30%), accompanied by lesser carbonate, epidote or actinolite alteration, which mask original textures and crystal habits.

The unit is magnetite-rich, and the highest magnetic susceptibility values are measured in layers and clasts of hematite-magnetite iron formation. In fact, up to 9 occurrences of brick-red, hematite-rich iron formation (Piercey, 2005) are reported near Joe Mountain and Teslin Mountain, in the form of layers of hematite-magnetite within a coherent basalt sequence, or as clasts of hematite-magnetite within the volcaniclastic unit mTJMvc (Fig. 8 a,b; Piercey, 2005). These occurrences are bright red, banded, highly silicified hematite-magnetite rich basaltic rocks, veins or clasts. Each occurrence has a small spatial footprint (no more than 5 by 5 m). This style of mineralization is interpreted as *in situ* metal concentrations forming in the vicinity of black-smokers, in a basaltic submarine environment. These occurrences are clearly syngenetic and Middle Triassic, and could indicate some VMS potential within the Joe Mountain Formation (Piercey, 2005; Chapter 6).

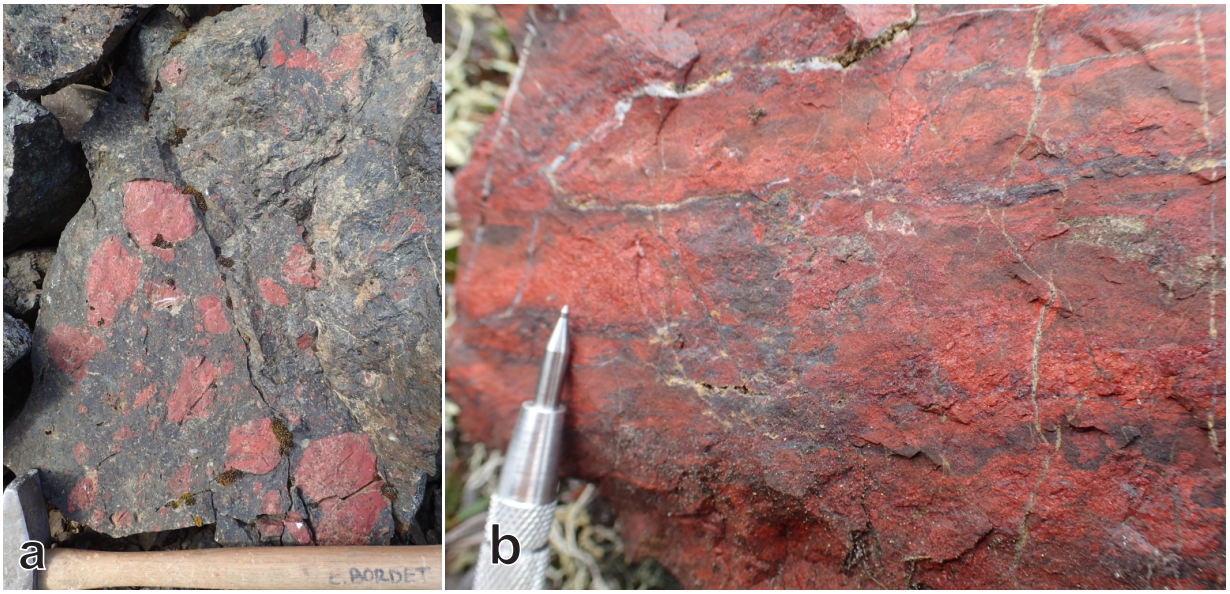

Figure 8. *Iron formation within the Joe Mountain Formation basalt at Teslin Mountain.* ***(a)*** *Iron formation clasts within volcaniclastic rocks; and* ***(b)*** *coherent pillowed basalt entirely hematite-altered.*

*Mafic tuff and volcanic breccia (*mTJMvc*)*

To the west and north of Teslin Mountain, an ~100 m thick volcaniclastic sequence includes poorly sorted volcanic conglomerate, volcanic sandstone, and mafic tuff interbedded with minor lenses of calcareous mudstone/sandstone (Fig. 6). This unit overlies the Joe Mountain Formation basalt. Thick-bedded, polymictic, chaotic volcaniclastic conglomerate displays boulder-size clasts (30–50 cm) of quartz-plagioclase-phyric diorite, cherty, glassy, basaltic ash tuff, dark green, finely crystalline basalt, and blocks of brick-red oxidized iron formation (Piercey, 2005). The conglomerate is interbedded with orange-brown-grey to tan weathering, pale grey-green, and medium-bedded volcaniclastic sandstone, with angular, dark basalt clasts (2%), and quartz eyes (up to 3%) in a pale grey-green very fine matrix (Fig. 9a). North of Teslin Mountain, this unit is dominated by south-dipping, pale green weathering, dark green to grey, silicified, laminated,

mafic ash tuff (Fig. 9b). Mafic ash tuff is interbedded with lenses of pale grey weathered, thin-bedded calcareous mudstone and sandstone. A reaction rind surrounds the limestone lenses at the contact with the mafic tuff north of Teslin Mountain, suggesting that limestone was incorporated as the tuff was still hot. The chaotic organization of the volcanic conglomerate and dominant volcanic clast composition indicate that only a minimum amount of reworking took place. Disseminated pyrite is observed locally.

Petrographic observations of the quartz-phyric volcaniclastic sandstone exposed at Teslin Mountain indicate a relatively equigranular, fine-grained texture (Fig. 9c). Subangular quartz crystals are intact, the rest of the rock comprises a groundmass completely recrystallized into fine microcrystalline quartz, and extremely altered olivine or pyroxene fragments. Possible fiammae are observed, which may correspond to compacted and elongated volcanic glass (Fig. 9c). The laminated mafic tuff displays a fine-grained texture and is dominated by isotropic ash material, with minor subangular quartz microcrysts (Fig. 9d). It is pervasively carbonate altered and displays parallel elongated fractures that may be the result of devitrification (Fig. 9d).

Volcanic breccia and conglomerate (mTJMbx***)***

A newly defined unit of volcanic conglomerate/breccia, locally interbedded with coherent pillowed to flow-banded basalt and mafic volcanic sandstone/mudstone covers an area ~12 by 4 km on the high alpine ridges between Teslin Mountain and Long Lake (Fig. 6). This sequence is dominated by thick-bedded (1–5 m), orange-brown-grey weathering, dark green, matrix-supported volcanic breccia and conglomerate (Fig. 9 e,f). Clasts are subangular to subrounded, range from lapilli to block size, and are poorly sorted. Clast composition is volcanic, but displays textural variability or various degrees of oxidation. Clasts include red oxidized pyroxene or plagioclase-phyric basalt/andesite, vesicular to massive andesite, and lapilli-size angular fragments of grey, grey-green to red aphanitic volcanic rock. The conglomerate matrix is a fine-grained, grey to green volcaniclastic sandstone, with ash to lapilli size fragments and disseminated plagioclase and pyroxene crystals. Fragmental rocks are locally interbedded with coherent pillowed to flow-banded basalt and mafic volcanic sandstone/mudstone. Frequent changes of dip, and a generally consistent east-west bedding strike suggest that this unit is deformed by east-trending folds similar to those affecting the underlying sedimentary sequence (Figs. 6).

Because of similarities to volcaniclastic conglomerate of the Lewes River Group, this unit was originally inferred to be Late Triassic (Bordet, 2016, 2017). However, stratigraphic ties imply that this unit is more likely to represent a volcaniclastic facies of the Joe Mountain Formation (Bordet, 2018, 2019).

Lewes River Group (Upper Triassic)

The Upper Triassic Lewes River Group is exposed along a north-northwest trending belt between Laurier Creek fault and the eastern shore of Lake Laberge (Fig. 6). A basal mafic volcanic sequence (~1000 m thick) is overlain by a laterally variable succession of carbonate and clastic sedimentary rocks (~1000–1500 m thick). Nine map units comprising clastic sedimentary, calcareous, volcaniclastic and mafic volcanic strata are defined based on lithology, stratigraphic associations and geographic distribution.

Limestone strata of the Lewes River Group overlie basalt of the Joe Mountain Formation along Laurier Creek, and volcaniclastic strata of the Joe Mountain Formation south of Long Lake and north of Teslin Mountain (Fig. 6). The contact between the Lewes River Group and the overlying Laberge Group is marked by an angular unconformity south of Long Lake (Bordet, 2019). The overall structural trend in the Upper Triassic sequence is north to north-northwest (Fig. 6).

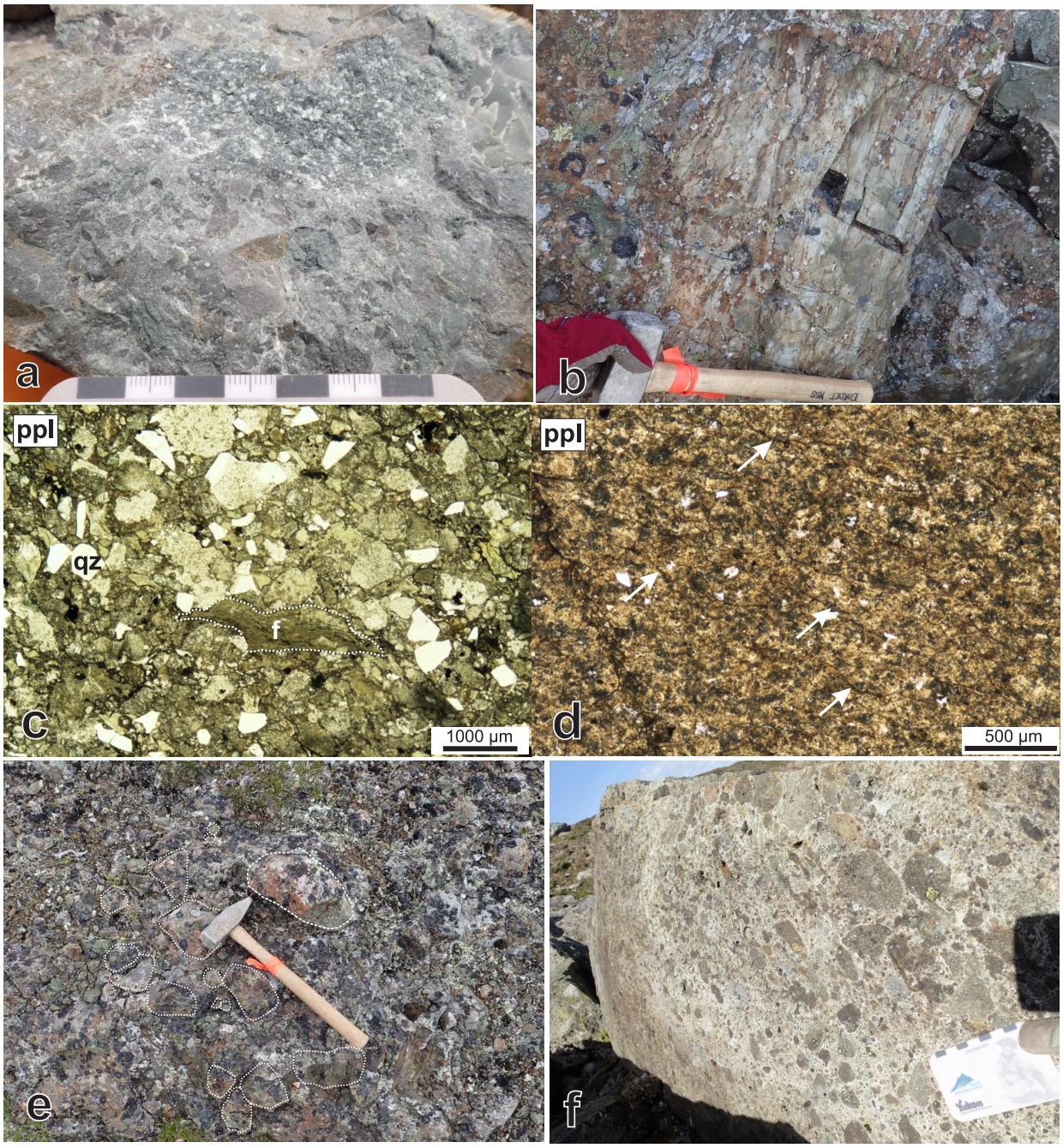

Figure 9. *Volcaniclastic units of the Joe Mountain Formation.* ***(a)*** *Angular volcanic breccia, contains clasts of plagioclase-phyric basalt-andesite, and aphyric basalt;* ***(b)*** *mafic laminated ash tuff at Teslin Mountain;* ***(c)*** *photomicrograph (plain polarized light) of quartz-phyric volcaniclastic sandstone: subangular quartz grains (intact or recrystallized; qz), possible fiammae (f; dashed white outline), mafic crystal fragments and opaque volcanic glass fragments form the sandstone matrix;* ***(d)*** *photomicrograph (plain polarized light) of a mafic ash tuff: isotropic, fine-grained ash, less than 1% very fine quartz crystals, pervasive carbonate alteration; fine dark brown fractures possibly represent compaction/devitrification features (indicated by white arrows);* ***(e)*** *partially reworked volcanic breccia: clasts of coherent basalt and volcaniclastic rocks shown by dashed outline; and* ***(f)*** *volcanic breccia northwest of Teslin Mountain.*

The total thickness of the group is >3000 m based on field estimates. Previous thickness estimates for the Lewes River Group range from 2100 m (Tozer, 1958) to greater than 3000 m (Hart, 1997a).

Povoas formation

The Povoas formation is the basal volcanic sequence of the Lewes River Group. It is exposed in the central part of the map area, along a north-trending belt extending more than 60 km from Mount Slim to Povoas Mountain (Fig. 6). The belt extends to the north beyond the limit of the map area past the Yukon River. It is characterized by a subdued, rolling topography, with extensive and thick tree cover in valleys and rare exposed hill tops in the Hancock Hills (Fig. 3b). The volcanic sequence is bounded to the east by the Laurier Creek fault and to the west by the Goddard fault (Fig. 6). No occurrences of the Povoas formation were observed west of the Goddard fault, except for a sliver of coherent, plagioclase-pyroxene-phyric basalt-andesite in a valley bottom that parallels the inferred trace of the Goddard fault.

Coherent basalt (uTLRb)

Between the Laurier Creek and Goddard faults, in the Hancock Hills, coherent, flow-banded and pillowed basalt dominate (Fig. 10a). The unit comprises coherent, dark green-grey to rusty brown weathering, dark green, flow-banded to pillowed aphyric to pyroxene-phyric basalt and plagioclase-phyric basalt or andesite, as well as primary volcanic breccia (Fig. 10b).

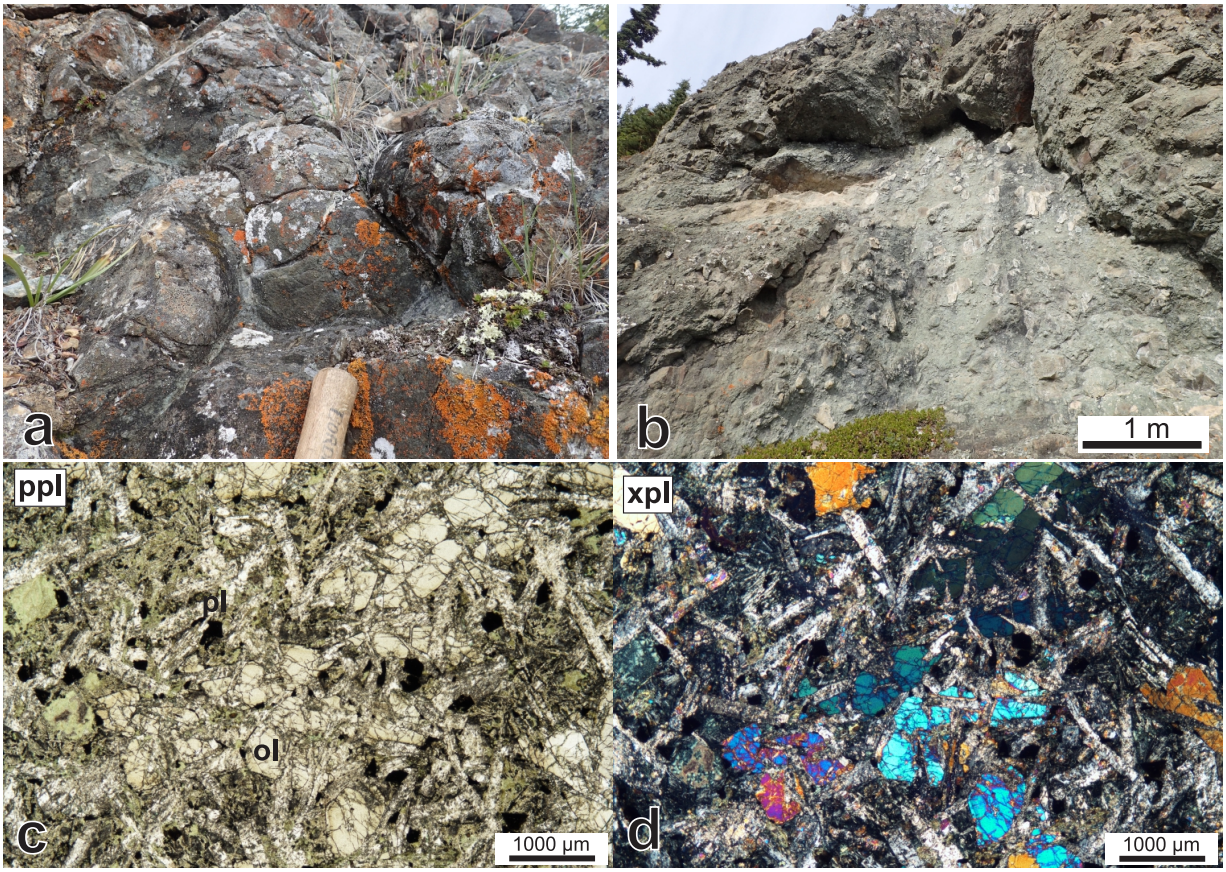

Figure 10. *Lewes River Group, Povoas formation coherent facies.* ***(a)*** *pillowed pyroxene-phyric basalt;* ***(b)*** *matrix-supported, primary volcanic breccia; and* ***(c,d)*** *photomicrograph of coherent basalt displays an intergranular texture formed by plagioclase laths (pl), interstitial space is occupied by olivine crystals (ol), pervasive chlorite and carbonate alteration (ppl = plain polarized light; xpl = cross-polarized light).*

Basalt of the Povoas formation is generally augite-phyric, although microcrystalline basalt with equigranular plagioclase microcrystals also occurs. Typically, basalt comprises very fine (<1 mm) plagioclase crystals (1–5%), small brown pyroxene crystals (1%) and minor olivine (<1%) in a finely crystalline aphyric groundmass. Amygdules, or sparse small rounded (1–2 mm) to larger irregularly shaped (1–2 cm) vesicles, are visible locally.

Most samples studied under the microscope display some level of brecciation, which is often associated with intense chloritic alteration. Petrographic observations of flow-banded to pillowed aphyric to pyroxene-phyric basalt display a porphyritic texture, with plagioclase, clinopyroxene and olivine phenocrysts in a microcrystalline, equigranular, plagioclase-rich groundmass (Fig. 10c,d). Mafic crystals are locally strongly altered to chlorite. Carbonate alteration is pervasive.

Fragmental facies (uTLRbx and uTLRvs)

Coherent basalt is interbedded with various volcanic breccia, volcaniclastic sandstone and conglomerate units (Fig. 11 a,b). A distinctive pale green, matrix-supported volcanic breccia with subrounded, pyroxene-phyric basalt blocks forms beds up to 10 to 20 m thick (Fig. 10b). At Povoas Mountain and in the Thirtymile area (Fig. 2), angular volcanic breccia and volcaniclastic sandstone dominate (Fig. 11c). Brown weathering, red-green, matrix-supported volcanic breccia contains angular, dark green clasts of microcrystalline basalt, in a dark brown, fine-grained plagioclase-rich groundmass (Fig. 11d).

Samples of matrix-supported volcanic breccia display a relatively homogeneous clast composition, as seen under the microscope. Typical clasts include plagioclase-clinopyroxene-phyric basalt with finely crystalline pyroxene-rich groundmass, and carbonate-filled vesicles (Fig. 11c). Petrographic observations of volcaniclastic sandstone units indicate equigranular, fine-grained crystal tuff comprising plagioclase, altered pyroxene crystals, as well as clasts of very finely crystalline plagioclase-phyric basalt and volcanic glass (Fig. 11d). Commonly, pervasive carbonate alteration masks the original mineralogy but preserves primary igneous textures. Plagioclase crystals are locally altered to sericite.

Aksala formation

The region between the Hancock Hills and the eastern shore of Lake Laberge is underlain by a succession of deformed sedimentary rocks overlying the basal mafic volcanic sequence, and referred to as the Aksala formation (Tempelman-Kluit, 1984, 2009). In particular, north to northwest-trending ridges of pale grey weathering, micritic limestone constitute visibly prominent stratigraphic marker beds (Fig. 3a) and outline structural features. Detailed mapping in 2016 and 2017 allowed the breakdown of a single carbonate sedimentary unit of the Lewes River Group (Hancock member of Tempelman-Kluit, 1984) into six units, distributed in two belts having distinct stratigraphy (Fig. 6; Bordet, 2019).

Eastern carbonate sequence (uTLRls, uTLRl and uTLRlms)

The eastern carbonate sequence is exposed on either side of the Lewes River Group mafic volcanic belt (Fig. 6). The stratigraphic framework includes prominent north to northwest-trending ridges of pale grey micritic limestone east of Mount Laurier, at Lime Peak, and east of Thirtymile (Figs. 6 and 12a).

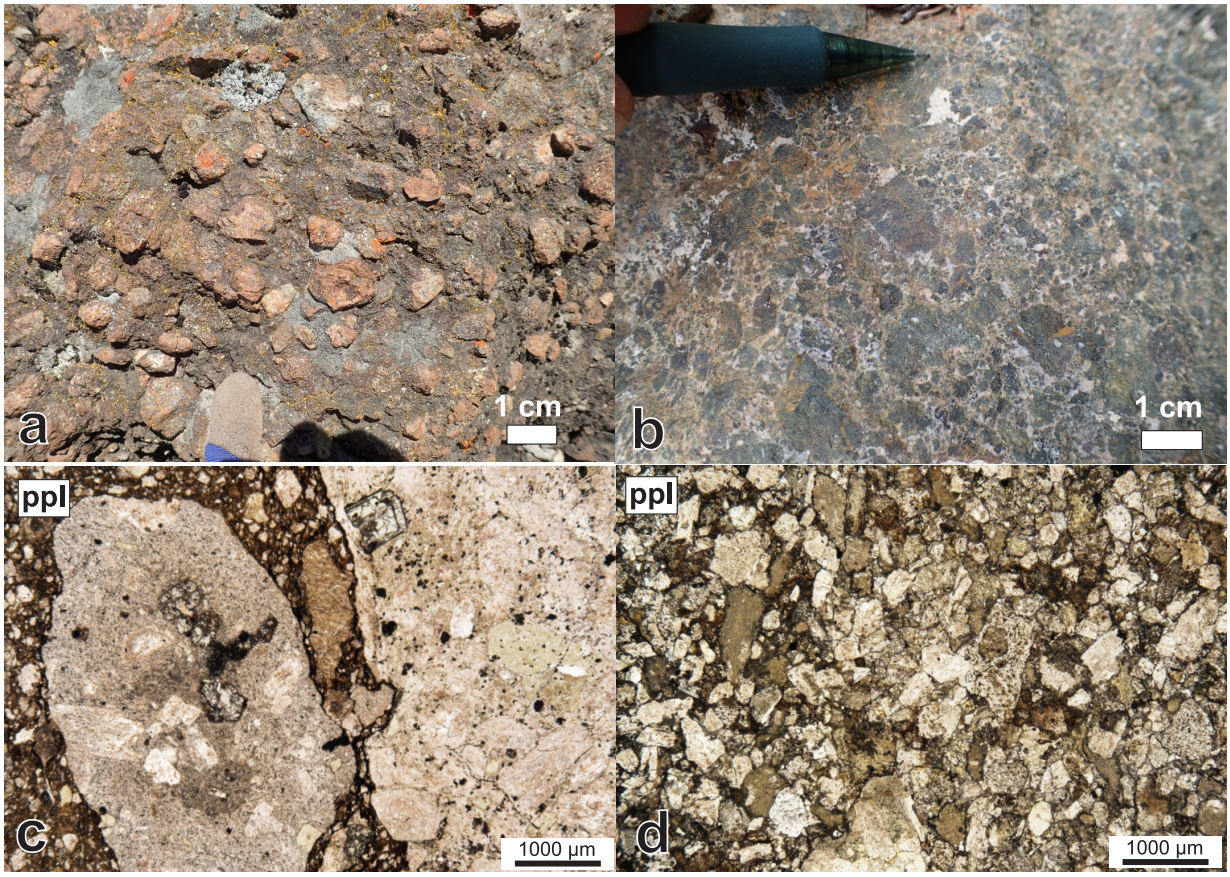

Figure 11. *Lewes River Group, Povoas formation fragmental facies;* **(a)** *matrix-supported pebble conglomerate east of Thirtymile: dark green, mafic matrix and clasts of plagioclase-phyric andesite, lime mudstone, and red-oxidized volcanic clasts;* **(b)** *pale grey-green, matrix-supported, carbonate altered volcanic breccia, clasts are granule size, angular, dark green aphyric lava;* **(c)** *photomicrograph (plain polarized light) of a volcanic breccia: clasts of volcaniclastic rocks in a very fine grained pyroxene-rich matrix; and* **(d)** *photomicrograph (plain polarized light) of a volcaniclastic sandstone: equigranular clasts and crystal fragments, grain-supported. Crystals include plagioclase and orthopyroxene, lithic fragments are very finely crystalline plagioclase-phyric basalt.*

Thin to medium-bedded calcareous mudstone and sandstone (uTLRls) are exposed along the Laurier Creek fault and overlie the Joe Mountain Formation basalt (Fig. 12b). Massive to thick-bedded, pale grey weathering, micritic and fossiliferous limestone is particularly well exposed at Lime Peak (uTLRl; Yarnell et *al.*, 1999), as well as along a north-trending belt that extends north and west of the Hancock Hills (Fig. 12a). The massive limestone generally overlies Middle and Upper Triassic volcanic rocks, or is locally interbedded with thin-bedded calcareous units (Fig. 12c). In the Hancock Hills (Fig. 2), massive limestone is locally interbedded with tan-grey weathering, clast-supported (locally matrix-supported), non-sorted, pebble to cobble calcareous conglomerate (Fig. 12d) and lenses of tan-orange weathering, fine-grained calcareous sandstone. The conglomerate comprises subrounded to subangular lime mudstone clasts in a pale yellow weathering, medium-grained calcareous sandstone matrix. Finally, east of the Yukon River at Thirtymile (Fig. 2), an east dipping sequence of argillaceous laminated mudstone and fine-grained sandstone is exposed (uTLRms; Fig. 12e). It comprises at least three levels of thick–bedded, massive micritic limestone, interbedded with intervals of medium to thin-bedded, brown weathered argillaceous mudstone and fine-grained sandstone.

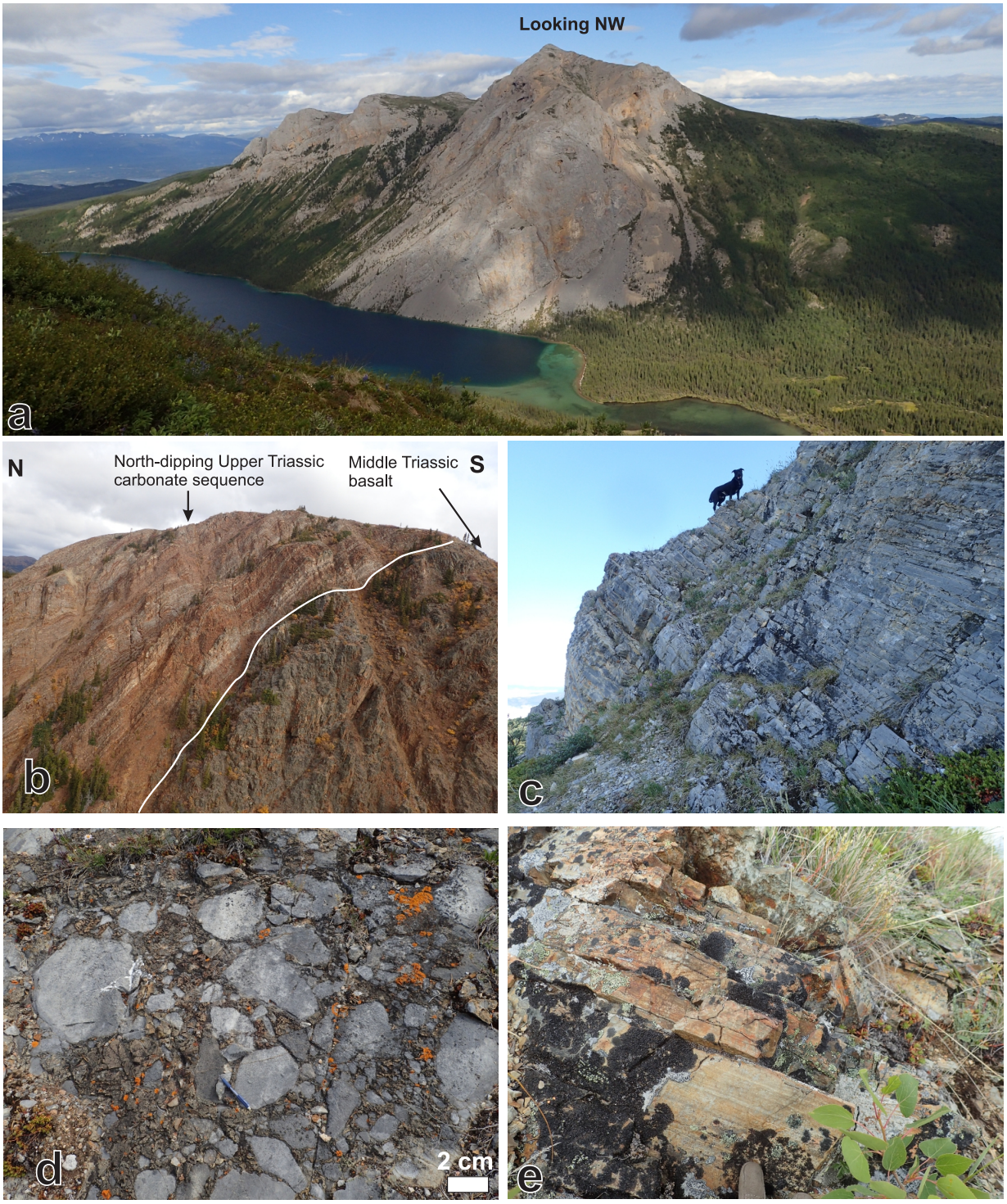

Figure 12. *Lewes River Group, eastern carbonate sequence of the Aksala formation.* **(a)** *looking northwest towards Thomas Lake (foreground) and Lime Peak. Lime Peak comprises several generations of reefal limestone attributed to unit* uTLRl; **(b)** *north-dipping sequence of medium-bedded calcareous sandstone, mudstone and conglomerate (*uTLRls*) overlying the Joe Mountain Formation basalt exposed east of Laurier Creek fault;* **(c)** *east-dipping medium to thick-bedded, pale grey limestone-mudstone. Lighter coloured intervals are very fine grained, argillaceous limestone;* **(d)** *clast-supported calcareous conglomerate of unit* uTLRlc*, comprising subrounded to subangular micritic limestone clasts in a tan to grey weathering, calcareous sandstone matrix; and* **(e)** *east-dipping thinly-bedded, laminated, non-calcareous mudstone.*

Western carbonate sequence (uTLRlf, uTLRst, uTLRul)

The western part of the map area is characterized by a distinctive carbonate sequence exposed along the eastern shore of Lake Laberge (Fig. 6). As in the rest of the map area, the stratigraphy includes prominent north to northwest-trending ridges of pale grey micritic limestone.

The following units form the core of an anticlinorium along the eastern shore of Lake Laberge (Fig. 6): a medium-bedded (30–50 cm), argillaceous, fossiliferous (bivalve or brachiopod shells, corals and burrows) wackestone (Fig. 13a); a thin-bedded, calcareous sandstone and mudstone (Fig. 13b); and a thick to medium-bedded, pale grey micritic limestone including lenses of rusty weathering, dark grey calcareous mudstone **(uTLRlf)**. These rocks are overlain by 5–10 m of brown to orange weathering, dark grey-green, non-calcareous, medium to coarse-grained sandstone with polymictic, matrix-supported granule conglomerate (Fig. 13c; **uTLRst**). A characteristic of this clastic lithology is its relatively high magnetic susceptibility (2-13 S.I. units). Overlying this sequence is a very thick bedded, pale grey to orange weathering, dark grey, finely to coarsely crystalline, micritic limestone (Fig. 13d; **uTLRul**), which is interbedded with minor bioclastic wackestone (Fig. 13e; corals, bivalve shells, brachiopods and crinoids), and minor calcareous sandstone and conglomerate.

Other units

The Sheldon Creek member is a unique unit recognized only east of Mount Byng (Hart, 1997a; Hart and Hunt, 1997b, 2003b). The original bedrock map describes "orange-weathering, resistant, light olive-green, locally pillowed and strongly silicified, andesitic and basaltic lava flows; locally with hyaloclastite and breccia that may be part of Joe Mountain Formation" (Hart and Hunt, 2003b). Hart (1997b) points out that the unit has an upper contact with massive limestone and a gradational lower contact with clastic sedimentary strata of the Lewes River Group, "although it is partly diachronous with both". The varied conglomerate beds that form the unit include rounded pebble, cobble and boulder-size clasts of volcanic, intrusive and sedimentary origin. The age of the unit is constrained to the Middle to Upper Norian by the presence of Upper Norian macrofossils within some fine-grained strata, and by the fact that stratigraphically underlying and overlying strata carry respectively Upper Carnian and Upper Norian conodonts (Hart, 1997a). Therefore, the Sheldon Creek member is interpreted here as a local variation of the Aksala formation. The deposition of these rocks likely occurred in a high energy, shallow marine environment proximal to a volcanic centre, leading to the formation of conglomerate containing clasts of both volcanic and carbonate origin.

Biostratigraphy

The carbonate sequence of the Aksala formation has been extensively sampled for microfossil and macrofossil identification since the first reconnaissance mapping programs took place in this area (Lees, 1934; Bostock and Lees, 1938; Tozer, 1958; Wheeler, 1961; Reid, 1980; Tempelman-Kluit, 1984, 2009; Hart, 1997a; Yarnell *et al.*, 1999). Results are summarized in Table 1. Appendix A includes original reports for macrofossils identification by R.B. Blodgett (Appendix A1) and conodonts by M. Golding (Appendix A2) conducted as part of this study. A compilation of all fossil collections from this and previous studies is in Appendix A3.

A new macrofossil collection from the Aksala formation includes specimens of bivalve and brachiopod shells (Fig. 14a,b), gastropods (Fig. 14c), scleractinian corals (Fig. 14d), columnal crinoid ossicles (Fig. 14e), and various sponge and other biotic debris (Table 1). Diagnostic fauna assemblages support a Late Triassic age, with some specimens restricted to the late Middle

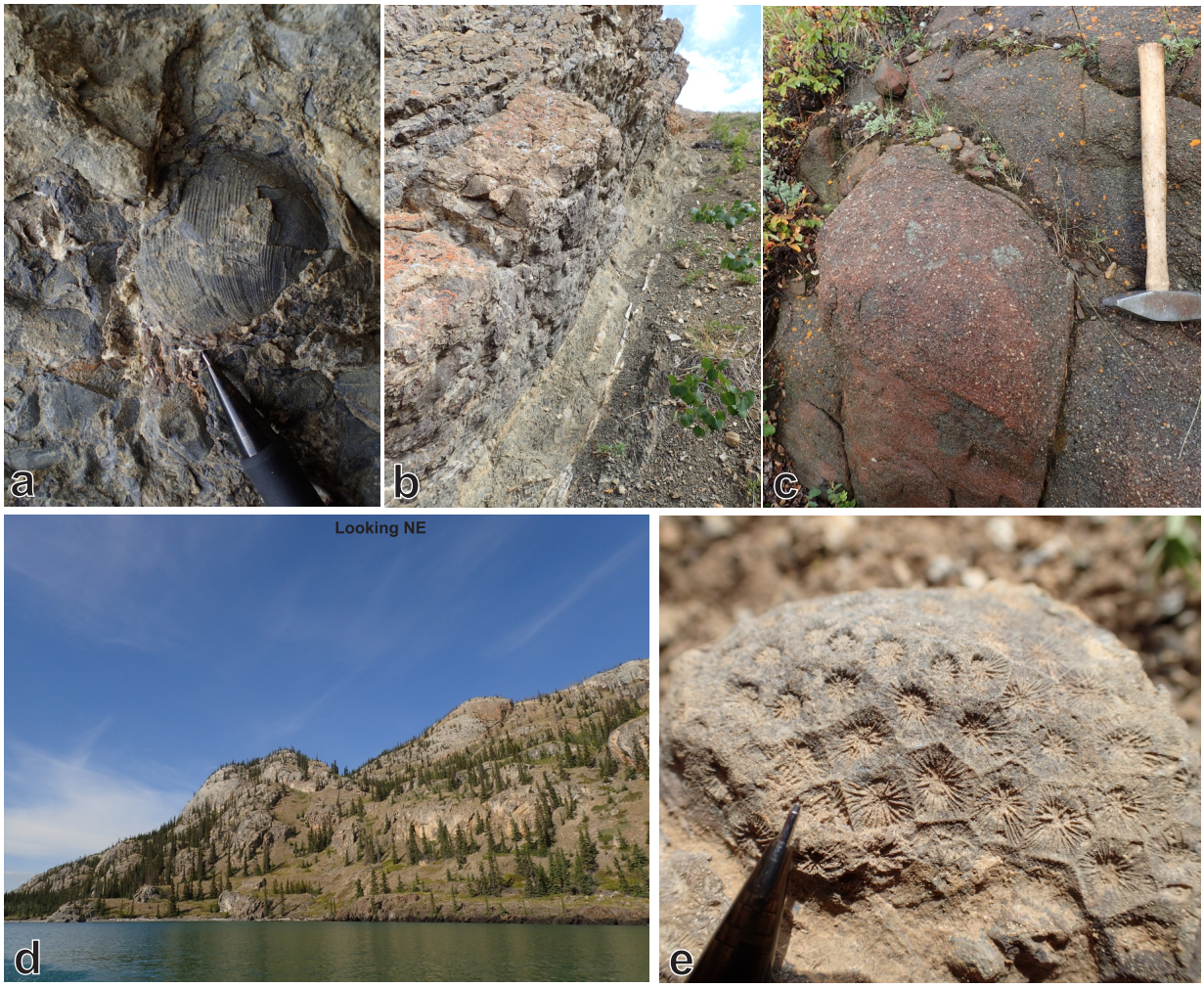

Figure 13. *Lewes River Group, western carbonate sequence of the Aksala formation.* **(a)** *shell fossil (bivalve or brachiopod) in calcareous mudstone wackestone (part of unit* uTLRlf*);* **(b)** *fossiliferous, medium-bedded calcareous mudstone of unit* uTLRlf; **(c)** *brown-weathering, non-calcareous, medium-grained sandstone and granule conglomerate of unit* uTLRst*; this sequence is about 5-10 m thick and underlies unit* uTLRul; **(d)** *thick-bedded micritic limestone beds (*uTLRul*) form a north-trending ridge along the east shore of Lake Laberge (lake in the foreground); and* **(e)** *scleractinian coral fossil from a fossiliferous interval of unit* uTLRul.

Norian (bivalves Halobia and Monotis, Table 1; Appendix A1). Environments of deposition are interpreted as shallow marine (inner platform or shelf) to open marine, with normal salinity and a tropical climate (Appendix A1 and Table 1).

Conodonts are sparse and often not preserved in carbonate rocks of the Lewes River Group. Of the 30 samples submitted, only 5 were conodont-bearing, and only 3 contained faunal assemblages that led to a constrained age (Appendix A2). In particular, identified specimens of *Mockina cf. englandi* (Orchard, 1991) restrict the age of deposition to the Norian–Rhaetian (Appendix A2). Overall, conodont identification supports a Late Triassic age for the Aksala formation.

Table 1. *Summary of new macrofossil collections from this study. Fossil identification, age interpretation and environment discussion after Blodgett (2016).*

Sample number	Host lithology	Host group/ formation	Estimated Age	Fossil content	Age	Environment
15EB-514-1	Bedded "fetid" mudstone limestone	Lewes River Group	Late Triassic	columnal crinoid ossicles; bivalve shells; undetermined solitary scleractinian corals	indeterminate, inferred Late Triassic	shallow water, shelfal depths
16EB-082-1	massive mudstone limestone to bioclastic limestone, fetid	Lewes River Group	Late Triassic	recrystallized biotics; possible sponge and crinoid ossicles	indeterminate, inferred Late Triassic	
16EB-101-1	Calcareous conglomerate, clast supported, polymictic	Lewes River Group	Late Triassic	rare to abundant small crinoid ossicles	uncertain, post-Cambrian	normal marine salinity, high energy environment with clasts from surrounding country rock
16EB-116-1	mudstone limestone, bioclastic, fetid	Lewes River Group	Late Triassic	crinoid ossicles; sponge; biotic debris	indeterminate, inferred Late Triassic	normal marine salinity
16EB-128-2	massive mudstone limestone	Lewes River Group	Late Triassic	disarticulated shells (bivalves or brachiopods); recrystallized scleractinian corals (*Retiophyllia*?); recrystallized calcareous sponge; crinoid ossicles; undetermined medium-sized, high-spired gastropods	Late Triassic	shallow water, open-marine
16EB-142-1	calcareous boulder conglomerate	Lewes River Group	Late Triassic	crinoid ossicles; undetermined solitary scleractinian corals; possible hydrozoan	Late Triassic	shallow water, carbonate platform
16EB-173-1	limestone, massive, bioclastic	Lewes River Group	Late Triassic	stromatactis-like structures	indeterminate	
16EB-284-1	light brownish-gray limestone mudstone to wackestone	Lewes River Group	Late Triassic	crinoid ossicles; bivalve shells	indeterminate, inferred Late Triassic	very shallow water, open-marine
16EB-287-1	medium to thick bedded musdtone limestone displays fossil traces and bioturbations	Lewes River Group	Late Triassic	recrystallized sponge; crinoid ossicles; fine-ribbed and disarticulated bivalves; *Lepismatina* (spiriferid brachiopod)	Middle to Late Triassic	shallow water, open marine (shelfal)
16EB-388-1	massive grey limestone, bioclastic	Lewes River Group	Late Triassic	large fasciculate coral; indeterminate solitary scleractinian corals; indeterminate ribbed bivalve fragments; small smooth ostracodes; crinoid ossicles	indeterminate, inferred Late Triassic	very shallow water, inner platform
16EB-433-2	limestone bed containing shells, bivalves	Lewes River Group	Late Triassic	ribbed bivalves: *Monotis*, *Halobia*, *Cassianella*; Gastropods: *Coelostyliolina*, *Zygopleura* (*Anoptychia*); crinoid ossicles (including *Pentacrinus*)	late middle Norian (Columbianus Zone)	normal marine salinity
16EB-457-1	limestone packstone	Lewes River Group	Late Triassic	colonial scleractinian corals: *Eocomoseris ramosa*, *Gablonzeria profunda*	Late Triassic (undifferentiated)	tropical water Tethyan

Table 1. *continued.*

Sample number	Host Lithology	Host group/ formation	Estimated age	Fossil content	Age	Environment
16EB-460-1	bioclastic wackstone	Lewes River Group	Late Triassic	rare crinoid ossicles; indeterminate small bivalves; indeterminate biotic debris; scleractinian coral with small corallites (*Distichomeandra*?); recrystallized coralline or sponge-like object; high-spired gastropods; stromatactis structures	Late Triassic	moderately open-marine
16EB-547-1	medium bedded limestone	Lewes River Group	Late Triassic	fine-ribbed bivalves; smooth brachiopod valves (terebratulids); Otapira (bivalve, one specimen); lesser gastropods and crinoid ossicles; indeterminate coral fragment	inferred Late Triassic	open-marine (normal salinity), in shelfal depths
16EB-600-1	fossil rich, red orange weathering, calcareous mudstone. bioclastic wackstone, clasts of shells and other fossils	Lewes River Group	Late Triassic	indeterminate ribbed spiriferid brachiopod fragment; smooth terebratulid brachiopod (*Coenothyris*); crinoid columnals	Late Triassic	shallow water, open marine conditions
16EB-477-1	dark gray (fresh and weathered), silty, limy argillite, weakly laminated	Laberge Group	Early Jurassic	rare bivalve shells; crinoid ossicle	indeterminate	quiet-water, offshore bio and lithofacies
16EB-539-1	macrofossil bearing sandstone	Laberge Group	Early Jurassic	common broken plant debris (carbonized)	none inferred	probably non-marine

U/Pb geochronology

U/Pb geochronology was conducted on Triassic volcanic rocks to further refine the age of volcanism for the Joe Mountain Formation, and provide age controls on the internal stratigraphy of the Lewes River Group. Triassic fossils were previously identified in both sequences (Hart, 1997a; Appendix A3). For instance, Ladinian conodonts were extracted from limestone lenses interbedded with mafic volcanic rocks of the Joe Mountain Formation (Hart, 1997a). In contrast, the Aksala formation contains a number of macrofossil and microfossil collections mostly ascribed to the Norian.

Triassic microcrystalline basalt and mafic volcaniclastic rocks typically lack crystals that can be dated by radiometric methods. Coarse-grained volcaniclastic sandstone and volcaniclastic tuffs were sampled to maximize detrital zircon yields, but the overall success rate was low (only 4 zircon bearing samples out of 13 samples processed). As a result, only one igneous age was obtained from the Joe Mountain Formation mafic sequence near Teslin Mountain, and three detrital zircon ages were obtained from clastic strata of the Aksala formation. Attempts at dating the Povoas formation were not successful. Geochronology results are summarized in Table 2. Complete data tables are in Appendix B (LA-ICPMS results: B1; CA-TIMS results: B2), and results of cathodoluminescence imaging are in Appendix B3. A compilation of all radiometric ages from this and previous studies is in Appendix B4.

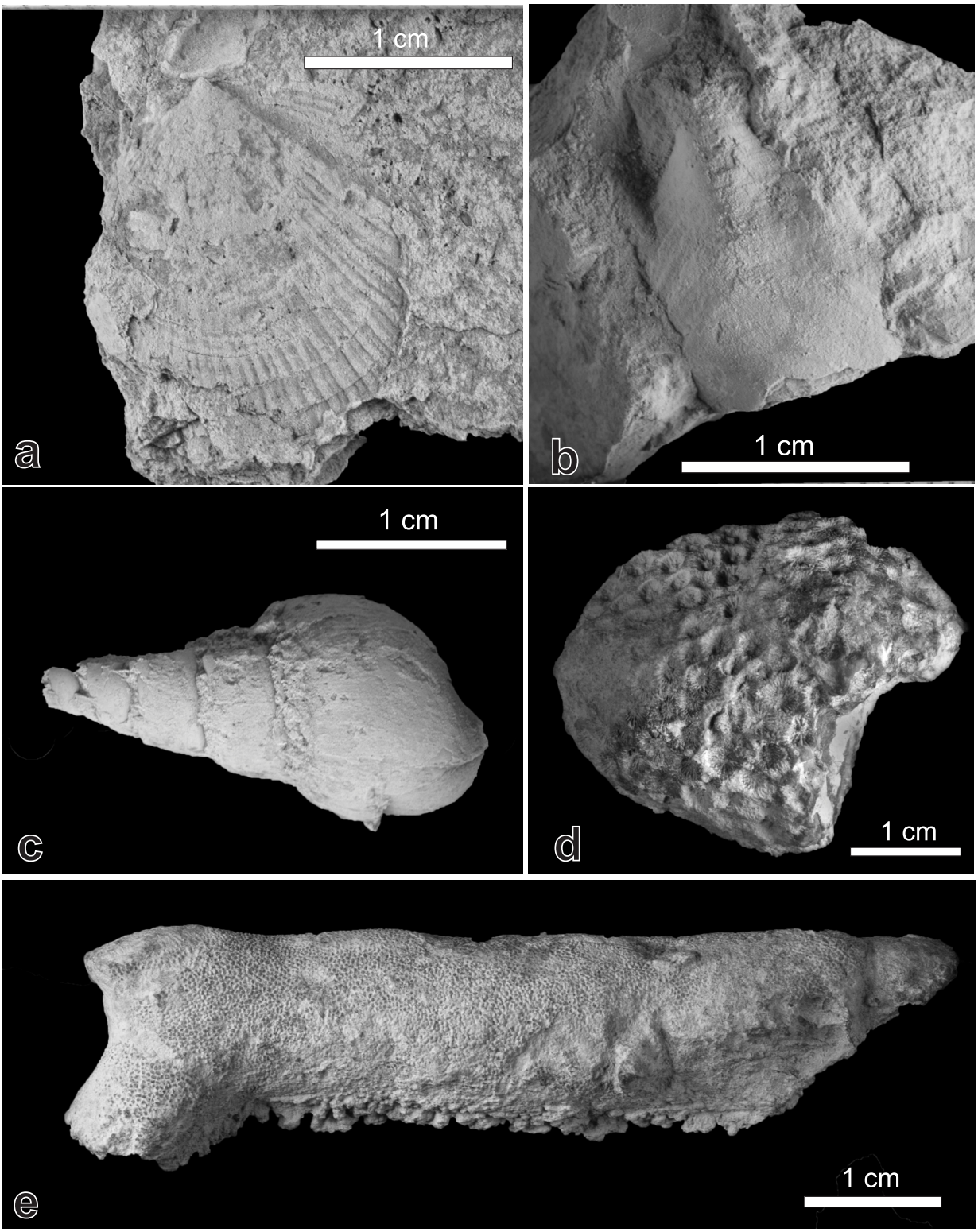

Figure 14. *Selected macrofossils collections from the Aksala formation. All photographs by R.B. Blodgett.* ***(a)*** *chlamys in sample 16EB-433-2;* ***(b)*** *plicate terebratulid in sample 16EB-460-1;* ***(c)*** *Zygopleura (Anoptychia) in sample 16EB-433-2;* ***(d)*** *colonial scleratinian coral in sample 16EB-457-1; and* ***(e)*** *Eocomersis ramosa in sample 16EB-457-1.*

Table 2. *Summary of U/Pb LA-ICPMS (LA) and CA-TIMS (TIMS) dates. Results are organized in chronological order, and grouped by unit, formation or group. White background indicates igneous crystallization ages, grey background indicates detrital zircon maximum depositional ages.*

Sample	Latitude	Longitude	Mineral	Method	Year	Rock Type	Location	Age	Error	Period/Epoch	Interpretation	Interpretation Unit
Cretaceous magmatic rocks												
15EB-109-1	61.0459	-134.5938	zircon	**TIMS**	2015	Granodiorite	Teslin Mountain	**78.14**	**0.03**	**Late Cretaceous (Campanian)**	**Crystallization age**	**Teslin Mnt pluton (Rancheria suite)**
17EB-016-1	61.1164	-134.5563	zircon	**TIMS**	2017	Crystal lithic lapilli tuff	north of Teslin Mountain, west of Open Creek	**79.05**	**0.03**	**Late Cretaceous (Campanian)**	**Crystallization age**	**Open Creek volcanic complex**
17EB-031-1	61.1276	-134.6048	zircon	**TIMS**	2017	Block and ash flow (matrix)	north of Teslin Mountain, west of Open Creek	**79.44**	**0.03**	**Late Cretaceous (Campanian)**	**Crystallization age**	**Open Creek volcanic complex**
16EB-267-1	61.2021	-135.1650	zircon	**LA + TIMS**	2016	Microcrystalline gabbro dike	East shore Lake Laberge	**105.91**	**0.04**	**Early-Mid Cretaceous (Albian)**	**Crystallization age**	**Whitehorse suite**
17EB-163-2	61.4224	-135.0989	zircon	**LA + TIMS**	2017	Intermediate dike	Thirtymile	**111.08**	**0.06**	**Lower Cretaceous (Aptian)**	**Crystallization age**	**Whitehorse suite**
17EB-177-1	61.3671	-135.1853	zircon	**LA + TIMS**	2017	Porphyritic diorite dike	west of Povoas Mountain	**113.94**	**0.04**	**Lower Cretaceous (Aptian)**	**Crystallization age**	**Teslin suite**
16EB-001-1	61.0233	-134.8040	zircon	**TIMS**	2016	Monzodiorite	East of Mount Laurier	**115.54**	**0.03**	**Lower Cretaceous (Aptian)**	**Crystallization age**	**Laurier Creek pluton (Teslin suite)**
15EB-222-1	61.1133	-134.7376	zircon	**TIMS**	2017	Quartz phyric rhyolite dike	south of Long Lake, intruding Laberge Group	**135.79**	**0.04**	**Early Cretaceous**	**Crystallization age**	**Goddard suite**
16EB-384-2	61.2106	-135.0755	zircon	**LA + TIMS**	2016	Diorite dike	East shore Lake Laberge	**138.06**	**0.04**	**Early Cretaceous**	**Crystallization age**	**Goddard suite**
Laberge Group												
16EB-181-1	61.0994	-135.0577	zircon	**LA + TIMS**	2016	Plag-quartz phyric sandstone	East shore Lake Laberge	**≤ 186.22**	**0.09**	**≤ Lower Jurassic (Sinemurian)**	**Maximum depositional age**	**Laberge Group**
16EB-384-1	61.2106	-135.0755	zircon	**LA + TIMS**	2016	Calcareous sandstone	East shore Lake Laberge	**≤ 186.38**	**0.07**	**≤ Lower Jurassic (Sinemurian)**	**Maximum depositional age**	**Laberge Group**
16EB-394-1	61.2503	-135.1888	zircon	**LA + TIMS**	2016	Sandstone to granule conglomerate	East shore Lake Laberge	**≤ 199.78**	**0.06**	**≤ Lower Jurassic (Hettangian)**	**Maximum depositional age**	**Laberge Group**
15EB-304-1	61.1042	-134.7580	zircon	**LA + TIMS**	2015	Conglomerate	south of Long Lake	**≤ 202.4**	**1.5**	**≤ Upper Triassic or younger (Rhaetian)**	**Maximum depositional age**	**Laberge Group (basal)**
16EB-257-1	61.1909	-135.1328	zircon	**LA + TIMS**	2016	Calcareous sandstone	East shore Lake Laberge	**≤ 203.46**	**0.14**	**≤ Upper Triassic or younger (Rhaetian)**	**Maximum depositional age**	**Laberge Group (basal)**

Table 2. *continued.*

Sample	Latitude	Longitude	Mineral	Method	Year	Rock Type	Location	Age	Error	Period/Epoch	Interpretation	Interpretation Unit
Lewes River Group												
16EB-421-1	61.2439	-135.1910	zircon	LA + TIMS	2016	Granule conglomerate	East shore Lake Laberge	≤ 212.3	0.14	≤ Upper Triassic (Norian)	Maximum depositional age	Aksala formation
17EB-225-1	61.3364	-135.2227	zircon	LA + TIMS	2017	Sandstone	east of Lake Laberge, west of Goddard fault	≤ 211.33	0.1	≤ Upper Triassic (Norian)	Maximum depositional age	Aksala formation
16EB-042-1	61.0346	-134.8245	zircon	LA	2016	Sandstone	East of Mount Laurier	≤ 230 Ma 117 Ma metam		≤ Upper Triassic (Carnian)	Maximum depositional age	Aksala formation, contact metamorphism Teslin Suite
17EB-900-1	61.0842	-134.7772	Zr	TIMS	2017	Andesite clast in volcanic conglomerate	ridge northwest of Teslin Mountain, east of Laurier Creek fault					
Joe Mountain Formation												
15EB-124-1	61.0501	-134.6147	zircon	LA + TIMS	2015	Volcanic sandstone	Teslin Mountain	244.74	0.09	Middle Triassic (Anisian)	Crystallization age	Joe Mountain Formation

Methods

Radiometric analyses were conducted by J.L. Crowley at Boise State University. The workflow for igneous samples involves separation of zircons followed by cathodoluminescence imaging. If zircon grains are homogeneous and do not present any inherited core, they are analyzed directly using the CA-TIMS method. If cathodoluminescence imaging indicates that there may be mixed zircon populations in the rock as a result of inheritance or contamination, zircons are first analyzed with LA-ICPMS. Then the youngest igneous zircons are selected and analyzed by CA-TIMS to obtain a crystallization age.

A similar process is applied to detrital samples. The maximum number of zircons obtained through separation will be dated by LA-ICPMS in order to generate a profile of the zircon populations that can be interpreted later in terms of source and basin evolution. If the youngest zircons identified are in sufficient number and of good quality (large enough, without core), they will be further tested by CA-TIMS to provide a more precise maximum age of deposition.

Laser Ablation Inductively Coupled Plasma Mass Spectrometry (LA-ICPMS)

Zircon grains were separated from rocks using standard techniques, annealed at 900°C for 60 hours in a muffle furnace, and mounted in epoxy and polished until their centres were exposed. Cathodoluminescence (CL) images were obtained using a JEOL JSM-1300 scanning electron microscope and Gatan MiniCL. Zircon was analyzed by laser ablation inductively coupled plasma mass spectrometry (LA-ICPMS) using a ThermoElectron X-Series II quadrupole ICPMS and New Wave Research UP-213 Nd:YAG UV (213 nm) laser ablation system. In-house analytical protocols, standard materials, and data reduction software were used for acquisition and calibration of U/Pb dates, and a suite of high field strength elements (HFSE)

and rare earth elements (REE). Zircon was ablated using a laser spot of 25 µm wide, having fluence and pulse rates of 5 J/cm^2 and 10 Hz, respectively, during a 45 second analysis (15 sec gas blank, 30 sec ablation) that excavated a pit ~25 µm deep. Ablated material was carried by a 1.2 L/min He gas stream to the nebulizer flow of the plasma. Dwell times were 5 ms for Si and Zr, 200 ms for ^{49}Ti and ^{207}Pb, 80 ms for ^{206}Pb, 40 ms for ^{202}Hg, ^{204}Pb, ^{208}Pb, ^{232}Th, and ^{238}U and 10 ms for all other HFSE and REE. Background count rates for each analyte were obtained prior to each spot analysis and subtracted from the raw count rate for each analyte. Ablations pits that have intersected glass or mineral inclusions were identified based on Ti and P. U/Pb dates from these analyses are considered valid if the U/Pb ratios appear to have been unaffected by the inclusions. Analyses that appear contaminated by common Pb were rejected based on mass 204 being above baseline. For concentration calculations, background-subtracted count rates for each analyte were internally normalized to ^{29}Si and calibrated with respect to NIST SRM-610 and -612 glasses as the primary standards. Temperature was calculated from the Ti-in-zircon thermometer (Watson *et al.*, 2006). Because there are no constraints on the activity of TiO_2, an average value in crustal rocks of 0.8 was used.

Data were collected in 13 experiments conducted between June 2016 and February 2018. For U/Pb and ^{207}Pb/^{206}Pb dates, instrumental fractionation of the background-subtracted ratios was corrected and dates were calibrated with respect to interspersed measurements of zircon standards and reference materials. The primary standard Plešovice zircon (Sláma *et al.*, 2008) was used to monitor time-dependent instrumental fractionation based on two analyses for every 10 analyses of unknown zircon. A secondary correction to the ^{206}Pb/^{238}U dates was made based on results from the zircon standards Seiland (530 Ma, *unpublished data*, Boise State University) and Zirconia (327 Ma, *unpublished data*, Boise State University), which were treated as unknowns and measured once for every 10 analyses of unknown zircon. These results illustrate a linear age bias of several percent that is related to the ^{206}Pb count rate. The secondary correction is thought to mitigate matrix-dependent variations due to contrasting compositions and ablation characteristics between the Plešovice zircon and other standards (and unknowns).

Radiogenic isotope ratio and age error propagation for all analyses include uncertainty contributions from counting statistics and background subtraction. For groups of analyses that are collectively interpreted from a weighted mean date, a weighted mean date is first calculated using Isoplot 3.0 (Ludwig, 2003) using errors on individual dates that do not include a standard calibration uncertainty, and then a standard calibration uncertainty is propagated into the error on the weighted mean date. This uncertainty is the local standard deviation of the polynomial fit to the interspersed primary standard measurements versus time for the time-dependent U/Pb fractionation factor. These uncertainties are 1.1–1.8% (2σ) for ^{206}Pb/^{238}U. Age interpretations are based ^{206}Pb/^{238}U dates. Errors on the dates are at 2σ.

Chemical abrasion thermal ionization mass spectrometry (CA-TIMS)

U/Pb dates were obtained by the chemical abrasion isotope dilution thermal ionization mass spectrometry (CA-TIMS) method from analyses composed of single zircon grains, modified after Mattinson (2005). Zircon was separated from rocks using standard techniques, placed in quartz beakers into a muffle furnace at 900°C for 60 hours, then mounted in epoxy, and polished until the centres of the grains were exposed. Cathodoluminescence (CL) images were obtained using a JEOL JSM-1300 scanning electron microscope and Gatan MiniCL. Twelve samples were first analyzed by LA-ICPMS. Zircon was removed from the epoxy mounts for dating based on LA-ICPMS data and CL images.

Zircon was put into 3 ml Teflon PFA beakers and loaded into 300 µl Teflon PFA microcapsules. Fifteen microcapsules were placed in a large-capacity Parr vessel and the zircon partially dissolved in 120 µl of 29 M HF for 12 hours at 190°C. Zircon was returned to 3 ml Teflon PFA beakers, HF was removed, and zircon was immersed in 3.5 M HNO_3, ultrasonically cleaned for an hour, and fluxed on a hotplate at 80°C for an hour. The HNO_3 was removed and zircon was rinsed twice in ultrapure H_2O before being reloaded into the 300 µl Teflon PFA microcapsules (rinsed and fluxed in 6 M HCl during sonication and washing of the zircon) and spiked with the Boise State University mixed $2^{33}U$-^{235}U-^{205}Pb tracer solution. Zircon was dissolved in Parr vessels in 120 µl of 29 M HF with a trace of 3.5 M HNO_3 at 220°C for 48 hours, dried to fluorides, and re-dissolved in 6 M HCl at 180°C overnight. U and Pb were separated from the zircon matrix using an HCl-based anion-exchange chromatographic procedure (Krogh, 1973), eluted together and dried with 2 µl of 0.05 N H_3PO_4.

Pb and U were loaded on a single outgassed Re filament in 5 µl of a silica-gel/phosphoric acid mixture (Gerstenberger and Haase, 1997), and U and Pb isotopic measurements made on a GV Isoprobe-T multicollector thermal ionization mass spectrometer equipped with an ion-counting Daly detector. Pb isotopes were measured by peak-jumping all isotopes on the Daly detector for 100 to 160 cycles, and corrected for 0.16 ± 0.03%/a.m.u. (1σ error) mass fractionation. Transitory isobaric interferences due to high-molecular weight organics, particularly on ^{204}Pb and ^{207}Pb, disappeared within approximately 60 cycles, while ionization efficiency averaged 104 cps/pg of each Pb isotope. Linearity (to ≥1.4 x 106 cps) and the associated deadtime correction of the Daly detector were determined by analysis of NBS982. Uranium was analyzed as UO_2^+ ions in static Faraday mode on 1012 ohm resistors for 300 cycles, and corrected for isobaric interference of $^{233}U^{18}O^{16}O$ on $^{235}U^{16}O^{16}O$ with an $^{18}O/^{16}O$ of 0.00206. Ionization efficiency averaged 20 mV/ng of each U isotope. U mass fractionation was corrected using the known $^{233}U/^{235}U$ ratio of the Boise State University tracer solution.

U/Pb dates and uncertainties were calculated using the algorithms of Schmitz and Schoene (2007), $^{235}U/^{205}Pb$ of 77.93 and $^{233}U/^{235}U$ of 1.007066 for the Boise State University tracer solution, and U decay constants recommended by Jaffey *et al.* (1971). $^{206}Pb/^{238}U$ ratios and dates were corrected for initial ^{230}Th disequilibrium using Th/U[magma] = 3.0 ± 0.3 (1σ) and the algorithms of Crowley *et al.* (2007), resulting in an increase in the $^{206}Pb/^{238}U$ dates of ~0.09 Ma. All common Pb in analyses was attributed to laboratory blank and subtracted based on the measured laboratory Pb isotopic composition and associated uncertainty. U blanks are estimated at 0.013 ± 0.009 pg (1σ).

Weighted mean $^{206}Pb/^{238}U$ dates were calculated from equivalent dates (probability of fit >0.05) using Isoplot 3.0 (Ludwig, 2003). Errors on the weighted mean dates are given as ± x / y / z, where x is the internal error based on analytical uncertainties only, including counting statistics, subtraction of tracer solution, and blank and initial common Pb subtraction, y includes the tracer calibration uncertainty propagated in quadrature, and z includes the ^{238}U decay constant uncertainty propagated in quadrature. Internal errors should be considered when comparing our dates with $^{206}Pb/^{238}U$ dates from other laboratories that used the same Boise State University tracer solution or a tracer solution that was cross-calibrated using EARTHTIME gravimetric standards. Errors including the uncertainty in the tracer calibration should be considered when comparing our dates with those derived from other geochronological methods using the U/Pb decay scheme (e.g., laser ablation ICPMS). Errors including uncertainties in the tracer calibration and ^{238}U decay constant (Jaffey *et al.*, 1971) should be considered when comparing our dates with those derived from other decay schemes (e.g., $^{40}Ar/^{39}Ar$, ^{187}Re-^{187}Os). Errors for weighted mean dates and dates from individual grains are given at 2σ.

For each sample analyzed by LA-ICPMS, errors on the dates are at 2σ. For each sample analyzed by CA-TIMS, weighted mean $^{206}Pb/^{238}U$ dates were calculated from equivalent dates (probability of fit >0.05) using Isoplot 3.0 (Ludwig, 2003). Errors on the weighted mean dates are given as ± x / y / z, where x is the internal error based on analytical uncertainties only, including counting statistics, subtraction of tracer solution, and blank and initial common Pb subtraction, y includes the tracer calibration uncertainty propagated in quadrature, and z includes the ^{238}U decay constant uncertainty propagated in quadrature. Errors for weighted mean dates and dates from individual grains are given at 2σ.

Joe Mountain Formation

Sample 15EB-124-1 was collected from the mafic tuff part of the Joe Mountain Formation volcaniclastic sequence (mTJMvc) at Teslin Mountain. The outcrop comprises brown to grey-weathering, fine to coarse-grained, laminated volcanic sandstone/mudstone. Quartz eyes constitute up to 3% of the rock composition.

LA-ICPMS analyses of 19 grains yielded equivalent dates with a weighted mean of 235 ± 4 Ma (MSWD = 1.0, probability of fit = 0.42; Fig. 15a; Appendix B1). The five youngest CA-TIMS dates from analysis of six grains yielded equivalent dates with a weighted mean of 244.74 ± 0.09 / 0.15 / 0.3 Ma (MSWD = 0.46, probability of fit = 0.77; Fig. 15b; Appendix B2), which is interpreted as the depositional age of the tuff. The other date is 245.15 ± 0.23 Ma. This age is the first radiometric age from the Joe Mountain Formation as defined by Hart (1997a). It confirms a Middle Triassic age and is compatible with Ladinian conodont ages obtained at Joe Mountain (Hart and Orchard, 1996; Hart, 1997a).

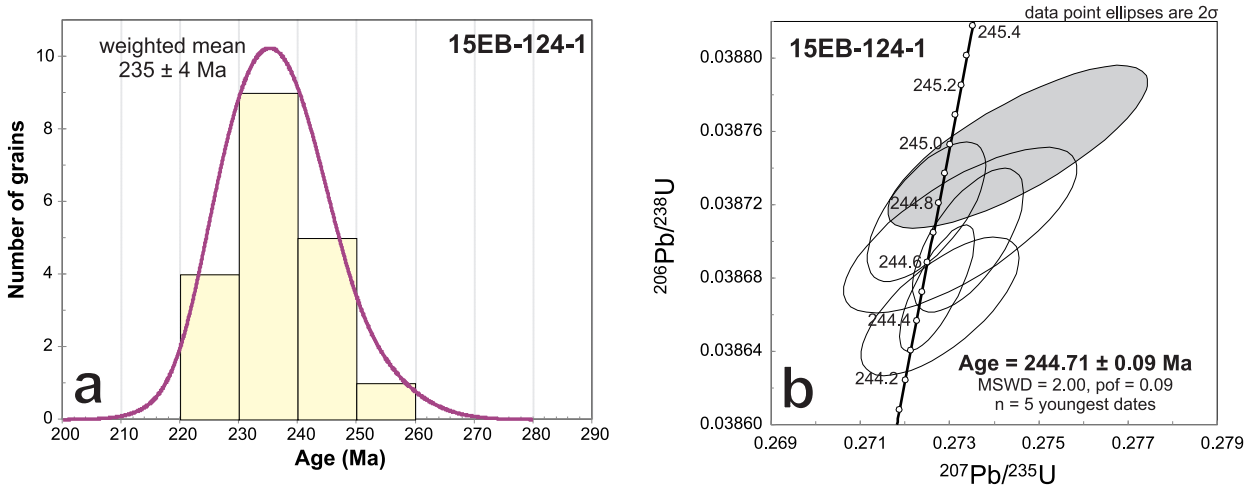

Figure 15. *U/Pb zircon geochronology for sample 15EB-124-1, collected from the mafic tuff sequence of the Joe Mountain Formation at Teslin Mountain.* ***(a)*** *Relative probability plot of LA-ICPMS analyses; and* ***(b)*** *Concordia plot of CA-TIMS analyses. Corresponding data tables are in Appendix 1. Ellipses in grey are not included in weighted mean calculations.*

Aksala formation

Detrital zircons from two samples of non-calcareous pebble conglomerate (uTLRst) underlying massive micritic limestone (uTLRul) were analyzed (Fig. 16; Table 2; Appendix B). These are the first available U/Pb dates for the Lewes River Group in this area.

Sample 16EB-421-1 was collected on the eastern shore of Lake Laberge from an ~5 m thick clastic interval, interbedded with carbonate strata of the Lewes River Group. It overlies a sequence of thin to medium-bedded calcareous sandstone and mudstone, and is directly overlain by thick-bedded micritic limestone that forms a ridge top at this location. Calcareous strata located below and above this interval are constrained to the Late Triassic by fossils (Table 1). In addition, the clastic interval can be followed for about 6 km, and similar stratigraphic relationships with carbonate strata are exposed all along the ridge.

LA-ICPMS analyses of 59 grains show 51 equivalent age dates with a weighted mean of 214 ± 3 Ma (MSWD = 1.1, probability of fit = 0.23; Fig. 16a). The six oldest grains yielded Mississippian dates (~310–350 Ma). CA-TIMS date from the analysis of the six youngest grains is 212.30 ± 0.07 / 0.12 / 0.26 Ma (MSWD = 1.34, probability of fit = 0.25), which is interpreted as the maximum depositional age. The other five dates are equivalent with a weighted mean of 214.75 ± 0.07 / 0.12 / 0.26 Ma (MSWD = 1.3, probability of fit = 0.25; Fig. 16b).

Sample 17EB-225-1 was collected east of Lake Laberge, west of the Goddard fault. It is from the same unit as 16EB-421-1 (uTLRst), but the sampling site is located more than 10 km to the north, south of Goddard Point. Similarly, the clastic interval is immediately underlying massive micritic limestone.

LA-ICPMS of 88 grains shows a large peak in the probability density plot at ~210 Ma and a small peak at 300–340 Ma (Fig. 16c). The two youngest CA-TIMS dates from analysis of the six youngest grains are equivalent with a weighted mean of 211.33 ± 0.10 / 0.15 / 0.27 Ma (MSWD = 2.2, probability of fit = 0.14, Fig. 16d), which is interpreted as the maximum deposition age. Four other grains yielded dates of 211.55 ± 0.15 to 215.65 ± 0.15 Ma.

16EB-042-1 was collected from a sequence of north-dipping, orange to brown weathering, thin to medium-bedded, non-calcareous and calcareous, fine-grained, laminated sandstone/mudstone, and coarse, calcareous sandstone to angular limestone pebble conglomerate, interbedded with fine-grained volcanic sandstone (uTLRls). This section is exposed across the valley east of Mount Laurier (Fig. 12b), and is in contact with the Laurier Creek pluton along the ridge to the east.

It yielded a small number of zircons, and as a result there are only eight LA-ICPMS analyses (Appendix B). The two largest grains yielded dates of ~230 Ma. Seven other dates are equivalent with a weighted mean of 117 ± 3 Ma (MSWD = 1.8, probability of fit = 0.10). These grains have an unusual chemistry, with very low total REE contents and low Th/U, which is characteristic of metamorphic or migmatitic zircon (Appendix B). Therefore, these results are interpreted to indicate deposition of the protolith during the Late Triassic, *ca.* 230 Ma or later, and subsequent metamorphism of these rocks during the mid-Cretaceous intrusion of the Laurier Creek pluton.

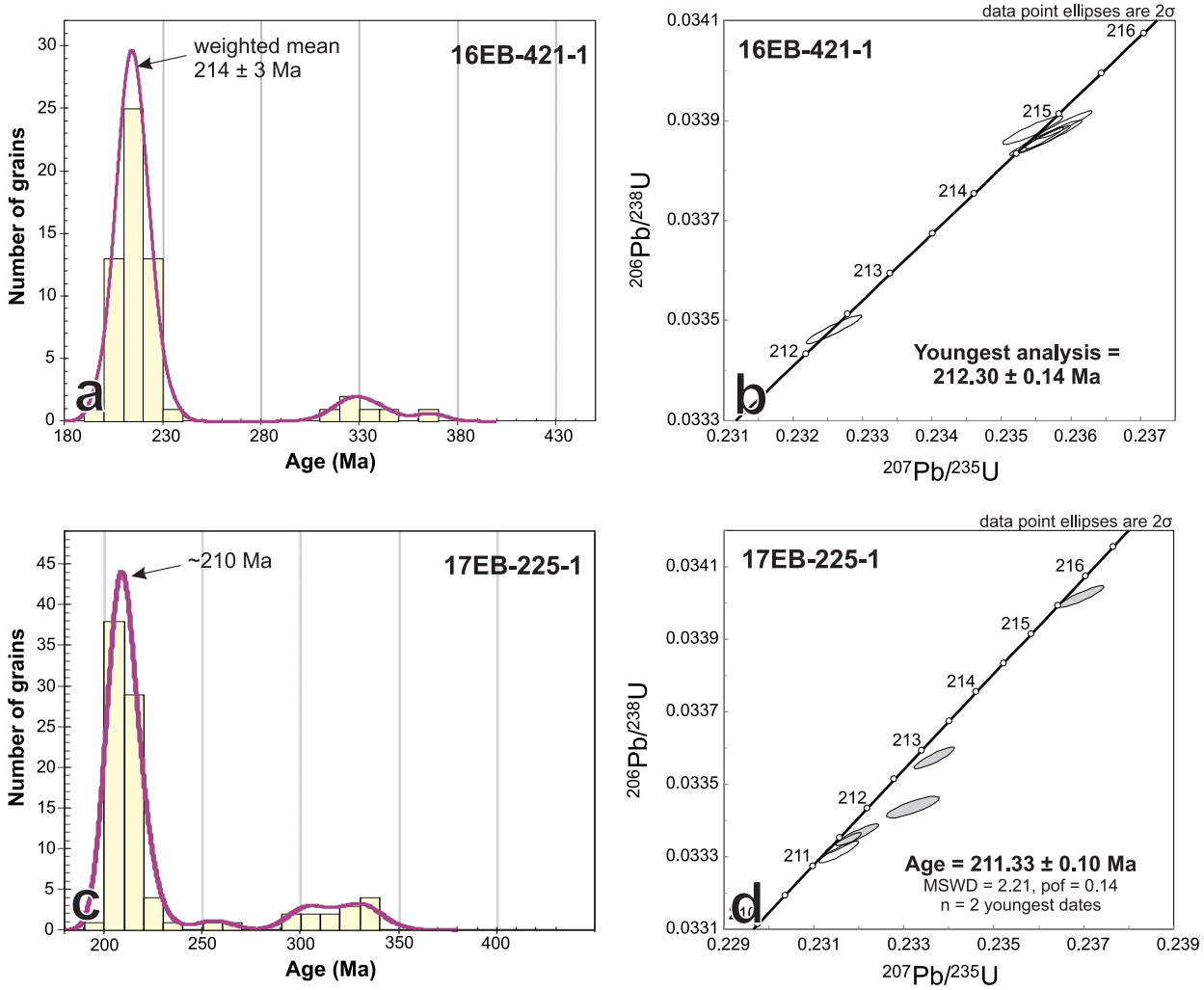

Figure 16. *U/Pb zircon geochronology for samples of the Aksala formation.* ***(a,b)*** *Relative probability plot of LA-ICPMS analyses and Concordia plot of CA-TIMS analyses for sample 16EB-421-1; and* ***(c,d)*** *relative probability plot of LA-ICP-MS analyses and Concordia plot of CA-TIMS analyses for sample 17EB-225-1. Ellipses in grey on Concordia plots are not included in weighted mean calculations.*

Geochemistry of Triassic volcanic rocks

Geochemical analyses were conducted to characterize the major and trace elements composition of the Joe Mountain Formation and Povoas formation volcanic rocks, to identify any spatial variations in composition within, and between the suites, and to support the complex volcanic stratigraphic framework and field relationships established during mapping. In addition, a subset of eight samples representative of the main isotopic signatures was selected within each volcanic suite to conduct radiogenic Nd-Hf isotopic analyses and to support interpretations of the tectonic setting in which these rocks were formed.

Analytical methods

Lithogeochemistry

Eighty-nine samples (Fig. 17a) were analyzed for major and trace elements at Activation Laboratories Ltd. in Ancaster, Ontario (4Lithoresearch package), and some samples were analyzed at the Ontario Geoscience Laboratories for trace elements. A first batch of samples (SJP prefixes) was collected regionally by S.J. Piercey from 2004 to 2006 at Joe Mountain and Mount Slim (NTS 105D/15), Mount Byng (NTS 105D/16), in the Miners Range west of Whitehorse (NTS 105D/13), and at Povoas Mountain (NTS 105E/6). This suite includes 21 samples from the Joe Mountain Formation (basalt, gabbro intrusive and mafic dikes), and 23 samples from Lewes River Group basalt, mafic tuff and volcanic breccia (Appendix C1). A second batch of samples (EB prefixes) was collected by E. Bordet from 2015 to 2018 as part of the present study. It includes 24 basalt samples from the Joe Mountain Formation, collected at Teslin Mountain, Joe Mountain and Mount Byng, and 14 samples from basalt and volcaniclastic rocks of the Povoas formation (Appendix C1). Patrick Sack (PS prefixes) collected 6 samples of basalt and gabbro from the Povoas formation west of Carcross (NTS 105D/3) and near Carmacks (NTS 115I/7, 115H/9, 16) during a regional-scale study of Late Triassic–Jurassic plutons in 2015 (Fig. 17a). Samples are representative of the different textures and compositions identified during mapping of the eastern Lake Laberge area.

Eleven major elements were analyzed by using lithium metaborate/tetraborate fusion on whole rock powders. Fused samples were dissolved in acid and analyzed by inductively coupled plasma mass spectrometry (ICP-MS) for trace elements. Samples prefaced by SJP were analyzed at the Ontario Geoscience Laboratories for trace elements using a closed-beaker digest of the whole rock powder and an ICP-MS finish. Major oxides concentrations were recalculated on an anhydrous basis to eliminate any potential bias due to fluid-related alteration. Petrographic observations were conducted as a complement to lithogeochemistry, to assess the texture and mineral composition of volcanic rocks, support chemical composition by mineral identification, and evaluate the nature and amount of alteration. Thin-section slabs were cut at Vancouver Petrographics.

Internal quality analysis and quality control included the random introduction of one blind duplicate, as well as standard pulp material, approximately every 10 samples. Standard pulp material is USGS Columbia River Basalt BCR-2 (Wilson, 1997) and Silver Plume granodiorite from Colorado GSP-2 (Wilson, 1998). Laboratory quality analysis/quality control consists of the inclusion of three blanks and five control samples (three before sample group and two after) analyzed per group of samples. Duplicates were fused and analyzed every 15 samples. Standard and duplicate samples analytical results confirm reliability and reproducibility of the analyses (Appendix C4).

Nd-Hf isotopic analyses

Radiogenic isotopic results for Nd and Hf were obtained on 28 samples from the Povoas and Joe Mountain formations within the map area (Fig. 17b). A first batch of Sm-Nd and Lu-Hf analyses was conducted in 2006 using a combination of CA-TIMS and MC-ICPMS on samples collected by Steve Piercey. The data set comprises samples from the Joe Mountain Formation (n = 9), and the Povoas formation (n = 8), as well as 3 samples from the Takhini assemblage for reference. These samples have MORB/BABB, IAT and CAB signatures (see below) based on trace elements results. A second batch of Sm-Nd and Lu-Hf analyses was conducted in 2017 on samples collected by Esther Bordet. These samples are representative of IAT and CAB signatures (see below) within the Joe Mountain Formation (n = 6) and basalt of the Povoas formation (n = 2).

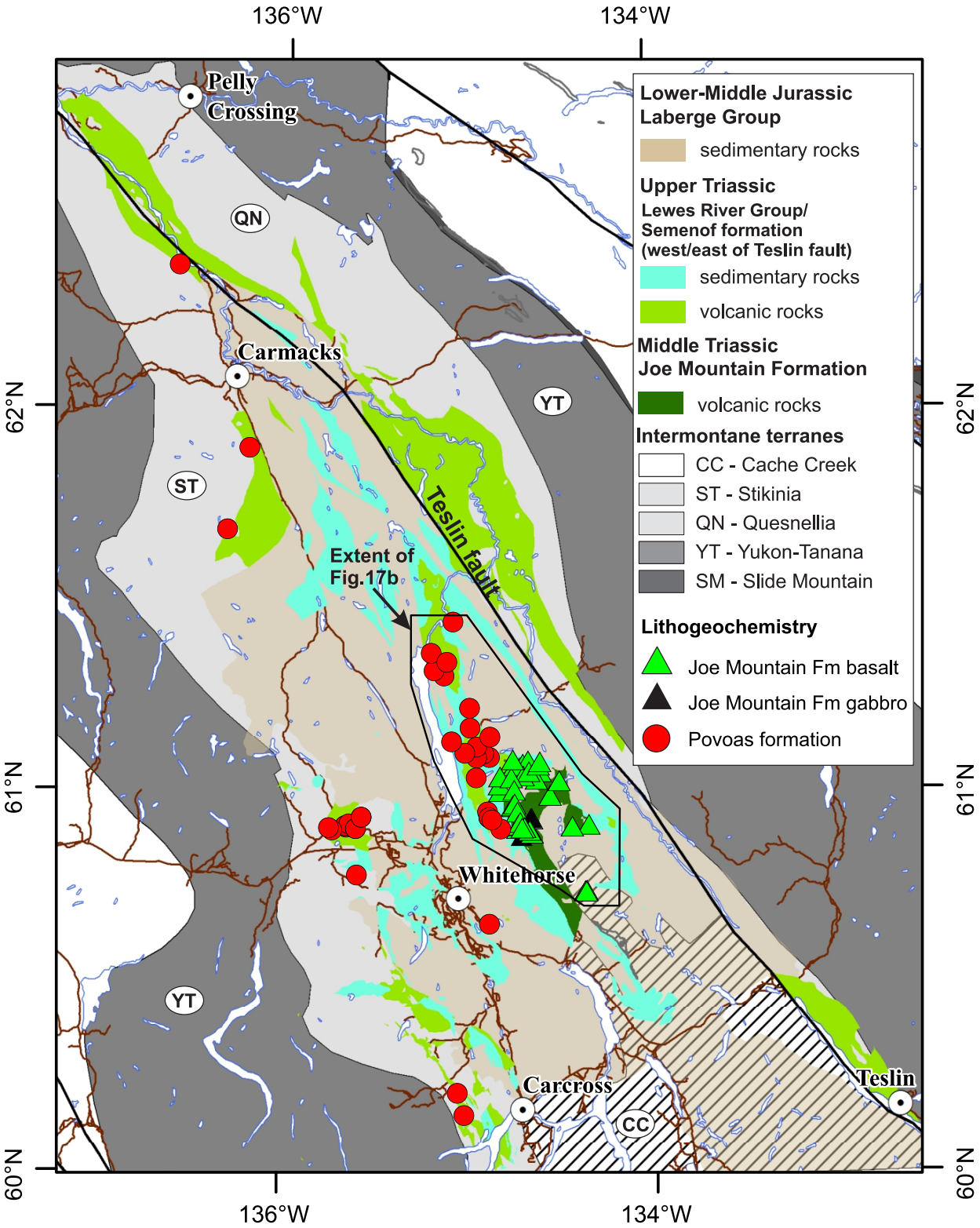

Figure 17. *Distribution of lithogeochemistry and Nd-Hf isotopic samples from Triassic rocks collected as part of this study.* ***(a)*** *Distribution of regional lithogeochemistry samples, including those collected by S.J. Piercey and P.J. Sack outside of the current map area during regional studies. Geology polygons after Colpron et al. (2016b); see* ***(b)*** *on next page.*

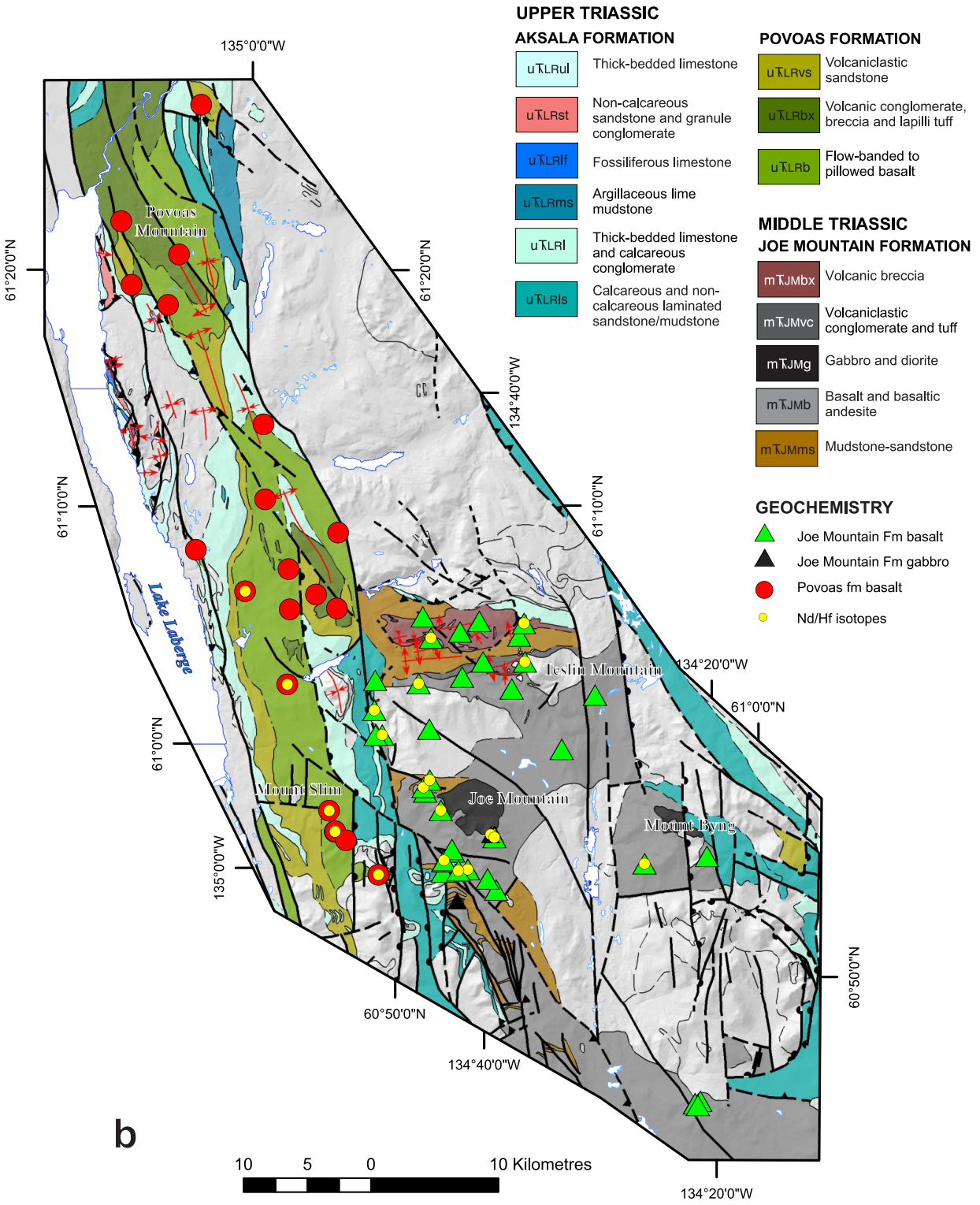

Figure 17 *continued.* ***(b)*** *Distribution of lithogeochemistry and Nd-Hf isotope samples in the eastern Lake Laberge map area.*

All samples were analyzed at the Pacific Center for Isotopic and Geochemical Research at the University of British Columbia following methods presented in Weis *et al.* (2005). Rock powders were dissolved using a conventional digestion in a closed beaker. For samples collected in 2006, Nd concentrations were measured using thermal ionization mass spectrometry (TIMS), and Hf concentrations were obtained by multi-collector ICP-MS. For the 2017 samples, both Nd and Hf concentrations were measured by multi-collector ICP-MS following methods detailed in Weis *et al.* (2006). Data are presented in Appendix C2.

Element mobility and utility

Isotopic tracers are used to identify igneous sources and magmatic processes, and therefore support interpretations of the tectonic settings in which the igneous rocks were formed. These tracers must be relatively immobile, so that effects of hydrothermal alteration and metamorphism are negligible, and that the measured concentrations of these elements is truly representative of igneous processes, whether it is mantle or crust melting. For instance, major elements, especially the alkalis and the LFSE, are highly mobile in fluids associated with hydrothermal alteration and metamorphism, and therefore arc rocks are enriched in those elements (Piercey *et al.*, 2006). In contrast, most HFSE (Ti, Zr, Hf, Nb, Ta), the REE (La, Lu and in a lesser way Eu) and some trace elements (Cr, Ni, Sc, V) are immobile in most conditions (English *et al.*, 2010; Piercey *et al.*, 2006). Th is the only LFSE that can be considered immobile and constitutes a good indicator of slab-derived fluid-flux (Piercey *et al.*, 2006). Therefore, the HFSE, REE, Th and selected trace elements can be used to reliably determine the tectonic setting in which magmas were formed, as well as the nature and type of mantle, crust and subducted slab components.

The system Nd-Hf represents a REE-HFSE pair of elements that can be used as a tracer of relative contribution of crust versus mantle in magmas. Nd shows global variations of concentration in the mantle (Indian *vs* Pacific reservoir; Pearce *et al.*, 1999). Because Nd is soluble in both aqueous fluids derived from subduction and in melts, its content can be modified due to processes like subduction and alteration (Pearce *et al.*, 1999). In contrast, Hf is incompatible, conservative (= not added to the mantle wedge during subduction), immobile during alteration, soluble in siliceous melts, but not in aqueous fluid derived from subduction. Therefore Hf is useful to characterize HFSE anomalies that define subduction-related lavas. Overall, Nd and Hf display varying incompatibility during mantle melting, thus varying sensitivities to crustal contamination allowing determination of mantle compositions and potential crustal contamination upon emplacement.

Geochemical composition

The bulk of the Povoas and Joe Mountain formations compositions are basalt, basaltic-andesite and andesite. The range of SiO_2 concentrations is 47–71% (Fig. 18a). Joe Mountain Formation coherent volcanic samples are dominantly subalkaline: they range in composition from basalt to basaltic-andesite, with a few samples plotting in the basaltic trachy-andesite field (Fig. 18a,b). The Povoas formation includes basalt, basaltic-andesite, andesite, and all their trachytic equivalents, as well as a few trachydacites. (Fig. 18a,b). The Povoas formation completely overlaps the range of compositions observed for the Joe Mountain Formation, but overall displays more alkaline-trachytic compositions.

Most major elements including Fe_2O_3, MnO, MgO, CaO and TiO_2 display a negative correlation with respect to SiO_2 (Fig. 19). The largest scatter of compositions is observed in the 47–60% SiO_2 range for all these elements. Na_2O displays a weak positive correlation with respect to SiO_2. These trends are all similar between the Povoas and Joe Mountain formations.

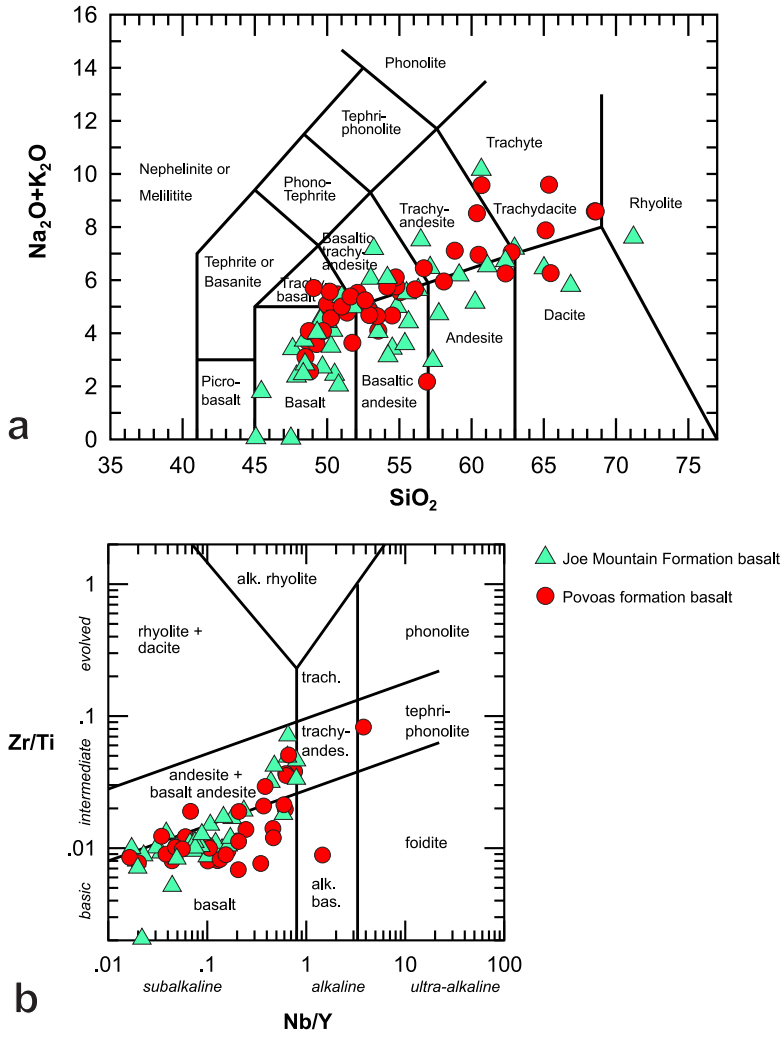

Figure 18. *Geochemical composition of volcanic rocks of the Joe Mountain Formation and Povoas formation.* ***(a)*** *Total Alkali Silica diagram after LeBas et al. (1986). Joe Mountain Formation samples with lowest alkali concentrations correspond to altered and deformed basalt and gabbro samples from the Michie Lake area. Povoas and Joe Mountain formation samples plotting in the trachydacite, dacite and rhyolite fields likely correspond to samples that were hydrothermally altered; and* ***(b)*** *Zr/Ti vs Nb/Y diagram of Pearce (1996), after Winchester and Floyd (1977). All samples plot in the basalt and basalt andesite field. Samples with higher Nb/Y were collected by P. Sack.*

Trace and rare earth elements

Trace element profiles normalized to primitive mantle compositions for basalts of the Povoas and Joe Mountain formations are relatively flat, with a marked Nb anomaly observed for most samples with minor exceptions (Fig. 20a; Sun and McDonough, 1989): such a profile is characteristic of subduction-related igneous rocks (Sun and McDonough, 1989; Pearce and Peate, 1995; Piercey et *al*., 2006). The variations in the trace element profiles on primitive mantle normalized trace element diagrams for the Joe Mountain and Povoas formations define three trends, representing potentially distinct tectonic environments (Fig. 20 b–d; Sun and McDonough, 1989):

1. MORB/BABB profile: these samples display a flat trace elements profile, with a minor Nb negative anomaly. This profile is prominent amongst Joe Mountain Formation samples (Fig. 20c), but a few occurrences exist within the Povoas formation (Fig. 20d). These signatures are interpreted to reflect rocks derived from depleted mantle sources with minor subduction influence and has undergone little differentiation, similar to primitive basalt found in MORB and BABB environments.
2. IAT profile: these samples display a relatively flat trace element profile, with slightly higher concentrations of LILE with respect to HFSE, and have a marked Nb negative anomaly, typical of subduction-related magmatic rocks and/or rocks contaminated by continental crust (e.g., Pearce and Peate, 1995; Fig. 20c,d).

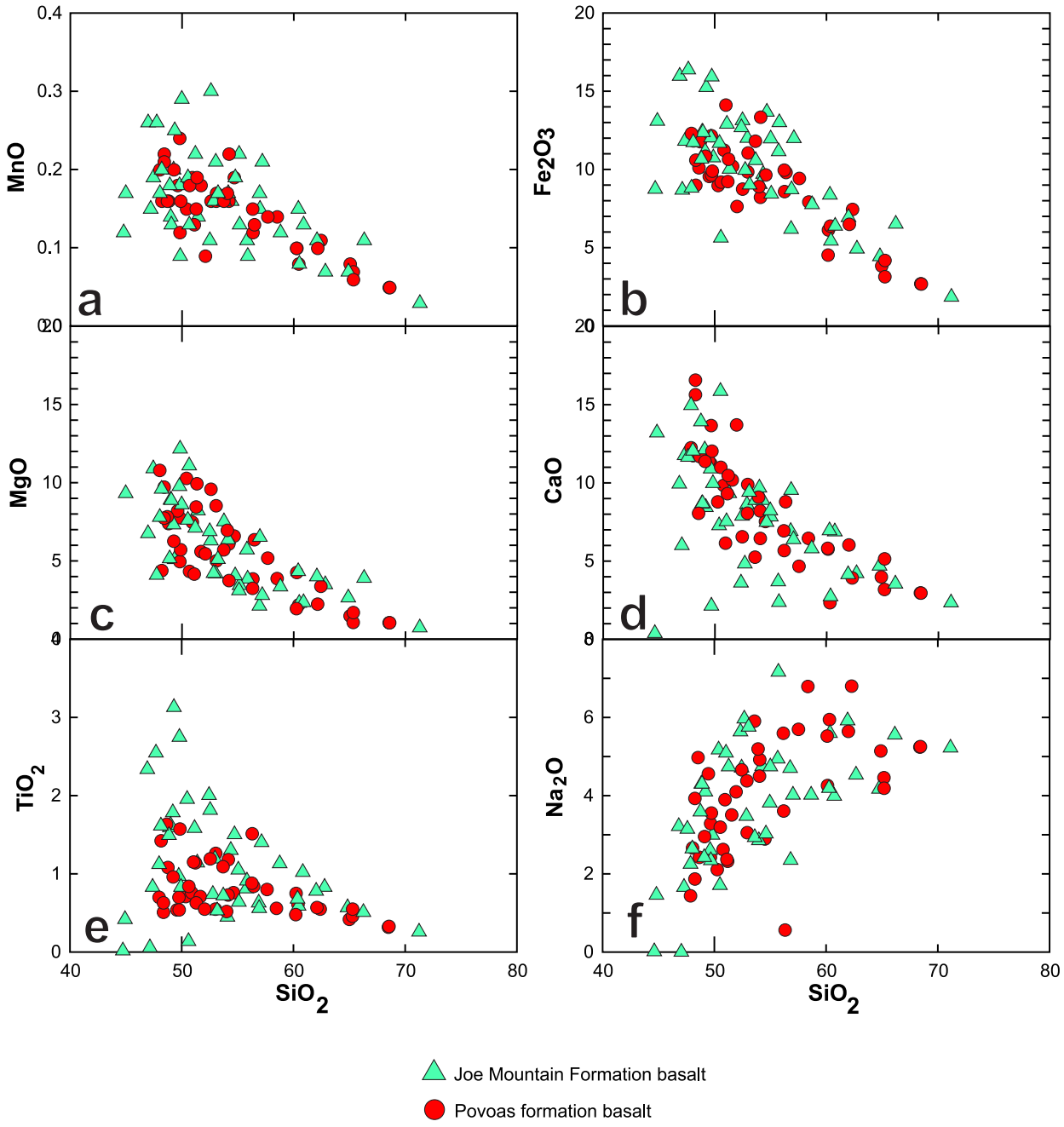

Figure 19. *Selected major element Harker diagrams for samples of the Joe Mountain Formation and Povoas formation.*

3. CAB profile: these samples display a marked negative slope, with significant LREE and LILE enrichment with respect to HREE and HFSE. The marked Nb and Ti negative anomalies are typical of calc-alkalic rocks with subducted slab signatures (Fig. 20c,d).

REE diagrams normalized to chondrites (Fig. 21; Sun and McDonough, 1989) also illustrate distinct trends between the different formations or tectonic groups. Most samples of Triassic volcanic rocks, whether they are part of Joe Mountain or Povoas formations, display a flat, undifferentiated REE profile with respect to chondrite (Fig. 21a), typical of rocks derived from juvenile depleted mantle sources (e.g., ocean-floor or island arc environment; Fig. 21b). Fewer samples show a higher concentration of the LREE versus HREE (Fig. 21a), which indicates a minor amount of

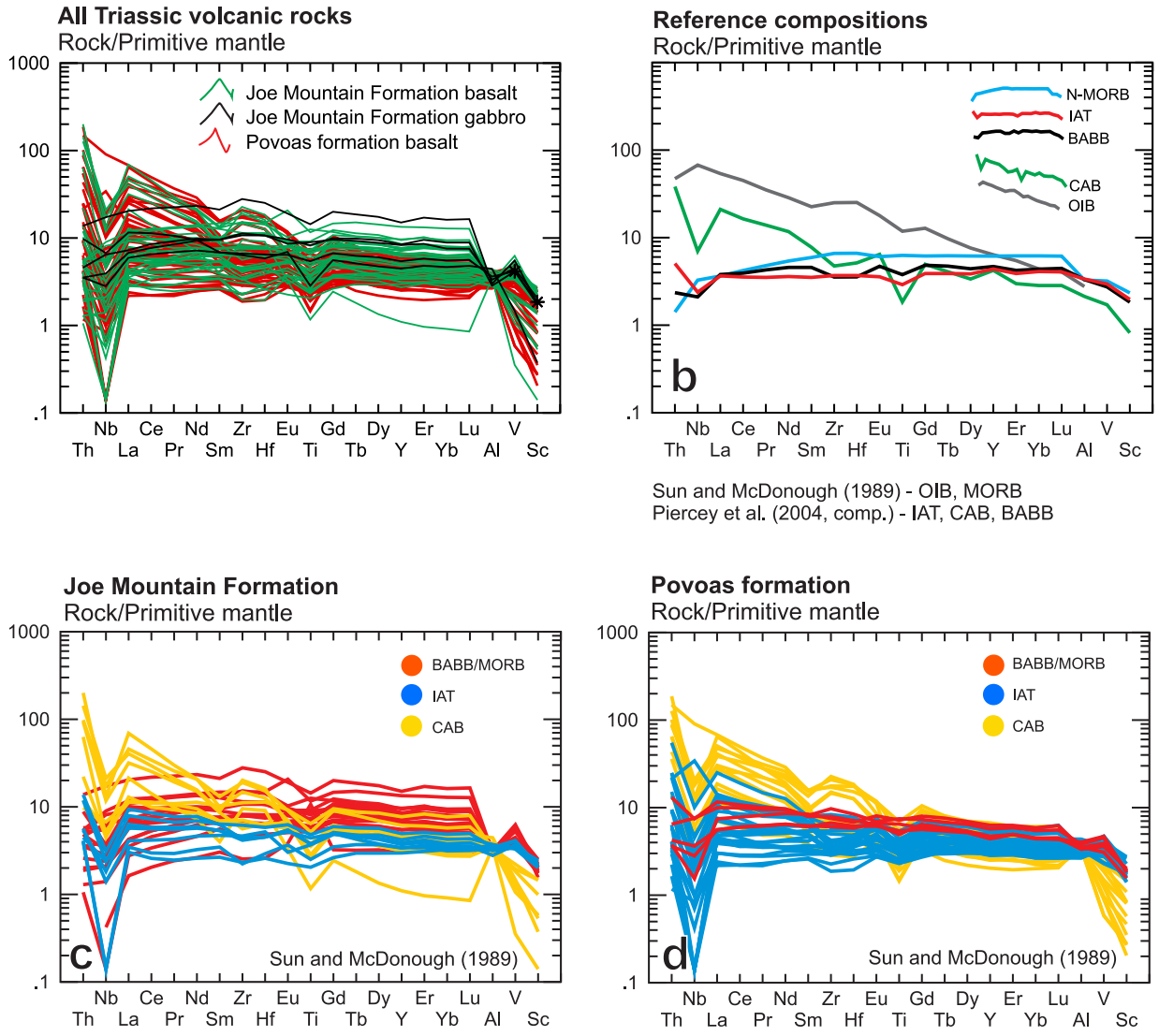

Figure 20. *Trace element spider diagrams for samples of the Joe Mountain Formation and Povoas formation. Primitive compositions of Sun and McDonough (1989).* **(a)** *Trace element profile for rocks of the Joe Mountain Formation and Povoas formation basalts;* **(b)** *trace elements reference compositions compiled from Sun and McDonough (1989) and Piercey et al. (2004).* **(c)** *Joe Mountain Formation samples with BABB/MORB, IAT and CAB affinities; and* **(d)** *Povoas formation samples with BABB/MORB, IAT and CAB affinities.*

differentiation with respect to chondrite compositions, and therefore suggest that some of these rocks have had either minor slab fluid input, lower degrees of melting, or have undergone minor crustal contamination leading to calc-alkaline signatures (Fig. 21b).

Tectonic discriminants

Binary and ternary trace elements diagrams for basaltic magmas are used to track elements behaviour and characterize the tectonic setting of the volcanic successions (Fig. 22a: Shervais, 1982; Fig. 22b: Pearce and Peate, 1995; Fig. 22c: Wood, 1980). Basalt of the Joe Mountain and Povoas formations include tholeiitic, transitional and calc-alkaline basalt compositions. Tectonic settings in which these rocks may have formed range from mid-oceanic ridge or back arc basin (MORB/BABB) to oceanic island arc (IAT, CAB). The Joe Mountain Formation is almost exclusively characterized by tholeiitic and transitional basalt with MORB/BABB and IAT signatures, whereas the Povoas formation shows a greater amount of CAB and lesser BABB/MORB compositions.

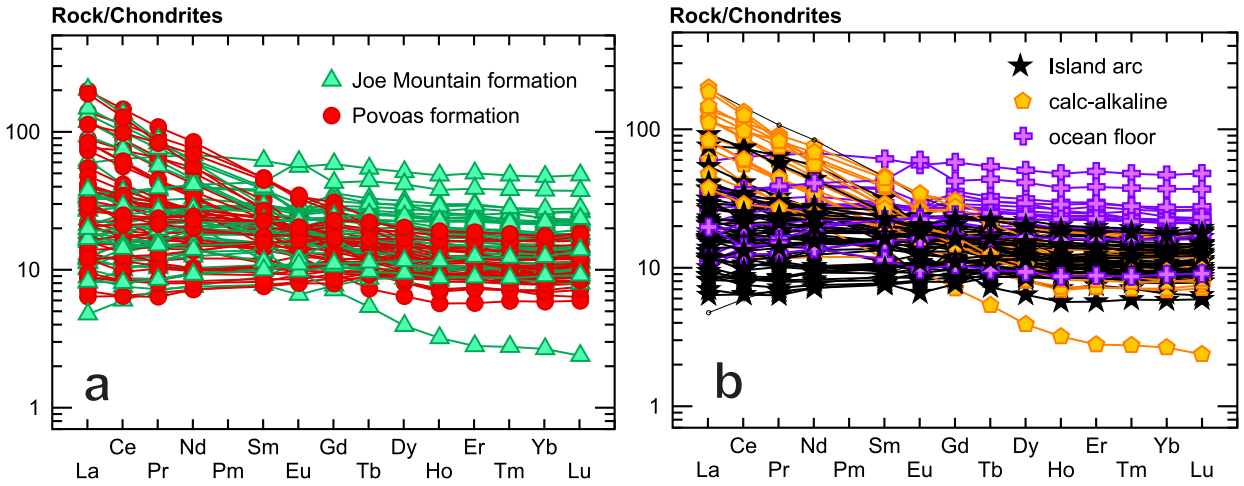

Figure 21. *Rare Earth Element plots vs chondrites compositions, with normalizing values after Sun and McDonough (1989).* ***(a)*** *Composition of Joe Mountain Formation and Povoas formation basalts; and* ***(b)*** *composition of Triassic mafic volcanic rocks by tectonic affinity group (island arc, calc-alkaline, ocean floor) defined after Pearce and Cann (1973).*

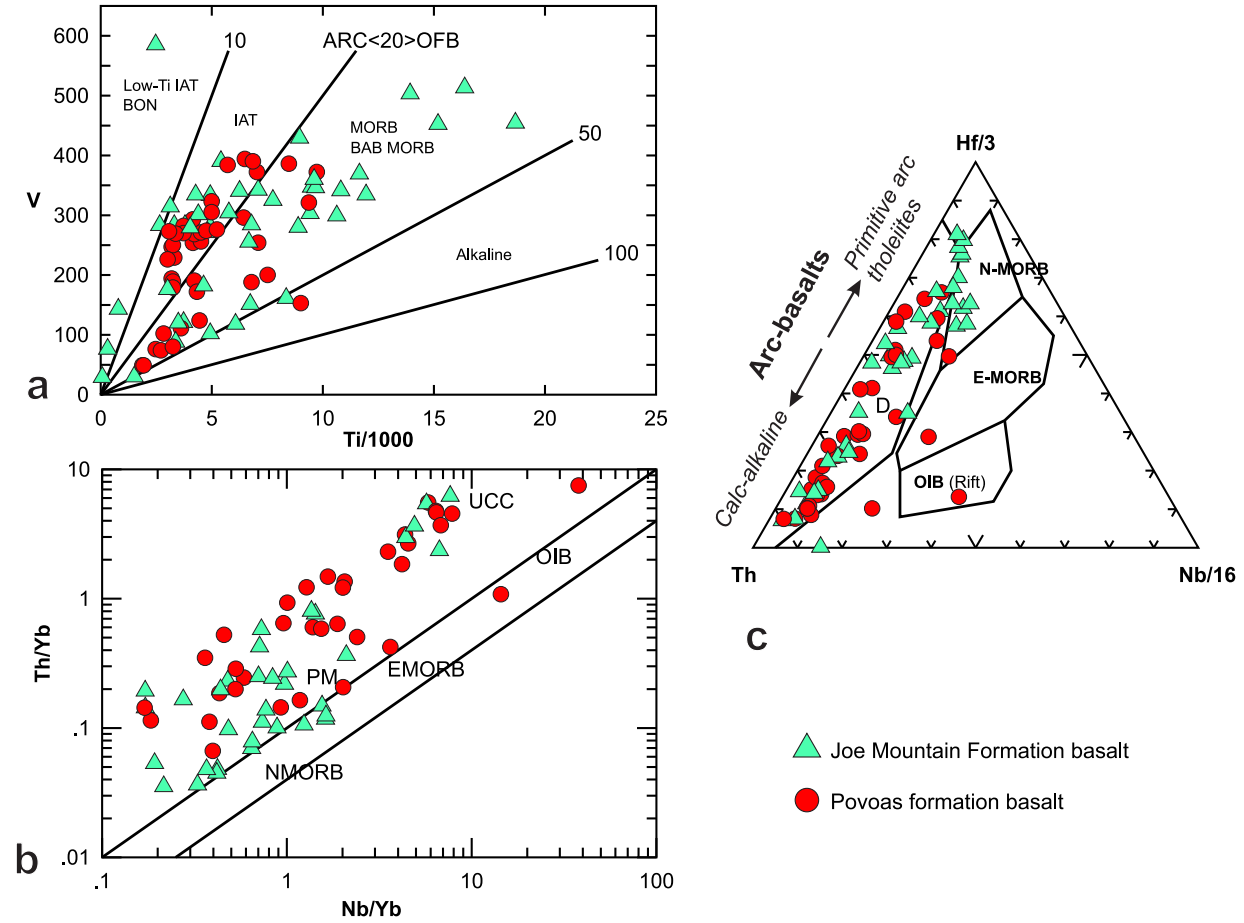

Figure 22. *Tectonic discrimination diagrams for mafic rocks of the Joe Mountain Formation and Povoas formation.* ***(a)*** *Ti/1000-V tectonic discriminant diagram from Shervais (1982);* ***(b)*** *Th/Yb vs Nb/Yb diagram of Pearce and Peate (1995). Most samples display higher Th/Yb ratios than MORB, highlighting the non-conservative behaviour of Th; and* ***(c)*** *Th-Hf/3-Nb/16 tectonic discriminant diagram from Wood (1980).*

A series of regional maps illustrate the spatial variations of geochemical signatures and tectonic affinity within, and between volcanic suites (Fig. 23). Spatially, the most juvenile compositions (MORB/BABB) are found within samples of the Joe Mountain Formation at Joe Mountain (Fig. 23a,b). CAB and IAT signatures are found across the entire study area independently of geographic location or host rock (Fig. 23a,b).

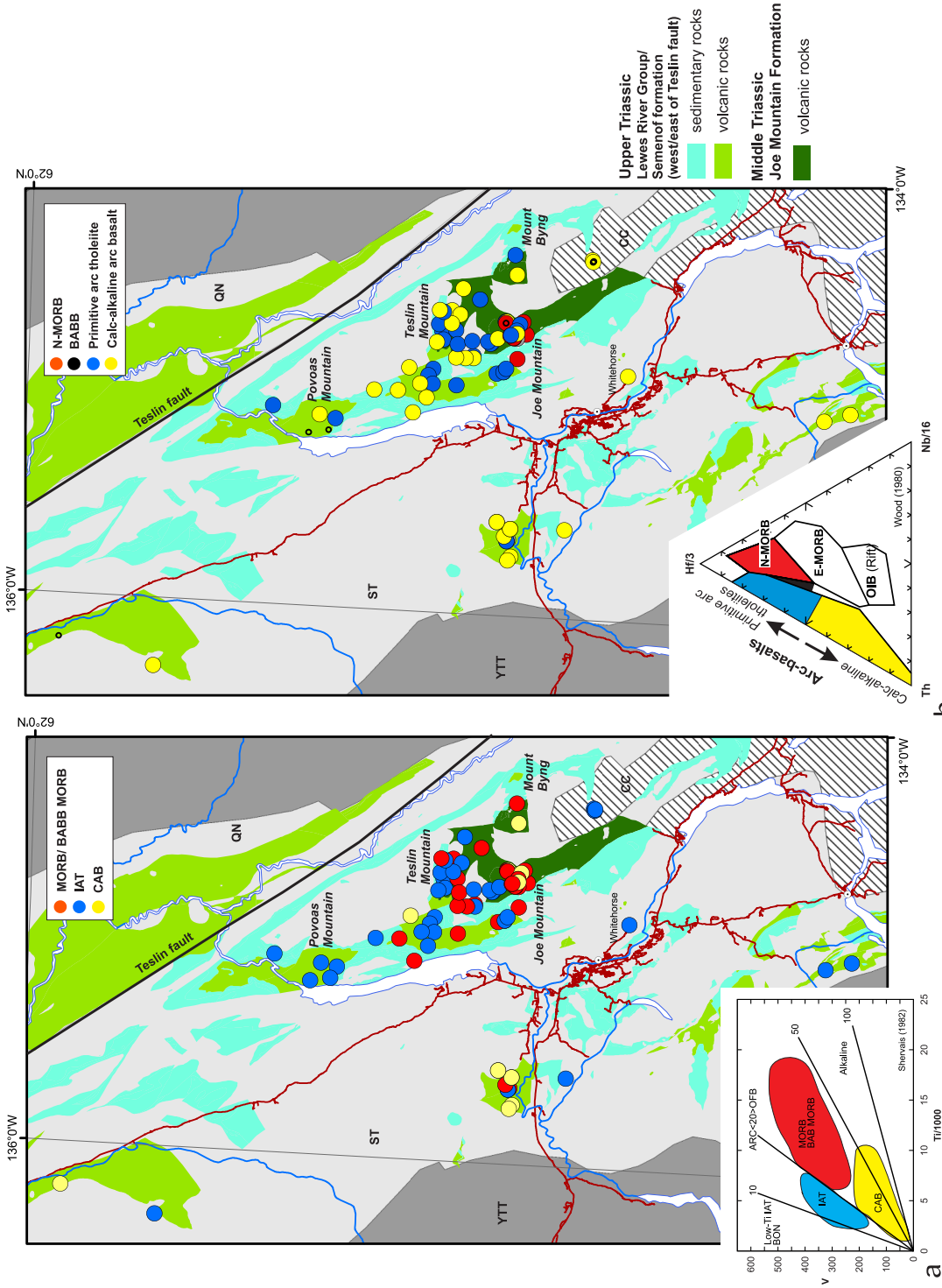

Figure 23. *Distribution and variations of tectonic character for mafic rocks of the Joe Mountain Formation and Povoas formation across the map area.* **(a)** *Classified according to Ti/1000-V tectonic discriminant diagram from Shervais (1982); and* **(b)** *classified using the Th-Hf/3-Nb/16 tectonic discriminant diagram from Wood (1980). ST = Stikinia, QN = Quesnellia, YTT = Yukon-Tanana (Colpron and Nelson, 2011). Geology after Colpron et al. (2016b).*

Nd-Hf isotopes

Samples selected for Nd and Hf include those with MORB/BABB, IAT and CAB signatures, and were chosen to test the potential variations in mantle versus basement contamination in the magmatic rocks. Isotopically, our data set (n = 28 samples) indicates εNd_t values ranging from + 1.1 to 11.3, with most samples having $\varepsilon Nd_t > 6$ (Fig. 24a), and εHf_t values ranging from + 3.5 to 10.6, with mainly $\varepsilon Hf_t > 5$ (Fig. 24b). The range of values for both εNd_t and εHf_t does not significantly vary between the two volcanic suites (Fig. 24). However, geochemical groups identified using tectonic discriminants show clear distinct patterns. The CAB samples are uniformly juvenile with εNd_t ranging between + 9.2 and + 11.3 and εHf_t between + 9.5 and + 10.1. MORB and BABB samples also display a narrow range of values, generally lower than those displayed by CAB, with εNd_t ranging between + 6.8 and 8.6 and εHf_t between + 6.2 and 9.6. The IAT and L-IAT category displays the most variability in isotopic values, with εNd_t ranging between + 1.1 and 9.6 and εHf_t between + 3.5 and 10.6. The IAT samples generally plot in the same range as MORB and BABB samples, with slightly lower εHf_t values down to + 3.5. MORB and BABB samples reflect a transition between low εHf_t IAT samples and higher εHf_t L-IAT samples.

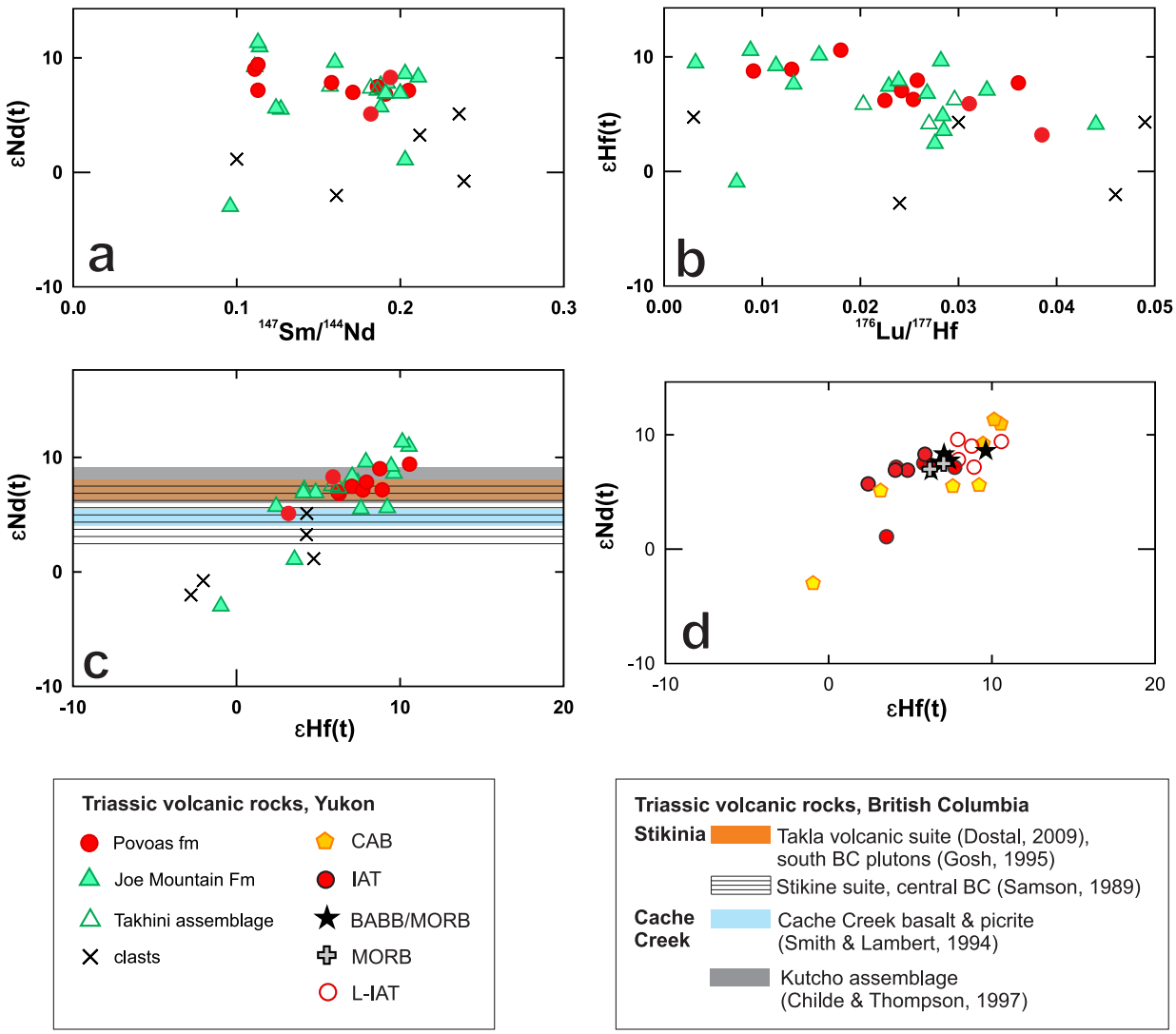

Figure 24. *Hf-Nd plots for mafic rocks of the Joe Mountain Formation and Povoas formation.* ***(a)*** *εNd(t) plot;* ***(b)*** *εHf(t) plot;* ***(c)*** *εHf(t) vs εNd(t) plot. εNd(t) values for various volcanic suites of Stikinia and Cache Creek are plotted for reference; and* ***(d)*** *εHf(t) vs εNd(t) plot based on the samples tectonic affinity.*

These observations are consistent with magma from both the Povoas and Joe Mountain formations being derived from predominantly juvenile, depleted mantle sources, and minor to no crustal contamination. The range of εNd(t) values displayed by the two volcanic suites is similar to analyses results from coeval volcanic suites in part of Stikinia or Cache Creek in British Columbia (Fig. 24c; Samson *et al.*, 1989; Smith and Lambert, 1995).

Summary

The Joe Mountain Formation comprises the oldest rocks in the map area. Units show a transition from coherent basalt to the south (Joe Mountain and Mount Byng areas), to sedimentary and volcaniclastic basin strata to the north (Teslin Mountain area). A sequence of fine-grained, thin-bedded, laminated clastic and calcareous mudstone/sandstone underlies, or is locally interbedded with the basalt (Hart and Hunt, 2003a), suggesting the existence of a basin prior to, or coeval with Joe Mountain volcanism. Pegmatitic and pyroxene-gabbro and diorite exposed at Joe Mountain and Mount Byng (Hart, 1997a) likely represent a juvenile subvolcanic intrusion that developed just beneath a volcanic arc centre and was later exposed by erosion. The bulk of the Joe Mountain Formation is composed of coherent, massive aphyric to microcrystalline basalt and volcanic breccia. Basalt is generally pillowed, with subaerial, flow-banded, vesicular lava locally observed. Regular lamination within the mafic tuff sequence, interbedded limestone lenses, and the presence of pillows suggests deposition under water for at least part of the formation. This unit also displays several occurrences of hematite-rich iron formation, likely formed as a result of black smoker pipe activity. A U/Pb zircon date of 244.74 ± 0.09 Ma constrains the Joe Mountain volcanism to the Middle Triassic.

The Lewes River Group refers to a sequence of volcano-sedimentary rocks, divided into a basal volcanic sequence possibly as old as Carnian (the Povoas formation), and an upper sedimentary sequence of laterally variable clastic and carbonate strata which are dominantly Norian, and locally as young as Rhaetian (the Aksala formation). The Povoas formation is dominated by volcaniclastic units (mafic sandstone, mudstone, volcanic conglomerate and breccia), and lesser subaerial and subaqueous coherent clinopyroxene basalt and basaltic andesite. Basalt is commonly altered to epidote or actinolite. Fragmental deposits of the Povoas formation are interpreted as proximal volcanic breccia resulting from mechanical fragmentation.

Overall, Triassic volcanic rocks in the map area likely represent primary, proximal flow deposits associated with andesitic-type eruptions from a stratovolcano. This type of eruption, associated with a dynamic convergent (subduction-related) tectonic environment, contributes to fast vertical accumulation of volcanic rocks. As a result, gravity-driven erosion of steep flanks of andesitic volcanoes produces large volumes of fragmental rocks. As the arc evolved, volcano-sedimentary basins developed along the rims of the volcanoes collecting materials formed during eruptions and subsequently eroded from the flanks of the volcano. The lithological, geochemical and temporal variability between, and within, the Joe Mountain and Povoas volcanic suites is similar to what can be observed in modern arcs (Izu Bonin Mariana arc: Brandl *et al.*, 2017; Ishizuka *et al.*, 2018; Luzon arc: Hollings *et al.*, 2011). Volcanic activity was likely initiated at Joe Mountain and Mount Byng around 245 Ma, in an intra-oceanic arc characterized by a juvenile IAT signature, and spatially restricted intra-arc rift basins with MORB/BABB signatures. The gabbro complexes at Joe Mountain and Mount Byng may represent the exhumed deepest root of the volcanic system. Povoas volcanism was probably active during the Carnian, and continued into the Norian synchronously with carbonate sedimentation. The maximum age of Povoas volcanism is unknown.

The Aksala formation is a heterogeneous combination of stratified sections that are time equivalent, but not laterally continuous across the basin. The thick (~2000–2500 m) carbonate sequence laterally overlying mafic volcanic rocks can be divided into at least two belts displaying spatially distinct stratigraphic successions of time-equivalent strata. Detrital zircon dates suggest maximum ages of deposition around 212–211 Ma for the Aksala formation. A subsidiary zircon population of Mississippian ages appears in all clastic samples, and corresponds to igneous events documented in Paleozoic successions of Stikinia and Quesnellia, and in the Yukon-Tanana terrane, which surrounds the map area on all sides (Fig. 1). Fossil ages constrain carbonate deposition during the Norian, with a few fauna assemblages suggesting a possible initiation of carbonate basin sedimentation as early as the Carnian. Original stratigraphic subdivisions by Tozer (1958) and Wheeler (1961) are most appropriate to describe the complex lateral stratigraphic variations and facies changes within the Aksala formation. However, subdivisions established by each author are only relevant to the specific areas they were mapping, and do not necessarily extend to the entire Stikinia in Yukon. Lateral stratigraphic boundaries within the Lewes River Group were later emphasized by regional faults. The Laurier Creek fault marks the eastern boundary of most Lewes River Group strata. Some carbonate strata of the Aksala formation overlie the Joe Mountain Formation south of Long Lake and east of Mount Laurier (Fig. 6). The Goddard fault marks the boundary between the eastern and western carbonate belts of the Aksala formation.

Basalt and basaltic-andesite rocks of the Joe Mountain and Povoas formations share similar compositions and textures. In both suites, mineralogy of coherent volcanic rocks typically includes plagioclase and augite. However, microcrystalline to aphyric basalt is found almost exclusively within the Joe Mountain Formation. These volcanic rocks have primitive geochemical compositions, with coherent volcanic rocks of the Joe Mountain Formation dominated by basalt and basaltic andesite and juvenile MORB/BABB and IAT signatures. Most IAT and CAB compositions of basalt and andesite are independent of geographic distribution and volcanic suite; such signatures are found across the entire map area within both the Joe Mountain Formation and Povoas formation. Trace and rare earth element geochemical data are consistent with them having tholeiitic, transitional to calc-alkaline juvenile arc basalt signatures formed in intra-oceanic arc to back-arc environments. Mafic intrusive rocks from the Joe Mountain Formation have the most juvenile signatures, suggesting that they were formed in a back-arc or intra-arc rift setting, where rifting was ongoing within the primitive arc. Nd-Hf isotope results confirm that all Triassic basaltic rocks were derived from a juvenile, depleted mantle source feeding a volcanic arc system that experienced potential rift episodes in the back-arc. There are no indications of significant crustal contamination.

Chapter 3 - Whitehorse Trough

The Joe Mountain Formation and Lewes River Group are unconformably overlain by the Lower to Middle Jurassic Laberge Group, which corresponds to deltaic and deep marine sedimentation in the Whitehorse trough following Triassic volcanic arc activity and related sedimentation (Colpron *et al.*, 2015; White *et al.*, 2012). The Laberge Group is volumetrically important in the map area (Fig. 6), and is mainly in contact with volcanic and sedimentary strata of the Lewes River Group, or locally with the Joe Mountain Formation near Joe Mountain. Mapping efforts and sampling focused at characterizing the nature and age of the contact between the Laberge Group and underlying Triassic strata.

Lithology and stratigraphy of the Laberge Group

Early–Middle Jurassic strata of the Laberge Group are dominated by thick-bedded, polymictic pebble to boulder conglomerate (JLcg) in the northeastern part of the map area and along the rugged ridge of Mount Laurier (Figs. 6 and 7). The conglomerate unit is bounded to the west by the Laurier Creek fault, and to the east by the Teslin fault (Fig. 1). Towards the south, units of the Laberge Group overlie the Middle Triassic Joe Mountain Formation. Fine-grained, thin-bedded clastic sedimentary rocks are exposed along the shore of Lake Laberge (JLst; Fig. 6). Two additional minor units are reported: a dark green, matrix-supported conglomerate (JLcbx) and an occurrence of the Nordenskiöld dacite (lJN; Bordet, 2019).

The contact between Laberge Group and the underlying Lewes River Group is either a disconformity (Mount Laurier), or an angular unconformity (south of Long Lake; Fig. 6). In fact, Laberge Group unconformably overlies various units of the Upper Triassic Lewes River Group, a relationship described in detail in van Drecht and Beranek (2018). Along the eastern shore of Lake Laberge, shallow to moderately dipping mudstone and sandstone strata of the Laberge Group abut against north-trending, competent massive limestone strata of the Aksala formation (Fig. 25). This relationship illustrates an uncomfortable depositional relationship likely controlled by pre-Jurassic topography. At Mount Byng, the contact between the Lewes River Group and Laberge Group may be conformable. Both groups include conglomeratic units characterized by rounded limestone clasts and/or igneous clasts (Hart and Hunt, 2003b). Furthermore, the areas where a contact should exist are either tree covered, or display a range of conglomeratic strata that transition continuously from one unit into the other.

The upper contact of the Laberge Group is not exposed in the Teslin Mountain area, therefore the estimated thickness of 2000 m for the Laberge Group is a minimum. Previous estimates report between 1000 and 3000 m (e.g., Hart, 1997a; White *et al.*, 2012) across the Whitehorse trough.

Sandstone/mudstone (JLst)

An ~30 m thick sequence of brown weathering, thin-bedded sandstone to mudstone (JLst) marks the base of the Laberge Group at Mount Laurier (Fig. 26a). This unit is also extensive along the eastern shore of Lake Laberge and on Richthofen Island (Fig. 26b), where it can reach several hundred metres thick.

At Mount Laurier, a west dipping fine clastic sequence overlies Lewes River Group limestone and underlies Laberge Group conglomerate (Fig. 26a). The sandstone contains fine mafic crystals (biotite, pyroxene) and minor plagioclase in a fine, dark grey groundmass. It displays cross-stratifications on weathered surfaces and grades upward into mudstone. Finely bedded,

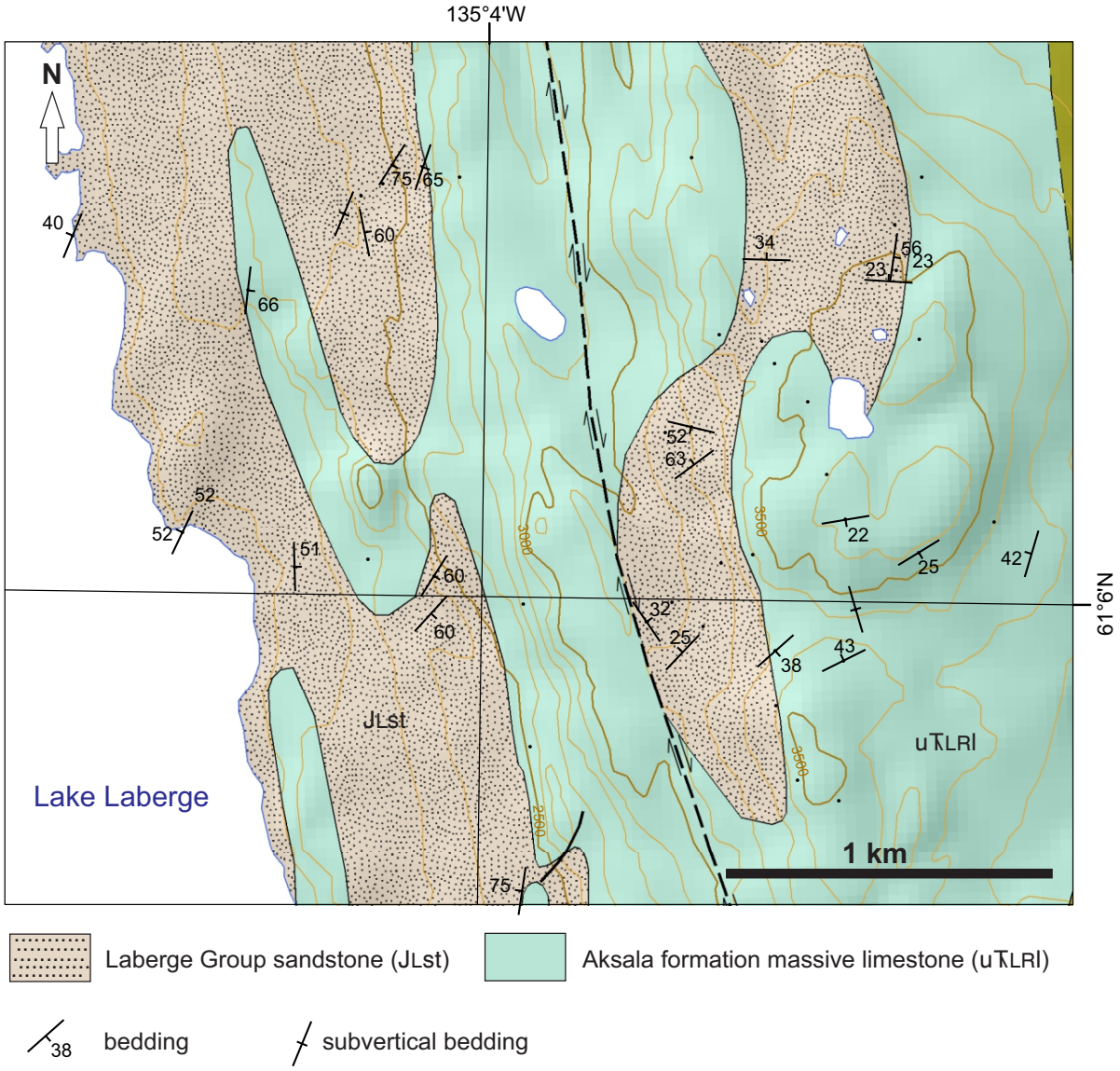

Figure 25. *Map relationships between Upper Triassic limestone of the Aksala formation, and Early-Middle Jurassic sandstone and mudstone of the Laberge Group, in the area east of Lake Laberge. Mapping shows folded Laberge Group strata with variable dips, abutting against north-trending Upper Triassic massive limestone beds acting as buttresses.*

laminated mudstone is grey-brown weathered, dark grey and very fine grained. A similar relationship between the Lewes River Group and Laberge Group conglomerate is mapped north of Teslin Mountain (Fig. 6). There, fine, brown weathering sandstone and mudstone dip north beneath thick beds of cobble conglomerate.

Fine-grained, thin-bedded clastic sedimentary rocks of the Early to Middle Jurassic Laberge Group are exposed along the western shore of Lake Laberge, on Richthofen Island, and as a discontinuous strip along the eastern shore of Lake Laberge (Fig. 6). Unit JLst comprises dark grey to brown weathering, thin-bedded, slightly calcareous to non-calcareous, dark grey turbiditic mudstone and siltstone (Fig. 26b). Dark grey, thin-laminated mudstone displays interbeds of pale yellow weathering sandstone with angular mudstone intraclasts. Load structures are common between sandstone beds and underlying mudstone, and generally indicate a stratigraphic polarity to the west (Fig. 26b).

Polymictic conglomerate (JLcg)

Grey-brown-rusty to tan weathering, thick-bedded, dominantly matrix-supported, poorly sorted, polymictic pebble to boulder conglomerate (**JLcg**; Fig. 26c) is exposed along steep ridges and cliffs. It includes rounded to subrounded clasts of a variety of compositions:

- sedimentary clasts: dark grey, very fine grained mudstone; pale grey, featureless limy mudstone or cherty limestone;
- intrusive clasts: dark grey-green, plagioclase ± hornblende-phyric diorite; medium-grained, biotite-plagioclase-phyric granodiorite with minor quartz; grey pyroxene-plagioclase-phyric gabbro; K-feldspar-porphyritic monzonite; and
- volcanic clasts: dark grey aphyric basalt; dark green amygdaloidal basalt; hornblende-phyric mafic volcanic rock; red-oxidized, finely vesicular aphyric, aphanitic volcanic rock.

Bedding thickness within the Laberge Group conglomerate ranges from 10 to 30 cm to locally metre-scale. The matrix is a pale yellow weathering, dark grey-green calcareous sandstone rich in biotite, quartz, feldspar and hornblende. Lithic sandstone forms metre-scale interbeds or lenses within the conglomerate.

Figure 26. *Field photographs of Laberge Group units.* ***(a)*** *West-dipping, basal sandstone/mudstone sequence at Mount Laurier;* ***(b)*** *load structures (white arrows) in a steep, west-dipping, slightly calcareous sandstone with dark grey mudstone interbeds;* ***(c)*** *boulder to cobble conglomerate underlain by thinly bedded mudstone and sandstone; and* ***(d)*** *cobble-boulder conglomerate mapped along the eastern shore of Richthofen Island (**JLcbx**), displaying clasts of pale grey micritic limestone (presumably from Upper Triassic Aksala formation), as well as andesite and fine-grained mudstone clasts, in a distinctive, bright, dark green matrix.*

*Dark green conglomerate (*JLcbx*)*

A distinct dark green conglomerate unit is exposed along the eastern shore of Richthofen Island and at several locations on the eastern shore of Lake Laberge, north of Goddard Point, and at Ptarmigan Point (Figs. 6 and 26d). It is composed of dark grey-green weathering, bright green, thick to medium-bedded, matrix-supported, immature, polymictic, poorly sorted cobble to boulder conglomerate locally interbedded with thin-bedded, lenticular mudstone/sandstone. The matrix is composed of pale green, fine-grained, non-calcareous volcanic sandstone with up to 3–4% quartz eyes. Subrounded clasts include pale grey micritic limestone, plagioclase-phyric rhyolite, andesite and dark grey mudstone (Fig. 26d). A maximum depositional age of *ca.* 202 Ma was obtained for this unit (van Drecht, *pers. comm.*).

Nordenskiöld facies

The Nordenskiöld facies (lJN) is a distinct crystal-lithic tuff (Tempelman-Kluit, 1984, 2009), occurring at multiple stratigraphic levels in both the Richthofen and Tanglefoot formations. It represents at least three distinct volcanic events between 188 and 186 Ma in the northern Whitehorse trough (Colpron and Friedman, 2008), but was also recognized and dated in the Lake Laberge area (184 ± 4 Ma; Hart, 1997a). Samples collected east of Lake Laberge were compared to Nordenskiöld samples collected regionally, and compositional and textural similarity was established based on petrographic observations.

Beige-tan weathering, medium-crystalline, equigranular crystal tuff was mapped near the eastern shore of Lake Laberge (Fig. 6). This unit is interbedded with pebble conglomerate and fine-grained sandstone and mudstone of the Laberge Group. The basal contact with thin-bedded mudstone-sandstone is erosive (Fig. 27a). The unit contains subrounded quartz crystals, hornblende and lithic fragments of plagioclase-phyric andesite in a microcrystalline plagioclase-phyric matrix (Fig. 27b). Small centimetre-scale lithic clasts of fine-grained grey mudstone are also present. Magnetic susceptibility for this unit is high (~25 S.I.). Petrographic observations (Fig. 27c) indicate a fragmental volcanic texture, with subrounded lithic fragments of plagioclase-phyric andesite (<1%). The matrix is plagioclase-rich. Crystals include quartz (1%), hornblende (3–5%), plagioclase (70%), opaque minerals (3%) and pyroxene (<1%).

Detrital zircon U/Pb Geochronology

The basal strata of the Laberge Group were sampled for detrital zircons near the contact with the underlying Lewes River Group. The objective was to refine the timing of basin sedimentation and deformation, as well as to identify the primary sources of sediments. Samples were collected in areas where mapping allowed sufficient confidence in the stratigraphy (*i.e.*, in Laberge Group strata immediately overlying confirmed Upper Triassic strata). The material collected ranges from coarse-grained sandstone to pebble-cobble conglomerate with a coarse sandy matrix. Methods are detailed in Chapter 2. Detrital geochronology results are summarized in Table 2, and complete data tables and cathodoluminescence images are in Appendix B.

For each sample analyzed by LA-ICPMS, errors on the dates are at 2σ. For each sample analyzed by CA-TIMS, weighted mean $^{206}Pb/^{238}U$ dates were calculated from equivalent dates (probability of fit >0.05) using Isoplot 3.0 (Ludwig, 2003). Errors on the weighted mean dates are given as ± x / y / z, where x is the internal error based on analytical uncertainties only, including counting statistics, subtraction of tracer solution, and blank and initial common Pb subtraction, y includes the tracer calibration uncertainty propagated in quadrature, and z includes the ^{238}U decay constant uncertainty propagated in quadrature. Errors for weighted mean dates and dates from individual grains are given at 2σ.

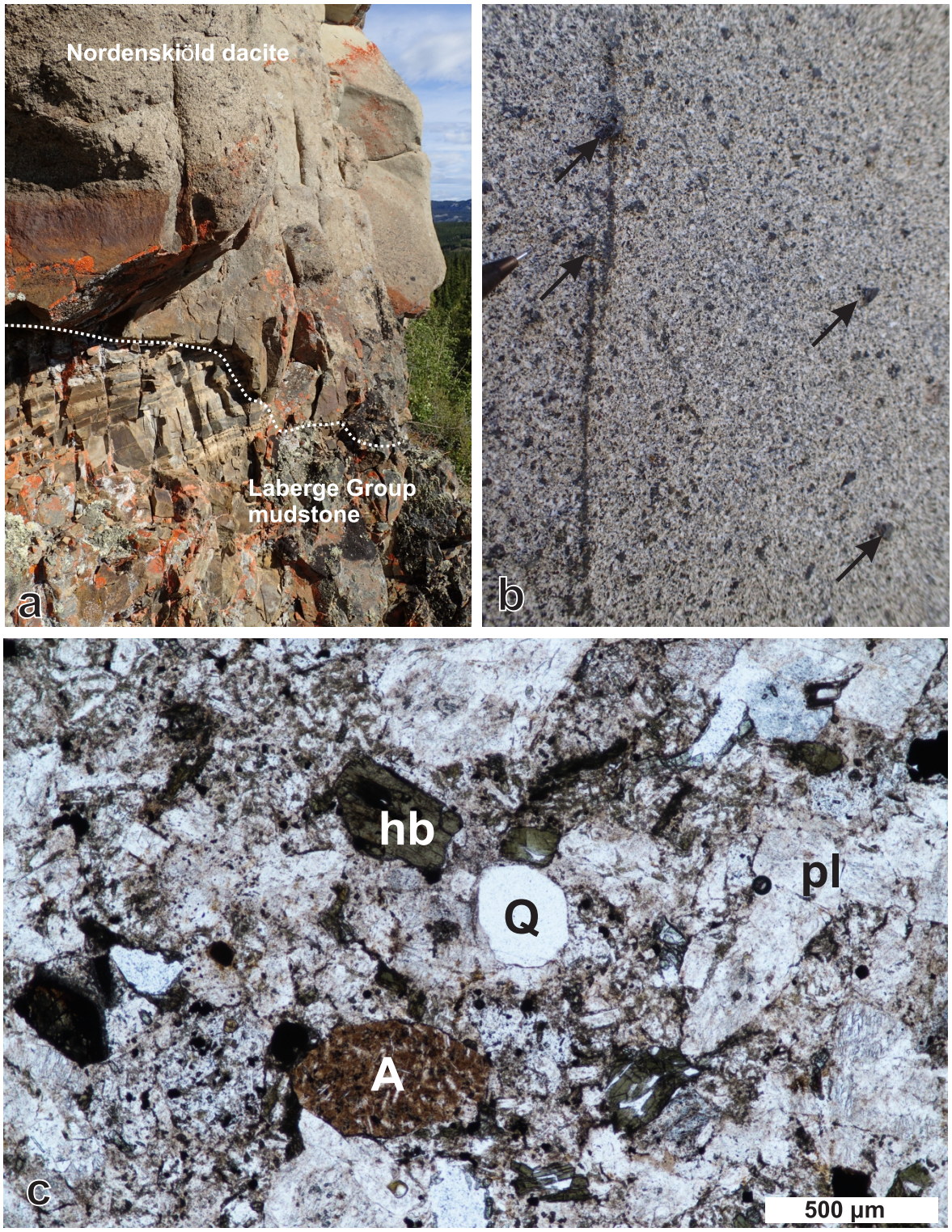

Figure 27. *Occurrence of the Nordenskiöld dacite east of Lake Laberge.* ***(a)*** *Erosional basal contact (white dashed outline) of the Nordenskiöld dacite with underlying thin-bedded, laminated mudstone-sandstone of the Laberge Group;* ***(b)*** *macroscopic view of the outcrop of the Nordenskiöld dacite displaying tan weathering, medium crystalline, equigranular crystal tuff; pencil tip for scale. The matrix contains plagioclase and hornblende, and angular lithic clasts are visible (black arrows); and* ***(c)*** *photomicrograph (plain polarized light) of the Nordenskiöld dacite, characterized by a fragmental volcanic texture. Includes subrounded quartz crystals (Q), lithic fragments of plagioclase-phyric andesite (A), hornblende (hb), plagioclase (pl).*

Sample 15EB-304-1 was collected from a conglomerate unit south of Long Lake (JLcg) immediately overlying the upper contact of Upper Triassic micritic limestone. The coarse sandstone conglomerate groundmass was collected for detrital zircon dating.

LA-ICPMS analyses of 55 grains shows that the youngest 40 dates are equivalent with a weighted mean of 203 ± 3 Ma (MSWD = 0.9, probability of fit = 0.60; Fig. 28a). The other grains yielded *ca.* 346 and 293 Ma dates (Mississippian to Pennsylvanian; Fig. 28a). CA-TIMS of eight grains yielded discordant analyses that form a line with a lower intercept of 202.0 ± 1.8 Ma and an upper intercept of 356 ± 12 Ma (MSWD = 0.45, probability of fit = 0.84). The good fit to the Discordia line indicates that the analyzed grains comprise two components of the same ages. Analyses plot much closer to lower intercept, indicating that the grains are mostly composed of *ca.* 202.0 Ma zircon. This is the interpreted maximum depositional age (Fig. 28b) and the upper intercept of *ca.* 356 Ma is interpreted as the age of inherited cores.

Sample 16EB-181-1 is a tan coloured, non-calcareous, coarse-grained plagioclase-quartz sandstone. It was collected east of Lake Laberge, in an area characterized by Jurassic sandstone and mudstone apparently abutting against Upper Triassic massive limestone strata (Fig. 25). This depositional pattern, likely enhanced by later deformation, makes it challenging to associate units to a single formation, and to distinguish between depositional and structural contacts. This sample was collected because of its apparent stratigraphic position between two massive beds of Upper Triassic limestone. Based on primary field evidence, there is no way to easily distinguish between these two beds, and to decide whether they are different or a single unit related to structural repetition through faulting and stacking, or simply folding.

LA-ICPMS analyses of 100 grains shows a peak at *ca.* 197 Ma and one grain at 349 ± 16 Ma (Fig. 28c). The two youngest dates from the six grains analyzed by CA-TIMS, are equivalent with a weighted mean of 186.22 ± 0.09 Ma (MSWD = 0.02, probability of fit = 0.88; Fig. 28d). The next two oldest grains are equivalent with a weighted mean of 186.49 ± 0.09 Ma (MSWD = 0.00, probability of fit = 0.98). Next oldest grain is 188.65 ± 0.13 Ma, and the oldest is a mixture of two or more components, one of which is older than 204.7 Ma.

Sample 16EB-257-1 was collected from a coarse calcareous sandstone along the eastern shore of Lake Laberge. The interval immediately underlies massive micritic limestone of the Lewes River Group. The contact is likely structural, based on field observations at several locations along this belt, and confirmed by dating.

LA-ICPMS analyses of 89 grains shows a peak at ~204 Ma (Fig. 28e) and several zircons with inherited Mississippian cores, as was observed for sample 15EB-304-1. Five of the six grains analyzed by CA-TIMS yielded discordant dates despite the lack of visible cores in cathodoluminescence images (Appendix B). The youngest date of 203.46 ± 0.14 Ma is a concordant analysis from a grain that is thought to lack a core (Fig. 28f), and thus this is interpreted as the maximum depositional age. The next oldest date at 204.06 ± 14 Ma is a slightly discordant analysis from a grain that likely has a small inherited core (Fig. 28f). Older dates are from moderately discordant analyses that do not form a Discordia line, likely as a result of the inherited cores differing in age. Samples 16EB-257-1 and 15EB-304-1 have similar U/Pb systematics, with inherited Mississippian cores and Late Triassic magmatic rims or whole grains. One difference is that 16EB-257-1 has variable ages of the inherited cores whereas the eight from 16EB-304-1 are the same age at *ca.* 356 Ma. It is likely that the samples have similar sources.

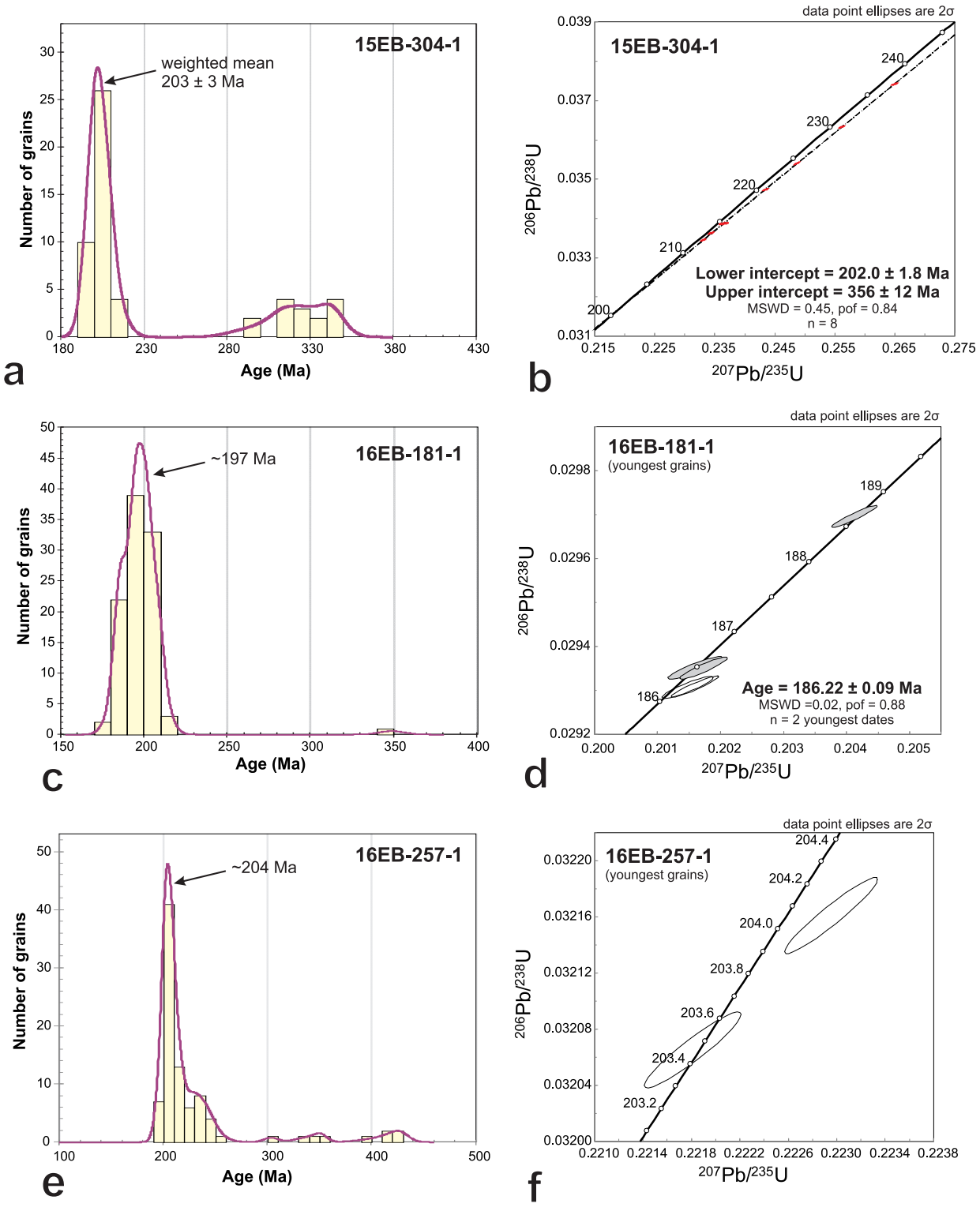

Figure 28. *U/Pb detrital zircon geochronology for samples of the basal Laberge Group. LA-ICPMS results are presented on relative probability plots and CA-TIMS results are presented on Concordia plots.* ***(a,b)*** *Relative probability and Concordia plots for sample 15EB-304-1;* ***(c,d)*** *relative probability and Concordia plots for sample 16EB-181-1;* ***(e,f)*** *relative probability and Concordia plots for sample 16EB-257-1; continued on next page.*

Sample 16EB-384-1 is a slightly calcareous sandstone collected about 6 km from the eastern shore of Lake Laberge. There, shallow dipping layers of sandstone and mudstone are intersected by a 5 m thick granodiorite dike.

LA-ICPMS analyses of 99 grains shows a peak at ca. 197 Ma (Fig. 28g). One older grain is 362 ± 15 Ma. The three youngest dates from the six grains analyzed by CA-TIMS are equivalent with a weighted mean of 186.38 ± 0.07 Ma (MSWD = 0.6, probability of fit = 0.54; Fig. 28h). Three other grains are 187.54 ± 0.13 to 189.30 ± 0.13 Ma.

Sample 16EB-394-1 is a non–calcareous, coarse crystal-rich sandstone to granule conglomerate from the eastern shore of Lake Laberge. It is located immediately east of the thrust fault contact with structurally overlying carbonate strata of the Lewes River Group.

LA-ICPMS analyses of 59 grains indicate that 54 dates are equivalent with a weighted mean of 200 ± 3 Ma (MSWD = 1.1, probability of fit = 0.25; Fig. 28i). The five youngest dates from six grains analyzed by CA-TIMS are equivalent with a weighted mean of 199.78 ± 0.06 / 0.12 / 0.24 Ma (MSWD = 2.2, probability of fit = 0.07; Fig. 28j), which is the interpreted maximum depositional age. One other grain yielded a date of 219.78 ± 0.06 Ma.

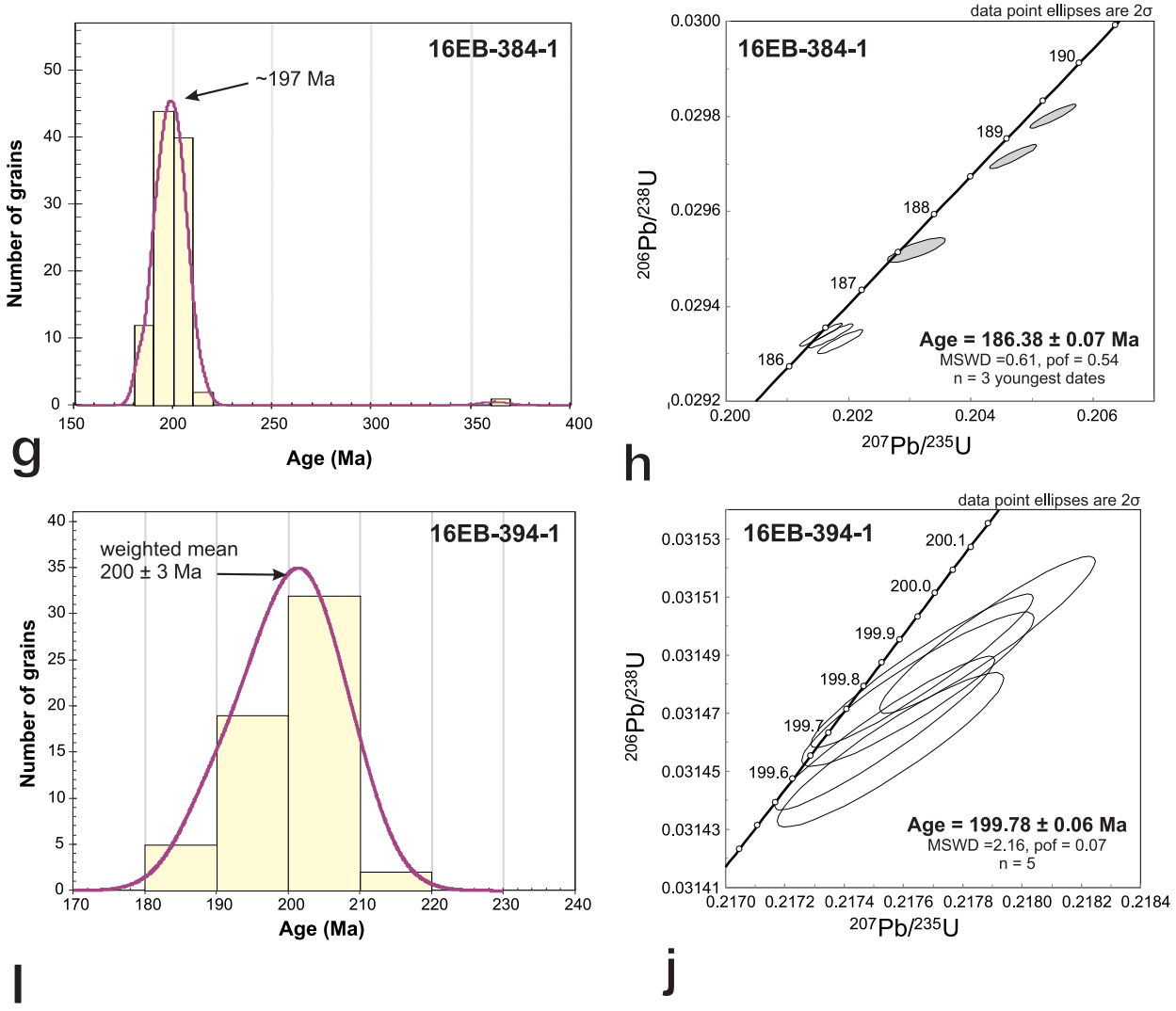

Figure 28 continued. ***(g,h)*** *relative probability and Concordia plots for sample 16EB-384-1; and* ***(i-j)*** *relative probability and Concordia plots for sample 16EB-394-1. Ellipses in grey on Concordia plots are not included in weighted mean calculations.*

Summary

Mapping suggests lateral facies changes within the Laberge Group from west to east. East of the Laurier Creek fault, the Laberge Group is dominated by cobble to boulder polymictic conglomerate interpreted to represent submarine fan channel deposits (Dickie and Hein, 1995; Lowey, 2005, 2008). The lithology west of the Laurier Creek fault, along Lake Laberge and on Richthofen Island, is dominated by fine-grained, thin-bedded turbiditic mudstone/sandstone, locally interbedded with granule to cobble polymictic conglomerate. This lithology is related to relatively deep-basin sedimentation. Limited conglomerate exposures within the turbiditic sequence to the west may be the result of localized channel activity.

Geochronology constrains the maximum deposition age for the basal strata of Laberge Group to between 203 and 186 Ma. Detrital zircon ages within rocks of the Laberge Group across the Whitehorse trough are consistent with these results with maximum deposition ages between 209 and 201 Ma (van Drecht, *pers. comm.*) and ~220 and 180 Ma (Colpron *et al.*, 2015). In addition, most Laberge Group samples display a subsidiary population of late Paleozoic detrital zircons, dominated by Mississippian dates. This observation is consistent with detrital zircon populations within the Aksala formation (Fig. 29). This suggests that both the youngest strata of the Lewes River Group and the basal Laberge Group strata were sourced from Paleozoic successions of Stikinia and Quesnellia, or the Yukon-Tanana terrane. A stratigraphic discontinuity is observed at the base of the Laberge Group in the map area, which indicates that latest Triassic deformation took place before deposition of the Laberge Group.

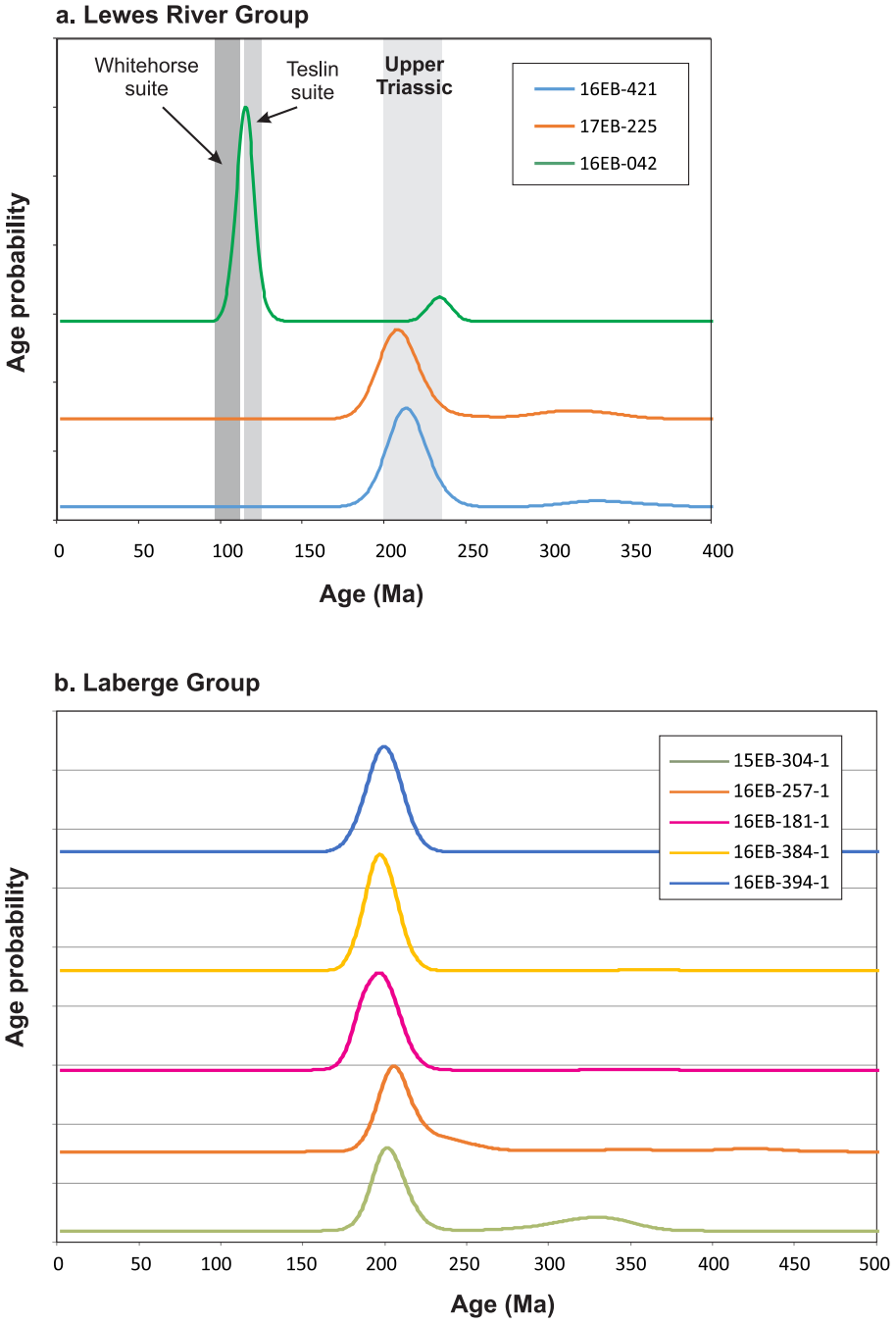

Figure 29. *Detrital zircon signatures for samples of* **(a)** *the Lewes River Group and* **(b)** *the Laberge Group.*

Chapter 4 – Post-Accretionary Magmatism

Bedrock mapping in the eastern Lake Laberge area identified several plutons and dikes intruding Middle Triassic to Middle Jurassic stratigraphy (Fig. 30). Field and petrographic descriptions of these rocks are presented below. The geochemical and trace elements signatures of dikes and plutons along with precise U/Pb radiometric dating highlight a complex evolution of magmatic and tectonic processes in this area.

Magmatic rock units

Igneous rocks in the map area include the Middle Jurassic Teslin Crossing pluton, the Early Cretaceous Cap Creek, M'Clintock (Hart, 1997a) and Laurier Creek plutons, and the Late Cretaceous Teslin Mountain pluton and its volcanic equivalent the Open Creek volcanic complex (Fig. 30). A few occurrences of mid-Cretaceous Byng Creek volcanic rocks (Byng suite) and its intrusive equivalent are reported south of Joe Mountain and described in previously published literature (Hart and Hunt, 1997a, 2003b; Hart, 1997a). In addition, a discrete but widespread intrusive igneous system is composed of hundreds of dikes (Fig. 30).

Plutonic rocks

*Teslin Crossing pluton (*MJB*)*

The Teslin Crossing pluton is an ~5 by 10 km body located in the northeastern part of the map area (Fig. 30). Limited exposures of the pluton are visible along a north-trending alpine ridge. Contact with Early-Middle Jurassic strata was mapped at the southern edge of the igneous body. The pluton is characterized by medium to coarse-grained monzonite, monzodiorite and syenite. Related dikes of dacite to andesite porphyry with euhedral andesine, hornblende and locally quartz in aphanitic greenish, or grey groundmass are also reported (Tempelman-Kluit, 1984, 2009). A U/Pb date of 171.62 ± 0.05 Ma is reported for the Teslin Crossing pluton (Yukon Geochronology, 2018). The Teslin Crossing pluton hosts the porphyry Cu-Mo-Au Mars prospect (Yukon MINFILE 105E 002).

*Laurier Creek pluton (*EKgT*)*

The Laurier Creek pluton is characterized by grey to tan-weathering, white to pale pink, equigranular, medium to coarse-grained granodiorite, monzonite, monzodiorite and quartz diorite. It forms an ~5 by 12 km pluton to the southwest of Teslin Mountain (Fig. 30). The M'Clintock plutons exposed near Mount Byng (Fig. 30) present similar compositions and textures (Hart, 1997a). The Laurier Creek pluton intrudes mainly Joe Mountain Formation aphyric basalt, but also the Lewes River Group sedimentary succession to the west. The following description is based on observations along the northern and western contacts of the intrusion with Joe Mountain Formation and Lewes River Group rocks. The intrusion is characterized by:

- equigranular, medium to coarse-grained granodiorite, which includes plagioclase (50%), biotite (25–30%), quartz (15%) and hornblende (up to 5%);
- equigranular, medium to coarse-grained monzonite and monzodiorite containing hornblende and lesser biotite to the west (up to 25%; Fig. 31a), and biotite (5–7%) and lesser hornblende (1–2%) towards the centre of the intrusion, in a plagioclase-rich groundmass. The rock locally displays up to 1–5% quartz (1–2 mm large crystals) and possible K-feldspar. A weak internal foliation is locally present; and

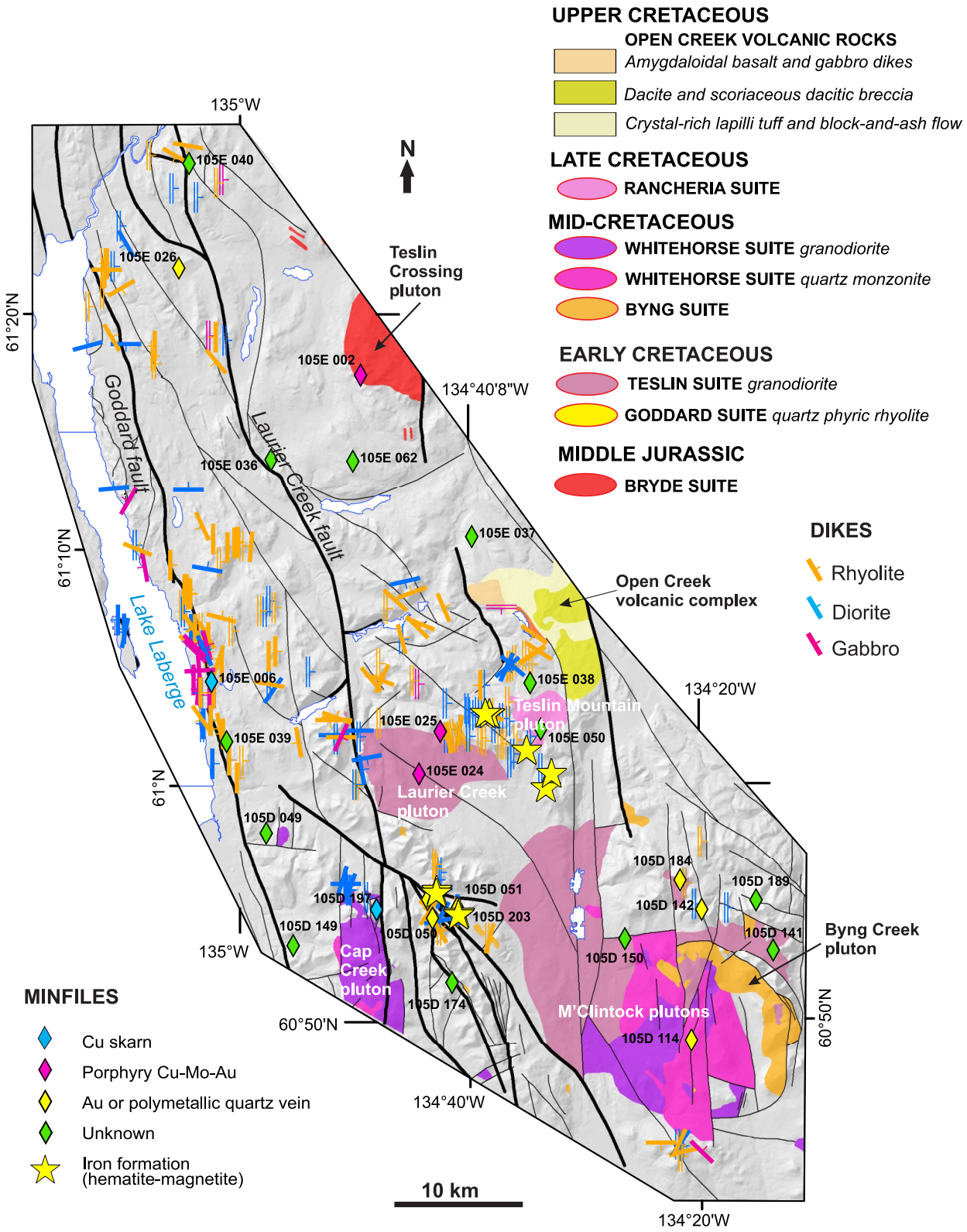

Figure 30. *Distribution of Cretaceous plutons, dikes and Yukon MINFILE occurrences in the map area (after Yukon MINFILE, 2018). Iron formation occurrences mapped for this study are indicated by yellow stars.*

- various dike phases are associated with the main intrusion, including a tan to yellow-weathering, pale pink, equigranular, fine to medium-grained quartz-rich granite composed of quartz (>50%), plagioclase (45%), biotite (5%) and hornblende-rich veins.

East of Mount Laurier, the contact between the monzodiorite and carbonate rocks of the Lewes River Group is marked by the development of skarn, characterized by garnet crystals, 1–2 cm in diameter, in a pale green carbonate matrix (Fig. 31b).

Teslin Mountain pluton (LKgR ***and*** LKdR***)***

The Teslin Mountain pluton is an ~4 by 3 km massive, blocky, medium-grained, grey weathering, pale grey to white monzodiorite (LKgR) that intrudes Joe Mountain Formation basalt at Teslin Mountain (Fig. 31c). It contains plagioclase (40–60%), K-feldspar (up to 15%), biotite (10–15%), hornblende (10–20%) and quartz (1–3%). Another phase (LKdR, Fig. 31d) comprises tan to grey weathering, massive, blocky, fine-grained, dark grey-green diorite (1–2% quartz) and quartz diorite (5–10% quartz), which contains plagioclase (10–15% and locally up to 50%), biotite or hornblende (5–15%).

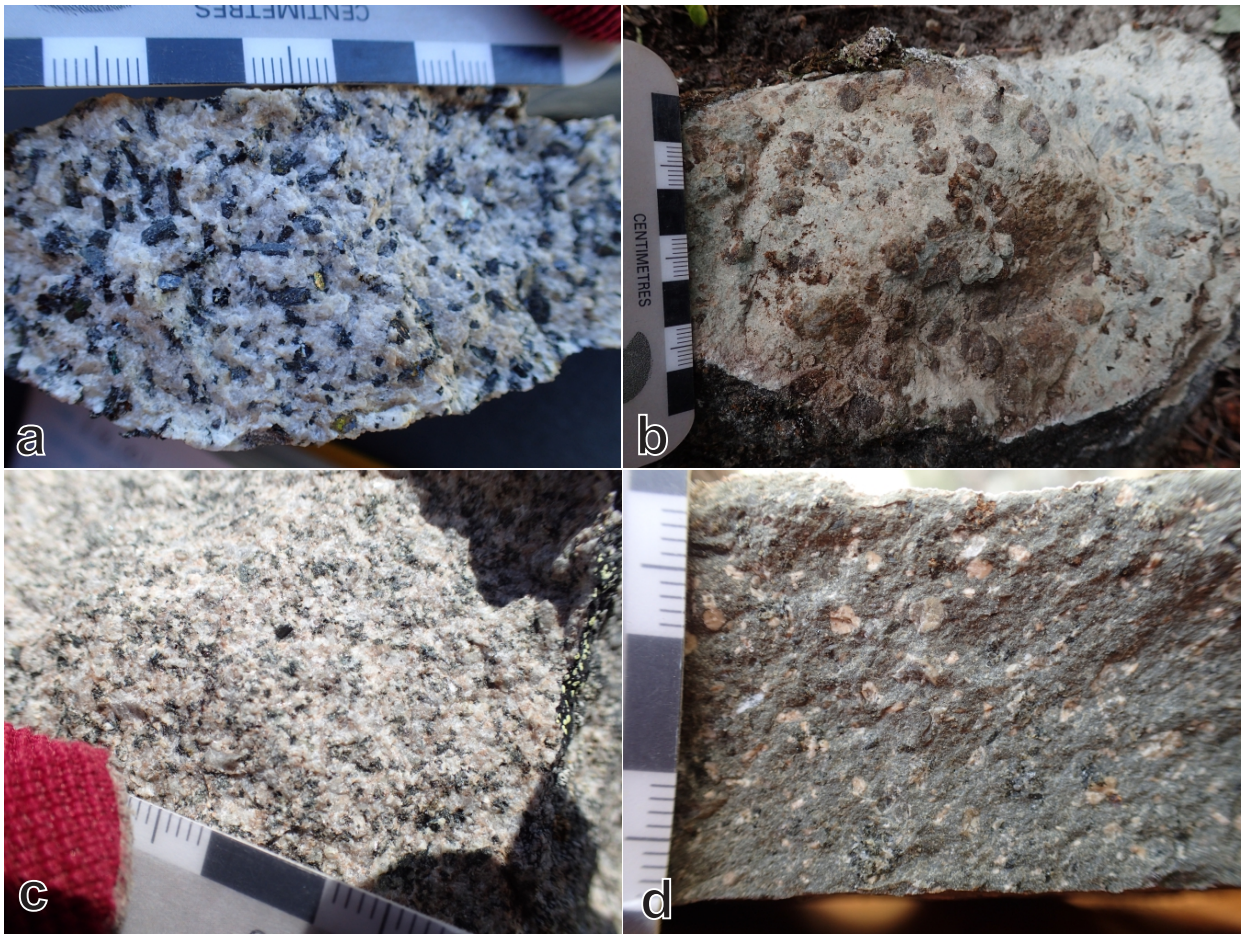

Figure 31. *Field photographs of intrusive units.* ***(a)*** *Coarse-crystalline, equigranular, hornblende-biotite porphyritic monzodiorite of the Laurier Creek pluton (*EKgT*);* ***(b)*** *skarn (cm-scale garnet crystals in a pale green calcareous matrix) resulting from contact metamorphism between the Laurier Creek pluton and Upper Triassic limestone;* ***(c)*** *medium-crystalline, equigranular, granodiorite of the Teslin Mountain pluton (*LKgR*); and* ***(d)*** *hornblende-plagioclase porphyritic diorite at Teslin Mountain (*LKdR*).*

Dikes

More than 200 dikes intrude the Triassic to Jurassic stratigraphy in the map area (Fig. 30). Petrography and mapping identified a variety of textures and compositions. Dikes locally display a magmatic foliation and are generally oriented north-south (see Chapter 5). At least three different dike compositions are reported:

- brown weathering, conchoidally fractured, dark grey-green gabbro dikes with pyroxene (1–2%) and plagioclase (5%) in a fine-crystalline, dark grey groundmass are less common (~8% of all dikes; Fig. 32a,b). They are spatially concentrated along the eastern shore of Lake Laberge, and crosscut massive micritic limestone of the Lewes River Group, as well as thin-bedded mudstone at the base of the Laberge Group (Bordet, 2017). These gabbro dikes appear to be folded along with the Upper Triassic-Jurassic sequence;
- grey to beige weathering, grey, porphyritic dacite and rhyodacite dikes are widespread (~36% of all the dikes; Fig. 32c,d). They have a grey-green, aphanitic to finely crystalline equigranular groundmass. Phenocrysts include plagioclase (5 mm to 2 cm; 10–15%, and up to 25%), hornblende (1–5%, and up to 10%; laths up to 1 cm) and quartz (<1%); and
- pale pink/orange/beige to tan weathering, massive to blocky or locally foliated rhyolite quartz-phyric dikes are most common (~56% of all the dikes; Fig. 32e,f). They display a fine to medium-crystalline, pale pink to grey groundmass, and contain up to 10–60% plagioclase. Phenocrysts include K-feldspar (5–25%), quartz (1–10%) and hornblende or biotite (1–5%). These dikes commonly display pervasive carbonate alteration of the cryptocrystalline groundmass. Biotite crystals are locally chlorite and carbonate altered.

Open Creek volcanic complex

Dark grey to brown weathering dacite lava, tephra and chaotic volcanic breccia are exposed northeast of Teslin Mountain and west of Open Creek (Fig. 29). These rocks were previously described by Tempelman-Kluit (1984, 2009), and informally named “Open Creek volcanics”. They cover an area of at least 5 by 10 km and are best exposed along the eastern flank of a north-trending ridge, which also marks the boundary of a landslide scarp. Open Creek volcanic rocks unconformably overlie the Laberge Group and Joe Mountain Formation, but contacts are not exposed.

The volcanic complex is dominated by a thick ignimbrite sequence (uKOt), overlain by indurated dacite lava and breccia (uKOd; Fig. 33a). Crystal-rich lapilli tuff and block-and-ash flow form a ≥400 m thick ignimbrite sequence. Grey to rainbow weathering, beige-tan coloured, lithic-crystal lapilli ash tuff (Fig. 33b) has up to 15% crystals (quartz, biotite, plagioclase), 5–10% angular and rounded lithic clasts (plagioclase-phyric andesite or dacite), and 2–5% pumice lapilli (Fig. 33c). Elongated vesicles are visible in the upper part of the ignimbrite below the contact with overlying dacite lava. The block-and-ash flow (Fig. 33d) has a white-pale green silicic ash matrix containing crystals (biotite, plagioclase and hornblende) and lapilli-sized lithic fragments. Blocks are up to 1 m in size, subrounded, and of intermediate-silicic composition. Composition of the ignimbrite sequence is rhyodacite to rhyolite.

The ignimbrite sequence is capped by brown-grey weathering, brown, aphyric to plagioclase (1-2%), pyroxene (2–3%) ± hornblende (1%) porphyritic, massive to columnar jointed or flow-banded indurated dacite (Fig. 33e–g). It includes brown to rusty weathering, matrix-supported scoriaceous dacite breccia and autobreccia.

Grey-brown weathering, massive, grey, plagioclase (20%), biotite (1–3%), hornblende (7–10%) coarsely porphyritic diorite (uKO) sits at the base of the volcanic complex, and is likely a feeder to the volcanic sequence.

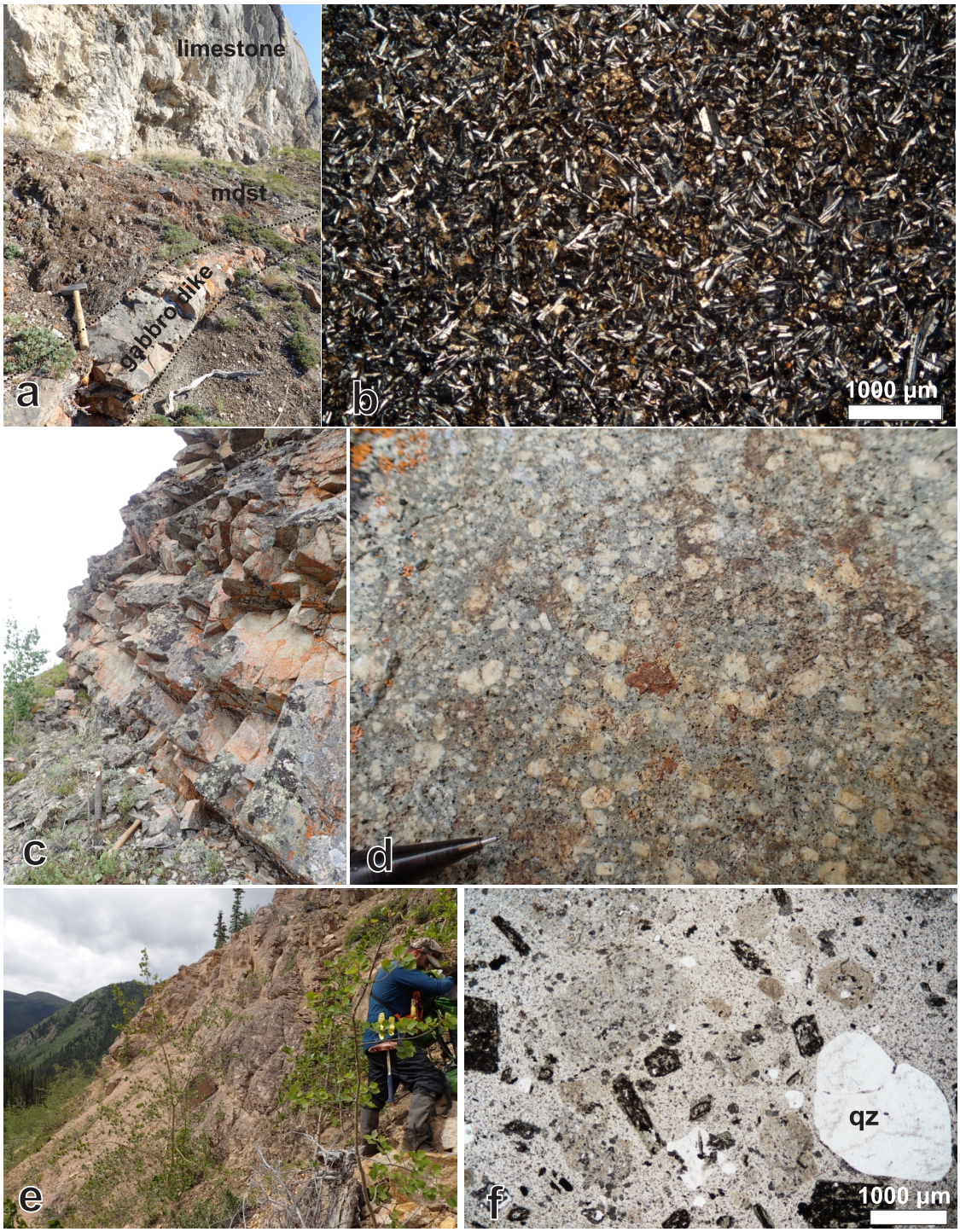

Figure 32. *Dikes textures and compositions.* ***(a)*** *Outcrop photograph of an ~30 cm thick gabbro dike. At this location, Upper Triassic limestone is thrust over Early-Middle Jurassic mudstone of the Laberge Group. The dike intrudes the Jurassic sequence and is parallel to bedding;* ***(b)*** *petrographic view (cross-polarized light) of the gabbro dike. Texture is equigranular, microcrystalline, essentially composed of plagioclase and pyroxene crystals;* ***(c)*** *outcrop photograph of an ~5 m wide rhyodacite dike intruding sedimentary strata of the Laberge Group;* ***(d)*** *macroscopic field photograph of the rhyodacite dike. Texture is porphyritic, with plagioclase phenocrysts, and biotite and hornblende microcrystals, in a pale grey aphanitic groundmass;* ***(e)*** *outcrop photograph of an ~10 m thick plagioclase-quartz porphyritic rhyolite dike intruding mudstone of the Laberge Group; and* ***(f)*** *petrographic view (plain polarized light) of a quartz-plagioclase-biotite porphyritic rhyolite dike. The groundmass is pervasively carbonate altered.*

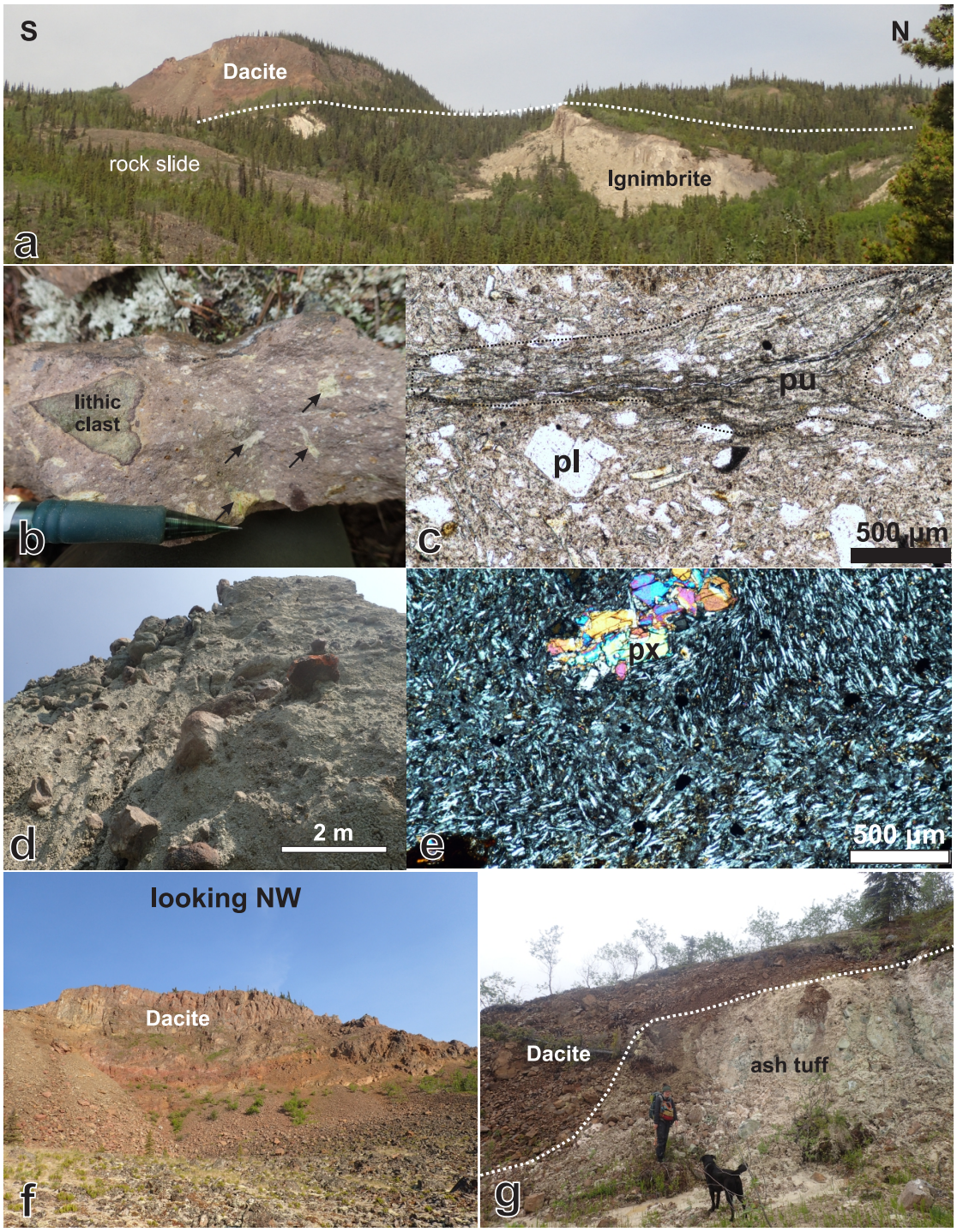

Figure 33. *Late Cretaceous Open Creek volcanic complex.* ***(a)*** *View looking west of the Open Creek volcanic complex. Indurated dacite lava and breccia cap an ~400 m thick ignimbrite sequence;* ***(b)*** *macroscopic view of the lapilli-ash tuff forming the ignimbrite. Pumice clasts indicated with black arrows;* ***(c)*** *petrographic view (plain polarized light) of the lapilli-ash tuff forming part of the ignimbrite sequence. Crystals include, plagioclase (pl), quartz. A pumice clast is outlined and labelled (pu);* ***(d)*** *block-and-ash flow sequence containing metre-sized blocks of dacitic lava in an ash-tuff matrix;* ***(e)*** *petrographic view (cross-polarized light) of the dacite lava. The groundmass comprises microcrystalline plagioclase crystals, rare pyroxene phenocrysts are observed (px);* ***(f)*** *close-up of the indurated dacite cap, looking NW; and* ***(g)*** *the contact between the basal clay-altered ignimbrite ash-tuff and overlying dacite lava.*

Isolated exposures of brown weathering, dark grey-brown, pyroxene-plagioclase porphyritic vesicular to amygdaloidal basalt and gabbro dikes (uKOb) are mapped to the west of the ignimbrite sequence (Fig. 29), but their relationship with the rest of the stratigraphy is unclear. Centimetre-scale quartz-filled amygdules within the basalt are similar to textures found in the Late Cretaceous Carmacks Group in the area west of Carmacks (Tempelman-Kluit, 2009). Therefore, it is possible that these basalts are correlative to those of the Carmacks Group rather than part of the Open Creek volcanic sequence.

The nature of the Open Creek volcanic succession suggests a period of explosive volcanism, leading to the deposition of an ignimbrite sequence at least 400 m thick. The ignimbrite comprises block-and-ash flow deposits, as well as crystal-lithic rich lapilli-ash tuff. Metre-sized blocks of dacite in the block-and-ash flow sequence, as well as primary volcanic textures in the rest of the ignimbrite sequence, suggest that these deposits are relatively proximal to a volcanic centre. The dacitic sequence capping the ignimbrite displays a range of textures from flow to monomictic breccia. Again, the texture of the flows and breccia suggest they were emplaced proximally relative to a volcanic centre.

The area where Open Creek volcanic rocks are exposed displays signs of active landslide and rockslide activity (Fig. 33a). In fact, the highly porous, ash matrix of the ignimbrite sequence is altered into clay-rich soil, creating an unstable slippery layer responsible for the collapse of the upper dacite lava.

U/Pb geochronology

Large plutons that intersect Triassic and Jurassic stratigraphy were previously dated using the K/Ar method on whole rock or minerals, and occasionally with U/Pb dating techniques on zircons (Stevens *et al.*, 1982; Hunt and Roddick, 1987; Hart, 1997a; Appendix B4). New, precise U/Pb dates from various plutonic suites and dikes are presented below to support interpretations of the magmatic evolution of the area. In addition, two samples of volcanic rocks from the Open Creek volcanic complex were dated.

Radiometric dating methods are described in Chapter 2. Results are summarized in Table 2, and complete data tables and cathodoluminescence images are in Appendix B3. For each sample analyzed by LA-ICPMS, errors on the dates reported below are at 2σ. For each sample analyzed by CA-TIMS, weighted mean $^{206}Pb/^{238}U$ dates were calculated from equivalent dates (probability of fit >0.05) using Isoplot 3.0 (Ludwig, 2003). Errors on the weighted mean dates reported below are given as ± x / y / z, where x is the internal error based on analytical uncertainties only, including counting statistics, subtraction of tracer solution, and blank and initial common Pb subtraction, y includes the tracer calibration uncertainty propagated in quadrature, and z includes the ^{238}U decay constant uncertainty propagated in quadrature. Errors for weighted mean dates and dates from individual grains are given at 2σ.

Laurier Creek pluton

Sample 16EB-001-1 was collected from a pink-grey-white weathered monzodiorite part of the Laurier Creek pluton, east of Mount Laurier. It comprises plagioclase (up to 75%), hornblende (20%, up to 5 mm elongate), and biotite (~5%, 2 mm). Six grains analyzed by CA-TIMS dates yielded equivalent dates with a weighted mean of 115.54 ± 0.03 / 0.07 / 0.14 Ma (MSWD = 1.7, probability of fit = 0.13), which is interpreted as the crystallization age (Fig. 34c). This is similar to a previous date of *ca.* 118 ± 3 Ma from the eastern part of the Laurier Creek pluton (K/Ar biotite; Stevens *et al.*, 1982; Bordet, 2019 and Appendix B4).

Teslin Mountain pluton

Sample 15EB-109-1 is a tan-grey weathered, massive blocky, pale white-pink granodiorite collected from the Teslin Mountain pluton. It contains plagioclase (40–50%), hornblende (15–20%), biotite (10%), quartz (~1–2%), and minor K-feldspar. Cathodoluminescence imaging indicates a homogeneous population of igneous zircons without cores (Appendix B). Five grains analyzed by CA-TIMS yielded equivalent dates with a weighted mean of 78.14 ± 0.03 / 0.05 / 0.10 Ma (MSWD = 0.5, probability of fit = 0.77), which is the interpreted igneous crystallization age (Fig. 34g).

Dikes

Sample 16EB-384-2 was collected from an ~5 m thick, tan weathering, pale grey porphyritic felsic dike. It contains plagioclase (30%), hornblende (5–10%) and minor biotite crystals in a pale grey, aphanitic groundmass. LA-ICPMS of 32 grains shows the youngest 26 dates are equivalent with a weighted mean of 136 ± 2 Ma (MSWD = 1.2, probability of fit = 0.20). Six grains analyzed by CA-TIMS grains yielded equivalent dates with a weighted mean of 138.06 ± 0.04 / 0.08 / 0.1 Ma (MSWD = 0.9, probability of fit = 0.47; Fig. 34a), which is the interpreted igneous crystallization age.

Sample 15EB-222-1 was collected from a pale pink-yellow weathered quartz-phyric rhyolite dike intruding Laberge Group strata south of Long Lake. The mineralogy is characterized by quartz phenocrysts (~5%) and plagioclase (~60%). Six grains analyzed by CA-TIMS yielded equivalent dates with a weighted mean of 135.79 ± 0.04 / 0.08 / 0.16 Ma (MSWD = 1.1, probability of fit = 0.37; Fig. 34b), which is the interpreted igneous crystallization age.

Sample 17EB-177-1 is from an ~10 m wide dark grey hornblende-plagioclase porphyritic diorite dike, intruding mafic volcaniclastic sandstone and breccia of the Lewes River Group. The rock has a grey-green aphanitic matrix with ~15% plagioclase crystals up to 1 cm diameter, and ~15% hornblende crystals up to 1 cm long. LA-ICPMS of 46 grains yielded 25 equivalent dates with a weighted mean of 114 ± 2 Ma (MSWD = 1.3, probability of fit = 0.15). Five grains analyzed by CA-TIMS yielded a weighted mean $^{206}Pb/^{238}U$ date of 113.94 ± 0.04 / 0.07 / 0.14 Ma (MSWD = 0.6, probability of fit = 0.66), which is the interpreted igneous crystallization age (Fig. 34d).

Sample 17EB-163-2 is from a coarse crystalline dioritic intrusion dominated by plagioclase (>70%), biotite (~20%), and hornblende (~5%). LA-ICPMS of 31 grains yielded dates of 122 ± 6 to 107 ± 5 Ma. The two youngest dates from the six grains analyzed by CA-TIMS are equivalent with a weighted mean of 111.06 ± 0.06 / 0.08 / 0.14 Ma (MSWD = 3.2, probability of fit = 0.07), which is the interpreted igneous crystallization age (Fig. 34e). Four other grains yielded dates of 111.31 ± 0.08 to 111.56 ± 0.08 Ma.

Sample 16EB-267-1 is from a microcrystalline gabbro dike intersecting Laberge Group sandstone and mudstone strata exposed on the eastern shore of Lake Laberge. Cathodoluminescence imaging shows that grains are highly elongate and prismatic (Appendix B), characteristic of zircons from mafic rocks; their chemistry confirms this, with high Th/U (~1.0), high total REE concentrations (1000–6000 ppm), high Ti-in-zircon temperatures (800°C), and small Eu anomaly (Eu/Eu* = 0.6). LA-ICPMS analyses of nine grains shows that the eight youngest dates are equivalent with a weighted mean of 105.4 ± 2.4 Ma (MSWD = 1.8, probability of fit = 0.084). Four grains analyzed by CA-TIMS yielded equivalent dates with a weighted mean of 105.91 ± 0.04 / 0.07 / 0.13 Ma (MSWD = 0.8, probability of fit = 0.51), which is the interpreted igneous crystallization age (Fig. 34f).

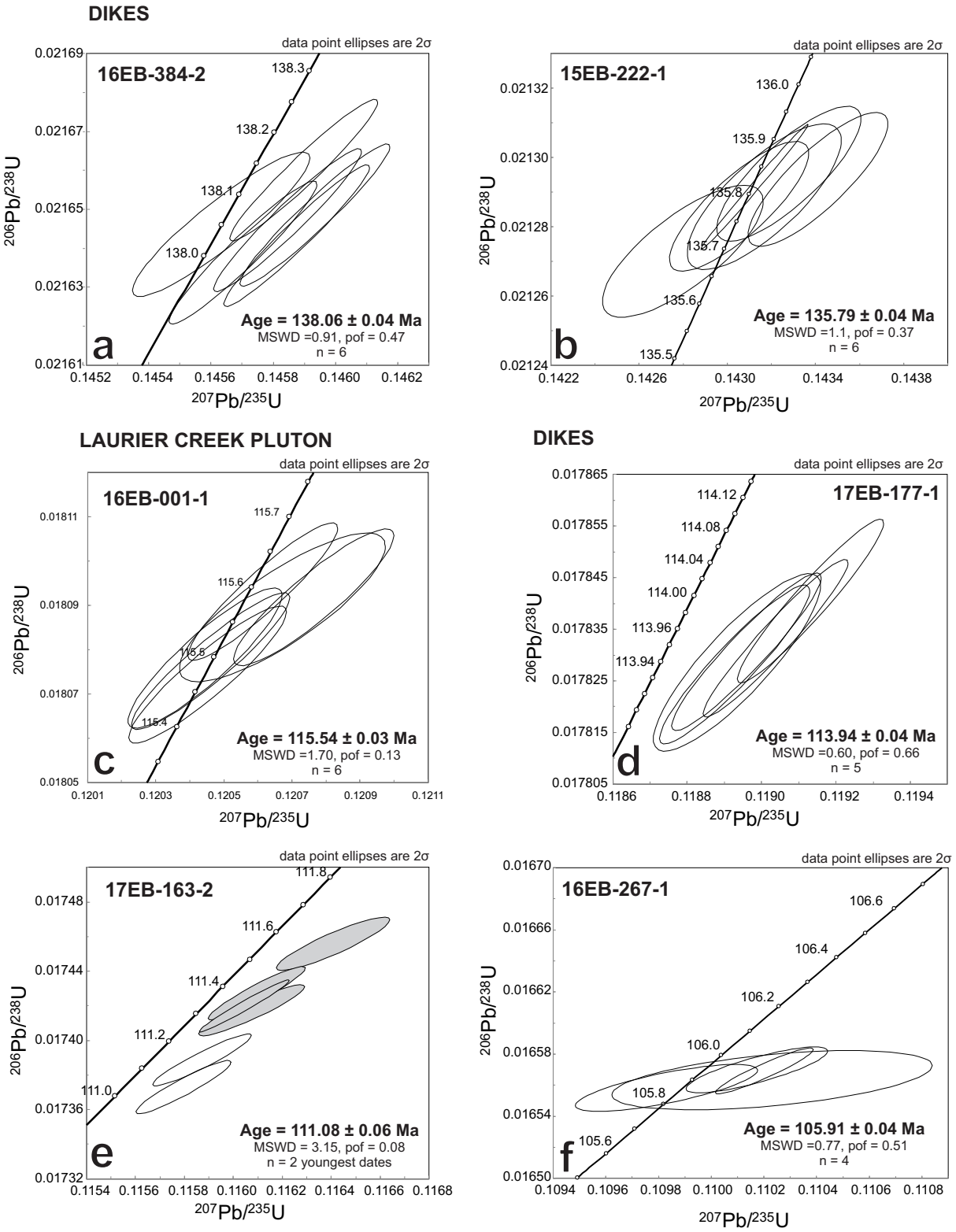

Figure 34. *Concordia plots of CA-TIMS analyses for Cretaceous plutons and dikes. Ellipses in grey are not included in weighted mean calculations.* ***(a,b)*** *Samples 16EB-384-2 and 15EB-222-1 collected from felsic dikes;* ***(c)*** *sample 16EB-001-1 from the Laurier Creek pluton;* ***(d)*** *sample 17EB-177-1 from an intermediate dike;* ***(e,f)*** *samples 17EB-163-2 and 16EB-267-1 from dikes; continued on next page.*

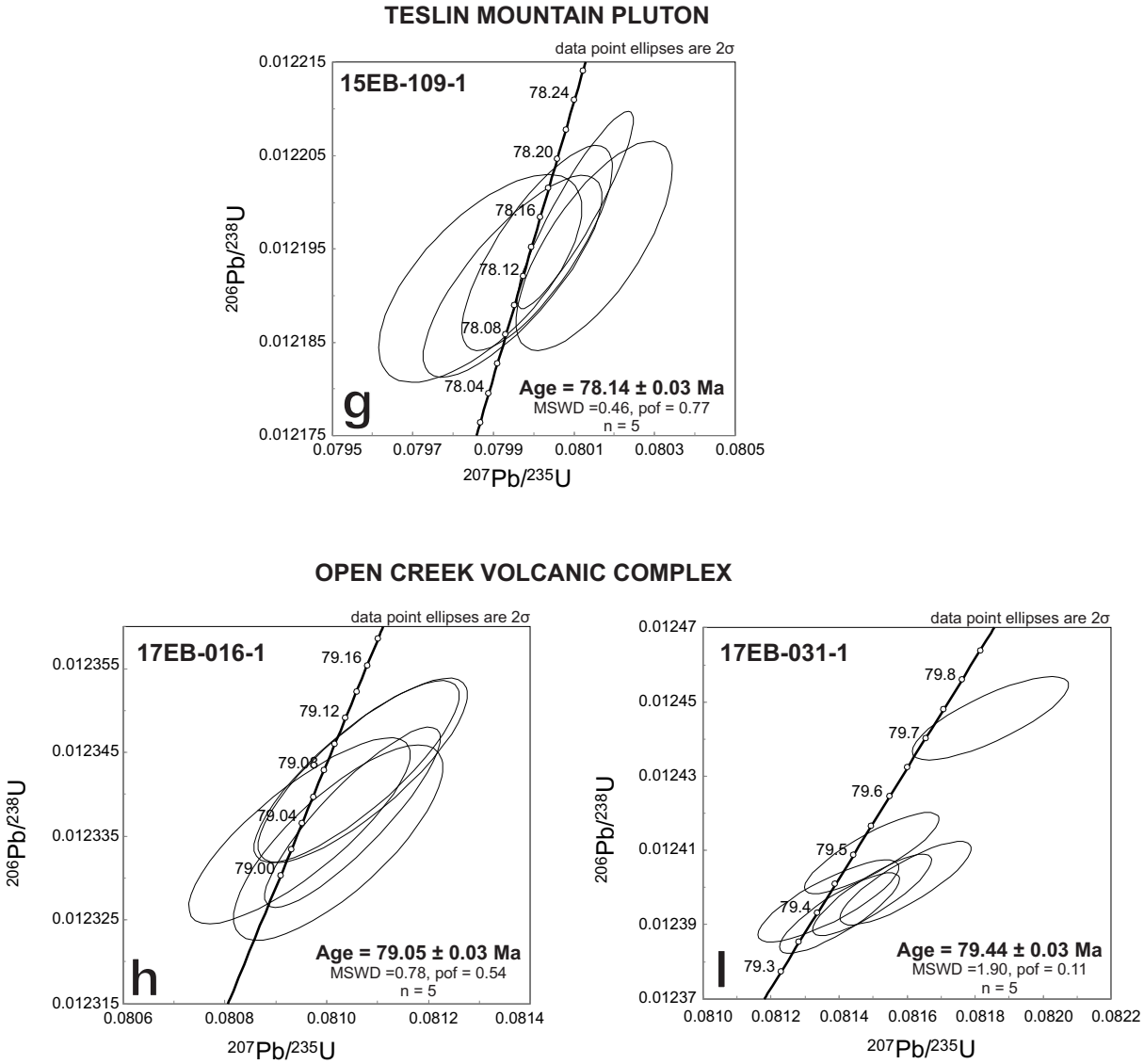

***Figure 34** continued. **(g)** sample 15EB-109-1 from the Teslin Mountain pluton; and **(h,i)** samples 17EB-016-1 and 17EB-031-1 from lithic-crystal tuff deposits part of the Open Creek volcanic complex.*

Open Creek volcanic complex

Sample 17EB-016-1 is a beige-brown weathering, pale beige crystal lithic lapilli tuff collected from the Open Creek volcanic complex. Lithic clasts are angular, dark grey dacite and plagioclase-phyric andesite. The pale beige tuffaceous matrix contains ~1% quartz and biotite, and ~2–5% pumice lapillis. Five grains analyzed by CA-TIMS yielded equivalent dates with a weighted mean of 79.05 ± 0.03 / 0.05 / 0.10 Ma (MSWD = 0.8, probability of fit = 0.54), which is the interpreted eruption age (Fig. 34h).

Sample 17EB-031-1 was collected from the matrix of a monomictic block–and-ash flow part of the Open Creek volcanic complex. The pale yellow clay-rich matrix supports crystals of biotite, plagioclase and hornblende, as well as lapilli-size lithic clasts and subrounded boulders of dacite. The five youngest dates from CA-TIMS analysis of six grains are equivalent with a weighted mean of 79.44 ± 0.03 / 0.05 / 0.10 Ma (MSWD = 1.9, probability of fit = 0.11), which is the interpreted pyroclastic eruption age (Fig. 34i). One other grain yielded a date of 79.73 ± 0.06 Ma.

The Open Creek volcanic rocks were originally dated at 80.0 ± 2.3 Ma (whole rock, K/Ar; Stevens *et al.*, 1982). This sample was collected from an exposure along Boswell River to the east of the present study area, and correlated with volcanic rocks exposures north of Teslin Mountain (Tempelman-Kluit, 2009). Two new U/Pb dates of 79.05 ± 0.03 Ma and 79.44 ± 0.03 Ma, obtained from the ignimbrite sequence, indicate that the volcanism is coeval with emplacement of the Teslin Mountain pluton, located just a few kilometres to the south.

Lithogeochemistry

Geochemical analyses were conducted to assess the geochemical composition of each of the Early Cretaceous, mid-Cretaceous, and Late Cretaceous magmatic pulses. Analytical methods are the same as those described in Chapter 2. Data tables are presented in Appendix C3. Thirty samples were selected; 2 samples from the Teslin Mountain pluton, 1 sample from the Laurier Creek pluton, 5 samples from the Open Creek volcanic rocks, 8 samples of intermediate dikes (diorite), 4 samples of mafic dikes (gabbro), and 10 samples of felsic dikes (rhyolite). Samples are representative of the range of ages and compositions within the Cretaceous magmatic rocks, and are distributed throughout the map area and across different units to identify possible spatial variations in composition.

Geochemical composition and classification

Geochemical compositions for Cretaceous plutons range from gabbro to granodiorite and diorite (Fig. 35a,b; LeBas *et al.*, 1986; Pearce, 1996 for intrusive rocks), with a majority being of granodiorite silicic composition. The Laurier Creek pluton (Early Cretaceous Teslin suite) and Cap Creek pluton (mid-Cretaceous Whitehorse suite) are dominated by granodiorite, quartz diorite, monzonite and monzodiorite. The Teslin Mountain pluton (Rancheria suite), as well as its volcanic equivalent Open Creek complex, display compositions ranging from gabbro/basalt to granite/rhyolite, with most compositions in the diorite-granodiorite/dacite-rhyodacite fields. Plutons and dikes are dominated by calc-alkaline, I-type granite and granodiorite (Fig. 35c) composed of plagioclase, quartz ± biotite and/or hornblende crystals.

The field classification of dikes is based on mineral assemblages, and matches their geochemical composition. Porphyritic dikes with a mineralogy dominated by quartz, plagioclase, and minor mafic minerals such as biotite and/or hornblende plot within the granite/granodiorite fields and are subalkaline (Fig. 35a). Other porphyritic dikes which do not contain quartz, and which have an increased proportion of hornblende/biotite and sometimes pyroxene, all plot within the granodiorite subalkaline field (Fig. 35a). Mafic to intermediate dikes (gabbro to diorite) are mainly reported along the regional Goddard dextral strike-slip fault, or associated with the Whitehorse suite (Fig. 29; Hart, 1997a). Gabbro dikes are generally finely crystalline, with a dark brown to black groundmass composed of mafic minerals. Their geochemical signature is equivalent to basalt or basaltic-andesite compositions (Fig. 35a).

Most intrusions display a decrease in major oxides (Fig. 36a–e: Al_2O_3, MnO, MgO, TiO_2, P_2O_5) with respect to SiO_2, and an increase of K_2O and Na_2O (Fig. 36f,g). A negative correlation is displayed by Fe_2O_3, CaO (Fig. 36h,i).

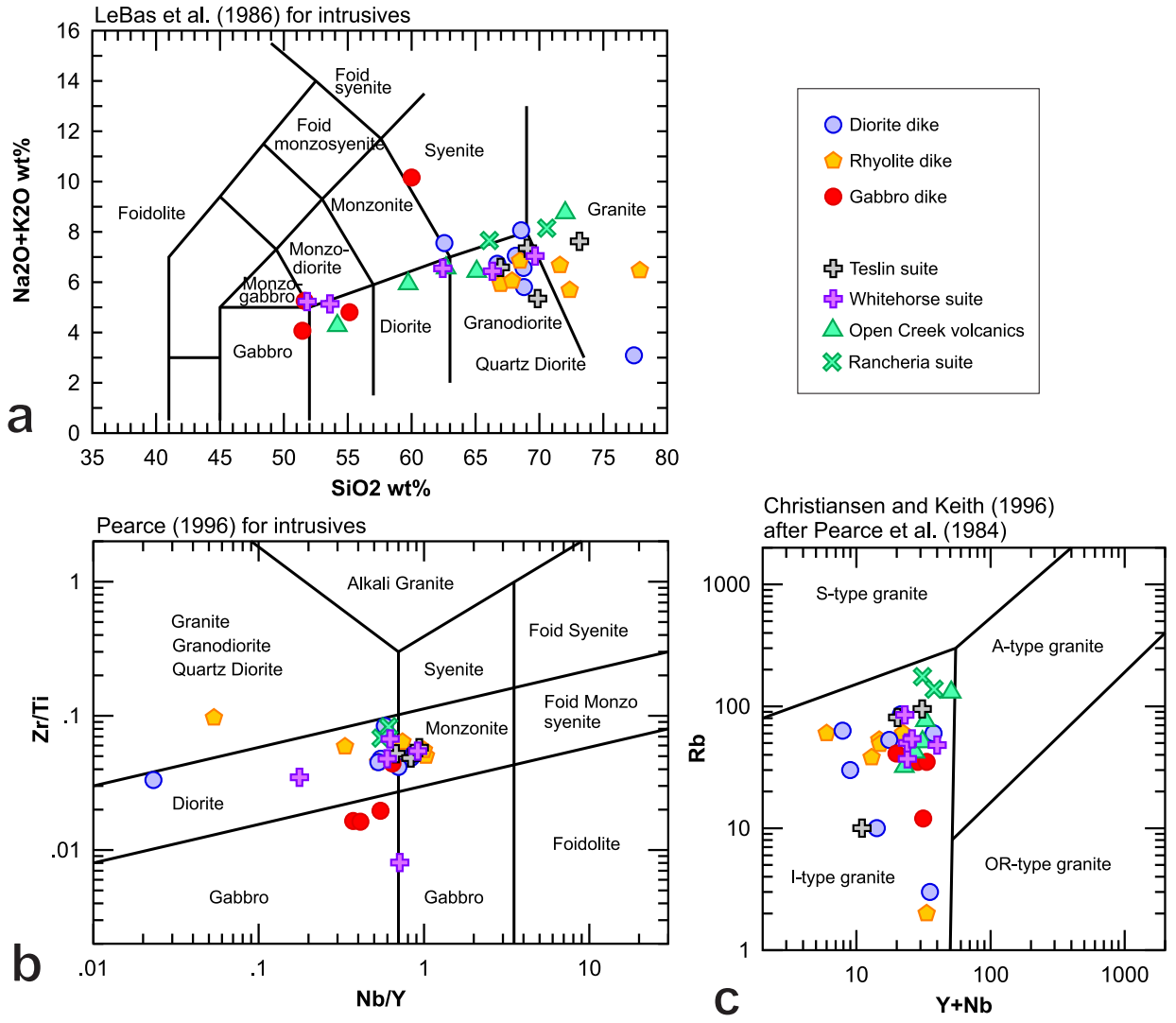

Figure 35. *Intrusive rocks compositions, including data compiled from Hart (1997a) for the Whitehorse and Teslin suites.* ***(a)*** *TAS diagram for intrusive rocks (LeBas et al., 1986);* ***(b)*** *Nb/Y vs Zr/Ti for intrusive rocks (Pearce, 1996); and* ***(c)*** *(Y + Nb) vs Rb (Christiansen and Keith, 1996).*

Tectonic discriminants and trace elements

All intrusive rocks have a volcanic arc signature, with most samples plotting in the calc-alkaline arc basalt field (Fig. 37a; Wood, 1980). Two of the diorite dike samples analyzed have a tholeiitic signature (Fig. 37; Barrett and MacLean, 1999; also in Wood, 1980). All rocks plot within the I-type granite field, corresponding to intrusive rocks related to partial melting of igneous protolith, likely sourced in the lower continental crust (Fig. 37b; Christiansen and Keith, 1996).

Four sub-trends can be identified based on REE signatures when normalized to chondrite (Fig. 38; Sun and McDonough, 1989).

- Two of the diorite dike samples (15EB-084-1 and 16EB-076-2) display a relatively flat profile with respect to chondrite (Fig. 38a). Their REE profile indicates derivation from a juvenile source (e.g., mafic crust). One sample shows a slight Eu anomaly, and the other sample shows little differentiation with respect to chondrite compositions. These two samples were collected from dikes that intersect coherent basalt of the Joe Mountain Formation in the Teslin Mountain area. On other tectonic discrimination plots (Fig. 37), these samples have

tholeiitic arc signatures. Similar trace elements and REE signatures and tectonic affinities are displayed by Middle Triassic dikes and intrusions from the Joe Mountain area (Fig. 38a). There are no dates available for these two dikes, however these comparative stratigraphic elements suggest that they may be part of the Middle Triassic magmatic suite rather than Cretaceous dikes.

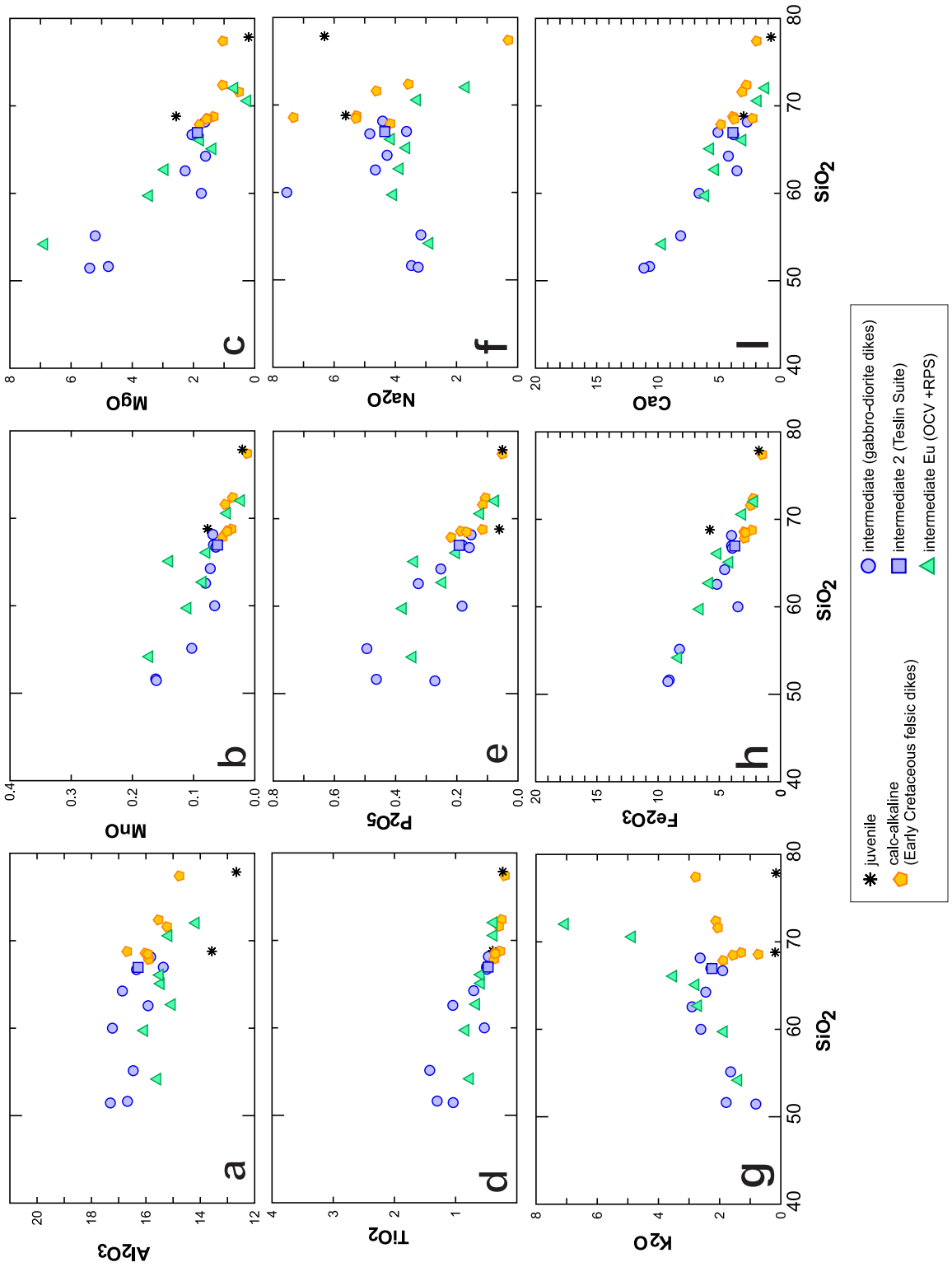

Figure 36. *Harker diagrams for Cretaceous plutons and dikes.*

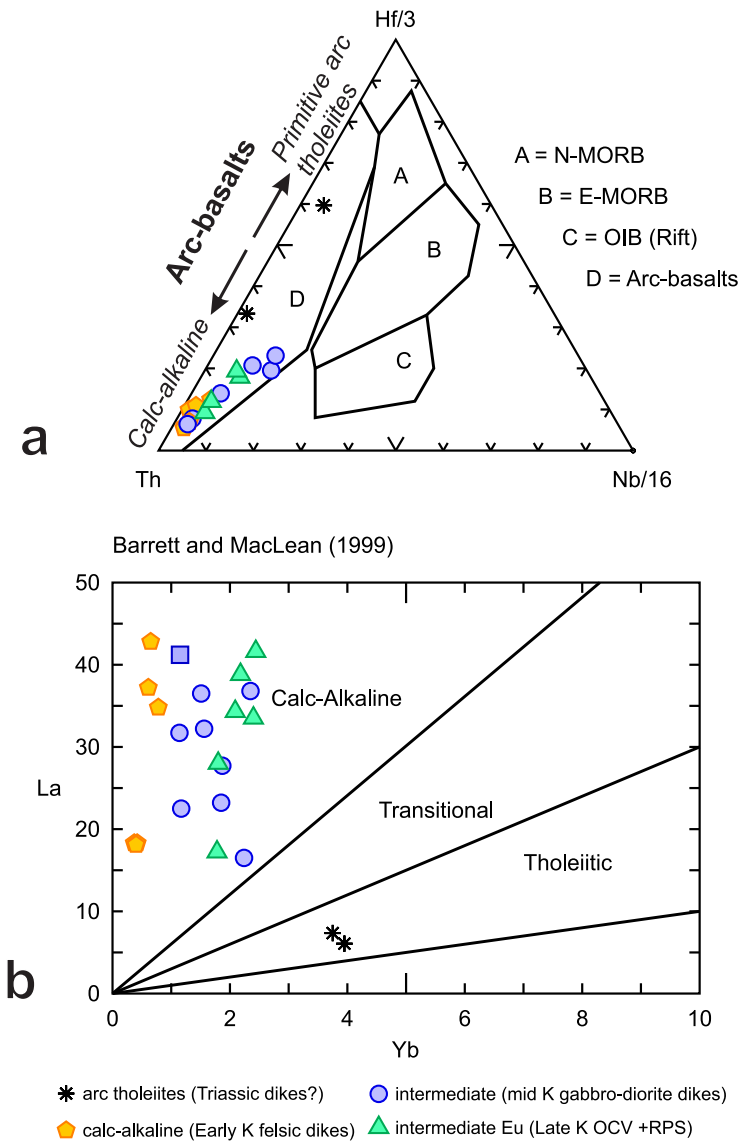

Figure 37. *Tectonic discriminant diagrams for Cretaceous plutons and dikes.* ***(a)*** *Arc basalt discrimination after Wood (1980); and* ***(b)*** *calc-alkaline vs tholeiitic series discrimination after Barrett and MacLean (1999).*

All other profiles are significantly different and show some level of differentiation relative to chondrite compositions.

- A set of intermediate and felsic dikes displays a steep negative slope, with enrichment in LREE and depletion in HREE (Fig. 38b). The profile flattens out for the heavy rare earth elements Er, Tm, Yb and Lu. The data set comprises the two dikes that were dated between 138–136 Ma (15EB-222-1 and 16EB-384-2). All other dikes on this graph have not been dated, but their geochemistry and petrography are all similar, including plagioclase-quartz-phyric rhyolite to rhyodacite. This REE profile is characteristic of calc-alkaline arc rocks.

The two other types of profiles are transitional between the juvenile profile (flat; Fig. 38a) and calc-alkaline profile (steep negative slope; Fig. 38b), suggesting derivation from sources that range from juvenile to evolved, as expected in most volcanic arc settings.

- The first transitional profile shows a negative slope with no particular anomaly observed for any of the elements (Fig. 38c). The data set here includes gabbro and diorite dikes ascribed to the Early Cretaceous Teslin plutonic and mid-Cretaceous Whitehorse suites, with dates ranging between ca. 116 Ma and ca. 106 Ma.

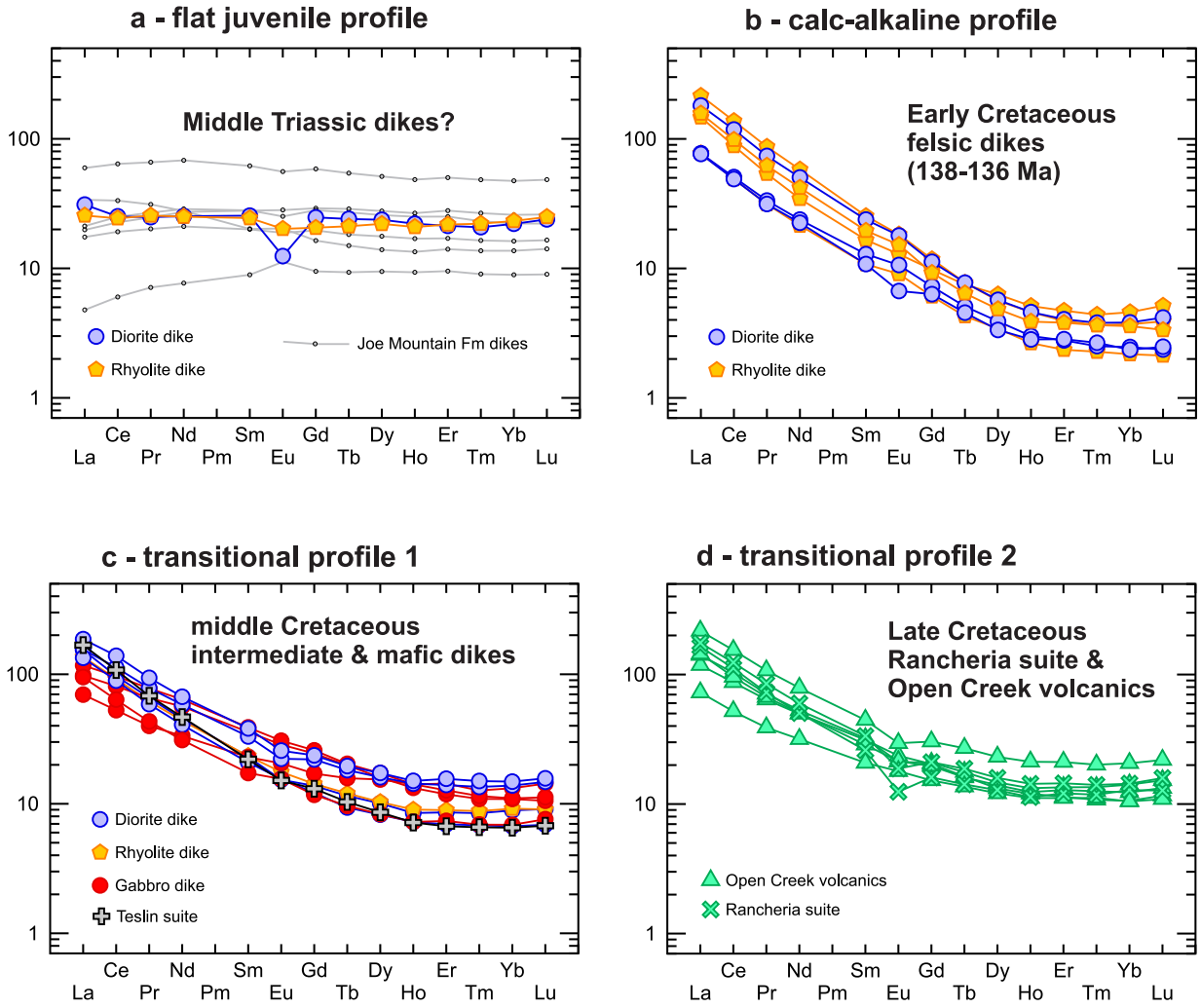

Figure 38. *REE vs chondrite diagrams for Cretaceous intrusion and dikes (Sun and McDonough, 1989). Four different trends are identified that defined distinct intrusive populations characterized by a unique REE-age signature.* **(a)** *Flat juvenile profile likely corresponding to Middle Triassic dikes;* **(b)** *calc-alkaline profile including at least two Early Cretaceous felsic dikes;* **(c)** *transitional profile 1 including mainly middle Cretaceous intermediate and mafic dikes; and* **(d)** *transitional profile 2 including Late Cretaceous Rancheria suite and Open Creek volcanic rocks.*

- The second transitional profile is almost identical to the one above, but displays a systematic slight negative Eu anomaly (Fig. 38d). This data set includes all of the Rancheria suite (Teslin pluton) and Open Creek volcanic complex samples, with dates between 79 and 78 Ma. A negative Eu anomaly can result from the removal of feldspar from the silicic melt by crystal fractionation or from the partial melting of a rock in which feldspar is retained in the source (Schnetzler and Philpotts, 1970).

Summary

Plutons in the eastern Lake Laberge area are dominated by felsic to intermediate compositions, lithologically characterized by plagioclase, quartz ± biotite and/or hornblende porphyritic or equigranular granodiorite, diorite, monzonite and monzodiorite. The compositional and textural diversity of magmatism is also reflected by the many dike occurrences that intersect Triassic and

Jurassic stratigraphy, ranging from fine-crystalline gabbro to porphyritic felsic dikes. In particular, mafic to intermediate dikes (gabbro to diorite) are clustered along the regional Goddard dextral strike-slip fault. Combined geochronology and lithogeochemistry analyses provide constraints on the signature and age of some of the dikes and plutons, and suggest associations to plutonic suites previously reported across the Yukon (Colpron *et al.*, 2016a). Dikes and plutons are dominantly Cretaceous (Fig. 39) and further discussed below. The older intrusion is the Middle Jurassic Teslin Crossing pluton, which is correlated to the Bryde plutonic suite (174–168 Ma; Colpron *et al.*, 2016a) based on age and composition characteristics. One set of juvenile felsic and intermediate dikes is inferred to be related to Joe Mountain volcanism based on their primitive REE signature completely distinct from the signature Cretaceous magmatic rocks. However, geochronological data are not available to confirm this hypothesis.

The Early Cretaceous Goddard suite is expressed only by quartz-phyric rhyolite and rhyodacite dikes dated between 138 and 136 Ma. The rare earth elements signature of these dikes displays a steep negative slope, with enrichment in LREE and depletion in HREE, which is characteristic of calc-alkaline magmatic rocks. Early Cretaceous igneous ages are rare in Yukon, and no igneous suite is defined so far that includes 138–136 Ma ages (Colpron *et al.*, 2016a). Detrital zircons within this age range are reported in the Blanchard River metasedimentary assemblage in southwestern Yukon (Vice, 2017). Together with the two dikes analyzed in this study they constitute the only known occurrence of zircons within this age range in Yukon, and indicate the potential for more igneous source rocks of this age.

Based on age and lithological characteristics, the Laurier Creek pluton (*ca.* 116 Ma) and one intermediate dike (ca. 114 Ma) are assigned to the Early Cretaceous Teslin suite (123–115 Ma; Colpron *et al.*, 2016a). The REE profile of these rocks is characterized by a moderate negative slope, which is a signature typical of calc-alkaline arc rocks. This profile can be distinguished from the steep negative slope of samples from the Goddard suite, and therefore the two suites can be discriminated based on their geochemical signature. The Laurier Creek pluton hosts the molybdenum porphyry Hig (Yukon MINFILE 105E 024) and Lori (Yukon MINFILE 105E 025) occurrences. The Cap Creek, M'Clintock Lakes, and M'Clintock River plutons (Hart, 1997a; Fig. 30) comprise hornblende-biotite granodiorite to quartz-monzonite, and are intruded by the Byng Creek pluton. They have reported U/Pb and K/Ar dates of 121 ± 5 Ma (Bremner, 1991) and 119 ± 1 Ma (Hart, 1997a), which also suggests an association of these plutons to the Teslin Suite.

The slightly younger Whitehorse suite is expressed by several mafic and intermediate dikes in the map area, with ages between *ca.* 111 and 106 Ma. This suite also comprises large plutons mapped in the Joe Mountain and Mount Byng areas, including the Cap Mountain pluton, Byng Creek pluton and Mount M'Clintock pluton (Hart, 1997a; Colpron *et al.*, 2016a).

Granodioritic and dioritic intrusions at Teslin Mountain (*ca.* 78 Ma) and felsic pyroclastic rocks and dacitic lavas of the nearby Open Creek volcanic complex (*ca.* 79 Ma), are ascribed to the Rancheria magmatic suite. The similar ages, identical geochemical signatures, and spatial proximity between the Teslin Mountain pluton and Open Creek volcanic rocks suggest that they are part of a same magmatic complex and share a common magmatic source. The Teslin Mountain pluton hosts the Debicki mineralized occurrence (Yukon MINFILE 105E 050). Based on geographic proximity, age and geological context, the Red Mountain porphyry (Yukon MINFILE 105C 009), located east of the Teslin fault, may be genetically related to the Teslin Mountain pluton. Late Cretaceous ages reported at Red Mountain (81–79 Ma, $^{40}Ar/^{39}Ar$; Joyce *et al.*, 2015) confirm association with the Rancheria suite.

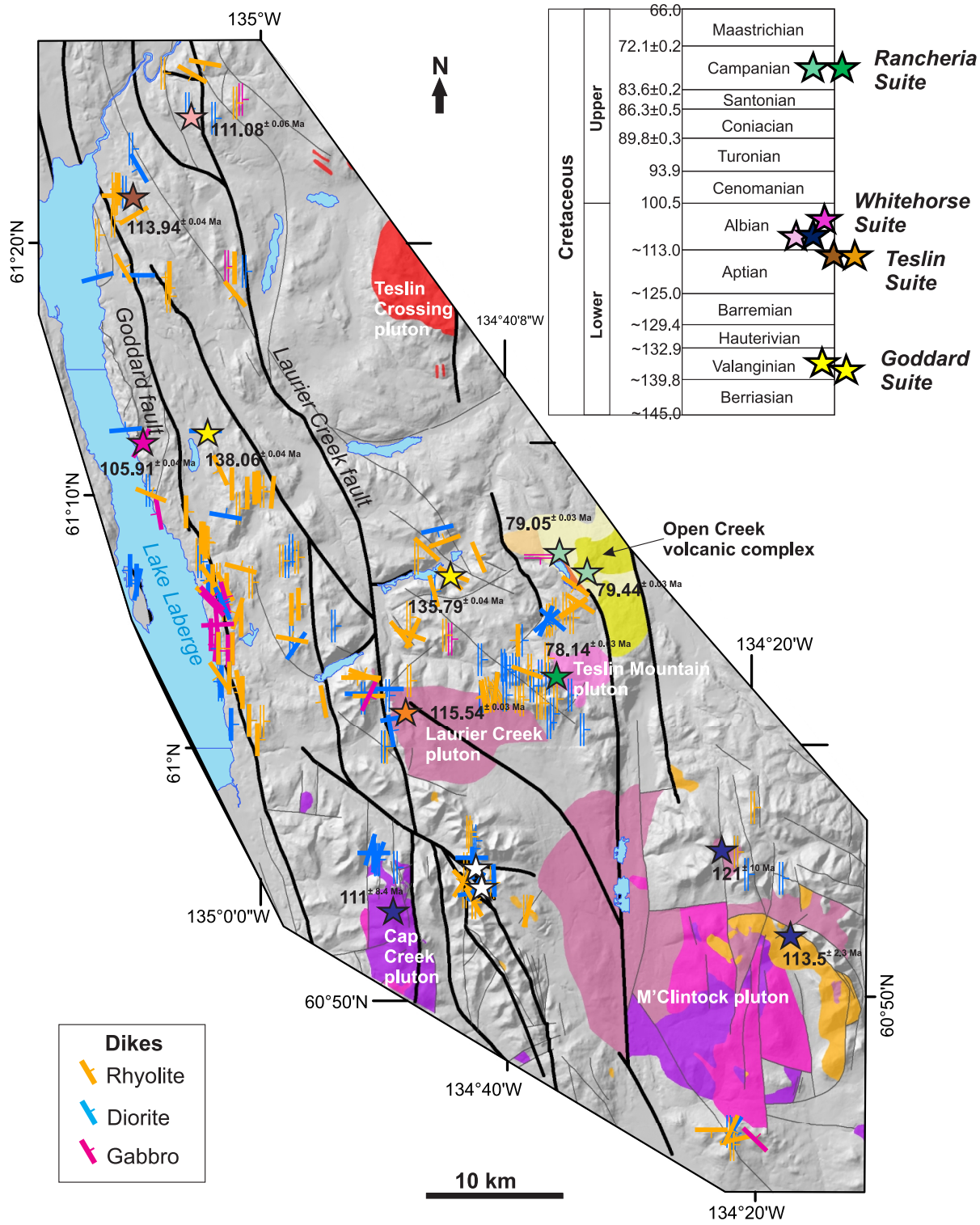

Figure 39. *Geochronology compilation for Cretaceous plutons and dikes. U/Pb ages generated in this study are from samples of the Rancheria suite (Teslin pluton, 78.14 ±0.03 Ma; Open Creek volcanic complex, 79.05 ± 0.03 Ma and 79.44 Ma ± 0.03 Ma), Whitehorse suite (gabbro dike, 105.91 ± 0.04 Ma; diorite dike, 111.08 ± 0.06 Ma), Teslin suite (diorite dike, 113.94 ± 0.04 Ma; Laurier Creek pluton, 115.54 ± 0.03 Ma), and from the newly defined Goddard suite (rhyodacite dikes, 138.06 ± 0.04 Ma and 135.79 Ma ± 0.04 Ma). Previous intrusive ages from Hart (1997) are from the Cap Creek pluton (111 ± 8.4 Ma and 105 ± 3 Ma) and M'Clintock pluton (Teslin Suite, 121 ± 10 Ma, Bremner, 1991; Byng Creek suite, 113.5 ± 2.3 Ma, Hart, 1997).*

Chapter 5 - Structures

The regional structural framework of the eastern Lake Laberge area is primarily controlled by Cordilleran-scale structures such as the Tintina and Teslin dextral strike-slip faults (Fig. 40a). In the map area, the Laurier Creek and Goddard faults dissect the Triassic to Jurassic stratigraphy (Fig. 40b), and folding is prevalent along the eastern shore of the lake where it is associated with near vertical bedding and steep topography. Two structural domains are defined on either side of the Laurier Creek fault. North to northwest-trending thrust and normal faults, and east-verging tight folds prevail in the western part of the map area, between the eastern shore of Lake Laberge and the Laurier Creek fault (Fig. 40b). East of the Laurier Creek fault, bedding measurements and cliff exposures of folds within the Middle Triassic sequence consistently indicate an east-trending structural fabric (Fig. 40b). In addition, numerous dikes, mainly north-trending, represent discrete but widespread expressions of extensional deformation associated with magmatism during the Cretaceous.

The structural framework in the eastern Lake Laberge area is primarily supported by field observations and air photograph interpretations. Unfortunately, outcrop-scale structural features are lacking in the map area. In fact, most of the regional-scale structures are located within broad, tree-covered valleys, or masked by thick glacial deposits (Fig. 3). An aeromagnetic survey (Kiss and Boulanger, 2018) allows better delineation of regional-scale structures and improves the existing regional structural framework (Bordet, 2019). The nature and style of faults, folds and dikes is reviewed below. The magnetic signature of faults, and of the units they intersect, is also discussed. A final discussion presents a tentative reconstruction of the structural evolution of the eastern Lake Laberge area.

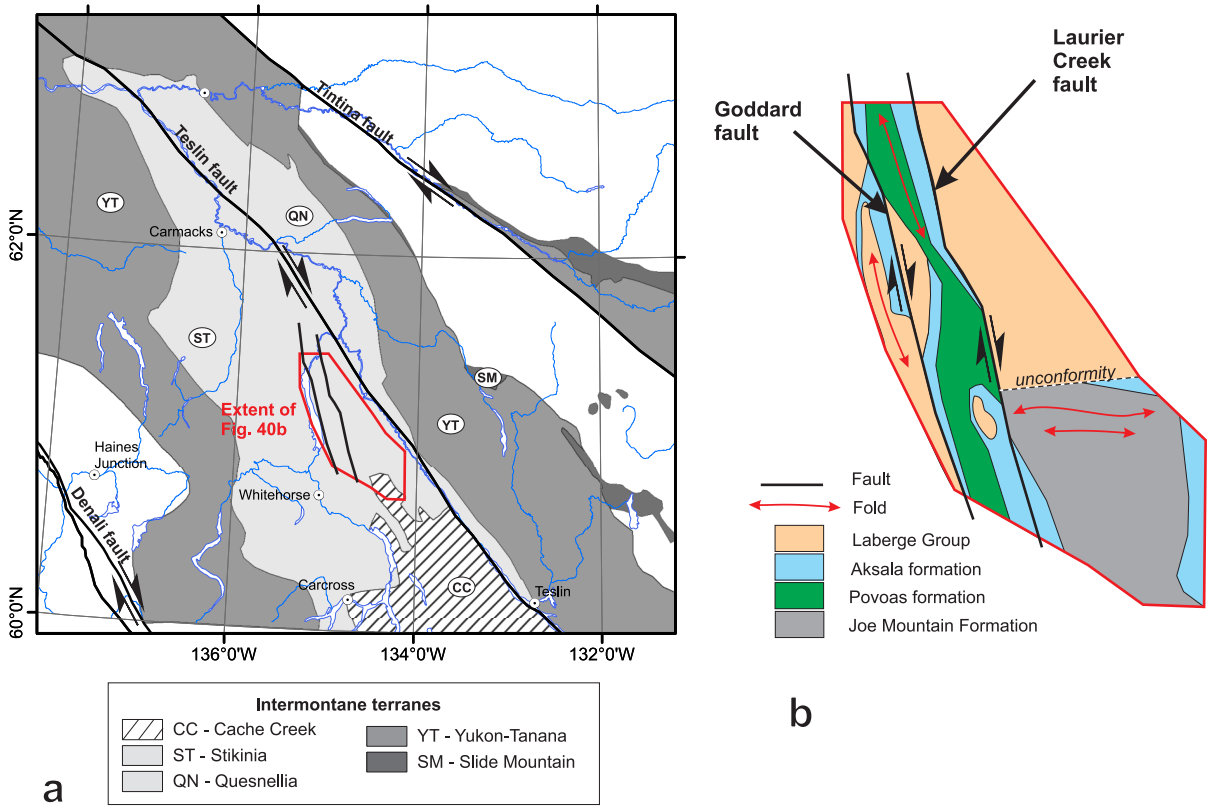

Figure 40. *Tectonic setting of southern Yukon.* ***(a)*** *Tintina, Teslin and Denali faults are Cordilleran-scale dextral strike-slip faults that control the orientation of regional structures across the Yukon; and* ***(b)*** *in the eastern Lake Laberge area, the Laurier Creek and Goddard faults are regional dextral strike-slip faults intersecting Triassic through Jurassic stratigraphy.*

Faults

Two dominant sets of faults are identified based on field observations combined with aeromagnetic imagery and Digital Elevation Model interpretations (Fig. 41): NNW-trending structures at least 60–70 km long, and NW-trending structures at least 10–40 km long, which are connected to the NNW-trending fault set. Minor faults (between 5 and 10 km long) are east-trending or NE-NNE trending.

Regional north-northwest trending faults constrain the geometry of rock units within the region east of Lake Laberge. They include the Goddard and Laurier Creek faults (Fig. 41), which deform rocks of the Lewes River and Laberge groups. These structures are located in covered valleys, and their presence is confirmed by field evidence such as discordant stratigraphic contacts, increased strata deformations such as brittle fractures, sharp topographic breaks or intense, localized rock alteration. Interpreted aeromagnetic patterns (Kiss and Boulanger, 2018) also confirm the existence of major structural breaks (Fig. 42a,b). The Open fault bounds part of the map area to the east (Fig. 41).

Laurier Creek fault

The Laurier Creek fault is a north to northwest-trending structure that separates the map area into two structural domains (Fig. 40b). To the east, east-striking strata of the Middle Triassic Joe Mountain Formation, Upper Triassic Aksala formation and Jurassic Laberge Group, define a north-younging succession. To the west of the Laurier Creek fault, a north-trending structural fabric prevails within the generally west-younging, volcano-sedimentary sequence of the Lewes River Group. The Laurier Creek fault also marks the western boundary of the Joe Mountain Formation in the Teslin Mountain area.

The Laurier Creek fault has a marked topographic expression, particularly in the steep valley that bounds Mount Laurier to the east (Fig. 43a). At this location, units are distinguished by contrasting lithology and a change of bedding orientation. Immediately east of the fault, a thick north-dipping succession of well-bedded calcareous sandstone and mudstone, and volcaniclastic rocks of the Lewes River Group is exposed. The sequence is folded and overlies Middle Triassic basalt of the Joe Mountain Formation (Fig. 43b). The contact is inferred to be unconformable. Across the valley, the base of Mount Laurier comprises 100 m thick, north-northwest dipping beds of Lewes River Group limestone unconformably overlain by Laberge Group sandstone and conglomerate. An outcrop of brecciated limestone that is part of the eastern carbonate belt of the Aksala formation is exposed at the valley bottom, a few metres away from exposures of the Joe Mountain Formation basalt, the oldest rocks identified in the field area. The fault follows Laurier Creek for ~20 km to the north, defining a structural contact between Laberge Group conglomerate to the east and Upper Triassic volcano-sedimentary successions exposed in the Hancock Hills to the west (Fig. 6). In addition, a fault contact is mapped between rusty-weathering, thick-bedded limestone of the Lewes River Group and thin-bedded, dark grey mudstone of the Laberge Group near the Aurier occurrence (Yukon MINFILE 105E 036; Fig. 30).

The magnetic signature of the Laurier Creek fault is marked by an ~5 km-wide negative magnetic anomaly corridor, bounded on either side by rocks dominated by higher, positive anomalies (Fig. 42a,b). The fault zone comprises dominantly carbonate rocks of the Lewes River Group characterized by a strong negative anomaly, and lesser volcanic and volcaniclastic strata highlighted by a positive anomaly.

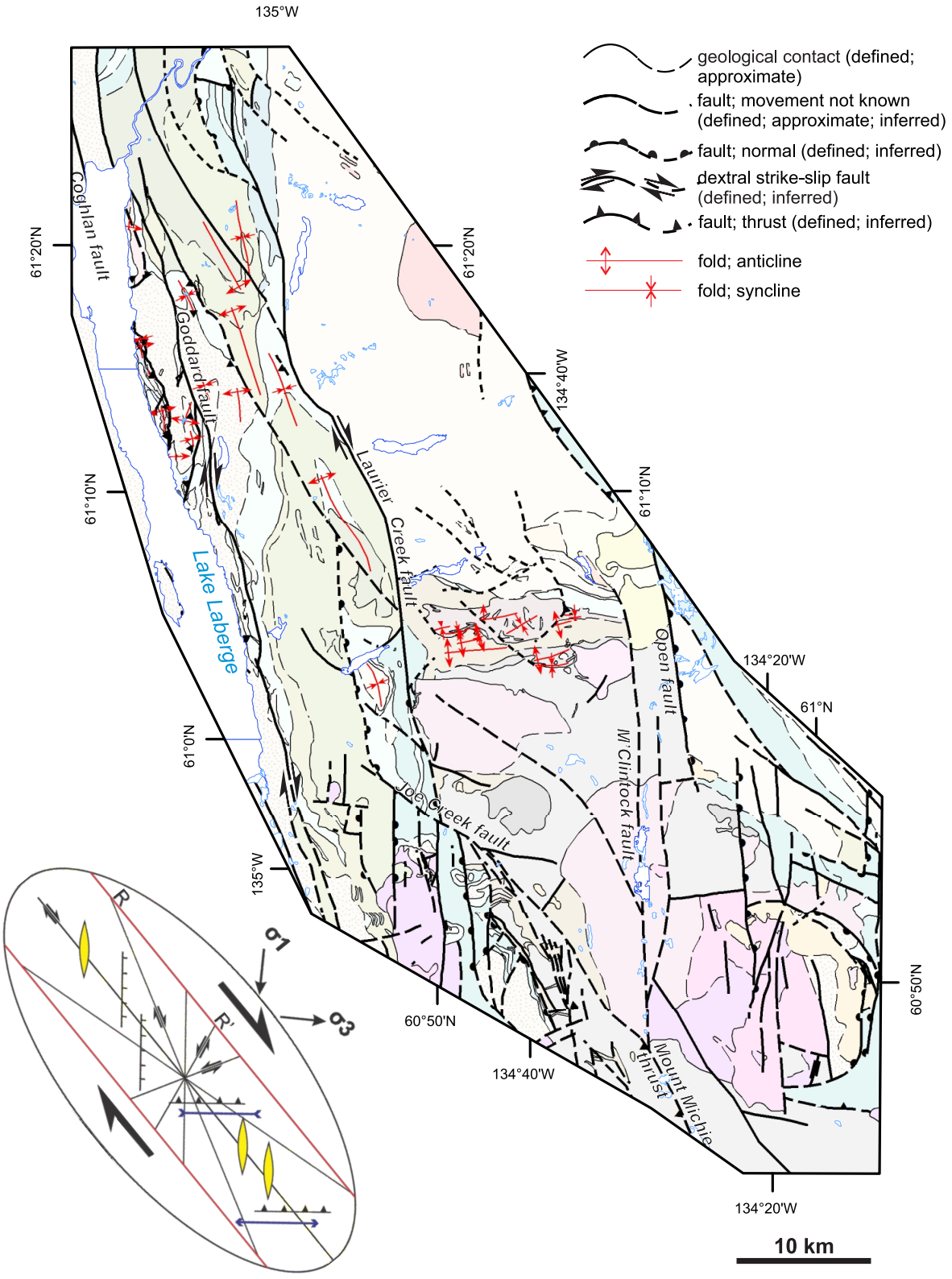

Figure 41. *Main structural features of the eastern Lake Laberge area. The structural interpretation is based on field observations integrated with aeromagnetic data (Kiss and Boulanger, 2018). The map displays faults classified by style (normal, thrust or strike-slip), folds and dikes. Diagram shows possible stress orientations associated with the development of most observed features.*

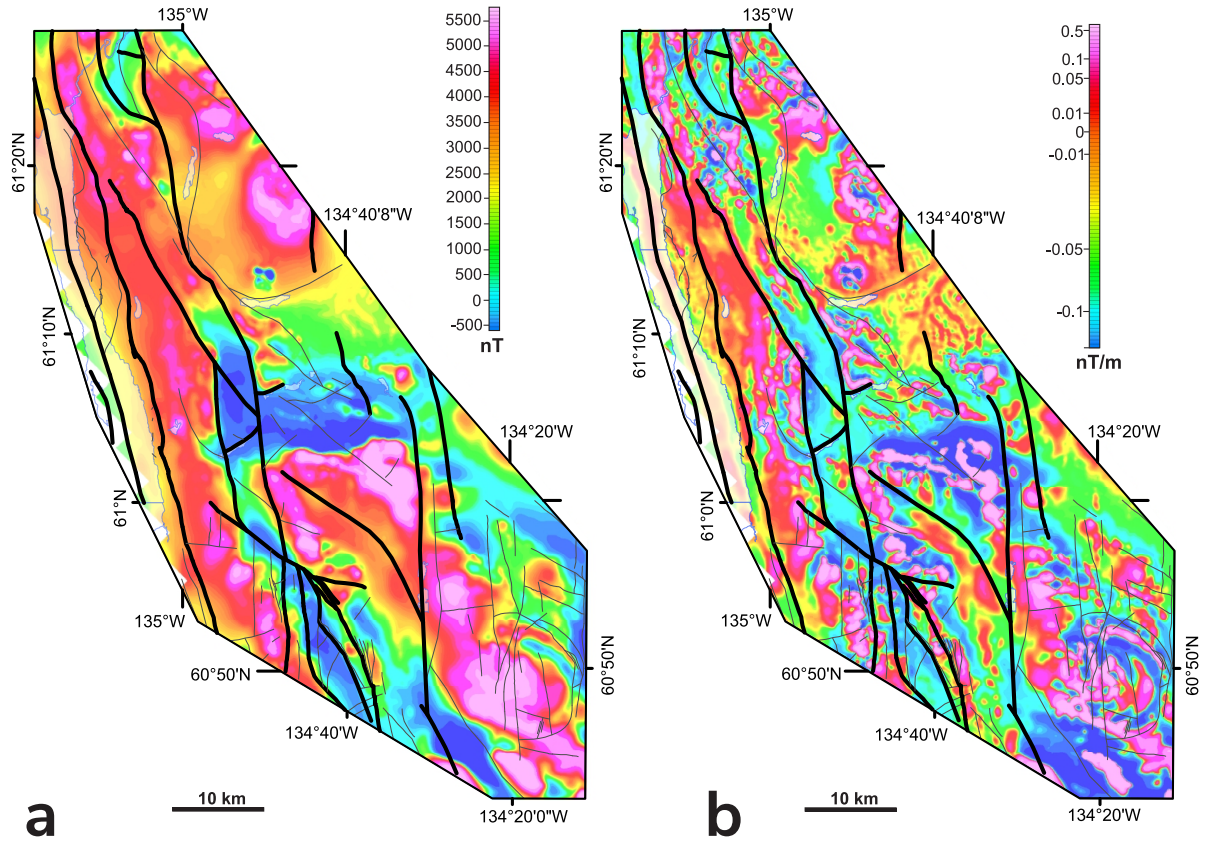

Figure 42. *Aeromagnetic data for the map area (after Kiss and Boulanger, 2018).* ***(a)*** *Residual Total Magnetic Field in nT (nT = nanoTesla); and* ***(b)*** *first vertical derivative of the magnetic field in nT/m.*

The latest displacement along the Laurier Creek fault may be Late Cretaceous or younger, as it exhumed Early and Late Cretaceous intrusive bodies. The Laurier Creek fault was previously interpreted as an extensional structure (Tempelman-Kluit, 1984). Based on mapping in the eastern Lake Laberge area, the motion along the Laurier Creek fault is dextral strike-slip, and locally normal (Fig. 6). In fact Laberge Group rocks are in contact with older rocks of the Lewes River Group to the north (Fig. 6), which suggests an east-side-down motion. However, towards the south, the oldest part of the stratigraphy is exhumed, and the fault juxtaposes rocks of the Joe Mountain Formation to the east with younger rocks of the Lewes River Group and Laberge Group to the west. This complex pattern results either from strike-slip motion along the Laurier Creek fault, and/or reactivation of a pre-existing structure.

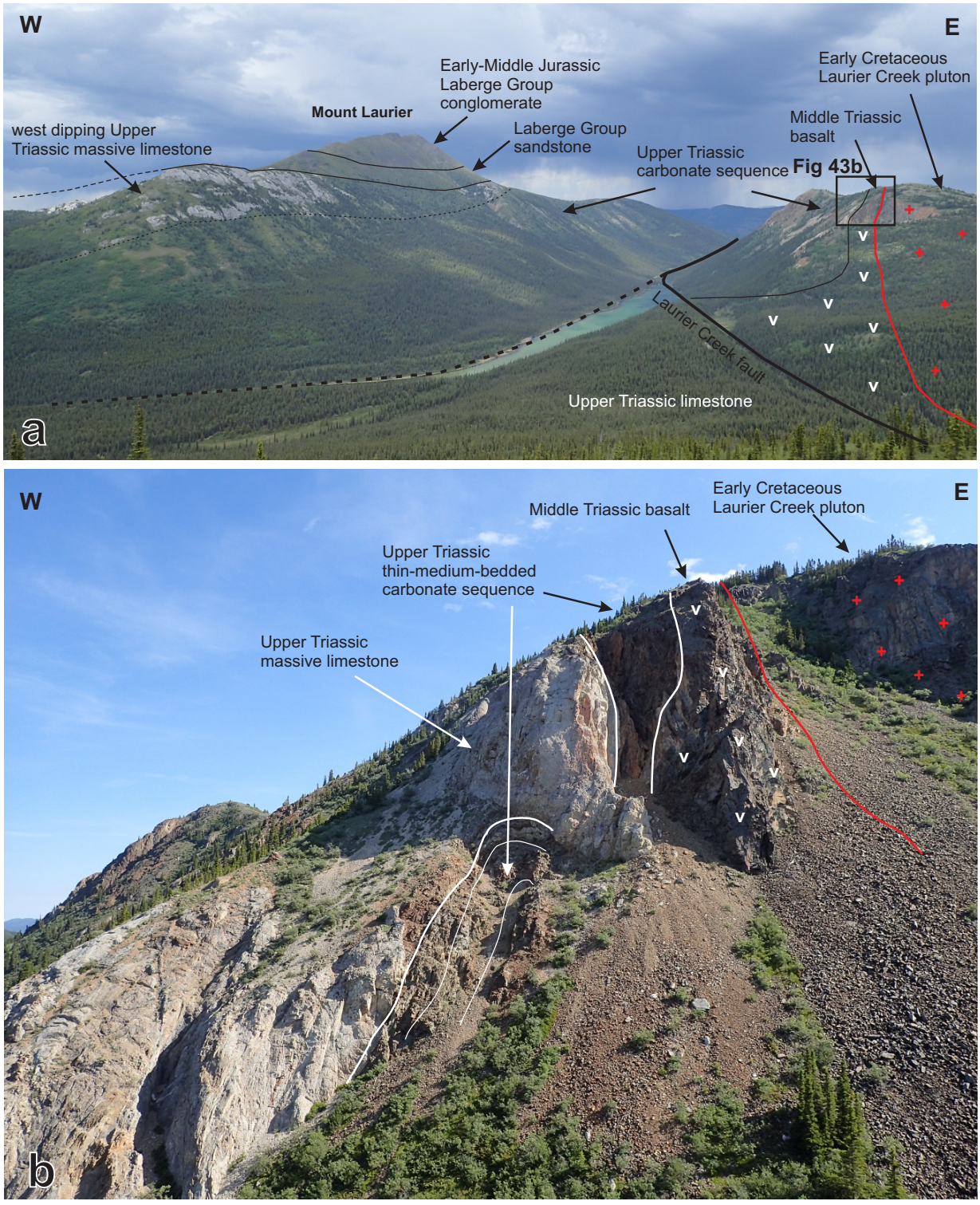

Figure 43. *Field characteristics of the Laurier Creek fault.* ***(a)*** *Looking north up Laurier Creek where the trace of the Laurier Creek fault is inferred. West of the fault, Laberge Group conglomerate and sandstone overlie west-dipping, pale grey massive limestone of the Upper Triassic Aksala formation; east of the fault, Middle Triassic Joe Mountain Formation basalt is overlain by the Aksala formation carbonate sequence, and both are intruded by the Early Cretaceous Laurier Creek pluton; and* ***(b)*** *close-up of exposures along the eastern side of Laurier Creek fault. The outcrop exhibits steeply west-dipping, tightly folded Aksala formation limestone overlying Joe Mountain Formation basalt, and intruded by the Laurier Creek pluton to the east.*

Goddard fault

The Goddard fault is a >100 km long, north to northwest-trending structure, located between 1.5 and 3.5 km east of Lake Laberge (Fig. 6). In the map area, the Goddard fault cuts across the carbonate sequence of the Aksala formation, as well as the Jurassic Laberge Group. It has a topographic expression indicated by steep cliff faces bounded by limestone and calcareous conglomerate ridges. In the field, the presence of a fault is suggested by the successive shifts in bedding along and across the fault trace.

The fault zone is exposed at several locations within kilometres northeast of the mouth of Laurier Creek and west of Goddard Point. One location, at the bottom of a narrow valley, displays a sliver of steeply dipping, blocky, vesicular, pyroxene-phyric basalt (Fig. 44a), whereas steep rock faces of Lewes River Group limestone conglomerate are exposed on either side of the valley. Due to its location at the bottom of a narrow, incised valley, and its restricted extent, the basalt exposure is interpreted as a sliver of rocks from the Povoas formation, exposed at the surface following upward and lateral motion along the fault. At a second location, an outcrop of dark grey limestone breccia is intersected by a steep (65° W to subvertical), north-striking, cataclasite. Elongated subangular limestone cobbles to boulders are aligned in a brown-weathering, dark grey, non-calcareous mudstone matrix (Fig. 44b). The northern part of the map area near Goddard Point displays a lack of continuous outcrop and thick tree cover. However, systematic mapping traverses conducted eastward from the shore of Lake Laberge identified associations between the topography (successions of NNW-trending ridges and valleys) and abrupt changes of lithology and bedding. At a few well exposed ridge tops, the fault trace is enhanced by thick (5–10m) north-trending rhyolite dikes (Fig. 44c).

The magnetic signature of the Goddard fault is marked by a sharp contrast between the Laberge Group sedimentary rocks to the west (uniform, positive anomaly), and the dominantly volcanic sequence of the Lewes River Group to the east, which overall displays a heterogeneous, “banded” anomaly pattern (Fig. 42a,b).

A dextral motion is inferred along the Goddard fault (Colpron, 2011). The Goddard fault intersects mainly Upper Triassic and Jurassic stratigraphy in the map area, with most field evidence of faulting in the form of intense, localized deformation (cataclastite) or localized extension (dikes).

Other faults

There are many normal faults mapped within the Lewes River Group. They are oriented north-south. Some of them are cut by the Joe Creek fault south of the map area (Bordet, 2019). Most of these faults are inferred from mapping, and based on discontinuity in stratigraphic relationships.

A north-trending normal fault is inferred west of Mount Laurier and Lime Peak (Fig. 41). It juxtaposes the Povoas formation to the west, with Lewes River Group massive limestone and overlying Laberge Group conglomerate at Mount Laurier to the east. This fault has a marked topographic expression. To the north, it is cut by a NW-trending fault that displays evidence of thrusting where exposed towards the north (Fig. 41).

North to northwest-striking, west-dipping thrust faults intersecting the Upper Triassic sequence and Laberge Group were mapped, or inferred, in the northern part of the map area, east of Goddard point (Fig. 41). They superpose thick competent limestone strata of the Lewes River Group to younger, thin-bedded mudstone and sandstone successions of the Laberge Group (Fig. 45). These thrusts are genetically associated with north-trending, east-verging anticlines, and together form a fold-and-thrust belt (Figs. 46 and 47; Bordet, 2019).

Figure 44. *Field characteristics of the Goddard fault.* **(a)** *Sliver of the interbedded basalt within calcareous conglomerate of the Lewes River Group along the Goddard fault;* **(b)** *elongated, deformed limestone boulders (white outline) in a thin-bedded mudstone matrix along the Goddard fault;* **(c)** *a north-trending plagioclase-hornblende porphyritic intermediate dike (bounded by a dashed white line) mapped along the trace of the Goddard fault trace east of Goddard point, eastern shore of Lake Laberge. At this location, the dike intersects a mafic volcaniclastic sequence of the Lewes River Group.*

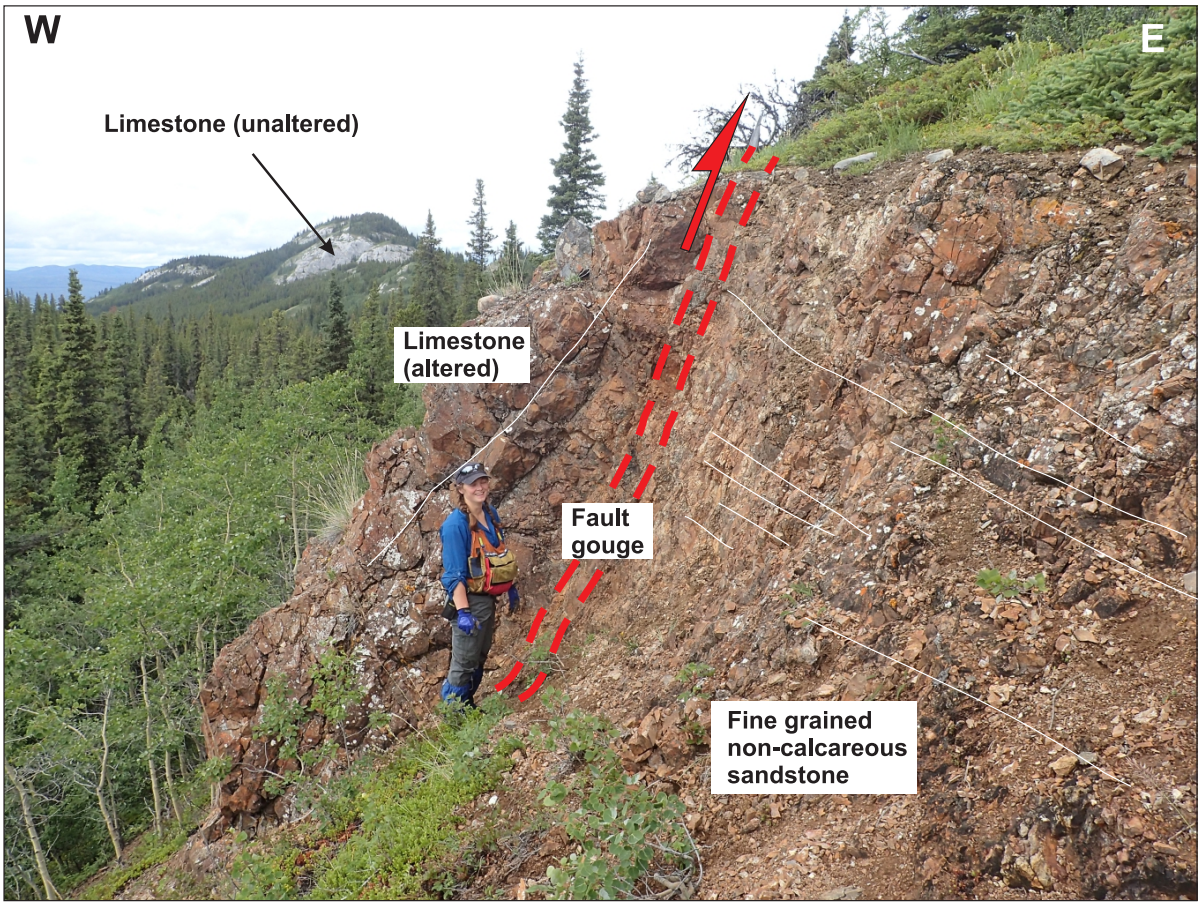

Figure 45. *Geometry of a thrust fault mapped north of the Hancock Hills. This orange-weathering outcrop marks a faulted contact between steeply west-dipping limestone to the west, and east-dipping, fine-grained, non-calcareous sandstone to the east. The fault zone is steeply dipping to the west and marked by a pebble-size, matrix-supported fault gouge intersected by numerous veins. Bedding is indicated by thin white full lines, the fault zone is in between the two thick dashed red lines.*

The topography of Richthofen Island is marked by a north-trending fault scarp along the eastern shore of the island. The fault crosscuts thin to medium-bedded mudstone/sandstone of the Laberge Group. Along the fault scarp, rocks are rusty weathering and crosscut by a network of north-trending quartz and carbonate veins. At the base of the fault scarp, along the eastern shore of the island, the mapped sequence includes a cobble to boulder conglomerate (JLcbx) overlying or interbedded with thin-bedded mudstone/sandstone sequence of unit JLst (see Chapter 2). An east-side-down motion is inferred along this fault to the north (Bordet, 2019).

Folds

At least two main orientations of fold axes are identified within the map area. Folding in the Lake Laberge area is inferred from variations of bedding attitude, but difficult to constrain due to the lack of foliation and cleavage planes, as previously noted by White et *al.* (2012).

North to northwest-trending thrust faults, bounding east-verging tight folds, prevail in the western part of the map area (Figs. 40, 46 and 47; Bordet, 2019), between the eastern shore of Lake Laberge and Laurier Creek fault. There, air photos of well-exposed ridges illustrate

the style of folding, the orientation of fold axis, and structural breaks that correspond to thrust faults within the Upper Triassic carbonate sequence (Figs. 45 and 46). Steep, west-dipping to subvertical limestone beds of the Lewes River Group represent the limbs of tight, east-verging folds along a narrow north to northwest-trending belt (maximum 2 km wide) along the eastern shore of Lake Laberge (Figs. 46 and 47). The difference of competency between strata within the carbonate sequence creates disharmonic folding. Thick-bedded micritic limestone is generally featureless, but thin to medium-bedded carbonate interbeds locally illustrate the nature and intensity of folding affecting these strata. Folds are generally north to northwest-trending, tight and overturned to the east, therefore interpreted as east-verging.

East of the Laurier Creek fault, near Teslin Mountain, flow-banding and bedding measurements indicate a sharp change of bedding polarity within the Joe Mountain Formation between the south (north dipping strata) and the north (south dipping strata). This suggests an east-trending synclinal fold axis, with outer basalt limbs wrapping around an inner core of younger volcaniclastic rocks (Figs. 6 and 41). This folding may be genetically related to an episode of northwest-directed thrusting inferred from mapping just north of Teslin Mountain (Fig. 6; Bordet, 2019).

Finally, variable bedding orientation of Laberge Group strata at Mount Laurier suggest folding of the sequence along a synclinorium axis (Figs. 6 and 41). North of Long Lake, bedding is relatively consistently steeply dipping to the north (50–70°).

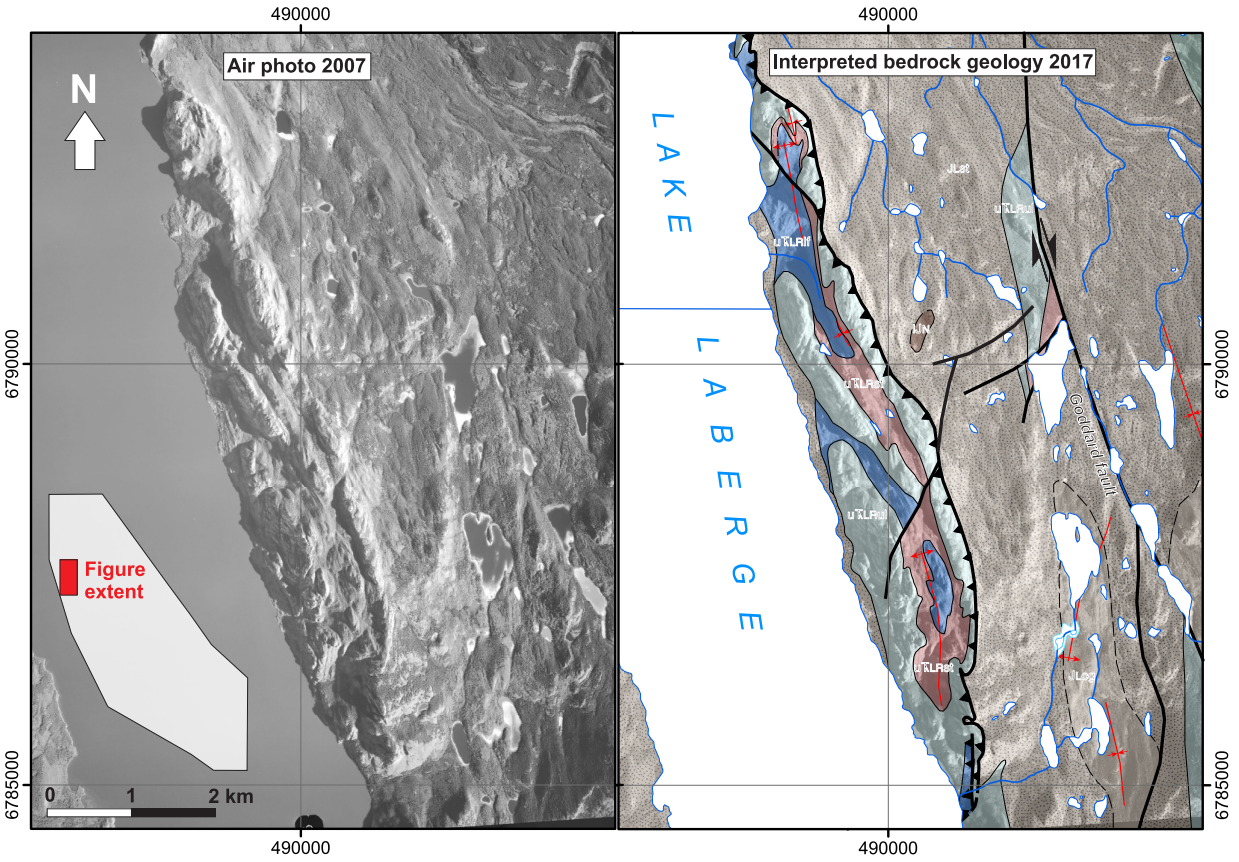

Figure 46. *Fold and fault geometry along the northeastern shore of Lake Laberge interpreted from air photos and field mapping. Geology legend as on Figure 6. Inset map shows extent of this detailed map.*

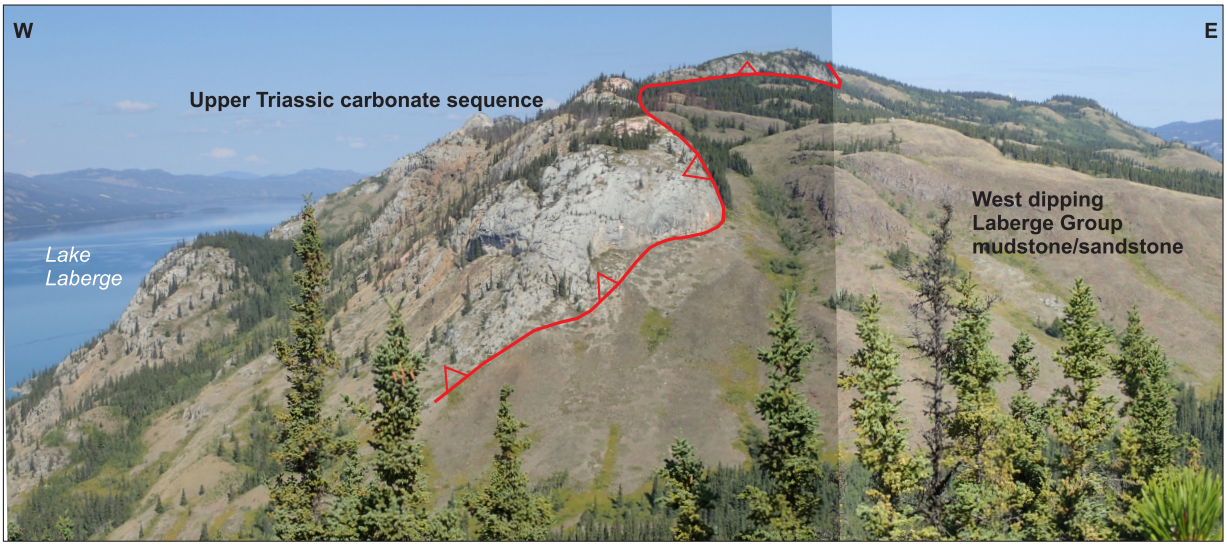

Figure 47. *North-looking view of the folded carbonate strata exposed at the northeastern end of Lake Laberge. Thick beds of Upper Triassic massive limestone are thrust over west dipping mudstone-sandstone strata of the Laberge Group.*

Dikes

More than 200 dikes were mapped in the area east of Lake Laberge. Rose diagrams illustrate clusters of preferred orientations of measured dikes (Fig. 48). Strike and dip information could be collected for only half of the dikes (Appendix D). When only a strike was measurable, a dip of 90° was assigned by default. Other dikes are known from limited field exposure, and were assigned a default north-strike and dip of 90°. Only dikes for which an orientation could be measured are displayed on Figure 48. The majority of dikes display a north-south orientation. Another dike orientation is east-west or northwest-southeast, which is mainly observed amongst rhyolite and intermediate dikes. There are not enough gabbro dikes to propose a statistically meaningful interpretation of their varying orientation. The majority of measured dikes display a steep dip (between 70 and 90°), while only 25% of the dikes have intermediate (between 70 and 45°) to shallow dips (less than 45°).

The distribution of dikes east of Lake Laberge is not homogeneous. There is a zone of higher dike frequency along the Goddard fault (Fig. 41). Another cluster of dikes is mapped between Laurier Creek and Teslin Mountain plutons. These dikes intersect Middle Triassic basalt of the Joe Mountain Formation (Fig. 41). Orientation of these dikes is poorly constrained because of their limited exposure. Their composition is intermediate to felsic, commonly plagioclase-phyric. None of these dikes were dated, however two of the dikes analyzed for lithogeochemistry from this area returned a significantly different REE signature than all other analyzed dikes. It is possible that some of these dikes represent older Triassic dikes, and therefore may result from different stress orientations and magmatic pulse than the dikes that are aligned with the Goddard fault.

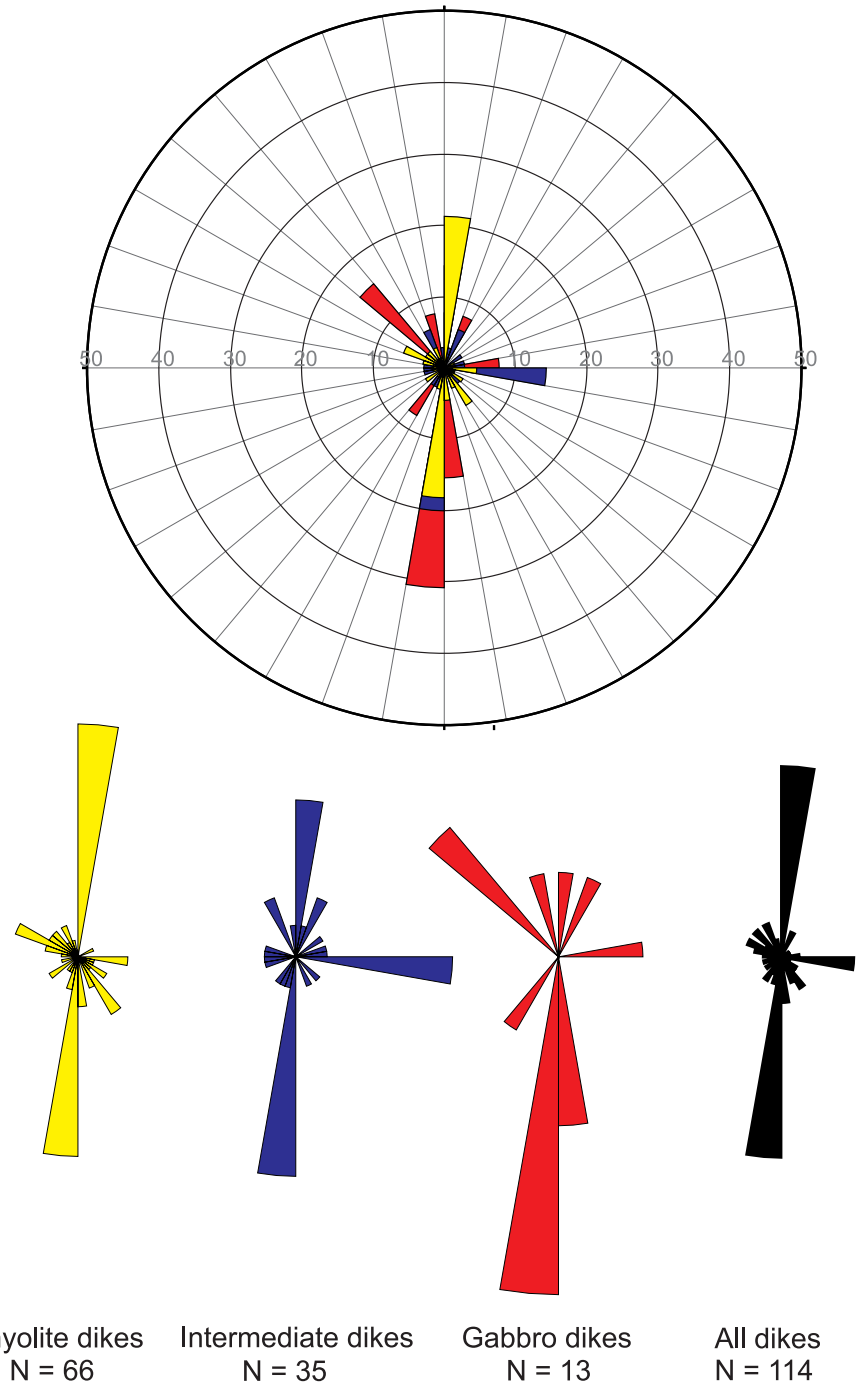

Figure 48. *Preferential orientation of measured dikes (N = 114) in the map area reported on a rose diagram. Dikes are plotted according to their composition.*

Chapter 6 - Mineralization

Several mineral occurrences are reported in the eastern Lake Laberge area, including iron formation, Cu-Mo porphyry, Cu or Mo skarn, and vein-associated Au. Some are spatially associated with Cretaceous plutons, whereas other indicate hydrothermal alteration of the Triassic volcanic rocks related to epithermal vein systems. These different mineralization styles are briefly reviewed below. Observations and analytical results are reported for the Hartless Joe property, which represents the most advanced exploration project in this area to date.

Mineralization styles

Mineral occurrences in the eastern Lake Laberge area are briefly described below (Table 3; Figs. 30 and 49). Enhanced interpretations of stream sediment geochemical data for NTS 105E (Mackie *et al.*, 2016) indicate high prospectivity for epithermal Au-Ag, polymetallic Ag-Pb-Zn, and Zn-Pb-Cu VMS-style mineralization north of the Joe Mountain area (90th to 100th percentile of the weighted sums models). The area between Teslin Mountain and Joe Mountain displays several catchment basins with high prospectivity for porphyry Cu-Mo mineralization. West and north of Teslin Mountain, several catchment basins show high prospectivity for both intrusion-related Au and epithermal Au-Ag. Prospectivity for W-skarn porphyry is relatively high in most of the southern part of the mapped area, and a few catchment basins with high prospectivity are identified east of Miller Lake (Mackie *et al.*, 2016). Most of these model predictions are confirmed by field observations.

Iron Formation

Iron occurrences composed of interlayered hematite and quartz, magnetite, and minor pyrite are interlayered with pillowed-basalt of the Joe Mountain Formation (Fig. 49a). An occurrence of reddish, jasperoidal iron formation at Joe Mountain was first described by Piercey (2005). Bedrock mapping in the Teslin Mountain area (105E/2) allowed the identification of several other similar occurrences (Fig. 30), suggesting that they are not anomalous within the Middle Triassic basalt sequence. All mapped exposures of iron formation are generally 2–3 m wide, and a few metres thick, but float can be found up to several kilometres away, suggesting possible lateral extent of each occurrence. Near Teslin Mountain, cobble to boulder-size clasts of the iron formation occur in the volcaniclastic sequence.

The occurrences are interpreted as Algoma-style iron formation (Piercey, 2005). They have anomalous metal concentrations and hydrothermal geochemical signatures (*e.g.*, high Fe/Al ratios) similar to hydrothermal sediments associated with seafloor hydrothermal vents (Piercey, 2005). This suggests that seafloor hydrothermal activity existed within the basin that the Joe Mountain Formation formed in, and that these occurrences likely result from black smoker activity during subaqueous volcanism in the Middle Triassic. Therefore, there may be potential for VMS mineralization in the Joe Mountain Formation.

Table 3. *Location and mineralization style for the Yukon MINFILE occurrences reported in the map area.*

MINFILE Number	Latitude	Longitude	UTM Zone	UTM Easting	UTM Northing	Name	Deposit Type
105D 049	60.966667	-134.961944	8	502060	6759075	LABE	Unknown
105D 050	60.9125	-134.801389	8	510771	6753057	POW	Skarn Mo
105D 051	60.913611	-134.684167	8	517128	6753206	ACE	Vein Polymetallic Ag-Pb-Zn±Au
105D 114	60.818889	-134.346111	8	535566	6742791	TEXEL	Vein Polymetallic Ag-Pb-Zn±Au
105D 141	60.881667	-134.226111	8	542011	6749854	GAMMON	Unknown
105D 142	60.917222	-134.250278	8	540654	6753799	BYNG	Unknown
105D 149	60.886944	-134.9225	8	504206	6750197	ERGE	Unknown
105D 150	60.890833	-134.441111	8	530331	6750757	UTSHIG	Unknown
105D 174	60.861944	-134.691389	8	516763	6747449	CAP CREEK	Unknown
105D 184	60.931944	-134.360278	8	534673	6755376	MOVEMENT	Vein Au-Quartz
105D 189	60.911111	-134.329444	8	536368	6753072	MT. BYNG	Vein Au-Quartz
105D 197	60.919167	-134.7275	8	514772	6753836	JOE CREEK	Vein Au-Quartz
105D 203	60.903889	-134.72	8	515179	6752122	GRUMPY	Vein Au-Quartz
105E 002	61.290278	-134.8225	8	509512	6795133	TUV	Porphyry Cu-Mo-Au
105E 006	61.073611	-135.041389	8	497766	6770987	LABERGE	Skarn Cu
105E 024	61.008056	-134.739167	8	514103	6763712	HIG	Porphyry Alkalic Cu-Au
105E 025	61.038056	-134.708056	8	515771	6767061	LORI	Porphyry Mo (Low F-Type)
105E 026	61.366111	-135.09	8	495188	6803570	MUSTARD	Vein Au-Quartz
105E 036	61.230556	-134.954167	8	502460	6788469	AURIER	Unknown
105E 037	61.175833	-134.660833	8	518242	6782419	CROST	Unknown
105E 038	61.072222	-134.576667	8	522844	6770905	SLINE	Unknown
105E 039	61.031389	-135.019722	8	498934	6766283	AKEL	Unknown
105E 040	61.44	-135.075278	8	495984	6811800	OVOAS	Unknown
105E 050	61.039444	-134.561111	8	523708	6767260	DEBICKI	Unknown
105E 062	61.229444	-134.834444	8	508893	6788349	EGYPT	Unknown

Porphyry-style mineralization

The Jurassic Teslin Crossing pluton hosts the Mars Cu-Mo-Au porphyry system (Yukon MINFILE 105E 002). The pluton consists of multiple high level intrusive phases of varying composition (syenite, monzonite and granodiorite). Extensive potassium metasomatism accompanied brecciation of the intrusion, and the surrounding monzonite exhibits weak propylitic alteration. Lamprophyre and hornblende-plagioclase porphyry dikes cut the main pluton following brecciation but prior to completion of mineralization. Mineralization is characterized by minor disseminated chalcopyrite associated with pyrite, magnetite and traces of molybdenite, galena, scheelite and purple fluorite. It is erratically distributed throughout the brecciated and altered areas of the pluton, locally associated with carbonate and quartz veining (e.g., Hart, 1997b; Lang and McClaren, 2003). Mineralization is inferred to be close to the age of the pluton (171.62 ± 0.05 Ma; Yukon Geochronology, 2018).

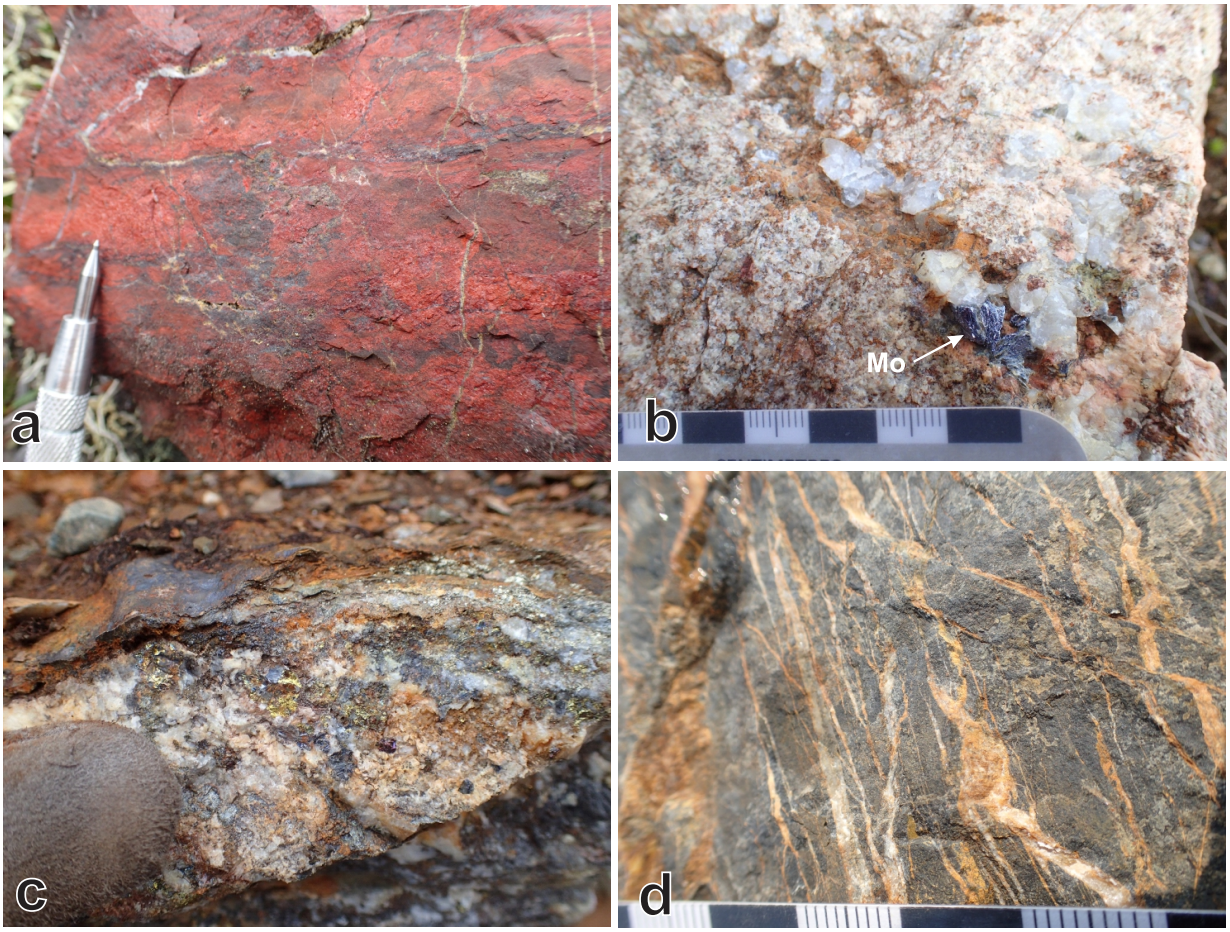

Figure 49. *Field photographs of selected mineralized occurrences.* ***(a)*** *Algoma-style iron formation hosted in Joe Mountain Formation pillow basalt, composed of interlayered hematite + quartz, magnetite, minor pyrite;* ***(b)*** *Hig (Cu-Mo; porphyry) hosted in ~116 Ma Laurier Creek pluton (Mo = molybdenite);* ***(c)*** *King showing at Hartless Joe displays chalcopyrite, sphalerite, galena, bornite in a quartz vein (60 g/t Au, 554 g/t Ag, 5.01% Pb, and 0.35% Cu across 1.2 m; www.strategicmetalsltd.com); and* ***(d)*** *carbonate veins through laminated mudstone near the Grumpy prospect, Joe Mountain area.*

Cu or Mo porphyry are hosted within large mid-Cretaceous plutons such as the Laurier Creek pluton (e.g., Hig occurrence, Yukon MINFILE 105E 024; Fig. 49b). The Hig occurrence is characterized by minor chalcopyrite and molybdenite in quartz veins and fractures. The mineralized area is weakly leached and exhibits possible low grade hydrothermal alteration. A selected specimen assayed 0.1% Mo and 0.03% Cu (Yukon MINFILE, 2018).

Finally, the Teslin Mountain pluton, dated at 78.14 ± 0.03 Ma, may be temporally and genetically related to the Red Mountain pluton, about 45 km to the east, which yielded Ar/Ar dates of 81.2 ± 0.9 Ma (biotite), 78.7 ± 0.9 Ma (whole rock), and 74.4 ± 0.8 Ma (whole rock; Brown and Kahlert, 1986; Joyce et *al*., 2015). The Red Mountain pluton hosts a Cu-Mo-Au-porphyry deposit (21.3 Mt at 0.293 % MoS_2; Turner and Sabag, 1995; Yukon MINFILE 105C 009) where at least four episodes of molybdenite mineralization are hosted within a quartz monzonite porphyry, and are genetically and spatially associated with hydrothermal phyllic and potassic alteration (Brown and Kahlert, 1986). A late event of base metal mineralization hosted in veins is also identified (Brown and Kahlert, 1986).

Skarn Mineralization

Cu or Mo skarn are found where the Upper Triassic carbonate sequence is intersected by Cretaceous dikes. At the Laberge prospect (Yukon MINFILE 105E 006), four small skarn showings containing magnetite and minor bornite and chalcopyrite occur at the contact of Aksala formation limestone and argillite with several Cretaceous feldspar porphyry dikes. The dikes show weak hydrothermal alteration with minor quartz veining containing chalcopyrite and molybdenite representing a second type of mineralization (Eaton, 1999). Best mineralization values were obtained from a trenching program that exposed a band of highly oxidized skarn comprising narrow veins and small lenses of semi-massive to massive pyrite and pyrrhotite with lesser sphalerite, chalcopyrite and galena (average values of 2.9% Zn, 0.17% Pb, 2.5% Cu, 66.9 g/t Ag and 9.1 g/t Au from seven grab samples; Eaton, 1999).

Epithermal vein-related mineralization

Quartz-vein related gold and polymetallic prospects (e.g., Hartless Joe prospect, Yukon MINFILE 105D 051) are hosted in the Joe Mountain Formation basalt (Hart, 1997a), however the mineralization itself is systematically associated with dikes and quartz veins that may be younger than the Triassic rocks (Fig. 49c,d). Mineralization at Hartless Joe is further described below.

Structurally controlled epithermal mineralization is also hosted in Open Creek volcanic rocks (R. Hulstein, *pers.comm.*) and likely associated with the emplacement of the Late Cretaceous volcanic complex.

Assays

During mapping 18 assay samples were collected from host rocks containing visible disseminated sulphides, or pervasive veining associated with oxidation or alteration at the outcrop scale. Most samples were collected in the vicinity of known showings. Samples were submitted to the Bureau Veritas Minerals processing facility in Whitehorse, Yukon, and analyzed at their laboratory in Vancouver, BC. Analytical procedures included splitting, crushing and pulverizing of 250 g of rock samples through a 200 mesh screen. Analysis of Au was done by fire assay fusion and an atomic absorption spectroscopy (AAS) finish. Nine other elements (Mo, Cu, Pb, Zn, Ag, As, Sb, Bl, Hg) were tested by Aqua Regia digestion with and inductively coupled plasma mass spectrometry (ICP-MS) finish.

Results are summarized in Table 4 and original certificates are in Appendix E. Most samples display concentrations below the detection limits for Mo, Ag, As, Sb, Bi and Hg. Au and Cu concentrations are not significant. Of the 18 samples tested, only two show noticeable values and are briefly discussed here.

Sample 15EB-043-1 was collected west of Joe Mountain near the Joe Creek (Yukon MINFILE 105D 197) and Grumpy (Yukon MINFILE 105D 203) Au-quartz vein prospects (Fig. 50). The sample was collected at an outcrop of brown-weathering, dark green basalt, intersected by a small fault zone along which the rock is altered to pale green chlorite or oxidized. Disseminated sulphides are seen along this small-scale structure. Assay analyses returned 0.1% Zn, 279 ppm As and 1.2 ppm Ag. Other reported mineral occurrences in this area include the Ace (Yukon MINFILE 105D 051) polymetallic veins prospect (Ag-Pb-Zn ± Au), and the Hartless Joe high-grade epithermal Au-Ag prospect (rock chip sample at 60 g/t Au, 554 g/t Ag, 5.01% Pb, and 0.35% Cu over 1.2 m; Eaton, 2016).

Table 4. *Assay results. Complete certificates in Appendix E.*

	UTM Coordinates Easting	Northing	Weight (kg)	Au (ppm)	Mo (ppm)	Cu (ppm)	Pb (ppm)	Zn (ppm)	Ag (ppm)	As (ppm)	Sb (ppm)	Bi (ppm)	Hg (ppm)
Detection limits			0.01	0.005	1	1	2	2	0.1	5	2	2	0.01
15EB-004-1	508670	6754569	0.65	-	-	12	31	60	0.3	-	-	-	-
15EB-043-1	515103	6753804	0.52	0.056	187	598	56	1111	1.2	279	9	-	0.01
15EB-045-1	514774	6752947	0.8	-	-	116	3	74	0.3	7	-	-	-
15EB-056-1	516572	6753538	0.66	0.206	-	20	-	125	-	-	-	-	-
15EB-144-1	521599	6767067	0.62	0.007	-	25	-	46	-	-	-	-	-
15EB-285-1	513090	6793619	0.55	0.008	9	146	4	16	0.1	-	-	-	-
15EB-285-2	513090	6793619	0.34	0.008	3	89	4	52	-	-	-	-	0.01
15EB-435-2	520893	6771263	0.51	0.006	-	22	-	66	-	-	-	-	-
16EB-007-1	510126	6763237	0.56	0.01	-	226	-	36	0.1	-	-	-	-
16EB-032-1	509519	6765413	0.48	0.011	1	125	15	39	0.1	-	-	-	-
16EB-074-1	511098	6768272	0.57	0.007	1	171	3	41	0.6	-	-	-	-
16EB-076-1	511032	6767763	0.75	0.008	-	105	4	52	0.1	-	-	-	-
16EB-084-1	516255	6766565	0.53	-	1	3	12	10	-	-	-	-	-
16EB-088-1	514494	6767795	0.62	0.009	-	53	4	62	-	9	-	-	-
16EB-202-1	497094	6774710	0.83	-	-	21	2	83	-	-	-	-	-
16EB-225-1	498195	6772755	1.02	0.02	30	662	74	67	2.8	15	-	14	0.11
16EB-364-2	500154	6788604	0.28	-	-	37	2	27	-	-	-	-	0.04
16EB-521-1	491201	6774353	0.66	0.01	-	11	9	27	-	16	-	-	0.02
18EB-009-2	534820	6734320		0.009	0.76	9	45	4	0.21	3.1	0.35	3.04	n/a
18EB-019-1	534701	6734562		0.01	0.24	5.9	8.3	2	0.1	47	2.1	0.07	n/a
18EB-019-2	534701	6734562		0.011	0.35	7.7	22.7	8	0.23	50.8	2.18	0.36	n/a
Note: "-" stands for below detection limit values													

Sample 16EB-225-1 was collected less than 2 km from the eastern shore of Lake Laberge, in the vicinity of the Laberge skarn prospect (Yukon MINFILE 105E 006). The rock is a rusty weathered, calcareous mudstone that is overlain by limestone conglomerate, and intruded by a medium-crystalline rhyolite dike. The sample returned 2.8 ppm Ag, but less than 1% is reported for Cu, Zn, Mo and Pb. The interplay between Cretaceous dikes, Lewes River Group carbonate rocks and volcanic mafic rocks, may be a geologically favourable location for skarn mineralization.

Geology and mineralization styles at Hartless Joe

The Hartless Joe property (Fig. 50) at Joe Mountain was studied in detail because it benefits from recent exploration efforts including trench sampling and drilling, in addition to having good rock exposures that were mapped in the 1990s (Hart and Hunt, 1997a, 2003a; Hart, 1997a) and were examined as part of this project. The Hartless Joe property encompasses several polymetallic Ag-Pb-Zn ± Au vein occurrences, and hematite-rich iron occurrences (Piercey, 2005). Mineralized vein occurrences include Grumpy, Joe Creek, and Ace. Work by Strategic Metals Ltd. (2015–2018) uncovered several new showings including Queen, King, Jack and Gusano (Fig. 50).

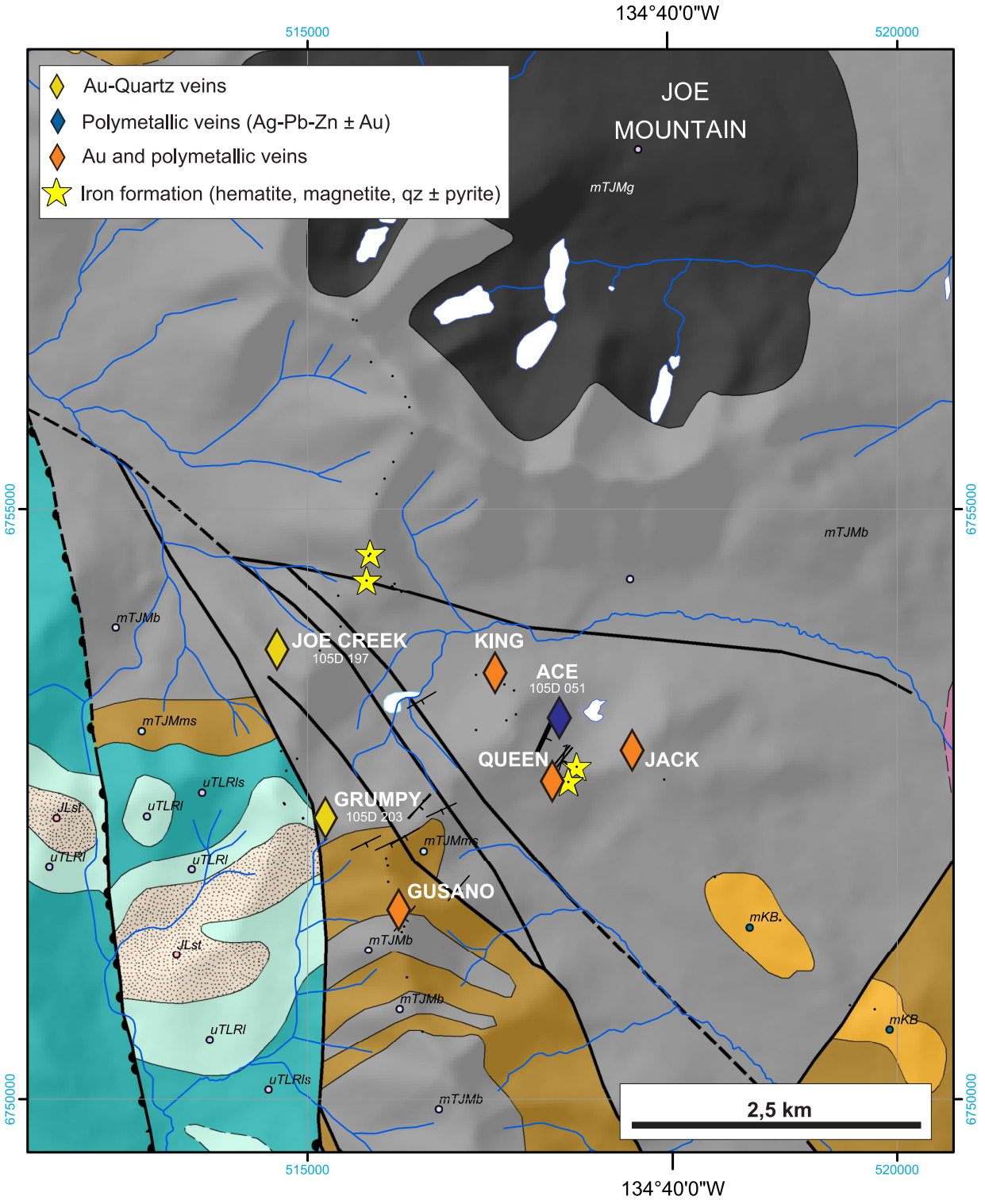

Figure 50. *Geological setting of the Hartless Joe property and location of mineral occurrences including recent discoveries by Strategic Metals Ltd. Geology legend as on Figure 6.*

Property geology

The Hartless Joe property is underlain by pillowed basalt, volcaniclastic strata, gabbro and diorite of the Middle Triassic Joe Mountain Formation (Chapter 2). Along the western edge of the property, Middle Triassic rocks are separated from carbonate strata of the Upper Triassic Lewes River Group by the Laurier Creek fault (Fig. 6; Hart and Hunt, 1997a, 2003a). To the north and east, the Teslin plutonic suite intrudes Joe Mountain Formation basalt (*ca.* 116 Ma Laurier Creek pluton, and *ca.* 120 Ma M'Clintock Lakes pluton; Hart, 1997a). Small felsic intrusions and dikes attributed to the Mount Byng suite are also mapped in the area (Hart and Hunt, 1997b, 2003b).

Characteristics of vein-related mineralization

At the King showing (Fig. 50), mineralization is characterized by pyrite, chalcopyrite, sphalerite and galena hosted in an ~50 cm thick flat-lying quartz vein in contact with rusty-brown weathered dark grey-green fine-grained volcaniclastic mudstone interbedded with mafic volcanic rocks. The subhorizontal quartz vein is located below the mudstone horizon. A rock chip sample collected during the 2015 exploration program returned 60 g/t Au, 554 g/t Ag, 5.01% Pb, and 0.35% Cu across 1.2 m (Eaton, 2016).

At the Ace and Queen occurrences (Fig. 50), shallow-dipping volcaniclastic mudstone and pillow basalt are intersected by an ~10–50 cm thick subhorizontal quartz vein and a silicified plagioclase-hornblende porphyritic dike, with up to ~1% quartz eyes. Precious metal mineralization is hosted in the quartz vein, and visible gold is present at the Queen occurrence (462 g/t Au, 79.6 g/t Ag, 1.02% Pb and 0.28% Cu across 0.4 m; Eaton, 2016). In both occurrences, the highly silicified dikes were sampled for trace element lithogeochemistry and U/Pb geochronology.

The Gusano prospect (Fig. 50; 1.31 g/t gold across 7 m; Eaton, 2018) is hosted in a sequence of grey-brown weathering, pale grey-brown volcaniclastic conglomerate unit interbedded with thin-laminated, very fine grained, dark grey non-calcareous mudstone and minor basalt. Clasts are subangular, aligned, rectangular, 2–3 cm long, and dominated by fine-grained volcanic mafic rock and/or mudstone. At the prospect, a quartz-phyric rhyolite dike and mineralized quartz vein intersect the volcaniclastic sequence. The dike is orange weathered, white, with up to 5% quartz eyes in an equigranular plagioclase-rich altered groundmass. The dike was sampled for trace element lithogeochemistry.

Analytical work

Several occurrences in the Joe Mountain area were visited during the summer of 2018 and samples were collected for geochemistry and geochronology to: (1)determine the age and composition of dikes spatially associated with mineralization, and (2) characterize the relationship between the host rocks, dikes and veins, and the mineralization history. Geochronology results were pending at time of writing this report, but lithogeochemistry results are briefly discussed below.

Three dikes were sampled in the Joe Mountain area at known gold mineral occurrences on the Hartless Joe property. One dike is a plagioclase-quartz-phyric, equigranular, rhyolite intersecting a basalt and chaotic volcaniclastic carbonate sequence at the Gusano showing (1.31 g/t Au across a 7 m trench; Eaton, 2018). The dike is overlain by a mineralized quartz vein. The second dike sampled is at the Ace showing (Yukon MINFILE 105D 051). It is a silicified, yellow-beige-weathered plagioclase-hornblende porphyritic intermediate dike, intersecting a sequence of basalt and interbedded mudstone. A quartz vein lies parallel to the bedding and dike. A similar setting is observed at the Queen occurrence (Yukon MINFILE 105D 051). Finally, a pale grey quartz-phyric rhyolite dike intersecting the Joe Mountain Formation volcaniclastic sequence is sampled south of Joe Mountain. It is possibly associated with the emplacement of the mid-Cretaceous Byng volcanic suite.

Results

All three dikes sampled at Hartless Joe returned REE signatures that correspond to some of the patterns identified in Chapter 4. Felsic plagioclase-quartz porphyric dikes at Ace and Gusano occurrences display a steep negative slope with enrichment in LREE and depletion in HREE (Fig. 51). This profile is characteristic of calc-alkaline arc rocks, and is similar to results obtained from other plagioclase-quartz-phyric rhyolite samples from the Goddard suite near Teslin Mountain (Fig. 38) and dated at 138–136 Ma (Fig. 34).

The pale grey quartz-phyric rhyolite dike, possibly associated with the mid-Cretaceous Byng volcanic suite, has a very distinct REE signature. The REE profile is flat with a slight Eu anomaly. A similar signature was observed in intermediate dikes that intersect the Joe Mountain Formation near Teslin Mountain (Fig. 38). There is no U/Pb age available for these dikes compositions.

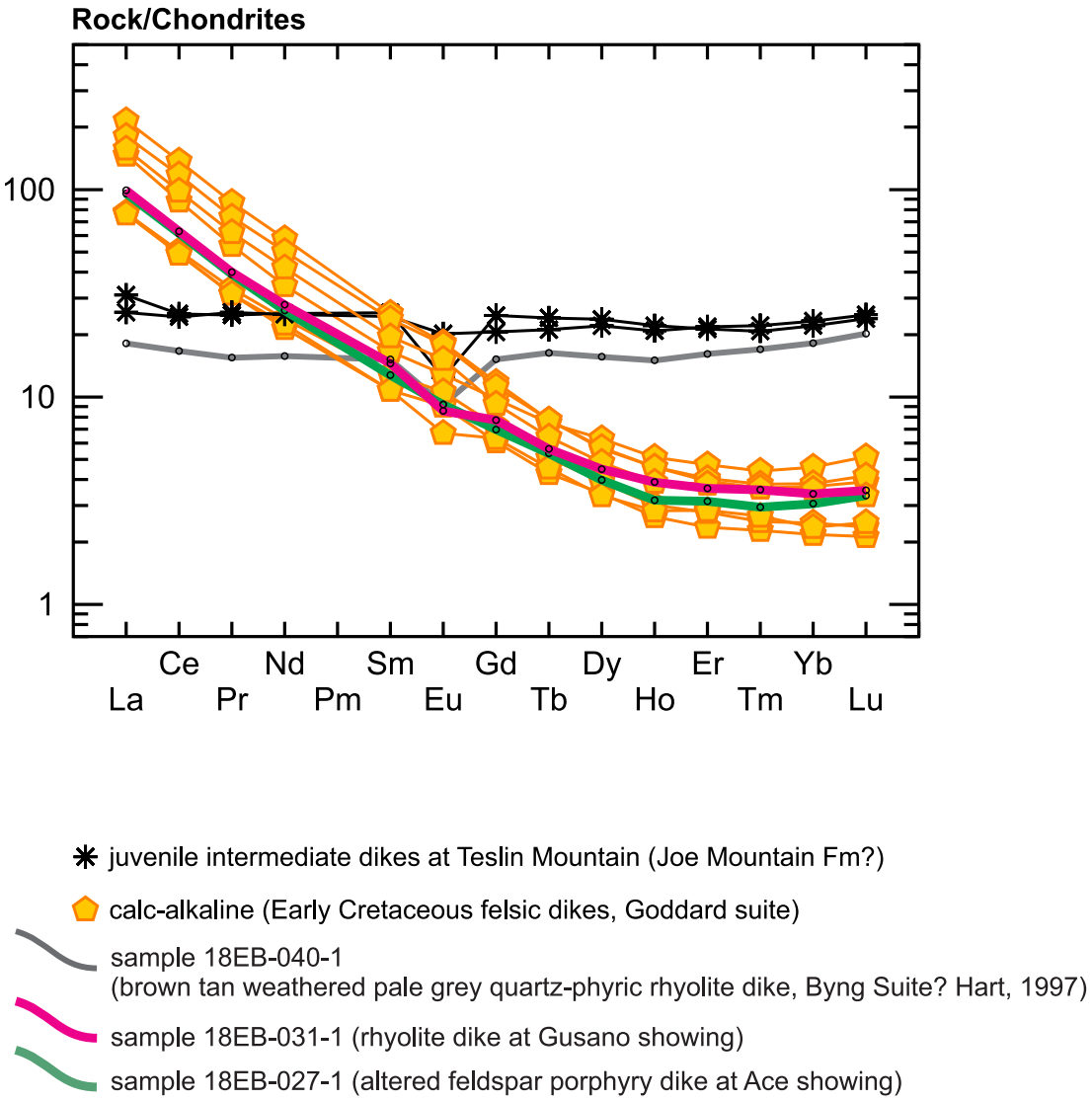

Figure 51. *REE vs chondrite diagram for Cretaceous dikes of the Hartless Joe property (Sun and McDonough, 1989). The dikes display signatures similar to two of the four different trends identified in Chapter 4, including the flat juvenile profile likely corresponding to Middle Triassic dikes, and the calc-alkaline profile that includes at least two Early Cretaceous felsic dikes.*

Interpretation

Mineralized occurrences at the Hartless Joe property are characterized by quartz veining and dikes intruding mafic and clastic strata of the Middle Triassic Joe Mountain Formation. Mineralization at Hartless Joe is classified as a low-sulphidation epithermal gold-silver type, based on the presence of epithermal vein textures and breccia with low base metal content (Pautler, 2018). Structurally controlled epithermal mineralization is further suggested by the presence of a complex extensional fault system, including a pull-apart basin (Pautler, 2018).

Work by Strategic Metals Ltd. in the area of the King and Queen occurrences identified subhorizontal bedding, interpreted as volcanic flows or volcaniclastic intervals, and spatially associated with mineralization. In the southwestern property area, a series of east-trending antiforms and synforms occur within Triassic and Early–Middle Jurassic strata. Hart (1997a) stated that the plagioclase-hornblende porphyritic dikes are related to the Teslin plutonic suite, whereas the quartz-phyric dikes and plugs are younger and genetically related to late phases of the Whitehorse suite and Byng Creek volcanic complex.

REE geochemical profiles for three felsic to intermediate dikes of the Hartless Joe property are similar to REE profiles identified to the north, in the eastern Lake Laberge area. Felsic plagioclase-quartz porphyric dikes at the Ace and Gusano occurrences are possibly related to the Early Cretaceous Goddard suite. If U/Pb geochronology confirms this association, there are several implications for mineral exploration:

- other plagioclase-quartz porphyric dikes in the eastern Lake Laberge area may be associated with mineralization. All dikes mapped in the eastern Lake Laberge area are reported in Appendix D, and are associated with a field description and UTM coordinates. A few dikes have geochronology and geochemical data available; and
- the age of epithermal mineralization at Hartless Joe may be constrained to the Early Cretaceous, based on the systematic association of these dikes with precious metals mineralization. This hypothesis will be confirmed once U/Pb dates are available. Orogenic gold mineralization in the Cariboo, Cassiar and Sheep Creek gold districts of BC is also associated with Early Cretaceous hydrothermal alteration events (Allan *et al.*, 2017).

Chapter 7 – Synthesis and Discussion

Field observations collected during mapping, combined with lithogeochemistry, Nd-Hf isotopic analyses, U/Pb geochronology, fossil identification, and structural interpretations are integrated to propose an interpretation of the tectonic evolution of the area east of Lake Laberge, south-central Yukon, from the Middle Triassic to the Cretaceous.

Triassic volcanic setting and evolution

Across the Canadian Cordillera, several Middle and Late Triassic arc volcanic assemblages are part of the Intermontane terranes (Fig. 52). Middle Triassic units include the Sitlika assemblage (*ca.* 258–241 Ma; Childe and Schiarizza, 1997), the Kutcho assemblage (*ca.* 252–242 Ma; Childe and Thompson, 1997; Childe *et al.*, 1997; Schiarizza, 2012), the Joe Mountain Formation (*ca.* 245 Ma, or Anisian to Ladinian; Hart, 1997a; this study), and the Michie formation (*ca.* 245–244 Ma; Bickerton, 2014). Upper Triassic volcanic units include the Nicola Group (*ca.* 238 Ma to *ca.* 202 Ma; Mihalynuk *et al.*, 2016), the Povoas formation (possibly as old as Early Carnian, and as young as Norian; Hart, 1997a; this study), the Stuhini Group (*ca.* 219–214 Ma; e.g. Simmons *et al.*, 2007) and the Takla Group (226–208 Ma; MacIntyre *et al.*, 2001).

Stratigraphic relationships, provenance studies, geochemical analyses and geochronology are key to determine whether these two sets of volcanic arcs (Middle Triassic and Late Triassic) evolved independently of each other until they were juxtaposed during Cordilleran orogenesis, or if they share common origins. Both scenarios have critical implications for models of Cordilleran terranes assembly.

Terrane affinity of Middle Triassic volcanic arcs

The Middle Triassic Joe Mountain Formation is coeval and spatially aligned with several volcanic arc assemblages in southern Yukon and northern BC, including the Michie formation, the Kutcho assemblage and the Sitlika assemblage.

The Michie formation is a volcaniclastic package that is gradationally overlying mafic volcanic rocks ascribed to the Cache Creek terrane south of Whitehorse (Bickerton, 2014). The formation is interpreted to represent fragmental rocks deposited on the flanks of a volcanic arc, and has yielded U/Pb zircon ages of 244.64 ± 0.08 Ma and 245.85 ± 0.07 Ma (Bickerton, 2014). Samples from mafic rocks stratigraphically related to clastic rocks of the Michie formation show a subalkalic signature, indicative of formation in a primitive arc tectonic setting.

Farther south, in the Dease Lake area of northern British Columbia, metavolcanic and metavolcaniclastic rocks of the Kutcho assemblage (Childe and Thompson, 1997; Schiarizza, 2011, 2012) form the basement to Upper Triassic and Lower Jurassic sedimentary rocks of the Whitehorse trough (English *et al.*, 2010). The assemblage is dominantly volcanic and composed of bimodal interbedded basalt and rhyodacite to rhyolite, and minor sedimentary intervals. The chemistry of tholeiitic volcanic rocks of the Kutcho assemblage also reflects a primitive arc tectonic setting (Childe and Thompson, 1997; Childe *et al.*, 1997). The age of the Kutcho assemblage is between 252 and 242 Ma (Childe and Thompson, 1997; Childe *et al.*, 1997; Schiarizza, 2012; Fig. 52). The Kutcho assemblage is correlated with the Sitlika assemblage in central BC (Monger *et al.*, 1978), dated at 241 ± 1 Ma and *ca.* 258 Ma (Childe and Schiarizza, 1997; Fig. 52).

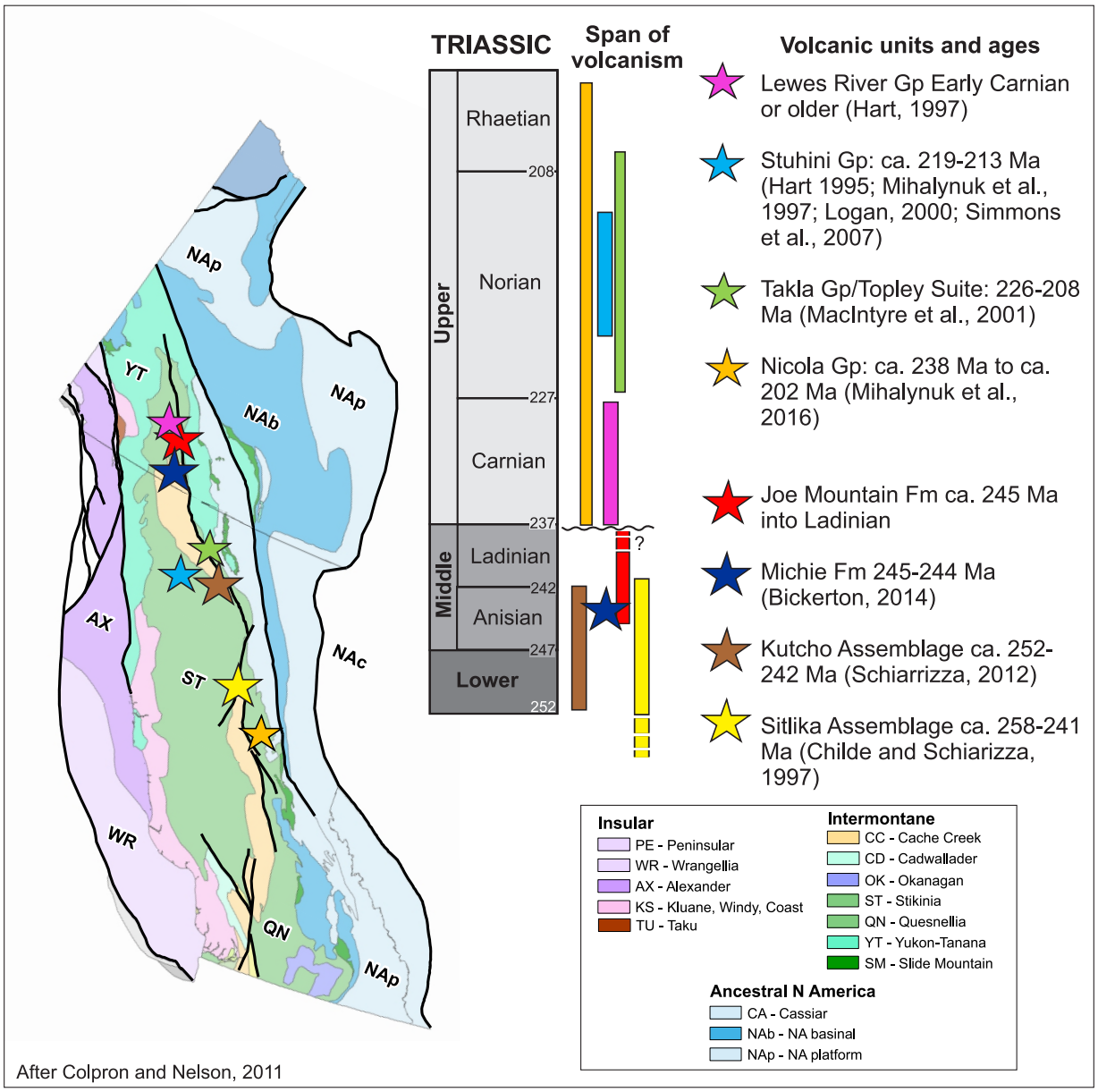

Figure 52. *Geochronology summary for Triassic volcanic arcs in the Intermontane terranes of BC and Yukon. Terrane map after Colpron and Nelson (2011).*

In addition to similar U/Pb ages, tholeiitic volcanic rocks of the Joe Mountain Formation and Kutcho assemblage show consistently depleted HFSE and flat to LREE-depleted REE patterns, suggesting they were both formed in an intra-oceanic arc environment (Fig. 53; e.g., Childe et *al.*, 1998). Isotopically, the Kutcho assemblage displays very similar primitive εNd(t) values to the Joe Mountain Formation (Fig. 54). Therefore, these Middle Triassic volcanic rocks are likely derived from similar primitive magmatic sources, with no significant incorporation of old, evolved sialic components.

Finally, the geochemistry of igneous zircon grains from the Joe Mountain and Michie formations were compared. Both sets of zircons display very high REE concentrations, with an average of 7900 ppm for samples of the Michie formation, and 5200 ppm in 15-EB124-1 from the Joe Mountain Formation at Teslin Mountain (J. Crowley, *pers. comm.*). Typical arc magmas usually

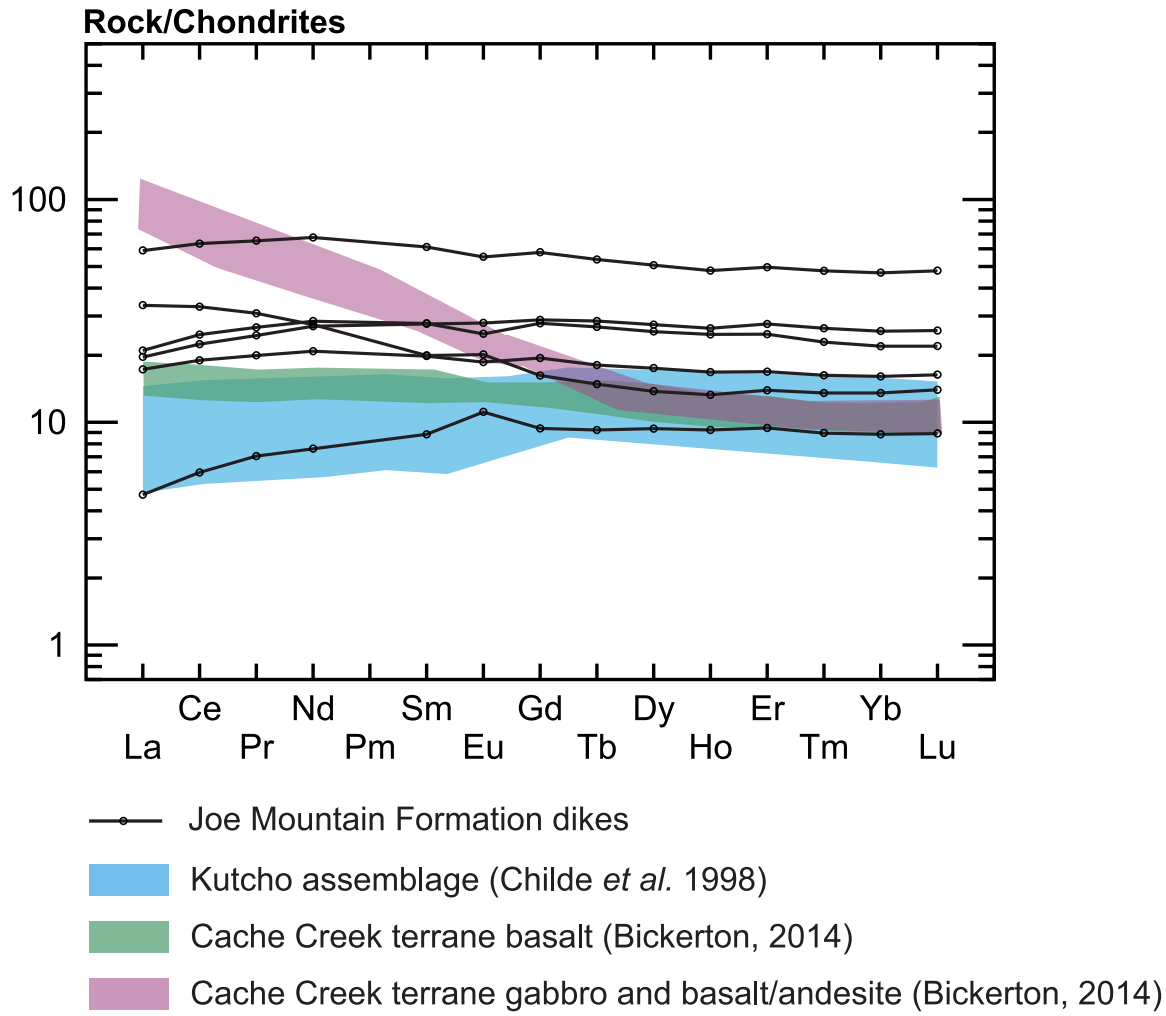

Figure 53. *REE composition of Middle Triassic mafic rocks including Joe Mountain Formation dikes, mafic volcanic rocks of the Kutcho assemblage in British Columbia (Childe et al., 1998), mafic volcanic rocks and gabbro of the Cache Creek terrane (Bickerton, 2014). Chondrite normalizing values after Sun and McDonough (1989).*

display 400–800 ppm REE concentrations. In addition, both sets of zircons are characterized by a very similar magnitude of Eu anomaly (Eu/Eu*; ~0.19 in the Michie formation, and ~0.23 in the Joe Mountain Formation), suggesting very similar magma sources for the two formations. In contrast, values in typical arc magmas are highly variable, from about 0.6 to 0.1. However, zircon geochemistry from the two sets display some significant differences in their Th/U, with an average of 0.98 in the Michie formation and 0.62 in the Joe Mountain Formation.

In conclusion, the Joe Mountain and Michie formations, and Kutcho and Sitlika assemblages are correlated based on lithological, chemical and geochronological evidence. This suggests that these primitive tholeiitic arc assemblages have a common magmatic origin and formed a single primitive volcanic arc that was subsequently dispersed by faulting. This primitive arc could have been part of one of the Intermontane terranes, as suggested by the current distribution of the Kutcho, Sitlika and Joe Mountain assemblages within the Canadian Cordillera. Alternatively, it could be a discrete, previously unrecognized intra-oceanic arc terrane.

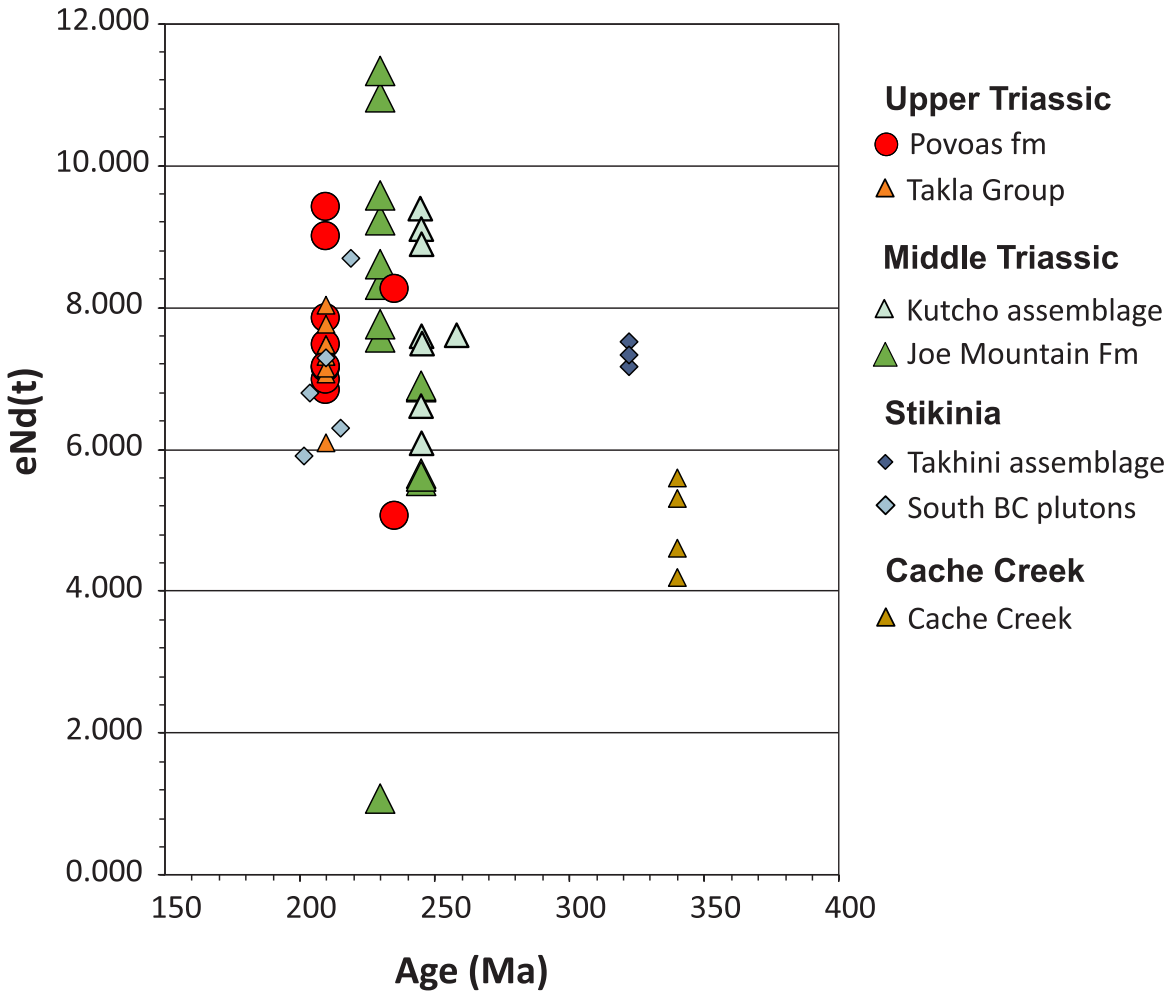

Figure 54. *Age vs eNd(t) plot for various Triassic volcanic suites of the Canadian Cordillera. Data from the Joe Mountain and Povoas formations are from this study. Other data include: Takla Group (Dostal et al., 2009), Takhini assemblage, southern BC plutons (Gosh, 1995), Cache Creek (Smith and Lambert, 1994), Kutcho assemblage (Childe et al., 1998; Childe and Schiarizza, 1997; Childe and Thompson, 1997).*

Several authors have indicated a structural contact and possible affiliation of Middle Triassic primitive arc assemblages to the Cache Creek terrane (Childe and Thompson, 1997; Schiarizza, 2012). The Cache Creek terrane is a Mississippian to Jurassic assemblage comprising chert, argillite, basalt, ultramafic rocks, extensive carbonate and locally blueschist (Monger *et al.*, 1982; Mihalynuk et *al.*, 2004), and is generally interpreted as a subduction-accretionary prism system that formed outboard of the Stikinia-Quesnellia arc terranes. It comprises ophiolites grouped with intraplate volcanic rocks, and carbonate successions with Early Permian fauna of Tethyan affinity being incorporated to the subducting slab of the Panthalassa ocean basin (Nelson et *al.*, 2013). Due to its origin as an accretionary complex, the Cache Creek terrane is formed of several fundamentally different associations of rocks, each of which could potentially be redefined as a distinct terrane (*i.e.*, a crustal block defined on the basis of its unique tectonostratigraphic record, that either is bounded by faults, or locally shares depositional and geodynamic ties with adjacent terranes; Gabrielse, 1991; Colpron et *al.*, 2007b).

It is suggested that a regionally extensive, primitive intra-oceanic volcanic arc system, including the Kutcho and Sitlika assemblages in northern BC, and the Joe Mountain and Michie formations in southern Yukon, was active during the Permo-Triassic, and formed an independent subterrane (Fig. 55a). This arc was situated outboard of Stikinia and Quesnellia, and was distinct from the seamounts and Tethyan carbonate assemblages later incorporated into a Cache Creek accretionary prism. This subterrane eventually became part of a Cache Creek composite terrane during amalgamation in Middle-Late Jurassic.

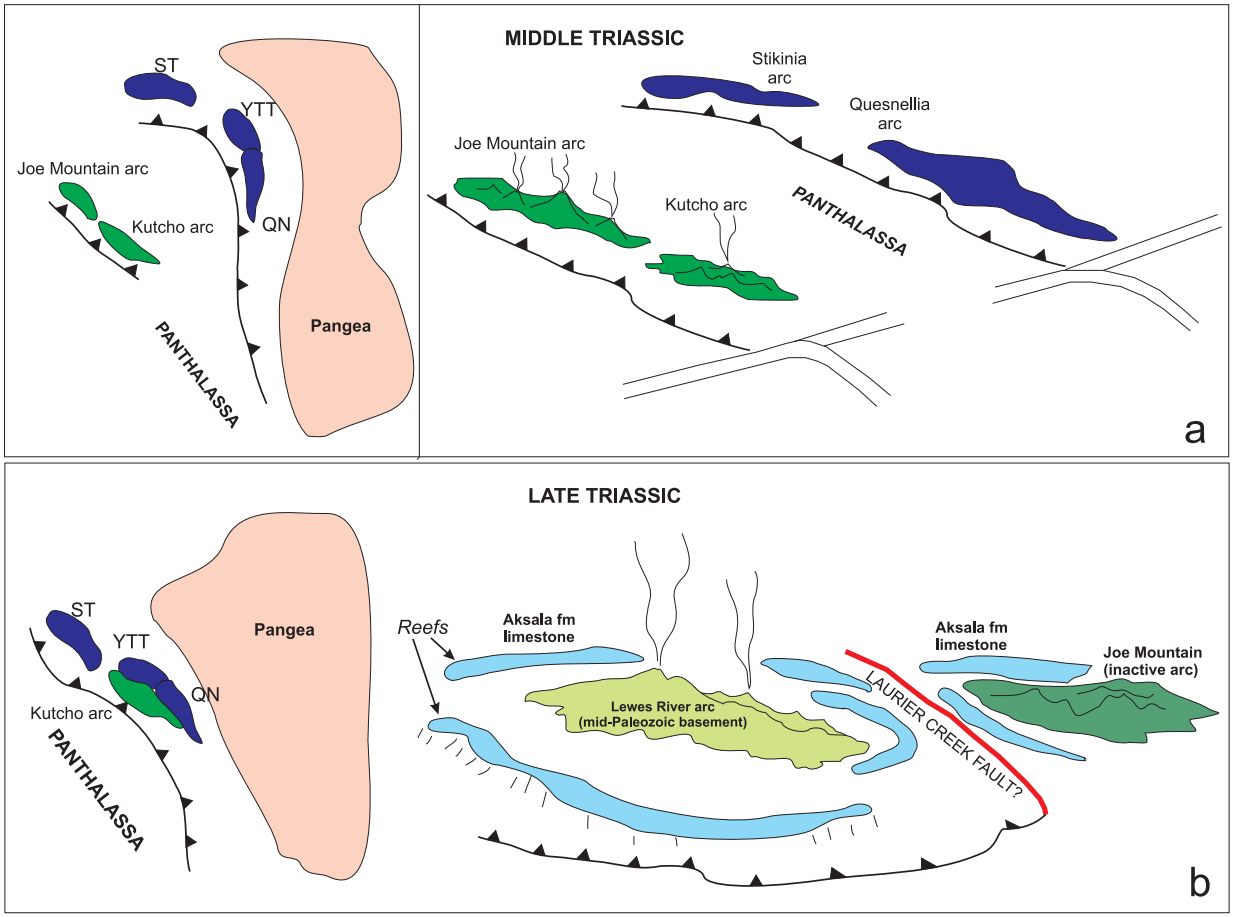

Figure 55. *Simplified sketches depicting the relationship between the main tectonic elements in the Middle and Late Triassic.* ***(a)*** *In the Middle Triassic, the Joe Mountain and Kutcho arc evolved in Panthalassa, away from the Laurentian margin, and constitute an independent oceanic arc system; and* ***(b)*** *by the Late Triassic, the Joe Mountain and Kutcho arcs must have been adjacent to the developing Lewes River arc. The latter likely built over older Intermontane crust, and was located at tropical latitudes. The Lewes River arc comprises a juvenile volcanic arc surrounded by shallow oceanic basins in which carbonate reefs strive, and are partially deposited over older Middle Triassic crust. The Laurier Creek fault marks the westernmost boundary of the Joe Mountain formation and may represent a reactivated terrane boundary.*

Stratigraphic links between Middle and Upper Triassic volcanic arcs

Upper Triassic volcanic assemblages (*e.g.*, Lewes River Group) were deposited onto older Paleozoic rocks of Stikinia (*e.g.*, Monger *et al.*, 1991; Simmons *et al.*, 2007). The older parts of Stikinia (Monger *et al.*, 1982) are represented by several upper Paleozoic arc assemblages in the northern Cordillera, including the Takhini assemblage in Yukon, and the Stikine and Asitka assemblages in northern BC. In Yukon, the relationship between the Takhini assemblage and Lewes River Group is unknown. The upper Paleozoic Takhini assemblage, exposed west of Whitehorse, is composed of variably deformed and metamorphosed mafic volcanic rocks, including greenstone, greenschist, metabasite, and minor amphibolite, gneiss, schist and felsic metavolcanic rocks (Hart, 1997a). This volcano-sedimentary package has a Mississippian age of *ca.* 323 Ma (Hart, 1997a). Similarly, the Stikine assemblage found in the Iskut River region of northern BC (Gunning *et al.*, 2006) is a Paleozoic assemblage recording the superposition of successive arcs over a span of 150 m.y. It is characterized by mixed igneous series recording the association of non-arc, enriched basalt with calc-alkaline magmatism, as a response to intra-rifting of the overriding plate. Regional structures are believed to have controlled the sites and nature of Stikine volcanism (Gunning *et al.*, 2006). On the basis of similar lithology and a late Paleozoic age date, the Takhini assemblage in Yukon is correlated with the Stikine assemblage in British Columbia. Both assemblages also display similar isotopic signatures, with $\varepsilon Nd(t)\sim 7$ for the Takhini assemblage (Fig. 54), and $\varepsilon Nd(t)\sim 2–8$ for the Stikine assemblage (Fig. 54; Gunning *et al.*, 2006).

Detrital zircon signatures of Middle and Late Triassic assemblages provide strong clues to establishing depositional links between these assemblages, and their relationship with underlying Paleozoic assemblages. For instance, two detrital zircon samples from the Aksala formation show a main peak in the Norian, as well as a subsidiary population of Paleozoic zircons (Chapter 2; Fig. 16). The presence of a Paleozoic signal amongst Lewes River Group detrital zircons suggests that Upper Triassic strata were deposited in proximity of upper Paleozoic rocks of Stikinia in Yukon. This observation contrasts with the detrital zircon signature of Joe Mountain and Michie formations, which lack an upper Paleozoic signal. In fact, Joe Mountain Formation age signatures show no input from zircons other than igneous grains dated at *ca.* 245 Ma (Fig. 15). Zircons from the Joe Mountain Formation are clearly equigranular, igneous grains, whereas grains from the Aksala formation display a variety of grain sizes and morphology (Appendix B3). An identical age signature to that of the Joe Mountain Formation is observed for several geochronology samples from the Michie formation (Bickerton, 2014). Finally, Norian strata of the Lewes River Group lack a Middle Triassic detrital zircon signature. Therefore, evidence from detrital zircon signatures in Middle and Upper Triassic rocks suggests that Middle Triassic primitive arcs (*e.g.*, Joe Mountain, Kutcho) were separated from the younger Lewes River-Stuhuni-Takla arcs until the Late Norian (*e.g.*, Nelson *et al.*, 2013).

Post-arc Norian carbonate overlaps the different Middle Triassic arc sequences, indicating that the Middle Triassic primitive arcs are adjacent to Upper Triassic volcano-sedimentary assemblages by the latest Triassic. For instance, in northern BC, Norian carbonate rocks of the Sinwa formation unconformably overlie the Kutcho volcanic assemblage (English and Johnston, 2005; Schiarizza, 2011). Similarly, carbonate rocks of the Aksala formation overlie basalt of the Joe Mountain Formation east of the Laurier Creek fault in south-central Yukon (Figs. 6, 56 and 57). Elsewhere in the map area (*i.e.*, west of the Laurier Creek fault), the Aksala formation is overlying basalt of the Povoas formation (Fig. 56).

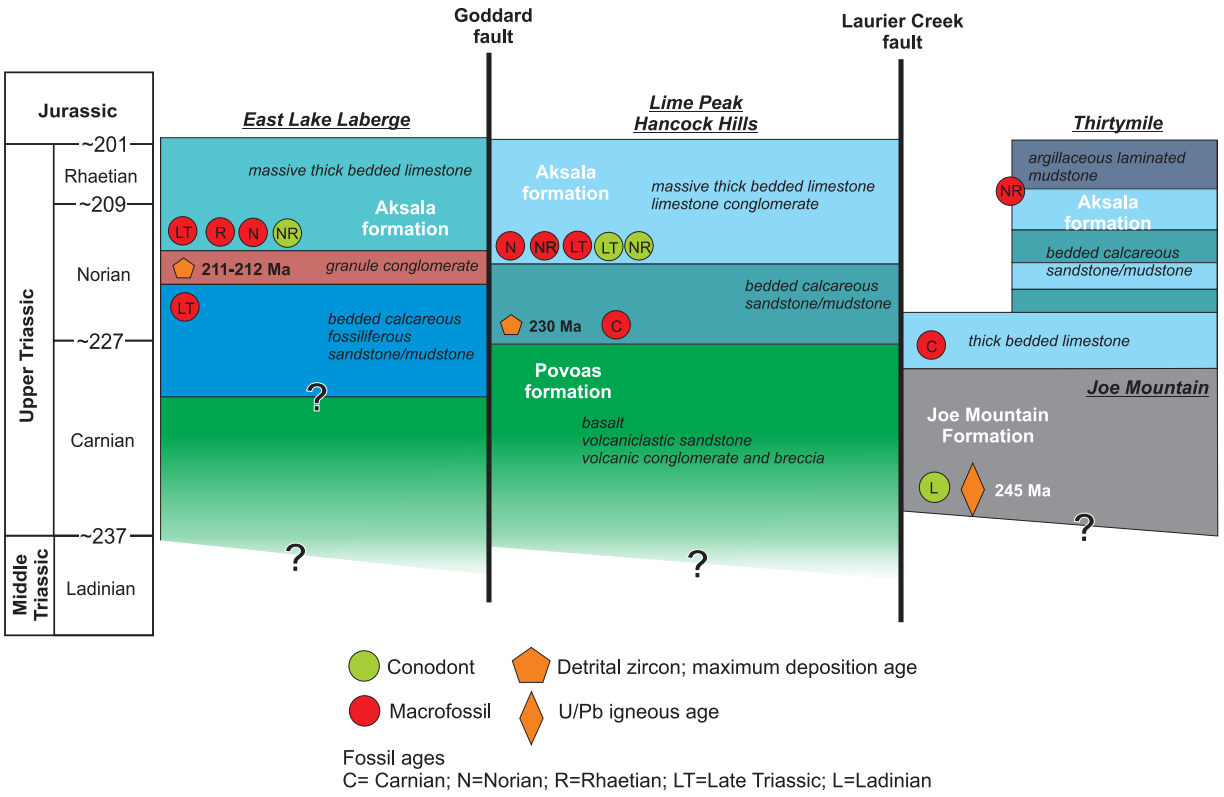

Figure 56. *Simplified stratigraphic relationships between units of the Lewes River Group and Joe Mountain Formation, constrained by field observations, fossils and detrital zircon ages. The existence of a volcanic basement is established in most areas, however no age constraint exists for the basal volcanic strata of the Povoas formation, which are therefore inferred to be Carnian or older. There is also no constraint on the nature of the contact between the Middle Triassic Joe Mountain Formation and basalt of the Povoas formation prior to faulting. The westernmost extend of the Joe Mountain Formation appears to be the Laurier Creek fault. At least two distinct but coeval sequences of carbonate and clastic strata overlie the Povoas formation volcanic rocks in the map area. The belts are now separated by the regional Goddard fault. At the time of deposition, the topography of the young volcanic arc likely controlled carbonate sedimentation in independent subbasins.*

Triassic through Cretaceous evolution

Triassic to Jurassic Arc to basin-related sedimentation

During the Late Triassic, the Lewes River volcanic arc formed a topographic high, later surrounded by a shallow oceanic basin in which carbonate sedimentation took place (Fig. 55b). Carbonate deposition and reef buildup occurred mainly post-volcanism or during the dying stages of volcanism, as indicated by field observations where the Aksala formation systematically overlies volcanic rocks of the Povoas formation. Carbonate sedimentation occurred in independent subbasins controlled by the physiography of this formerly active central volcanic arc highland. Sedimentation was locally controlled by minor variations of the depositional environment, size of the subbasin, volume and frequency of volcanic input, etc. Massive micritic limestone strata represent reef buildup structures (Reid, 1980; Yarnell *et al.*, 1999), whereas calcareous conglomerate likely represents a high-energy zone along the slope in front of the reef.

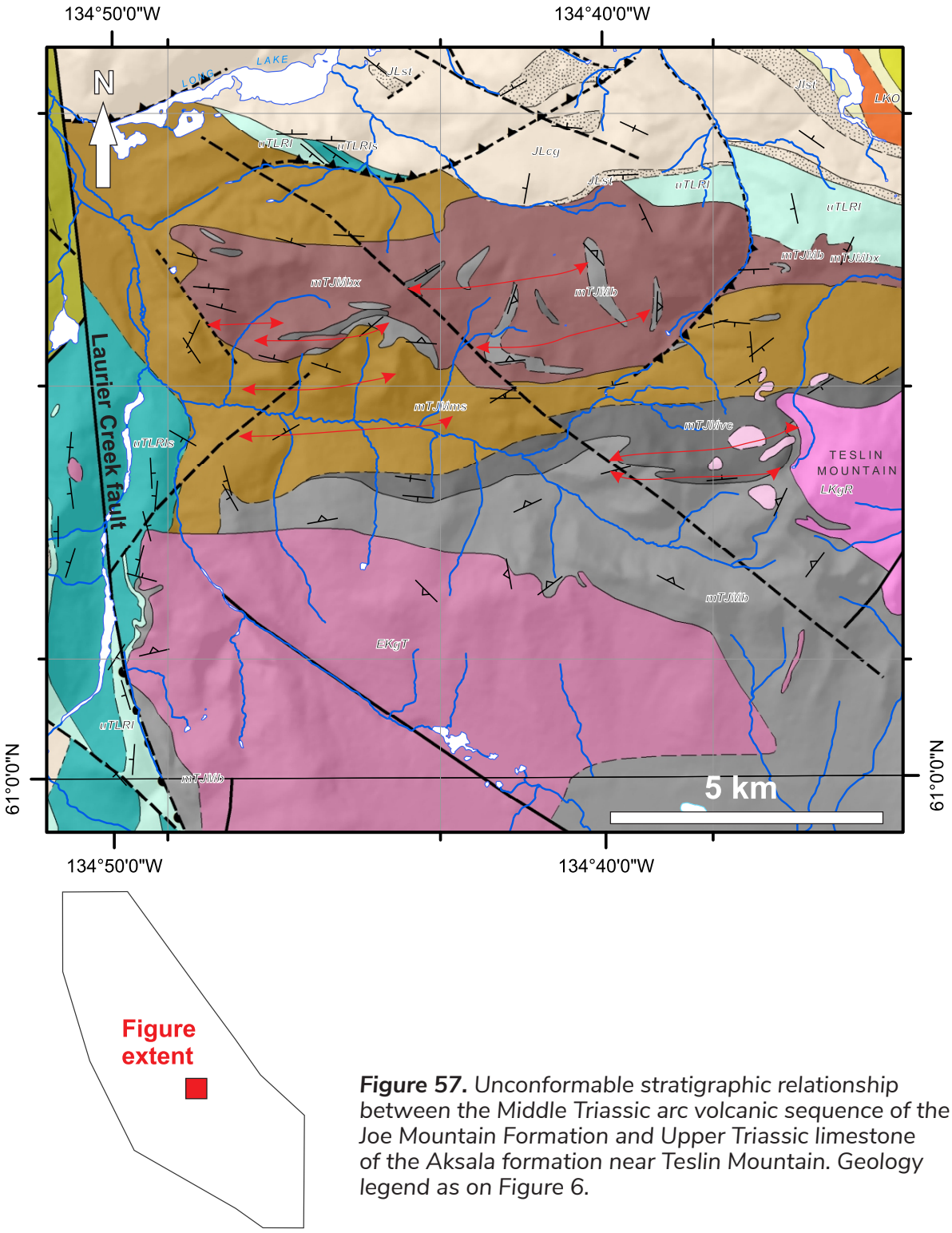

Figure 57. *Unconformable stratigraphic relationship between the Middle Triassic arc volcanic sequence of the Joe Mountain Formation and Upper Triassic limestone of the Aksala formation near Teslin Mountain. Geology legend as on Figure 6.*

Based on macrofossil analyses, environments of deposition for the carbonate sequence are interpreted as shallow marine (inner platform or shelf) to open marine, with normal salinity and a tropical climate. Fine-grained, thin-bedded, argillaceous units are interpreted as forming in deeper parts of the basin, or in shallow lagoons located between the reef and the arc. Erosion of the arc provided a steady supply of volcanic material throughout the Late Triassic. The westernmost

strata of the Lewes River Group may have originally formed in a shallow subbasin distal from the arc, and were later stacked over and against the eastern carbonate belt during Late Triassic or post-Triassic deformation.

Late Triassic clastic and carbonate sedimentation was followed by clastic sedimentation in the Whitehorse trough, and deposition of the Laberge Group. The contact relationship between the Lewes River and Laberge groups has been variably described as a conformity (Bostock and Lees, 1938; Tempelman-Kluit, 1984; Hart and Radloff, 1990), a disconformity (Hart and Radloff, 1990; Hart, 1997a), an angular unconformity (Wheeler, 1961; Lowey, 2008), or as changing from a disconformity on the western margin of the basin to a conformity in the central region (Wheeler, 1961). Lowey (2008) proposed that the contact is an unconformity that spans the entire Whitehorse trough, typically marked by conglomerate in the Richthofen and Tanglefoot formations. Most recent studies also support a regional unconformity at the base of the Laberge Group (e.g., Lowey, 2004, 2005, 2008; Lowey *et al.*, 2009; van Drecht and Beranek, 2017, 2018). Observations at Mount Byng suggest that a conformable contact between the Aksala formation and Laberge Group may exist in that area. An angular unconformity was mapped south of Long Lake, just across the Laurier Creek fault (Fig. 58). At Mount Laurier, the contact is a disconformity. These observations are consistent with a period of deformation during the latest Triassic, followed by Jurassic erosion and/or non-deposition in the central part of the map area, and finally deposition of Laberge Group strata across the Whitehorse trough.

In the region east of Lake Laberge, the Laberge Group shows a lateral transition from the polymictic conglomerate mapped east of the Laurier Creek fault, towards a fine-grained turbiditic sequence dominating the eastern shore of Lake Laberge. The base of the group comprises 10–30 m of sandstone, overlain by cobble to boulder conglomerate (e.g., Mount Laurier, Fig. 26a). The deposition of Laberge Group sediments in the Early Jurassic and their subsequent erosion was likely controlled by pre-existing Triassic topography. Massive micritic limestone beds of the Aksala formation constitute present-day, prominent topographic features (Figs. 3a and 12a), and their reefal origin suggests that they were probably already shaping the landscape during the Late Triassic and Early Jurassic. These reefs formed buttresses, constraining the deposition of both Upper Triassic argillaceous sediments, and Laberge Group turbiditic or deltaic fan deposits. Therefore, abutting relationships between Triassic and Jurassic strata (Fig. 25) results from deposition of Laberge Group sediments over pre-existing Triassic topography. This pattern was further emphasized by later deformation that thrusted sheets of Triassic rocks over younger Jurassic strata.

Deformation

Deformation in the eastern Lake Laberge area affects Triassic through Jurassic stratigraphy and is expressed by faulting, folding, and several unconformable stratigraphic relationships. Deformation is likely controlled by the Goddard and Laurier Creek fault systems. These faults are parallel, and both form a 30–40° angle with the NW-trending Teslin fault (Fig. 40). Dextral deformation along the Teslin fault, in particular, was active at the latest in the Late Cretaceous and Tertiary (Larson, 2002), but could have taken place as early as the late Early Cretaceous (*ca.* 115–100 Ma; Gabrielse *et al.*, 2006). In this stress regime, the principal stress $\sigma 1$ would be oriented north-south, while $\sigma 3$ would be east-west (Fig. 41, inset). This stress regime also implies a general dextral motion along the Goddard and Laurier Creek faults. Either these faults are dextral Riedel shears formed under the same stress regime as the Teslin fault, or the Laurier Creek and Goddard faults are older structures that were reactivated during motion along the Teslin fault. This stress regime is also compatible with normal motion along NNW-trending faults, such as along the Laurier Creek fault in the Mount Laurier area, and west of Joe Mountain (Fig. 41).

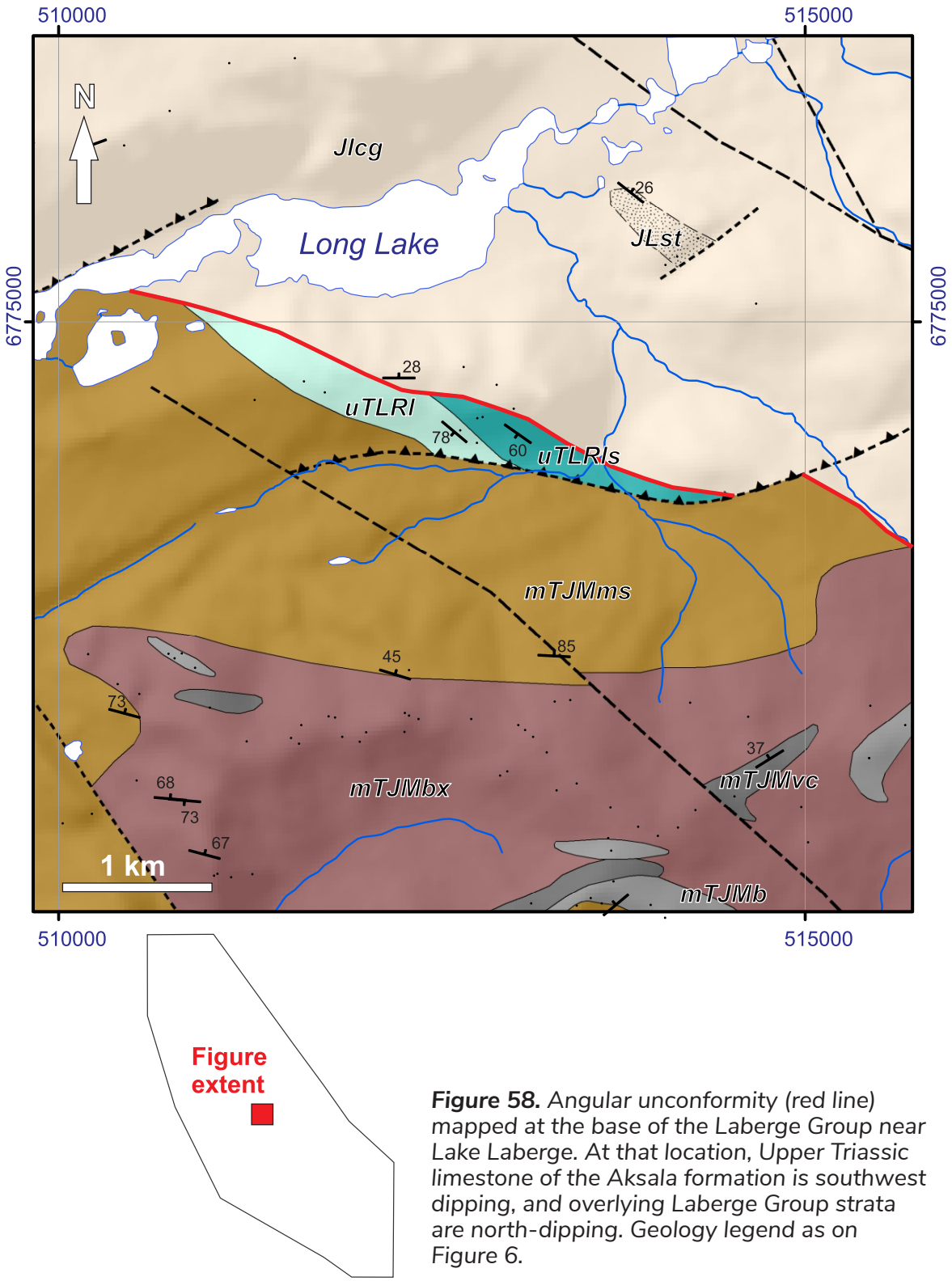

Figure 58. *Angular unconformity (red line) mapped at the base of the Laberge Group near Lake Laberge. At that location, Upper Triassic limestone of the Aksala formation is southwest dipping, and overlying Laberge Group strata are north-dipping. Geology legend as on Figure 6.*

In the eastern Lake Laberge area, east of the Laurier Creek fault, there is an angular unconformity between Upper Triassic Aksala formation strata and the base of the Laberge Group (Chapter 2; Fig. 58). In other parts of the Whitehorse trough, Laberge Group strata are commonly observed overlying different stratigraphic levels of the Lewes River Group (e.g., Colpron *et al.*, 2007a, 2015; White *et al.*, 2012; van Drecht and Beranek, 2018). These observations confirm that Upper Triassic strata were deformed and eroded prior to deposition of the Laberge Group, in the latest Triassic.

Folding likely occurred concurrently with lateral displacements along the Goddard and Laurier Creek faults. The Upper Triassic-Jurassic stratigraphic sequence is characterized by north to northwest-trending thrusts and tight folds particularly well exposed along the eastern shore of Lake Laberge (Fig. 6). At Teslin Mountain, east-trending folds are observed within the Middle Triassic Joe Mountain Formation sequence, and Laberge Group strata dip moderately to the north in a fashion consistent with these folds (Fig. 6). Folding affects both the Upper Triassic and Jurassic sequences, therefore it took place at the earliest during the Middle Jurassic. Similarly, most of the thrusting, as well as strike-slip motion along the Goddard and Laurier Creek faults, must have at least a syn or post-Jurassic component because these faults intersect rocks as young as the Early Jurassic. This event is likely related to the dominant stress regime that affected Yukon during the Mesozoic, and controlled by north-northwest-trending regional dextral strike-slip faults such as the Teslin fault (Fig. 40, inset on Fig. 41).

Therefore, at least two deformation events are identified: 1) in the latest Triassic, immediately prior to deposition of the Laberge Group basal strata; and 2) from the Middle Jurassic through Cretaceous, as part of a Yukon-wide transpressional deformation. The Goddard and Laurier Creek fault systems are definitely involved in the latest Middle Jurassic though Cretaceous transpressional event that affected southern Yukon. The implication of these faults in earliest deformation events is unclear, but they may correspond to the reactivation of an earlier contact. Observations in the eastern Lake Laberge area support previous studies in the northern Whitehorse trough that suggested that northwest-trending open folds, southwest-verging thrusts and folds, and extensional structures developed under a dextral transpressive regime controlled by regional northwest and north-striking strike-slip faults (White *et al.*, 2012). This stress regime also supports most dikes being oriented north-south. However, the timing of magmatism is not necessarily coeval with displacement along faults, because dike emplacement could occur along pre-existing structures.

Cretaceous magmatism and mineralization

The region east of Lake Laberge records magmatic activity throughout the Cretaceous. Plutons are exposed south and west of Mount Byng (M'Clintock plutons, *ca.* 121–118 Ma; Hart, 1997a), southwest of Joe Mountain (Cap Creek pluton, 111 ± 8.4 Ma; Hart, 1997a), southwest of Teslin Mountain (Laurier Creek pluton; *ca.* 116 Ma), and at Teslin Mountain (Teslin Mountain pluton; *ca.* 78 Ma). The Open Creek volcanic complex (*ca.* 79 Ma) is spatially and temporally related to the Teslin Mountain pluton. In addition, a discrete but pervasive intrusive igneous system is composed of hundreds of dikes mainly related to the Teslin and Whitehorse plutonic suites. Two of the dated dikes returned dates between 138 and136 Ma, a previously unrecognized magmatic suite in Yukon, and informally named the Goddard suite.

Each intrusion is the result of the tectonic and magmatic setting at a given time, and therefore the geochemical and trace element signatures of these intrusions, combined with U/Pb geochronology, provide insight into the tectonic evolution of the northern Cordilleran orogen throughout the Cretaceous. Each intrusion and group of dikes is characterized by a distinct U/Pb and REE signature. The latter indicates varying degrees of crustal contribution to the magmas. The most juvenile dikes are interpreted to be Middle Triassic, because they intersect only mafic and volcaniclastic rocks of the Joe Mountain Formation, and their REE profile matches the signature of known juvenile Middle Triassic dikes. In contrast, Early Cretaceous dikes display a calc-alkaline signature. This suggests that a major shift in tectonic environment occurred between the Triassic and Early Cretaceous. The initial stages of Cordilleran terrane accretion took place during the Jurassic and the changing dike geochemistry between the Triassic and Early Jurassic may reflect that. Middle and Late Cretaceous dikes and intrusions are still calc-alkaline with a slightly shallower slope and a distinct Eu anomaly for the Rancheria suite intrusive and volcanic rocks, suggesting that these rocks were probably derived from crustal melts.

Plutons and dikes represent significant volumes of magma, either fully expressed as batholith-size intrusions, or as discrete dike occurrences. The cluster of dikes in some areas may be the surface expression of an underlying pluton (e.g., west of Teslin Mountain), or may be related to extension transfer zones along a dominantly strike-slip fault (e.g., along the Goddard fault; Fig. 40). This active magmatic environment is consistent with the setting of an active orogen building, and characterized by local crustal extension and transtensional deformation.

Mineral occurrences in the eastern Lake Laberge area are mainly spatially associated with Cretaceous dikes and plutons, which highlights the relationship between an active magmatic system throughout the Cretaceous and a resulting mineral endowment. Large plutons such as the Laurier Creek (*ca.* 116 Ma) and Teslin plutons (*ca.* 78 Ma) are associated with porphyry-style mineralization. Cu-Mo mineralization is observed at the Laurier Creek pluton (Fig. 49b). In addition, possible genetic associations exist between the Teslin Mountain pluton and Red Mountain Cu-Au-Mo porphyry (Yukon MINFILE 105C 009) based on lithological and geochronological correlations between the two plutons. Other styles of mineral occurrences indicate the presence of gold associated with dikes and veins, and are only poorly characterized so far.

Acknowledgements

Several field assistants were involved in this mapping project: Kyle Orr, Sarah Ellis, Daphnee Tuzlak, Galena Roots and Alexina Boileau Morrisson. Their hard work in the field is greatly appreciated. Heli Dynamics Ltd. provided safe helicopter support for four consecutive summers. The Geological Survey of Canada GEM-2 program (Evaluation of the Geo-Mapping for Energy and Minerals) is thanked for supporting part of the analytical and logistical expenses for this project including lithogeochemistry, geochronology, conodont analyses and isotopic analyses. Strategic Metals Ltd. provided access to their Hartless Joe camp and property during the summer of 2018. Hf-Nd isotopic analyses were conducted at the Pacific Center for Isotopic and Geochemical Research at the University of British Columbia. Robert Blodgett analyzed 16 macrofossil samples collected during mapping. Martyn Golding conducted analyses and identification of 25 conodont samples. Patrick Sack provided geochemical data for 5 samples of Triassic volcanic rocks. Finally, discussions with Steve Israel, Maurice Colpron and Patrick Sack helped in developing a better understanding of the complex geology in the eastern Lake Laberge area. Maurice Colpron provided a detailed and constructive review of the text and figures presented in this report.

References

Aitken, J.D., 1959. Atlin Map-area, British Columbia. Geological Survey of Canada, Memoir 307, 89 p.

Allan, M.M., Rhys, D.A. and Hart, C.J.R., 2017. Orogenic gold mineralization of the eastern Cordilleran gold belt, British Columbia: Structural ore controls in the Cariboo (093A/H), Cassiar (104P) and Sheep Creek (082F) mining districts. Geoscience BC Report 2017-15, 108 p.

Barrett, T.J. and MacLean, W.H., 1999. Volcanic sequences, lithogeochemistry, and hydrothermal alteration in some bimodal volcanic-associated massive sulfide systems. Reviews in Economic Geology, vol. 8, p. 101–131.

Bickerton, L., 2014. The northern Cache Creek terrane: record of Middle Triassic arc activity and Jurassic-Cretaceous terrane imbrication. Unpublished MSc thesis, Simon Fraser University, 95 p.

Bickerton, L., Colpron, M. and Gibson, D.W., 2013. Cache Creek terrane, Stikinia, and overlap assemblages of eastern Whitehorse (NTS 105D) and western Teslin (NTS 105C) map areas. *In:* Yukon Exploration and Geology 2012, K.E. MacFarlane, M.G. Nordling and P.J. Sack (eds.), Yukon Geological Survey, p. 1–17.

Bond, J.D., 2004. Late Wisconsinan McConnell glaciation of the Whitehorse map area (105D), Yukon. *In:* Yukon Geological Survey (ed.), Yukon Exploration and Geology 2003, p. 73–88.

Bordet, E., 2016. Preliminary results on the Middle Triassic-Middle Jurassic stratigraphy and structure of the Teslin Mountain area, southern Yukon. *In:* Yukon Exploration and Geology 2015, K.E. MacFarlane and M.G. Nordling (eds.), Yukon Geological Survey, p. 43–61.

Bordet, E., 2017. Updates on the Middle Triassic-Middle Jurassic stratigraphy and structure of the Teslin Mountain and east Lake Laberge areas, south-central Yukon. *In:* Yukon Exploration and Geology 2016, K.E. MacFarlane and L.H. Weston (eds.), Yukon Geological Survey, p. 1–24.

Bordet, E., 2018. Bedrock geology of the Teslin Mountain and east Lake Laberge areas, south-central Yukon. *In:* Yukon Exploration and Geology 2017, K.E. MacFarlane (ed.), Yukon Geological Survey, p. 1–24.

Bordet, E., 2019. Bedrock geology map of the eastern Lake Laberge area; parts of Teslin Mountain, Lake Laberge, Lower Laberge, Mason Landing, Joe Mountain and Mount M'Clintock (NTS 105E/2, 3, 6, 7 and 105D/15, 16). Yukon Geological Survey, Geoscience Map 2019-1, 2 sheets, 1:50 000 scale

Bostock, H.S. and Lees, E.J., 1938. Laberge map-area, Yukon. Department of Mines and Resources, Geological Survey of Canada, Ottawa, ON, Canada, Memoir 217, 33 p.

Brandl, P.A., Hamada, M., Arculus, R.J., Johnson, K., Marsaglia, K.M., Savov, I.P., Ishizuka, O. and Li, H., 2017. The arc arises: The links between volcanic output, arc evolution and melt composition. Earth and Planetary Science Letters, vol. 461, p. 73–84,

Bremner, T., 1991. Mount Byng property, south Yukon. Yukon Geology 1990. Indian and Northern Affairs Canada, Exploration and Geological Services Division, Yukon, p. 52–56.

Brown, P. and Kahlert, B., 1986. Geology and mineralization of the Red Mountain porphyry molybdenum deposit, south-central Yukon. *In:* Mineral Deposits of Northern Cordillera, J.A. Morin (ed.), Special Volume 37, p. 288–297.

Cairnes, D.D., 1910. Preliminary memoir on the Lewes and Nordenskiold rivers Coal District, Yukon Territory. Geological Survey of Canada, Memoir 5, 87 p.

Childe, F.C. and Schiarizza, P., 1997. U-Pb geochronology, geochemistry and Nd isotopic systematics of the Sitlika Assemblage, central British Columbia. *In:* Geological Fieldwork 1996, B.C.G. Survey (ed.), Paper 1997-1, p. 69–79.

Childe, F.C. and Thompson, J.F.H., 1997. Geological setting, U-Pb geochronology, and radiogenic isotopic characteristics of the Permo-Triassic Kutcho Assemblage, north-central British Columbia. Canadian Journal of Earth Sciences, vol. 34, p. 1310–1324.

Childe, F.C., Friedman, R.M., Mortensen, J.K. and Thompson, J.F.H., 1997. Evidence for Early Triassic felsic magmatism in the Ashcroft (92I) map area, British Columbia. *In:* Geological Fieldwork 1996, British Columbia Geological Survey (ed.), Paper 1997-1, p. 117–124.

Childe, F.C., Thompson, J.F.H., Mortensen, J.K., Friedman, R.M., Schiarizza, P., Bellefontaine, K. and Marr, J.M., 1998. Primitive Permo-Triassic volcanism in the Canadian Cordillera: tectonic and metallogenic implications. Economic Geology, vol. 93, p. 224–231.

Christiansen, E.H. and Keith, J.D., 1996. Trace element systematics in silicic magmas: a metallogenic perspective. *In:* Trace element geochemistry of volcanic rocks: applications for massive sulfide exploration, D.A. Wyman (ed.), Short Course notes, vol. 12, p. 115–151.

Cohen, K.M., Finney, S.C., Gibbard, P.L. and Fan, J.-X., 2013; updated. The ICS International Chronostratigraphic Chart. Episodes, vol. 36, p. 199–204.

Colpron, M., Gordey, S., Lowey, G., White, D. and Piercey, S., 2007a. Geology of the northern Whitehorse trough, Yukon (105E/12, 13 and parts of 11 and 14; 105L/4 and parts of 3 and 5; parts of 115H/9 and 16; 115I/1 and part of 8). Yukon Geological Survey Open File 2007-6, scale 1:150 000.

Colpron, M., Nelson, J.L. and Murphy, D.C., 2007b. Northern Cordilleran terranes and their interactions through time. GSA Today, vol. 17, p. 4–10.

Colpron, M. and Friedman, R.M., 2008. U-Pb zircon ages for the Nordenskiold formation (Laberge Group) and Cretaceous intrusive rocks, Whitehorse trough, Yukon. *In:* Yukon Exploration and Geology 2007, D.S. Emond, L.R. Blackburn, R.P. Hill and L.H. Weston (eds.), Yukon Geological Survey, p. 139–151.

Colpron, M. and Nelson, J.L., 2011. A Digital Atlas of Terranes for the Northern Cordillera. Yukon Geological Survey, www.geology.gov.yk.ca [accessed Nov. 2015].

Colpron, M., 2011. Geological compilation of Whitehorse trough - Whitehorse (105D), Lake Laberge (105E), and part of Carmacks (115I), Glenlyon (105L), Aishihik Lake (115H), Quiet Lake (105F) and Teslin (105C). Yukon Geological Survey, Geoscience Map 2011-1, scale 1:250 000.

Colpron, M., Crowley, J.L., Gehrels, G., Long, D.G.F., Murphy, D.C., Beranek, L. and Bickerton, L., 2015. Birth of the northern Cordilleran orogen, as recorded by detrital zircons in Jurassic synorogenic strata and regional exhumation in Yukon. Lithosphere, vol. 7, p. 541–562, doi:10.1130/l451.1.

Colpron, M., Israel, S. and Friend, M. (compilers), 2016a. Yukon Plutonic Suites. Yukon Geological Survey, Open File 2016-37, scale 1:750 000.

Colpron, M., Israel, S., Murphy, D., Pigage, L. and Moynihan, D., 2016b. Yukon bedrock geology map. Yukon Geological Survey, Open File 2016-1, scale 1:1 000 000, map and legend.

Coney, P.J., Jones, D.L. and Monger, J.W., 1980. Cordilleran suspect terranes. Nature, vol. 288, p. 329–333.

Crowley, J.L., Schoene, B. and Bowring, S.A., 2007. U-Pb dating of zircon in the Bishop Tuff at the millennial scale. Geology, vol. 35 p. 1123–1126.

Dickie, J.R. and Hein, F.J., 1995. Conglomeratic fan deltas and submarine fans of the Jurassic Laberge Group, Whitehorse trough, Yukon Territory, Canada – Fore-arc sedimentation and unroofing of a volcanic island-arc complex. Sedimentary Geology, vol. 98, p. 263–292.

Dostal, J., Keppie, J.D. and Ferri, F., 2009. Extrusion of high-pressure Cache Creek rocks into the Triassic Stikinia–Quesnellia arc of the Canadian Cordillera: implications for terrane analysis of ancient orogens and palaeogeography. Geological Society, London, Special Publications, vol. 327, p. 71–87.

Eaton, D.W., 1999. Assessment Report Describing Geological Mapping, Prospecting and Soil Geochemistry on the DDL Property, for Nordac Resources Ltd. Yukon Energy, Mines and Resources, Assessment Report 093953, 47 p.

Eaton, D.W., 2016. Strategic Metals Ltd. reports more high grade assays from its Hartless Joe Property in Yukon Territory including 462 g/t gold over 0.40 m. Strategic Metals Ltd. news release, www.strategicmetals.com.

Eaton, D.W., 2018. Strategic Metals Ltd. announces new high-grade gold discoveries that expand the precious metal system at its Hartless Joe property, Yukon. Strategic Metals Ltd. news release, http://www.strategicmetalsltd.com.

English, J.M. and Johnston, S.T., 2005. Collisional orogenesis in the northern Canadian Cordillera; implications for Cordilleran crustal structure, ophiolite emplacement, continental growth, and the terrane hypothesis. Earth and Planetary Science Letters, vol. 232, p. 333–344.

English, J.M., Mihalynuk, G.M. and Johnston, S.T., 2010. Geochemistry of the northern Cache Creek terrane and implications for accretionary processes in the Canadian Cordillera. Canadian Journal of Earth Sciences, vol. 47, p. 13–34.

Gabrielse, H., 1991. Late Paleozoic and Mesozoic terrane interactions in north-central British Columbia. Canadian Journal of Earth Sciences, vol. 28, p. 947–957.

Gabrielse, H., Murphy, D.C. and Mortensen, J.K., 2006. Cretaceous and Cenozoic dextral orogen-parallel displacements, magmatism, and paleogeography, north-central Canadian Cordillera. *In:* Paleogeography of the North American Cordillera: Evidence For and Against Large-Scale Displacements, J.W. Haggart, R.J. Enkin and J.W.H. Monger (eds.), Geological Association of Canada,, Special Paper 46, p. 255–276.

Gerstenberger, H. and Haase, G., 1997. A highly effective emitter substance for mass spectrometric Pb isotope ratio determinations. Chemical Geology, vol. 136, p. 309–312.

Gosh, D.K., 1995. Nd-Sr isotopic constraints on the interactions of the Intermontane Superterrane with the western edge of North America in the southern Canadian Cordillera. Canadian Journal of Earth Sciences, vol. 32, p. 1740–1758.

Gunning, M.H., Hodder, R.W.H. and Nelson, J.L., 2006. Contrasting volcanic styles and their tectonic implications for the Paleozoic Stikine assemblage, western Stikine terrane, northwestern British Columbia. *In:* Paleozoic Evolution and Metallogeny of Pericratonic Terranes at the Ancient Pacific Margin of North America, Canadian and Alaskan Cordillera, M. Colpron and J.L. Nelson (eds.), Geological Association of Canada, Special Paper 45, p. 201–227.

Hart, C.J.R., 1997a. A transect across northern Stikinia: geology of the northern Whitehorse map area, southern Yukon Territory (105D/13-16). Indian and Northern Affairs Canada, Exploration and Geological Services Division, Yukon Region, Bulletin 8, 77 p.

Hart, C.J.R., 1997b. Geology and geochemistry of the Teslin Crossing Pluton: A gold rich alkalic porphyry target. *In:* Yukon Exploration and Geology, 1996, Exploration and Geological Services Division, Yukon, Indian and Northern Affairs Canada, p.131–137.

Hart, C.J.R. and Hunt, J.A., 1997a. Geology of the Joe Mountain area, southern Yukon (105D/15). Exploration and Geological Services Division, Yukon Region, Indian and Northern Affairs Canada, scale 1:50 000.

Hart, C.J.R. and Hunt, J.A., 1997b. Geology of Mount M'Clintock map area, southern Yukon (105D/16). Exploration and Geological Services Division, Yukon Region, Indian and Northern Affairs Canada, scale 1:50 000.

Hart, C.J.R. and Hunt, J.A., 2003a. Geology of Joe Mountain map area (105D/15), southern Yukon (1:50 000 scale). Yukon Geological Survey, Energy, Mines and Resources, Yukon Territorial Government, Geoscience Map 2003-4.

Hart, C.J.R. and Hunt, J.A., 2003b. Geology of Mount M'Clintock map area (NTS 105D/16), southern Yukon (1:50 000 scale). Yukon Geological Survey, Energy, Mines and Resources, Yukon Territorial Government, Geoscience Map 2003-5.

Hart, C.J.R. and Orchard, M.J., 1996. Middle Triassic (Ladinian) volcanic strata in southern Yukon Territory, and their Cordilleran correlatives. Geological Survey of Canada, Current Research no. 1996-A, p. 11–18.

Hart, C.J.R. and Radloff, J.K., 1990. Geology of Whitehorse, Alligator Lake, Fenwick Creek, Carcross and part of Robinson map areas (105 D/11, 6, 3, 2, 7). Exploration and Geological Services Division, Department of Northern and Indian Affairs, Whitehorse, Open File 1990-4, 126 p.

Hollings, P., Wolfe, R., Cooke, D.R. and Waters, P.J., 2011. Geochemistry of Tertiary Igneous Rocks of Northern Luzon, Philippines: Evidence for a Back-Arc Setting for Alkalic Porphyry Copper-Gold Deposits and a Case for Slab Roll-Back? Economic Geology, vol. 106, p. 1257–1277.

Hoover, P.R., 1991. Late Triassic cyrtinoid spiriferinacean brachiopods from western North America and their biostratigraphic and biogeographic implications. Bulletins of American Paleontology, vol. 100, p. 63–109.

Hunt, J.A. and Roddick, J.A., 1987. A compilation of K-Ar ages. Geological Survey of Canada, Paper 87-2, 143–210 p.

Ishizuka, O., Hickey-Vargas, R., Arculus, R.J., Yogodzinski, G.M., Savov, I.P., Kusano, Y., McCarthy, A., Brandl, P.A. and Sudo, M., 2018. Age of Izu–Bonin–Mariana arc basement. Earth and Planetary Science Letters, vol. 481, p. 80–90.

Jaffey, A.H., Flynn, K.F., Glendenin, L.E., Bentley, W.C. and Essling, A.M., 1971. Precision measurements of half-lives and specific activities of 235U and 238U. Physical Review C, vol. 4, p. 1889–1906.

Joyce, N.L., Ryan, J.J., Colpron, M., Hart, C.J.R. and Murphy, D.C., 2015. A compilation of $^{40}Ar/^{39}Ar$ age determinations for igneous and metamorphic rocks, and mineral occurrences from central and southeast Yukon. Geological Survey of Canada, Open File 7924, 229 p.

Kiss, F. and Boulanger, O., 2018. Aeromagnetic Survey of the Marsh Lake Area, Yukon, Part of NTS 105D/North. Geological Survey of Canada, Open File 8418.

Klassen, R.W. and Morison, S.R., 1987. Surficial geology, Laberge, Yukon Territory. Geological Survey of Canada, Map 8-1985, 1:250 000 scale.

Krogh, T.E., 1973, A low contamination method for hydrothermal decomposition of zircon and extraction of U and Pb for isotopic age determination. Geochimica et Cosmochimica Acta, vol. 37, p. 485–494.

Lang, J.R. and McClaren, M., 2003. Hydrothermal alteration, mineralization and exploration potential of the Mars alkalic copper-gold-molybdenum porphyry occurrence, Laberge map area (105E/7), Yukon. *In:* Yukon Exploration and Geology 2004, D.S. Emond and L.L. Lewis (eds.), Yukon Geological Survey, p. 261–269.

Larson, K.P., 2002. Microstructural Analysis of the Teslin Fault, Northwestern British Columbia. *In:* Geological Fieldwork 2001, British Columbia Geological Survey Survey (ed.), Paper 2002-1, p. 31–34.

Le Bas, M.J., Le Maitre, R.W., Streckeisen, A. and Zanettin, B., 1986. A chemical classification of volcanic rocks based on the total alkalis-silica diagram. Journal of Petrology, vol. 27, p. 745–750.

Lees, E.J., 1934. Geology of the Laberge area, Yukon. Transactions, Royal Canadian Institute, vol. 20, p. 1–48.

Long, D.G.F., 2015. Provenance and depositional framework of braided and meandering gravel-bed river deposits and associated coal deposits in active intermontane piggyback basins: The Upper Jurassic to Lower Cretaceous Tantalus Formation, Yukon. Yukon Geological Survey, Open File 2015-23, 80 p. plus appendices.

Lowey, G.W., 2004. Preliminary lithostratigraphy of the Laberge Group (Jurassic), south-central Yukon: Implications concerning the petroleum potential of the Whitehorse Trough. *In:* Yukon Exploration and Geology 2003, D.S. Emond and L.L. Lewis (eds.), Yukon Geological Survey, p. 129–142.

Lowey, G.W., 2005. Sedimentology, stratigraphy and source rock potential of the Richthofen formation (Jurassic), northern Whitehorse Trough, Yukon. *In:* Yukon Exploration and Geology 2004, D.S. Emond, L.L. Lewis and G. Bradshaw (eds.), Yukon Geological Survey, p. 177–191.

Lowey, G.W., 2008. Summary of the stratigraphy, sedimentology and hydrocarbon potential of the Laberge Group (Lower-Middle Jurassic), Whitehorse trough, Yukon. *In:* Yukon Exploration and Geology 2007, D.S. Emond, L.R. Blackburn, R.P. Hill and L.H. Weston (eds.), Yukon Geological Survey, p. 179–197.

Lowey, G.W., Long, D.G.F., Fowler, M.G., Sweet, A.R. and Orchard, M.J., 2009. Petroleum source rock potential of Whitehorse trough: a frontier basin in south-central Yukon. Bulletin of Canadian Petroleum Geology, vol. 57, p. 350–386.

Ludwig, K.R., 2003, User's Manual for Isoplot 3.00. Berkeley Geochronology Center, Berkeley, CA, 70 p.

MacIntyre, D.G., Villeneuve, M.E. and Schiarizza, P., 2001. Timing and tectonic setting of Stikine Terrane magmatism, Babine–Takla lakes area, central British Columbia. Canadian Journal of Earth Sciences, vol. 38, p. 579–601.

Mackie, R., Arne, D. and Pennimpede, C., 2016. Enhanced interpretation of stream sediment geochemical data for NTS 105E. Yukon Geological Survey, Open File 2016-9, scale 1:250 000, 13 sheets.

Mattinson, J.M., 2005. Zircon U-Pb chemical abrasion ("CA-TIMS") method: combined annealing and multi-step partial dissolution analysis for improved precision and accuracy of zircon ages. Chemical Geology, vol. 220, p. 47–66.

Mihalynuk, G.M., Diakow, L.J., Friedman, R. and Logan, J.M., 2016. Chronology of southern Nicola arc stratigraphy and deformation. British Columbia Ministry of Energy and Mines, British Columbia Geological Survey, Geological Fieldwork 2015, Paper 2016-1, p. 31–63.

Mihalynuk, M.G., Erdmer, P., Ghent, E.D., Cordey, F., Archibald, D.A., Friedman, R.M. and Johannson, G.G., 2004. Coherent French Range blueschist: Subduction to exhumation in <2.5 m.y.? GSA Bulletin, vol. 116, p. 910–922.

Mihalynuk, M.G., Mountjoy, K.J., Smith, M.T., Currie, L.D., Gabites, J.E., Tipper, H.W., Orchard, M.J., Poulton, T.P. and Cordey, F., 1999. Geology and mineral resources of the Tagish Lake area (NTS 104M/8, 9, 10E, 15 and 104N/12W), northwestern British Columbia. B.C. Ministry of Energy and Mines, Bulletin 105, 217 p.

Mihalynuk, M.G., Nelson, J. and Diakow, L.J., 1994. Cache Creek terrane entrapment: Oroclinal paradox within the Canadian Cordillera. Tectonics, vol. 13, p. 575–595.

Monger, J.W.H., Price, R.A. and Tempelman-Kluit, D.J., 1982. Tectonic accretion and the origin of two metamorphic and plutonic welts in the Canadian Cordillera. Geology, vol. 10, p. 70–75,

Monger, J.W.H., Wheeler, J.O., Tipper, H.W., Gabrielse, H., Harms, T., Struik, L.C., Campbell, R.B., Dodds, C.J., Gehrels, G.E. and O'Brien, J., 1991. Part B. Cordilleran terranes, Upper Devonian to Middle Jurassic assemblages (Chapter 8). *In:* Geology of the Cordilleran orogen in Canada, H. Gabrielse and C.J. Yorath (eds.), Geological Survey of Canada, Geology of Canada 4, p. 281–327; *also* Geological Society of America, The Geology of North America, vol. G-2.

Mortensen, J.K. and Jilson, G.A., 1985. Evolution of the Yukon-Tanana terrane: evidence from southeastern Yukon Territory. Geology, vol. 13, p. 806–810.

Mortensen, J.K., 1992. Pre-Mid-Mesozoic tectonic evolution of the Yukon-Tanana terrane, Yukon and Alaska. Tectonics, vol. 11, p. 836–853.

Nelson, J.L., Colpron, M. and Israel, S., 2013. The Cordillera of British Columbia, Yukon, and Alaska: Tectonics and metallogeny. *In:* Tectonics, Metallogeny and Discovery: The North American Cordillera and Similar Accretionary Settings, M. Colpron, T. Bissig, B.G. Rusk and J.F.H. Thompson (eds.), Society of Economic Geologists, Special Publication 17, p. 53–103.

Orchard, M.J., 1991. Upper Triassic conodont biochronology and new index species from the Canadian Cordillera. Geological Survey of Canada Bulletin 417, p. 299–335.

Orchard, M.J., 1995. Report on conodonts and other microfossils from the Whitehorse (105D) and Lake Laberge (105E) map areas. Geological Survey of Canada, MJO-1997-10.

Pautler, J., 2018. Technical report on the Hartless Joe project, Yukon Territory. Strategic Metals Ltd. technical report, 48 p., www.sedar.com [accessed November 2018].

Pearce, J.A. and Cann, J.R., 1973. Tectonic Setting of Basic Volcanic Rocks Determined Using Trace Element Analyses. Earth and Planetary Science Letters, vol. 19, p. 290–300.

Pearce, J.A. and Peate, D.W., 1995. Tectonic implications of the composition of volcanic arc magmas. Annual Reviews of Earth and Planetary Science, vol. 23, p. 251–285.

Pearce, J.A., 1996. A user's guide to basalt discrimination diagrams. *In:* Trace element geochemistry of volcanic rocks: Applications for massive sulphide exploration, D.A. Wyman (ed.), Geological Association of Canada, Short Course Notes, vol. 12, p. 79–113.

Pearce, J.A., Kempton, P.D., Nowell, G.M. and Noble, S.R., 1999. Hf-Nd element and isotope perspective on the nature and provenance of mantle and subduction components in Western Pacific arc-basin systems. Journal of Petrology, vol. 40, p. 1579–1611.

Piercey, S.J., 2005. Reconnaissance geological and geochemical studies of the Joe Mountain Formation, Joe Mountain region (NTS 105D/15), Yukon. *In:* Yukon Exploration and Geology 2004, D.S. Emond, L.L. Lewis and G.D. Bradshaw (eds.), Yukon Geological Survey, p. 213–226.

Piercey, S.J., Murphy, D.C., Mortensen, J.K. and Creaser, R.A., 2004. Mid-Paleozoic initiation of the northern Cordilleran marginal backarc basin: Geologic, geochemical, and neodymium isotope evidence from the oldest mafic magmatic rocks in the Yukon-Tanana terrane, Finlayson Lake district, southeast Yukon, Canada. GSA Bulletin, vol. 116, p. 1087–1106.

Piercey, S.J., Nelson, J., Colpron, M., Dusel-Bacon, C., Simard, R.-L. and Roots, C.F., 2006. Paleozoic magmatism and crustal recycling along the ancient Pacific margin of North America, northern Cordillera. *In:* Paleozoic Evolution and Metallogeny of Pericratonic Terranes at the Ancient Pacific Margin of North America, Canadian and Alaskan Cordillera, M. Colpron and J. Nelson (eds.), Geological Association of Canada, Special Paper 45, p. 281–322.

Rasmussen, K.L., 2013. The timing, composition, and petrogenesis of syn- to post-accretionary magmatism in the northern Cordilleran miogeocline, eastern Yukon and southwestern Northwest Territories. PhD thesis, University of British Columbia, 810 p.

Reid, R.P., 1980. Report of field work on the Upper Triassic reef complex of Lime Peak, Laberge map area, Yukon. *In:* Geology and Exploration 1979-80, D.J. Tempelman-Kluit (ed.), Indian & Northern Affairs Canada/Department of Indian & Northern Development: Exploration & Geological Services Division, p. 110–114.

Samson, S.D., McClelland, W.C., Patchett, P.J., Gehrels, G.E. and Anderson, R.G., 1989. Evidence from neodymium isotopes for mantle contributions to Phaneroizoic crustal genesis in the Canadian Cordillera. Nature, vol. 337, p. 705–709.

Schiarizza, P., 2011. Bedrock geology of the Andrea Creek area, part of NTS 104I/01. British Columbia Ministry of Energy and Mines, 1:25 000 scale.

Schiarizza, P., 2012. Geology of the Kutcho assemblage between the Kehlechoa and Tucho Rivers, northern British Columbia (NTS 104I/01, 02). *In:* Geological Fieldwork 2011, British Columbia Ministry of Energy, Mines and Petroleum Resources, Paper 2012-1, p. 75–98.

Schmitz, M.D. and Schoene, B., 2007. Derivation of isotope ratios, errors and error correlations for U-Pb geochronology using 205Pb-235U-(233U)-spiked isotope dilution thermal ionization mass spectrometric data. Geochemistry, Geophysics, Geosystems (G3), vol. 8, Q08006, doi:10.1029/2006GC001492.

Schnetzler, C.C. and Philpotts, J.A., 1970. Partition coefficients of rare-earth elements between igneous matrix material and rock-forming mineral phenocrysts. Geochimica et Cosmochimica Acta, vol. 34, p. 331–340.

Senowbari-Daryan, B., 1990. Die systematische Stellung der thalamiden Schwämme und ihre Bedeutung in der Erdgeschichte. Münchner Geowissenschaftliche Abhandlungen, vol. A 21, p. 5–326.

Shervais, J.W., 1982. Ti-V plots and the petrogenesis of modern and ophiolitic lavas. Earth and Planetary Science Letters, vol. 59, p. 101–118.

Simmons, A.T., Tosdal, R.M., Awmack, H.J., Wooden, J.L. and Friedman, R.M., 2007. Early Triassic Stuhini Group and Tertiary Sloko Group Magmatism (NTS 104K/10W), Northwestern British Columbia: New U-Pb Geochronological Results. *In:* Geological Fieldwork 2006, Ministry of Energy, Mines and Petroleum Resources (ed.), Paper 2007-1, 211–224 p.

Sláma, J., Košler, J, Condon, D.J., Crowley, J.L., Gerdes, A., Hanchar, J.M., Horstwood, M.S.A., Morris, G.A., Nasdala, L., Norberg, N., Schaltegger, U., Schoene, B. Tubrett, M.N. and Whitehouse, M.J. 2008. Plešovice zircon — A new natural reference material for U–Pb and Hf isotopic microanalysis. Chemical Geology, vol. 249, p. 1-35.

Smith, A.D. and Lambert, R.S., 1995. Nd, Sr, and Pb isotopic evidence for contrasting origins of late Paleozoic volcanic rocks from the Slide Mountain and Cache Creek terranes, south-central British Columbia. Canadian Journal of Earth Sciences, vol. 32, p. 447–459.

Stevens, R.D., Delabio, R.N. and Lachance, G.R., 1982. Age Determinations and Geological Studies, K-Ar Isotopic Ages. Geological Survey of Canada, Report 16, Paper 82-2, 56 p.

Struik, L.C., Schiarizza, P., Orchard, M.J., Cordey, F., Sano, H., MacIntyre, D.G., Lapierre, H. and Tardy, M., 2001. Imbricate architecture of the upper Paleozoic to Jurassic oceanic Cache Creek Terrane, central British Columbia. Canadian Journal of Earth Sciences, vol. 38, p. 495–514.

Sun, S.S. and McDonough, W.F., 1989. Chemical and isotopic systematics of oceanic basalts: implications for mantle composition and processes. Geological Society, London, Special Publications, vol. 42, p. 313–345.

Tempelman-Kluit, D.J., 1984. Geology, Laberge (105E) and Carmacks (115I), Yukon Territory. Geological Survey of Canada, Open File 1101, 10 pages and two maps, scale 1:250 000.

Tempelman-Kluit, D.J., 2009. Geology of Carmacks and Laberge map areas, central Yukon: Incomplete draft manuscript on stratigraphy, structure and its early interpretation (*ca.* 1986). Geological Survey of Canada, Open File 5982, 399 p.

Tozer, E., 1958. Stratigraphy of the Lewes River Group (Triassic), central Laberge area, Yukon Territory. Geological Survey of Canada, Bulletin 43, p. 1–28.

Turner, A. and Sabag, S.F., 1995. A Preliminary Evaluation of Gold Potential, Red Mountain Molybdenum Deposit. Yukon Energy, Mines and Resources Assessment Report 093354, 353 p.

van Drecht, L. and Beranek, L.P., 2018. New investigations of basal Laberge Group stratigraphy, Whitehorse trough, central Yukon. *In:* Yukon Exploration and Geology 2017, K.E. MacFarlane (ed.), Yukon Geological Survey, p. 151–163 p.

van Drecht, L., Beranek, L.P. and Hutchison, M., 2017. Jurassic stratigraphy and tectonic evolution of the Whitehorse trough, central Yukon: Project outline and preliminary field results. *In:* Yukon Exploration and Geology 2016, K.E. MacFarlane and L.H. Weston (eds.), Yukon Geological Survey, p. 207–223 p.

Vice, L., 2017. Late Cretaceous to Paleocene evolution of the Blanchard River assemblage, southwest Yukon; implications for Mesozoic accretionary processes in the northwestern Cordillera. MSc thesis, Simon Fraser University, Vancouver, BC, 224 p.

Watson, E.B., Wark, D.A. and Thomas, J.B. 2006. Crystallization thermometers for zircon and rutile. Contributions to Mineralogy and Petrology, vol. 151, p. 413–433.

Weis, D., Kieffer, B., Maerschalk, C., Barling, J., De Jong, J., Williams, G., Hanano, D., Pretorius, W., Mattielli, N., Scoates, J.S., Goolaerts, A., Friedman, R. and Mahoney, J.B., 2006. High-precision isotopic characterization of USGS reference materials by TIMS and MC-ICP-MS. Geochemistry, Geophysics, Geosystems, vol. 7, p. 1–30.

Weis, D., Kieffer, B., Maerschalk, C., Pretorius, W. and Barling, J., 2005. High-precision Pr-Sr-Nd-Hf isotopic characterization of USGS BHVO-1 and BHVO-2 reference materials. Geochemistry, Geophysics, Geosystems, vol. 6, p. 1–10.

Wheeler, J.O., 1961. Whitehorse map area, Yukon Territory. Geological Survey of Canada Memoir 312, 183 p.

Wheeler, J.O., Brookfield, A.J., Gabrielse, H., Monger, J.W.H., Tipper, H.W. and Woodsworth, G.J., 1991. Terrane map of the Canadian Cordillera. Geological Survey of Canada, Map 1713A, scale 1:2 000 000.

White, D., Colpron, M. and Buffett, G., 2012. Seismic and geological constraints on the structure and hydrocarbon potential of the northern Whitehorse trough, Yukon, Canada. Bulletin of Canadian Petroleum Geology, vol. 60, p. 239–255.

Wilson, S.A., 1997. The collection, preparation, and testing of USGS reference material BCR-2, Columbia River, Basalt. US Geological Survey, Open File Report 98-00x.

Wilson, S.A., 1998. Data compilation for USGS reference material GSP-2, Granodiorite, Silver Plume, Colorado. US Geological Survey, Open File Report.

Winchester, J.A. and Floyd, P.A., 1977. Geochemical discrimination of different magma series and their differentiation products using immobile elements. Chemical Geology, vol. 20, p. 325–343.

Wood, D.A., 1980. The application of a ThHfTa diagram to problems of tectonomagmatic classification and to establishing the nature of crustal contamination of basaltic lavas of the British Tertiary Volcanic Province. Earth and Planetary Science Letters, vol. 50, p. 11–30.

Yarnell, J.M., Stanley, G. and Hart, C.J.R., 1999. New paleontological investigations of Upper Triassic shallow-water reef carbonates (Lewes River Group) in the Whitehorse area, Yukon. *In:* Yukon Exploration and Geology 1998, C.F. Roots and D.S. Edmond (eds.), Exploration and Geological Services Division, Yukon, Indian and Northern Affairs Canada, p. 179–184.

Yukon Geochronology, 2018. Yukon Geochronology – A database of Yukon geochronology sample locations, M. Colpron (compiler). Yukon Geological Survey,<http://yukon2.maps.arcgis.com/home/item.html?id=0fa83ba4a4794b9d8432d4d1b44da967> [accessed November 22, 2018].

Yukon MINFILE, 2018. Yukon MINFILE – A database of mineral occurrences. Yukon Geological Survey, <http://data.geology.gov.yk.ca> [accessed November 2018].